

**Carbon nanotube membranes for brackish groundwater desalination and removal of  
organic micropollutants from water**

by

NOZIPHO NONSIKELELO GUMBI

submitted in accordance with the requirements for the degree of

DOCTOR OF PHILOSOPHY

in the subject

CHEMISTRY

at the

UNIVERSITY OF SOUTH AFRICA

SUPERVISOR : Prof EN Nxumalo

CO-SUPERVISORS : Prof BB Mamba

: Prof J-X Li

July 2019

## DECLARATION

---

Name: Ms N.N. Gumbi

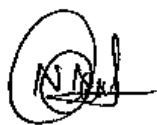
Student number: 57404755

Degree: PhD in Chemistry

Exact wording of the title of the thesis as appearing on the copies submitted for examination:

**Carbon nanotube membranes for brackish groundwater desalination and the removal of organic micropollutants from water**

I declare that the above thesis is my own work and that all the sources that I have used or quoted have been indicated and acknowledged by means of complete references.



---

SIGNATURE

04/07/2019

---

DATE

## **DEDICATION**

---

This work is dedicated to my very first teacher and late grandfather, Mr Themba Gumbi, my dearest moms Mrs Nelisiwe Nguse and Mrs Hlengiwe Ngcobo, my supportive partner Mr Sydney Madzivha, and to all the loved ones that I have lost during the course of this degree.

## ACKNOWLEDGEMENTS

---

*“I come as one, but I stand as ten thousand.” – Maya Angelou*

First and foremost, I would like to thank God Almighty, with whom none of this would have been possible. Thank you for seeing it fit that this journey comes to pass.

I wish to extend my deepest gratitude to my supervisors, Prof Edward Nxumalo and Prof Bhekie Mamba for their constant support, guidance and patience, and their timeous feedback on the thesis corrections. I truly appreciate the meticulous efforts in mentoring and moulding me into the developing researcher that I am today.

Prof Jianxin Li, I wish to thank you for unravelling my understanding of membrane microstructures and for allowing me to work with your group of researchers at Tianjin Polytechnic University (TJPU) in China.

I am indebted to Prof Andrea Schaefer of Karlsruhe Institute of Technology (Institute of Functional Interfaces, Membrane Technology group) who hosted me in her laboratories for 6 months. Your teachings on the importance of devising a concept note prior to starting experimental work remain instilled in me.

I am grateful to Prof Rong Wang of Nanyang Technological University (Singapore) for the enlightening discussions that we had on the manufacture of thin film composite membranes during the AMSIC-2 conference in Johannesburg and for sharing tips on what makes a successful academic scholar.

I would like to render my warmest thanks to Prof Sabelo Mhlanga who has become my cheerleader on the side-lines and for being genuinely interested in my professional career.

I wish to thank Prof Neil Coville of the University of the Witwatersrand (Wits) for allowing me access to his laboratories for carbon nanotube synthesis and I wish to thank Dr Ranganathan Kamalakannan for assisting me during the synthesis process. To Dr Manoko Maubane at Wits, I am thankful for your assistance with TEM analysis of the membrane

samples. To Dr Keneiloe Sikhwivhilu at Mintek, thank you for your assistance with TOC measurements and for creating other opportunities for my career development.

I am indebted to Mr Saood Qaseem and his family for making sure that I settle well at TJPU and for being readily available to provide various forms of assistance when I needed them. To Mr Wang Zhen also at TJPU, thank for your time and assistance with antimicrobial testing of my membrane samples. I thank my new friends which I made at TJPU in China: Zhang Lei, Mengyang Hu, Li Jian and Zhou Xue.

I have received generous support from Mr Darlington Ikegwuoha and Ms Zakithi Dube of UNISA civil engineering department who provided alternative working laboratory space. Thank you for creating a comfortable and friendly working environment. I thank Mr Senzo Mdletshe at the UNISA Department of chemistry, for his kind assistance and getting permission for me to utilise various resources in the Chemistry department.

My deepest appreciation goes to the technical and administrative staff of the Nanotechnology and Water Sustainability (NanoWS) Research Unit, in particular, Dr Hlengilizwe Nyoni, Ms Gcinaphi Shabalala and Ms Kamogelo Musi, for their support.

I gratefully acknowledged the funding agencies (UNISA, DAAD-NRF and TATA Africa) for funding my studies.

I thank all the members of the Membrane Technology Research Group at UNISA who have contributed immensely to my personal and professional growth. The group has been a source of friendship, laughter, advice and partnerships.

Dr Machawe Motsa, our discussions on phase-inversion membranes have been particularly insightful and I appreciate you for being a helpful hand at all times. To Dr Lindani Mdlalose at CSIR, thank you for being my confidant and for being readily available to provide assistance with some instrumental techniques. To my friends, Sindisiwe Chauke, Dipuo Sethaba, Sania Kadanyo, Phakeme Sibiyi, Naledi Raleie, Diseko Boikanyo, Kholiswa Yokwana, Lebea Nthunya, Sithembela Zikalala and Nqobile Ndlangamandla - thank you all for being there for me at all times throughout the journey and for providing emotional support.

I am sincerely grateful to my sons, Thendo and Mukhethwa Madzivha, for being patient and understanding that I sometimes needed to spend extended time away from home. May you grow to be wise and respectful men. To my dear partner, Sydney Madzivha, I am deeply grateful for your continued support of my dreams and for holding the fort while I was away on research visits or attending conferences. Thank you also, for the tough love which helped me greatly in shaping up and completing the thesis.

Finally, I must express my very profound gratitude to all my family members, my greatest support structure and cheerleaders, for providing me with unfailing support and continuous encouragement throughout all my years of study and through the process of researching and writing this thesis. I truly personify the line “*I come as one, but I stand as ten thousand*” from Maya Angelou’s “our grandmothers” poem, for the sacrifices that you have all made in making sure that I get to realise my dreams and further my studies. May God bless you all abundantly.

## PUBLICATIONS AND PRESENTATIONS

---

Several research publications and conference presentations have emanated from this thesis.

### Publications

1. N.N. Gumbi, T.G. Tshabalala, S.D. Mhlanga, B.B. Mamba, A.I. Schäfer, E.N. Nxumalo, Prospects and State-of-the-Art of Carbon Nanotube Membranes in Desalination Processes, Chapter 8 in **Desalination Sustainability, A Technical, Socioeconomic, and Environmental Approach**, Elsevier, 2017, pp. 305-339.  
<https://doi.org/10.1016/B978-0-12-809791-5.00008-0>
2. N.N. Gumbi, M. Hu, B.B. Mamba, J. Li, E.N. Nxumalo, Macrovoid-free PES/SPSf/O-MWCNT ultrafiltration membranes with improved mechanical strength, antifouling and antibacterial properties, **Journal of Membrane Science**, **566** (2018) 288-300.
3. N.N. Gumbi, B.B. Mamba, J. Li, E.N. Nxumalo, Relating the performance of sulfonated polyamide thin-film composite nanofiltration membrane to structural properties of macrovoid-free polyethersulfone/sulfonated polysulfone/O-MWCNT support membranes, **Desalination**, **474** (2020), 114176.
4. N.N. Gumbi, B.B. Mamba, J. Li, and E.N. Nxumalo, Polyethersulfone/carbon nanotube mixed-matrix membrane for water treatment: Current status and future prospects (Manuscript submitted to **Chemical Engineering Journal**, 2019).

### Conferences and symposium presentations

1. **Nozipho N. Gumbi**, Bhekhe B. Mamba, Edward N. Nxumalo. Energy efficient carbon nanotube membranes for brackish ground water desalination. **Poster presentation**. Savitribai Phule Pune University, AVISHKAR competition, India, December 2015.

2. **Nozipho N. Gumbi**, Edward N. Nxumalo, Bhekie B. Mamba, Andrea I. Schäfer. Synthesis and characterisation of carbon nanotube composite membranes for water treatment. **Poster presentation**. Advanced Membrane Technology, Maryborough Hotel and Spa, Cork, Ireland, 11 – 16 September 2016.
  
3. **Nozipho Gumbi**, Zhenyu Cui, Benqiao He, Bhekie Mamba, Edward Nxumalo, Jianxin Li. A macrovoid-free PES/SPSf/O-MWCNT support membrane with improved mechanical strength, antifouling and performance properties. **Poster presentation**. 11th International Congress on Membranes and Membrane Processes (ICOM2017), San Francisco, CA USA, 29 July – 4 August 2017.
  
4. **Nozipho Gumbi**, Bhekie Mamba, Edward Nxumalo, Jianxin Li. Fabrication of macrovoid-free PES/SPSf/O-MWCNT support membrane with improved mechanical strength, antifouling and performance properties. **Oral presentation**. SACI Young Chemists Symposium, University of Johannesburg, Kingsway Campus, 30 November 2017.
  
5. **Nozipho Gumbi**, Bhekie Mamba, Jianxin Li, Edward Nxumalo. The role of macrovoid-free PES/SPSf/O-MWCNT support membranes in the fabrication of sulfonated TFC NF membranes with high monovalent/bivalent salt selectivity. **Oral presentation**. 2nd African Membrane Society International Congress (AMSIC-2), South Africa, 29 July–2 August 2018.

**Achievements and awards received during the course of the PhD study:**

- 2015 Best poster presentation, 1st Prize, at University of South Africa’s Research and Innovation showcase.
- 2016 Women in science award issued by Department of Science and Technology, South Africa which was accompanied by Tata doctoral scholarship, sponsored by Tata Africa.
- 2016 Deutscher Akademischer Austauschdienst (DAAD) short-term research scholarship recipient.

- 2016 Six-month research visit to Karlsruhe Institute of Technology, Institute of Functional Interfaces.
- 2016 Famelab South Africa 2016 winner; and Top 10 finalist at the Famelab international competition, Cheltenham, London, U.K.
- 2016 Mail&Guardian's 200 Young South Africans list for 2016, in the field of science.
- 2016 Media interviews (Metro FM, UKhozi FM, Ligwalagwala FM, channel Africa, and eNCA).
- 2017 Best presentation by a PhD student, 2<sup>nd</sup> Prize at the South African Chemical Institute (SACI) Young Chemists' Symposium, University of Johannesburg, South Africa.
- 2017 Panellist during the discussions on the role of scientists in society (Science Forum South Africa, CSIR international convention center.
- 2017 Six-month research visit to State key laboratory Tianjin Polytechnic University (TJPU to Karlsruhe Institute of Technology, Institute of Functional interfaces
- 2018 Best presentation by a PhD student, 1st Prize at the 2nd African Membrane Society International Congress (AMSIC-2), UNISA, South Africa.
- 2019 Represented and gave a talk on behalf of young African scholars, under the Young Scientists of the World category, at the International Year of The Periodic Table (IYPT2019) opening ceremony at UNESCO headquarters in Paris, France.

## ABSTRACT

---

This thesis reports on the synthesis and characterisation of various types of oxidised multi-walled carbon nanotubes (O-MWCNTs) modified polymeric membranes. These O-MWCNT modified polymeric membranes were then assessed in terms of their remediation potential, in particular for the removal of estrogenic hormones, dissolved proteins and salts from brackish water sources. The fabricated O-MWCNT-based polyethersulfone (PES) membranes were applied as (i) adsorptive membranes, (ii) molecular-sieving membranes and (iii) as membrane substrates for thin-film composite nanofiltration (NF) membrane preparation.

The research work commences with the preparation of MWCNTs via a facile catalytic chemical vapour deposition method and their chemical oxidation with strong acids in order to introduce hydrophilic carboxylic ( $-\text{COOH}$ ) and hydroxyl ( $-\text{OH}$ ) surface functional group moieties on the MWCNT outer walls. Intrinsically, MWCNTs are chemically inert and tend to form agglomerated nanoclusters (due to van der Waals interaction forces), which induce further difficulties in their homogenous dispersion in polar solvents (such as N-methyl-2-pyrrolidone and dimethylacetamide) employed to dissolve the polymers in the study. The introduction of these oxygen-containing moieties was therefore necessary to aid the dispersion of MWCNTs in organic solvents and for their enhanced interaction with PES and sulfonated polysulfone (SPSf).

The PES/O-MWCNT ultrafiltration (UF) membranes were produced via a non-solvent induced phase separation (NIPS) method and employed in the adsorptive removal of natural hormone estrone (E1). The PES/O-MWCNT UF membranes thus prepared were

characterised using SEM, AFM, zeta potential measurements and MWCO experiments. It was found that the adsorption of E1 initially increased with an increase in O-MWCNT content followed by a constant decline on further increments. Moreover, the inclusion of O-MWCNTs (0.5 wt.%) in the PES membrane matrix resulted in an increase in the maximum adsorption capacity for E1 compared to pristine PES membrane, *i.e.*, 31.25 mg/g adsorption capacity was achieved for PES/O-MWCNT compared to 23.81 mg/g for bare PES UF membrane. Based on the correlation coefficients, the Freundlich isotherm provided a better fit for the adsorption data and the adsorption kinetics followed the pseudo-second order kinetic model. Interestingly, after five regeneration cycles, the PES/O-MWCNT membranes were found to maintain similar adsorption efficiencies. The PES/O-MWCNT membranes thus prepared, present a viable approach for the removal of natural hormones and other endocrine disruptors present in water systems compared to the use of common adsorbents such as activated carbon, which end up generating large amounts of chemical sludge that require disposal in the environment.

The third part of the study focused on the controlled formation of macrovoid-free polyethersulfone/sulfonated polysulfone (PES/SPSf) UF membranes with high water permeabilities, mechanical strength and antifouling properties, in the presence of O-MWCNTs. To date, the majority of polymeric nanocomposite membranes modified with O-MWCNTs as nanofillers, generally have finger-like structures and macrovoids in the membrane sublayer. While the presence of finger-like structures is favoured for the reduction in mass flow resistance, their presence induces mechanically weak points in the membrane and reduces the nanocomposite membranes' mechanical strength properties and long-term performance stability. As such macrovoid-free PES/SPSf/O-MWCNT membranes were fabricated via the NIPS techniques, using H<sub>2</sub>O and polyethylene glycol (PEG 20 kDa) as

non-solvent additives. The SEM cross-sectional images showed that a fully sponge-like morphology of the PES/SPSf membrane can be achieved in the presence of different loadings of O-MWCNTs. This was attributable to the formation of stronger hydrogen bonds between the SPSf polymer and non-solvent additives *i.e.*, H<sub>2</sub>O, PEG 20kDa and O-MWCNTs. The combination of the macrovoid-free morphology and homogenous distribution of high mechanical strength O-MWCNTs in the membrane matrix provided excellent mechanical strength enhancements for PES/SPSf/O-MWCNT membranes. Additionally, pure water flux initially increased from 598 L/m<sup>2</sup>.h to 713 L/m<sup>2</sup>.h followed by a decline to 578 L/m<sup>2</sup>.h upon further increments in O-MWCNT contents, due to agglomeration of O-MWCNTs at higher loadings. The fabricated PES/SPSf/O-MWCNT membranes also displayed superior antifouling properties (FRR > 90%) and antibacterial properties (99% bacterial killing ratio) against *E. coli* bacteria. The fabricated support fabric-free PES/SPSf/O-MWCNT UF membranes with macrovoid-free sublayer morphologies displayed attractive features for use as UF membranes in the pre-treatment stages of water treatment and as support substrates for the preparation of TFC membranes.

In general, sponge-like and macrovoid-free membrane structures are regarded as unfit for use as support membranes for TFC membrane preparation since they increase the membrane's resistance to water flow, thereby reducing the overall TFC membrane permeability. This assumption has largely been based on sponge-like and macrovoid-free membranes structures achieved through the use of extremely high polymer concentrations, particularly using polysulfone (PSf) polymer. Hence, the sponge-like structures formed are very dense and less porous. Nevertheless, the macrovoid-free PES/SPSf/O-MWCNT membranes produced in this study, consisted of open cellular network microstructures within the membrane sublayer, which could be visualised at higher SEM magnifications.

This part of the work therefore investigated the role of hydrophilic, macrovoid-free PES/SPSf and PES/SPSf/O-MWCNT as support membranes on the performance of TFC NF membranes. The TFC NF membranes were prepared via an efficient interfacial polymerization reaction between piperazine (PIP) and trimesoyl chloride (TMC). The deposition of the polyamide thin-film layer was confirmed by ATR-FTIR, SEM, AFM, contact angle and zeta potential measurements. Membrane performance results showed that TFC NF membranes fabricated on PES/SPSf/O-MWCNT support membranes displayed a 35% improvement in pure water flux with comparable salt rejections from those prepared on bare PES/SPSf support membranes. Salt rejection followed the order of  $\text{Na}_2\text{SO}_4 > \text{MgSO}_4 > \text{NaCl}$ , which is typical for negatively charged NF membranes. It was established that the presence of hydrophilic O-MWCNTs in the support membrane allowed for the formation of a thin polyamide layer on the top surface of the support membrane, which gave rise to enhanced water permeability of the TFC NF membrane and the possibility of polyamide rejection layer within the support membrane pore channels. To further improve the performance of the TFC NF membranes, in particular, the monovalent/bivalent salt selectivity, a mixture of PIP and 2,4-diaminobenzene sulfonic acid (2,4-DABSA) at different weight ratios was prepared in the aqueous solution and reacted with TMC in the organic phase solution. It was found that the addition of low monomer weight ratio of 2,4-DABSA in the amine mixture, lead to the generation of a sulfonated TFC NF membrane with superior membrane performance in terms of pure water permeability ( $30.2 \text{ L/m}^2\cdot\text{h}$ ), monovalent/bivalent salt selectivity ( $\alpha_{\text{NaCl}/\text{Na}_2\text{SO}_4} = 25.0$ ) at low operating pressures (3 bar) and salt concentrations in the range of brackish waters. This was attributable to the combined presence of sulfonic acid groups on the membrane surface and the formation of the thin polyamide layer. Moreover, sulfonated TFC NF membranes exhibited good antifouling properties against bovine serum albumin (BSA), with FRR of 96.4% after three

cycles of fouling and cleaning, with a fairly stable membrane performance over a 10-day period of pure water flux and Na<sub>2</sub>SO<sub>4</sub> rejection testing. Indeed, the use of a macrovoid-free PES/SPSf/O-MWCNT support membrane did not only provide the mechanical strength for the deposition of TFC NF membrane, but also their open, cellular network microstructure, combined with high hydrophilicity and large surface pore sizes were beneficial in the reduction of polyamide layer thickness, and subsequently in the enhancement of TFC NF membrane performance.

The study provided insightful information on lesser known aspects of O-MWCNT incorporated polymeric membranes, with regards to membrane structural configurations in relation to the membrane structure-performance relationships. It has been deduced that (i) the right combination of membrane surface characteristics and adsorbate solution chemistry is necessary for an open UF membrane to display reasonable removal efficiencies for low molecular-weight solutes, (ii) the combination of macrovoid-free membrane morphology with good dispersion of O-MWCNTs in the polymer matrix is necessary to realise significant enhancements in the mechanical properties of sulfonated membrane and (iii) formation of a thin sulfonated polyamide layer on top of the hydrophilic PES/SPSf/O-MWCNT support membrane is necessary to achieve high salt selectivity, and allow for the sulfonated TFC NF membrane to be operated at low pressures.

**Key terms:** carbon nanotubes, polyethersulfone, sulfonated polysulfone, polyamide composite membrane, structural morphology, macrovoid-free structure, hydrophilicity, antifouling, mechanical strength, hormones, desalination, monovalent/bivalent salt selectivity

## TABLE OF CONTENTS

---

DECLARATION.....	i
DEDICATION .....	i
ACKNOWLEDGEMENTS .....	ii
PUBLICATIONS AND PRESENTATIONS.....	v
ABSTRACT .....	viii
TABLE OF CONTENTS .....	xiii
LIST OF FIGURES .....	xix
LIST OF TABLES .....	xxv
LIST OF ABBREVIATIONS .....	xxvi
<b>CHAPTER 1 INTRODUCTION.....</b>	<b>1</b>
1.1. Background and Problem statement .....	1
1.2. Justification of the study .....	7
1.3. Aims and objectives.....	9
1.4. Thesis outline.....	11
1.5. References.....	14
<b>CHAPTER 2 PROSPECTS AND STATE-OF-THE-ART OF CARBON NANOTUBE MEMBRANES IN DESALINATION PROCESSES .....</b>	<b>18</b>
2.1. Introduction.....	19
2.2. Types of CNTs used in membrane fabrication .....	24
2.2.1. CNT configurations.....	24
2.2.2. CNT tip functionalisation and alignment .....	26
2.3. Types of CNT composite membranes .....	28
2.4. Fabrication processes for CNT membranes for desalination.....	30
2.5. Solute transport properties of CNT membranes .....	36
2.6. Characterisation tools for CNT-based membranes .....	42
2.6.1. Introduction to techniques used to probe CNT Membranes .....	42
2.6.2. Microscopic Investigation of CNT membranes .....	43
2.6.3. Mechanical strength analysis .....	48
2.6.4. Contact angle analysis .....	49
2.6.5. Atomic force microscopy (AFM) analysis.....	50
2.6.6. Streaming potential and surface charge analysis .....	51
2.6.7. Other characterisation techniques .....	52

2.7. Environmental sustainability of CNT membranes .....	52
2.7.1. Energy demand.....	52
2.7.2. Disposal.....	54
2.7.3. Toxicity of CNT membranes .....	55
2.8. Challenges and future perspectives .....	58
2.9. Conclusions.....	61
2.10. References.....	62

**CHAPTER 3 POLYETHERSULFONE/CARBON NANOTUBE MIXED-MATRIX MEMBRANES FOR WATER TREATMENT: CURRENT STATUS AND FUTURE PROSPECTS ..... 70**

3.1. Introduction.....	70
3.2. Synthesis procedures for preparing PES/MWCNT mixed-matrix membranes	75
3.2.1. Phase-inversion by immersion precipitation.....	76
3.2.1.1. Phase diagrams for predicting the structural properties of membranes...	86
3.2.1.2. PES/MWCNT membrane configurations: Flat-sheet versus hollow fibre .....	88
3.2.2. Interfacial polymerisation .....	90
3.2.3. Spray-assisted layer-by-layer assembly .....	94
3.3. Morphological structures of PES/MWCNT membranes .....	95
3.3.1. Finger-like structures with macrovoids versus sponge-like structure .....	96
3.3.1.1. Evolution of finger-like structure and macrovoids .....	96
3.3.1.2. Mechanisms of macrovoid formation .....	97
3.3.1.3. Formation of sponge-like structures .....	100
3.3.1.3.1. Effect of casting solution thickness on membrane structure .....	103
3.3.1.3.2. Addition of solvent into the coagulation bath .....	104
3.3.1.3.3. Addition of non-solvent additives .....	105
3.3.1.3.4. Coagulation bath temperature.....	107
3.4. Influence of PES/MWCNT cross-sectional structure on membrane performance as measured by permeability and selectivity .....	108
3.5. Modification strategies for PES/MWCNT mixed-matrix membranes .....	110
3.5.1. Functionalisation of MWCNTs prior to inclusion in the PES matrix .....	110
3.5.1.1. Oxidation of MWCNTs to MWCNT-COOH and MWCNT-OH.....	110
3.5.1.2. Amination of MWCNTs to NH <sub>2</sub> -MWCNTs.....	113

3.5.1.3. Polymer-functionalised MWCNTs (by polymer grafting and polymer wrapping) .....	114
3.5.1.4. MWCNT/hybrid nanocomposites as new generation materials for PES modification .....	116
3.5.1.4.5. MWCNT/GO or MWCNT/graphene .....	117
3.5.1.4.6. MWCNT/TiO <sub>2</sub> polymer membranes.....	119
3.5.1.5. Polymer grafting and polymer blending of PES .....	121
3.6. Properties of PES/MWCNT membrane.....	126
3.6.1. Surface roughness .....	126
3.6.2. Surface charge .....	127
3.6.3. Surface hydrophilicity in relation to pure water flux in PES/MWCNT membranes .....	129
3.6.4. Antifouling and antimicrobial properties .....	132
3.6.5. Porosity and pore size .....	135
3.6.6. Mechanical properties .....	138
3.7. PES/MWCNT membrane performance indicators .....	140
3.8. Performance of PES/MWCNT membranes in water treatment applications .	143
3.9. Outlook and future perspectives .....	147
3.10. References.....	152
<b>CHAPTER 4 POLYETHERSULFONE/MULTI-WALLED CARBON NANOTUBE ULTRAFILTRATION (UF) MEMBRANES FOR ADSORPTIVE REMOVAL OF NATURAL HORMONE ESTRONE.....</b>	<b>165</b>
4.1. Introduction.....	165
4.1.1. Techniques for the removal of estrogenic EDCs from water systems .....	165
4.1.2. Theory on membrane separation mechanisms .....	169
4.2. Experimental.....	171
4.2.1. Materials.....	171
4.2.2. Membrane preparation .....	172
4.2.3. Membrane characterization .....	173
4.2.4. Static adsorption experiments .....	176
4.2.5. Regeneration of PES/O-MWCNT membranes .....	179
4.3. Results and discussion .....	180
4.3.1. FTIR analysis of PES/O-MWCNT membranes.....	180

4.3.2. Morphological characterisation of PES/O-MWCNT membranes .....	181
4.3.3. MWCO characterisation of PES/O-MWCNT membranes .....	185
4.3.4. Contact angle and pure water flux measurements of PES/O-MWCNT membranes .....	186
4.3.5. Zeta potential of PES/O-MWCNT membranes .....	189
4.3.6. Removal of natural hormone estrone (E1) .....	191
4.3.6.1. Effect of membrane area and O-MWCNT content on E1 adsorption ...	192
4.3.6.2. Effect of contact time on E1 adsorption .....	197
4.3.6.3. pH dependence of E1 adsorption by PES/O-MWCNT membranes .....	202
4.3.6.4. Regeneration of PES/O-MWCNT membranes .....	204
4.4. Limitations of the study and further work .....	205
4.5. Conclusion .....	206
4.6. References .....	208
<b>CHAPTER 5 MACROVOID-FREE PES/SPSF/O-MWCNT ULTRAFILTRATION MEMBRANES WITH IMPROVED MECHANICAL STRENGTH, ANTIFOULING AND ANTIBACTERIAL PROPERTIES .....</b>	<b>215</b>
5.1. Introduction .....	215
5.2. Experimental .....	219
5.2.1. Materials .....	219
5.2.2. Preparation of O-MWCNTs .....	219
5.2.3. Membrane preparation .....	220
5.2.4. Membrane characterisation .....	221
5.2.5. Membrane performance tests .....	224
5.3. Results and discussion .....	226
5.3.1. Dispersion of O-MWCNTs in PES/SPSf matrix .....	226
5.3.2. Viscosity measurements .....	229
5.3.3. ATR- FTIR analyses of PES/SPSf and PES/SPSf/O-MWCNT membranes .....	232
5.3.4. Morphological studies .....	233
5.3.5. Contact angle and tensile strength measurements .....	239
5.3.6. Performance tests: Pure water flux and BSA rejection .....	242
5.3.7. Antifouling and antibacterial tests .....	247

5.4. Conclusion .....	250
5.5. References.....	252
<b>CHAPTER 6 RELATING THE PERFORMANCE OF SULFONATED THIN-FILM COMPOSITE NANOFILTRATION MEMBRANE WITH STRUCTURAL PROPERTIES OF MACROVOID-FREE PES/SPSF/O-MWCNT SUPPORT MEMBRANES .....</b>	<b>258</b>
6.1. Introduction.....	258
6.2. Experimental.....	263
6.2.1. Materials.....	263
6.2.2. Preparation of thin-film composite nanofiltration (TFC NF) membrane .....	264
6.2.3. Membrane characterization .....	265
6.2.4. Membrane performance tests .....	266
6.3. Results and discussion .....	269
6.3.1. Effect of TMC concentration on TFC NF membrane performance: PES/SPSf versus PES/SPSf/O-MWCNT support membranes .....	269
6.3.2. Effect of interfacial polymerisation reaction time on pure water flux and Na <sub>2</sub> SO <sub>4</sub> rejection .....	273
6.3.3. Effect of monomer weight ratio on membrane separation performance of TFC NF membranes .....	275
6.3.4. ATR- FTIR analyses of TFC NF membranes .....	281
6.3.5. Microstructure analysis .....	283
6.3.6. Contact angle and surface charge measurements.....	288
6.3.7. Antifouling tests and performance stability .....	290
6.4. Conclusion .....	292
6.5. References.....	294
<b>CHAPTER 7 GENERAL CONCLUSIONS AND RECOMMENDATIONS.....</b>	<b>297</b>
7.1. General conclusions.....	297
7.2. Recommendations.....	299
7.3. Reference .....	301
<b>APPENDICES.....</b>	<b>302</b>
Appendix A-Supplementary material .....	302
Appendix B. Supplementary material.....	304

S5.6.1. Synthesis and characterisation of O-MWCNTs using nebulized spray pyrolysis method .....	304
S5.6.2. Characteristic properties of O-MWCNTs .....	305
S5.6.2.1. TEM analysis of MWCNT and O-MWCNTs .....	305
S5.6.2.2. FTIR spectroscopy analysis of MWCNTs.....	306
S5.6.2.3. Raman spectroscopy analysis .....	307
S5.6.2.4. TGA analysis .....	308
Appendix C- Supplementary materials.....	325

## LIST OF FIGURES

---

<b><u>Figure</u></b>	<b><u>Description</u></b>	<b><u>Page</u></b>
<b>Figure 2.1</b>	Sketches depicting structures of (a) SWCNT, (b) MWCNT and (c) N-CNT (bamboo-shaped CNT).....	<b>25</b>
<b>Figure 2.2</b>	Schematic representation of the fabrication of VA-CNT membranes by filtration method.....	<b>28</b>
<b>Figure 2.3</b>	Water transport and solute rejection of CNT membranes through (a) vertically aligned CNT membranes and (b) CNT mixed-matrix membranes.....	<b>29</b>
<b>Figure 2.4</b>	Molecular dynamic simulation depicting water configuration or formation of “water wires” in differently sized armchair carbon nanotubes..	<b>38</b>
<b>Figure 2.5</b>	Illustration of slip length at the liquid/solid interface.....	<b>39</b>
<b>Figure 2.6.</b>	SEM cross-sectional images of MWCNT/PSf blend membranes with different loadings of MWCNTs; (A) 0 wt%, (B) 1.0 wt% (C) 2.0 wt%, and (D) 4.0 wt%. Images A1 to D1 are high magnification (20000×) images of A to D, showing the presence of MWCNTs in the surface layer of the membrane.....	<b>46</b>
<b>Figure 2.7</b>	SEM micrographs for (a) CNT film (b) the middle of the CNT film, (c) HR-TEM micrographs for CNTs, and (d) patterned CNTs using a TEM grid prepared using the nanotemplate method.....	<b>47</b>
<b>Figure 2.8</b>	SEM micrographs of VA-CNT membranes (in different forms) prepared using the filtration method.....	<b>48</b>
<b>Figure 2.9</b>	AFM topographic images depicting changes in surface structure of cellulose acetate/polyethylene glycol polymer matrix (PM).....	<b>51</b>
<b>Figure 2.10</b>	Potential performance versus commercial viability of nanotechnology-enabled membrane.....	<b>57</b>
<b>Figure 3.1</b>	Schematic depiction of membrane fouling in UF membranes.....	<b>71</b>
<b>Figure 3.2</b>	Cross-sectional depiction of: (a) an asymmetric structure; and (b) thin-film composite membrane structure.....	<b>76</b>
<b>Figure 3.3</b>	Phase-inversion by immersion precipitation process for preparation of UF membranes.....	<b>77</b>
<b>Figure 3.4</b>	Schematic representation of a ternary phase diagram.....	<b>87</b>
<b>Figure 3.5</b>	Photographic images of O-MWCNT containing polymer composite membranes with different configurations (a) flat-sheet and (b) hollow fiber membrane.....	<b>89</b>
<b>Figure 3.6</b>	Schematic diagram of the interfacial polymerisation method.....	<b>91</b>

<b>Figure 3.7</b> Interfacial polymerisation reaction between TMC and PIP for the formation of the polyamide film.....	<b>91</b>
<b>Figure 3.8</b> Schematic diagram of TFC RO membrane fabricated on PES/fMWCNT substrate.....	<b>93</b>
<b>Figure 3.9</b> Spray-assisted layer-by-layer deposition method used for the preparation of polyelectrolyte multilayer PES/MWCNT membranes..	<b>95</b>
<b>Figure 3.10</b> Phase-inversion phenomena of sPPSU/NMP dope solutions modified with various compositional contents of PEG 400 Da: (A) 0 wt.% (PEG0), (B) 2 wt.% (PEG2), (C) 4 wt.% (PEG4) and (D) 8 wt.% (PEG8) in water. ....	<b>99</b>
<b>Figure 3.11</b> SEM images of the flat-sheet membranes cast from 26% 2.5sPPSU polymer solution with the casting gap height of (A) 100 $\mu\text{m}$ (B) 150 $\mu\text{m}$ and (C) 200 $\mu\text{m}$ ....	<b>104</b>
<b>Figure 3.12</b> Schematic representation for functionalisation of MWCNTs.....	<b>112</b>
<b>Figure 3.13</b> (a) Procedure for amine functionalisation of MWCNTs; and (b) mechanism for amine functionalisation of MWCNTs. ....	<b>114</b>
<b>Figure 3.14</b> Digital photographs showing the appearance of (A) raw MWCNTs and (B) PAA modified MWCNTs in water: (i) 30 min; (ii) 1 day; and (iii) 1 week after ultrasonication. ....	<b>115</b>
<b>Figure 3.15</b> Digital photographs showing the dispersion of MWNTs and MWNT-HPAE in DMF (a and b) and in PVDF casting solutions: (c and e) MWCNT-HPAE dispersion and (d and f) raw MWCNT dispersion.....	<b>116</b>
<b>Figure 3.16</b> TEM image showing the distribution of MWCNT/GnP nanohybrids for a MWCNT:GnP ratio of 9:1.....	<b>118</b>
<b>Figure 3.17</b> Schematic illustration of photocatalytic activity of ZnO coated MWCNTs.	<b>121</b>
<b>Figure 3.18</b> Mixing enthalpies of PES/PSf and PES/SPSf blend systems. ....	<b>124</b>
<b>Figure 3.19</b> DSC thermograms of (a) PES/PSf and (b) PES/SPSf at different weight ratios. ....	<b>125</b>
<b>Figure 3.20</b> Schematic representation of a hydrophilic PES/MWCNT membrane surface. ....	<b>130</b>
<b>Figure 3.21</b> Pure water flux of pristine and modified PES UF membranes at different trans-membrane pressures..	<b>132</b>
<b>Figure 3.22</b> Synergistic antibacterial effect between hybrid SLS-PES membrane and electric field against <i>E. coli</i> . ....	<b>135</b>
<b>Figure 3.23</b> Schematic diagram of membrane porosity versus membrane pore size and their effect on membrane performance indicators. ....	<b>136</b>

<b>Figure 3.24</b> TEM observation of crack nucleation and propagation in MWCNT-polystyrene thin films as induced by thermal stresses.. .....	<b>139</b>
<b>Figure 3.25</b> Experimental set-up of SWCNTs-UF membrane testing unit used by Heo et al .....	<b>146</b>
<b>Figure 3.26</b> Number of research papers published between the years 2010 – 2018 on the subject of PES/MWCNT MMMs for various water treatment applications (Search results obtained upon entering the following keywords on Web of Science and Scopus: “carbon nanotube polyethersulfone composite membranes for water treatment”). ..	<b>148</b>
<b>Figure 4.1</b> Membrane separation mechanisms. ....	<b>170</b>
<b>Figure 4.2</b> FTIR spectra of PES/O-MWCNT membranes.....	<b>181</b>
<b>Figure 4.3</b> SEM surface and cross-sectional images of PES/O-MWCNT membranes: (a) M0, (b) M1, (c) M2 and (d) M3. ....	<b>183</b>
<b>Figure 4.4</b> Molecular weight cut-off profiles of PES/O-MWCNT membranes. ....	<b>186</b>
<b>Figure 4.5</b> Contact angles of PES/O-MWCNT membranes.....	<b>187</b>
<b>Figure 4.6</b> Effect of transmembrane pressure on pure water flux of PES/O-MWCNT membranes.....	<b>189</b>
<b>Figure 4.7</b> Surface zeta potential as a function of electrolyte pH for PES/O-MWCNT membranes.....	<b>191</b>
<b>Figure 4.8</b> E1 adsorption on PES membranes containing various loadings of O-MWCNTs after 72 h contact time as a function of membrane area.. .....	<b>194</b>
<b>Figure 4.10</b> Hydrogen bonding interactions between E1 and PES/O-MWCNT membranes. ....	<b>195</b>
<b>Figure 4.11</b> Comparison of partition coefficients of E1 between the PES/O-MWCNT membranes and the bulk E1 solution.....	<b>196</b>
<b>Figure 4.12</b> Time-dependent E1 removal by O-MWCNTs and by PES membranes containing various loadings of O-MWCNTs.. .....	<b>198</b>
<b>Figure 4.13</b> Isotherm data fitting for adsorption of E1 by PES/O-MWCNT membranes (a) linear regression form of Langmuir isotherm and (b) linear regression form of the logarithmic form of the Freundlich isotherm. ....	<b>200</b>
<b>Figure 4.14</b> Influence of pH on E1 removal by PES/O-MWCNT membranes.....	<b>203</b>
<b>Figure 4.15</b> Regeneration efficiency of PES/O-MWCNT membranes.. .....	<b>205</b>
<b>Figure 5.1</b> Digital photographs of PES/SPSf/O-MWCNT casting solutions (a) taken immediately after preparation, (b) taken after 4 weeks of preparation and (c) photograph showing the physical appearance of PES/SPSf/O-MWCNT membranes. ....	<b>228</b>

<b>Figure 5.2</b> TEM images of (a) O-MWCNTs and (b) microtomed specimen of PES/SPSf/O-MWCNT membrane (M5).....	<b>229</b>
<b>Figure 5.3</b> Effect of temperature on viscosity of PES/SPSf and PES/SPSf/O-MWCNT casting solutions. ....	<b>231</b>
<b>Figure 5.4</b> Hydrogen bonding interaction between SPSf, H <sub>2</sub> O and O-MWCNTs. ....	<b>231</b>
<b>Figure 5.5</b> ATR-FTIR spectra of PES/SPSf and PES/SPSf/O-MWCNT membranes. ....	<b>233</b>
<b>Figure 5.6</b> SEM surface and cross-sectional images of PES/SPSf/O-MWCNT membranes: M0, M1, M2, M3, M4 and M5. ....	<b>236</b>
<b>Figure 5.6</b> continued .....	<b>237</b>
<b>Figure 5.7</b> SEM cross-sectional images of PES/SPSf/O-MWCNT membranes (a) M0-1 and (b) M5-1.....	<b>238</b>
<b>Figure 5.8</b> AFM topographical images and surface roughness values of PES/SPSf/O-MWCNT membranes (a) M0, (b) M1, (c) M2, (d) M3, (e) M4, and (f) M5.....	<b>239</b>
<b>Figure 5.9</b> Water contact angle values of the pristine PES/SPSf membrane and PES/SPSf/O-MWCNT blend membranes.....	<b>240</b>
<b>Figure 5.10</b> Tensile strength and elongation at break of the pristine PES/SPSf membrane and PES/SPSf/O-MWCNT blend membranes. ....	<b>242</b>
<b>Figure 5.11</b> Flux variation of membranes during the pure water filtration and fouling operation with 1g/L BSA solution (stages I, III and V: pure water filtration and II, IV: fouling stage).....	<b>248</b>
<b>Figure 5.12</b> Flux recovery ratios of PES/SPSf/O-MWCNT membranes after the second fouling stage (after stage IV).....	<b>248</b>
<b>Figure 5.13</b> Photographs of agar plates of <i>E. coli</i> suspension treated with PES/SPSf membranes: (a) control (without membrane), (b) M0 and (c) M5. ....	<b>250</b>
<b>Figure 6.1</b> Interfacial polymerisation reaction scheme between PIP, 2,4-DABSA and TMC. ....	<b>263</b>
<b>Figure 6.2</b> Schematic diagram of stirred-cell membrane permeation test unit.....	<b>268</b>
<b>Figure 6.3</b> Effect of TMC concentration on pure water flux of TFC membranes. Experimental conditions: PIP concentration = 2 wt.%, IP reaction time = 30 s. ....	<b>271</b>
<b>Figure 6.4</b> Salt rejection performance of (a) NF_M0 and (b) NF_M1 membranes. Experimental conditions: PIP concentration = 2 wt.%, IP reaction time = 30 s. ....	<b>272</b>
<b>Figure 6.5</b> SEM surface images of NF_M1 membranes prepared from different concentrations of TMC: (a) 0.05 wt.%, (b) 0.1wt.%, (c) 0.2 wt.% and (d) 0.3 wt.%. Experimental conditions: PIP concentration = 2 wt.%, IP reaction time = 30 s. ....	<b>273</b>

<b>Figure 6.6</b> Effect of IP reaction time on pure water flux and salt rejection of NF_M1 membrane. Experimental conditions: PIP concentration = 2 wt.%, TMC concentration = 0.1 wt.%.....	<b>275</b>
<b>Figure 6.7</b> Effect of 2,4-DABSA monomer weight on pure water flux and salt rejection of TFC NF membranes. ....	<b>278</b>
<b>Figure 6.8</b> Pure water flux of TFC NF membranes as a function of operating pressure..	<b>279</b>
<b>Figure 6.9</b> Salt flux of TFC NF membranes prepared from different 2,4-DABSA monomer weight ratios. ....	<b>280</b>
<b>Figure 6.10</b> FTIR spectra of TFC NF membranes prepared from different 2,4-DABSA monomer weight ratios. ....	<b>283</b>
<b>Figure 6.11</b> SEM surface (1) and cross-sectional images (2 and 3) of UF support and TFC NF membranes; (a) M1 support UF membrane, (b) NF_M1_0, (c) NF_M1_25, (d) NF_M1_50 and (e) NF_M1_100.....	<b>285</b>
<b>Figure 6.12</b> AFM topographic images of support UF and TFC NF membranes; (a) M1 support UF membrane, (b) NF_M1_0, (c) NF_M1_25, (d) NF_M1_50 and (e) NF_M1_100. ....	<b>287</b>
<b>Figure 6.13</b> Contact angle values of TFC NF membranes prepared from different 2,4-DABSA monomer weight ratios. ....	<b>289</b>
<b>Figure 6.14</b> Zeta potential of TFC NF membranes prepared with different 2,4-DABSA monomer weight ratios. ....	<b>290</b>
<b>Figure 6.15</b> Normalised flux of TFC NF membranes using BSA as model foulant. ....	<b>291</b>
<b>Figure 6.16</b> Performance stability of NF_M1_25 membrane based on pure water flux and Na <sub>2</sub> SO <sub>4</sub> rejection. ....	<b>292</b>
<b>Figure S4.1</b> Comparison of E1 adsorption on PES/O-MWCNT membranes vs PSf/MWCNT membranes.....	<b>302</b>
<b>Figure S4.2</b> Chemical structures of PSf and PES.....	<b>302</b>
<b>Figure S4.3</b> SEM surface image of M2 after five adsorption-regeneration cycles.....	<b>303</b>
<b>Figure S4.4</b> Regeneration efficiency of M1 using Milli-Q water at 20 °C as a washing solvent.....	<b>303</b>
<b>Figure S5.1</b> Experimental set-up for the nebulized spray pyrolysis method.....	<b>305</b>
<b>Figure S5.2</b> TEM analysis of (a) as-synthesized MWCNTs and (b) O-MWCNTs.....	<b>305</b>
<b>Figure S5.3</b> FTIR spectra of as-synthesized MWCNTs and O-MWCNTs. ....	<b>306</b>
<b>Figure S5.4</b> Raman spectra of as-synthesized MWCNTs and O-MWCNTs. ....	<b>308</b>

<b>Figure S5.5</b> TGA and DTA curves for (a) pristine MWCNTs and (b) functionalized O-MWCNTs .....	<b>309</b>
<b>Figure S5.6</b> SEM cross-sectional image of PES/SPSf membrane with 0.03wt.% O-MWCNT (5s of solvent evaporation) prepare in the absence of PEG20kDa and H <sub>2</sub> O; Pure water flux (17.55 L/m <sup>2</sup> .h at 0.2MPa).....	<b>310</b>
<b>Figure S5.15</b> Pure water flux and BSA rejection of PES/SPSf/O-MWCNT membranes containing various contents of PEG 20kDa (O-MWCNT content = 0.005wt.%, PEG 20kDa content = 16, 18, 20, 22 and 24 wt.%). .....	<b>324</b>
<b>Figure S6.1.</b> MWCO determination of M0 and M1 support membranes used for fabrication of TFC NF membranes. ....	<b>325</b>

## LIST OF TABLES

---

<b><u>Table</u></b>	<b><u>Description</u></b>	<b><u>Page</u></b>
<b>Table 2.1</b>	Different fabrication techniques for CNT membranes. ....	<b>32</b>
<b>Table 2.2</b>	Properties of different membrane processes used in water treatment (adapted from Das et al. [34]. ....	<b>33</b>
<b>Table 2.3</b>	Comparison of VA-CNT membranes and mixed-matrix CNT membranes (adapted from Ahn et al.[3]). ....	<b>36</b>
<b>Table 2.4</b>	Water and ion conductance of nanotubes under 209 MPa Pressure at 250 mM ion concentration (reproduced from [42]). ....	<b>42</b>
<b>Table 3.1</b>	A summary of the structural properties and performance of PES/MWCNT membranes prepared via phase-inversion method for water treatment applications...	<b>82</b>
<b>Table 4.1</b>	Physicochemical properties of estrone (E1) .....	<b>171</b>
<b>Table 4.2</b>	Composition of the casting solutions for the preparation of PES/O-MWCNT membranes.....	<b>172</b>
<b>Table 4.3</b>	Roughness parameters, average surface pore size and thickness of PES/O-MWCNT membranes. ....	<b>185</b>
<b>Table 4.4</b>	Kinetic model parameters for E1 adsorption by PES/O-MWCNT membranes. ....	<b>199</b>
<b>Table 4.5</b>	Langmuir and Freundlich fitted parameters for E1 adsorption by PES/O-MWCNT membranes.....	<b>201</b>
<b>Table 5.1</b>	Composition of casting solutions for PES/SPSf/O-MWCNTs membrane blends. ....	<b>221</b>
<b>Table 5.2</b>	Solubility parameters of different solvents and PES [19, 28].....	<b>227</b>
<b>Table 5.3</b>	Effect of SPSf, H <sub>2</sub> O and O-MWCNT interaction on membrane porosity, mean pore radius and thickness.....	<b>245</b>
<b>Table 5.4</b>	BSA rejection and water permeability values for various UF membranes. ....	<b>246</b>
<b>Table 6.1</b>	PES/SPSf support membranes physicochemical characteristics*. ....	<b>266</b>
<b>Table 6.2</b>	Compositions of aqueous and organic phase solutions for TFC NF membrane preparation.....	<b>266</b>
<b>Table 6.3</b>	Comparison of sulfonated TFC NF membrane performance in terms of pure water permeability and salt selectivity. ....	<b>281</b>
<b>Table 6.4</b>	Antifouling performance parameters of TFC NF membranes.....	<b>292</b>
<b>Table S5.1</b>	Characteristics of MWCNTs.....	<b>306</b>

## LIST OF ABBREVIATIONS

---

AFM	atomic force microscopy
AgNPs	silver nanoparticles
BSA	bovine serum albumin
DMAc	dimethylacetamide
DI H <sub>2</sub> O	deionised water
E1	estrone
EDCs	endocrine disrupting compounds
EMPs	emerging pollutants
FO	forward osmosis
FTIR	Fourier Transform Infrared spectroscopy
GnP	graphene nanoplatelets
HTI	Hydration Technology Innovations
ICP	internal concentration polymerisation
IP	interfacial polymerisation
LMW-DOMs	low molecular-weight dissolved organic matter
MMM(s)	mixed-matrix membrane(s)
MWCNTs	multi-walled carbon nanotubes
NF	nanofiltration
O-MWCNTs	oxidised multi-walled carbon nanotubes
PA	polyamide
PAA	polyacrylic acid
PAAm	polyacrylamide
PAC	polycitric acid
PAC	powdered activated carbon
PANI	polyaniline
PCL	polycaprolactone
PES	polyethersulfone
PEG	polyethylene glycol
PEGMA	poly(ethylene glycol) methyl ether methacrylate
PMTAC	polymethyl triethyl ammonium chloride
PSS	poly(sodium 4-styrenesulfonate)

PSf	polysulfone
PVP	polyvinylpyrrolidone
PWP	pure water permeability
RO	reverse osmosis
SBMA	sulfobetaine methacrylate
SEM	scanning electron microscopy
SLS	sodium lignosulfonate
SPSf	sulfonated polysulfone
SWCNTs	single-walled carbon nanotubes
SWRO	seawater reverse osmosis
TEM	transmission electron microscopy
TFC	thin-film composite membrane
TFN	thin-film nanocomposite membrane
TGA	thermogravimetric analysis
TiO <sub>2</sub>	titanium dioxide
TNRs	titanium dioxide nanoribbons
UF	ultrafiltration
XPS	X-ray photoelectron spectroscopy

# CHAPTER 1

## INTRODUCTION

---

### 1.1. Background and Problem statement

The global water crisis is a two-fold crisis which encompasses water shortage and the deteriorating water quality. Water shortage is associated with water stress due to the increase in population growth and natural disasters such as recurring droughts, while the deteriorating water quality aspect is related to water pollution as a result of human, industrial and agricultural activities. Both poor water quality and water shortage have a negative impact on the quality of life for human beings, especially for the most vulnerable – usually women and children in underdeveloped countries.

As such, there is a growing demand for potable water sources worldwide but more specifically in the sub-Saharan Africa [1]. Moreover, the continual changes in human lifestyles and technological advances made in industrial processes, contributes to the introduction of both traditional and newly emerging contaminants into freshwater sources. Contaminants of emerging concern (CECs) are either naturally occurring (or synthetic) chemicals and microorganisms which are generally not monitored in the environment but have the capability to cause known or suspected human health effects [2]. The CECs originate from various sources which include among others, the use of agrochemicals such as organochlorine pesticides, brominated flame retardants, endocrine disrupting chemicals (EDCs), antimicrobial growth inhibitors, pharmaceutical and personal health care products [3, 4]. The CECs can find their way into surface water sources through agricultural run-off, wastewater treatment plant, effluents and negligent waste disposal in the environment

which can result in leaching of these compounds into both groundwater and surface water sources [5].

In particular, EDCs have emerged as a serious health concern as a result of their interfering with the normal functioning of the endocrine systems of humans and animals, and therefore affect animal and human reproduction and development in the long term [6]. In UK alone, several cases of abnormalities and feminisation in reproductive systems of male fish species related to the presence of EDCs in rivers have been reported [7-9]. In addition, a number of studies have already identified the presence of EDCs in South African waters and wastewater sources [10-13], which makes it imperative to identify potential methods for their removal. One notorious class of EDCs is steroid hormones which can be further categorized into natural and synthetic estrogens. Examples of steroid hormones include estrone (E1), 17- $\beta$ -estradiol (E2), estriol (E3), 17 $\alpha$ -ethinylestradiol (EE2), mestranol (*mes*), testosterone (*tes*) and progesterone (*pro*) [14]. Natural hormones E1, E2 and E3 are responsible for maintaining the health of reproductive tissues, skin, breasts and brain cells in females, whereas synthetic hormones EE2, *mes* and *pro* are used as contraceptives [15]. Steroid hormones are excreted by humans in urine in a conjugated and inactive form, but become reactivated by the bacteria present in water sources [16]. While they occur at relatively low concentrations (ng/L range) in water sources, the endocrine-disrupting potency of steroid hormones is several orders of magnitude higher than that of organic micropollutants such as pesticides and alkyl phenols [17]. This fact validates further the need to seek alternative means by which hormones can be removed from water sources. The natural hormone E1, is the breakdown product of E2 and EE2 in wastewaters and is therefore a suitable indicator for the

presence of estrogenic EDCs. Therefore, it was chosen in the present study for adsorption by polymeric membranes.

Several measures to improve water quality and relieve strain on the limited water supply have been introduced including the implementation of stringent legislations for permissible levels of pollutants in water, water harvesting, and the repair of leakages in the piping systems to promote efficient distribution of water [18]. However, these measures are only able to improve the quality and use of existing water resources to a certain extent and do not lead to an increase in water supplies. The only methods that are capable of increasing water supply to beyond that which is currently available are water reuse and desalination [19]. As such, wastewater treatment industries treat and recycle the already used inadequate water and redistribute it for human consumption and for irrigation purposes. On the other hand, desalination of saline waters (seawater and brackish water) using reverse osmosis (RO) membrane technologies have gained popularity over the years as a means of providing freshwater [20, 21].

Reverse osmosis membranes are preferable for desalination processes due to their intrinsically small pore sizes (0.3 – 0.6 nm) [10], which allows for effective removal of the  $\text{Na}^+$  (0.716 nm) and  $\text{Cl}^-$  (0.664 nm) ions while enabling the permeation of pure water molecules by solution-diffusion mechanism. Nonetheless, full adaptation of membrane-based RO technologies in water desalination processes is hindered by their high energy costs as a consequence of extremely high operating pressures necessary to filter saline feed waters through the membrane to obtain pure water on the permeate side, and in the case of seawater desalination, the incurred cost of pumping water from the sea to the desalination plant [18]. Although major technological advances have

been made in recent years in the production of RO membranes with reduced energy consumption for desalination processes (from 8.0 kWh/m<sup>3</sup> to 3.4 kWh/m<sup>3</sup>), this energy consumption is still far greater than the theoretical minimum energy of 1.06 kWh/m<sup>3</sup> required for desalination of seawater with a total dissolved solids (TDS) concentration of 35 000 mg/L, at a recovery rate of 50% [19, 22]. However, the energy requirement for RO membranes is still far better than that of thermal-based desalination processes. Seawater desalination is more beneficial for providing freshwater for coastal areas, while the desalination of brackish waters with a salinity of between that of seawater and freshwater, presents a viable option for alternative water supply for inland regions [23]. In both cases, the discharge of brine generated from the desalination process back into the environment remains a major hindrance towards implementation of these processes, as it poses a major threat to the ecosystem and species in the water. However, several disposal options for waste brines have been proposed, which include deep well injection, solar evaporation in shallow evaporation ponds to produce solid salts, and irrigation of plants with high salinity tolerance [24-26].

Nanofiltration (NF) membranes have been used to treat different kinds of waters including groundwater, surface water, and wastewater. NF membranes also display attractive features to be used as pretreatment membranes during the desalination processes [27]. The use of NF membranes as pretreatment membranes for RO desalination processes in particular, is prompted by the fact that they are capable of removing turbidity, microorganisms, hardness, and a significant fraction of dissolved salts [28, 29]. With regards to the removal of dissolved salts, NF membranes are capable of near-complete removal of multivalent salts and reduction of monovalent salts by about 10 – 50%, depending on the type of NF membrane used [30]. The effectiveness in the removal of

dissolved salts by NF membranes results in the reduction of feed salt concentrations, thereby reducing the osmotic pressure and lowering the operating pressure (and energy costs) for the RO membrane desalination process. Nonetheless, the susceptibility of NF membranes to fouling limits their effective use.

Membrane fouling is a major hurdle that limits the large-scale implementation of polymeric membranes in general, in water treatment applications. Most of the commercial polymeric membranes manufactured to date have satisfactory permeation and rejection properties, but their antifouling properties are inferior [31]. Fouling refers to the accumulation of organic, inorganic particulate and microbiological matter on the surface of a membrane or within the membrane pores [32]. Consequently, severe membrane fouling causes partial obstruction inside the pores, resulting in an increase in permeation resistance, which necessitates chemical cleaning using harsh chemicals to reverse fouling and restore membrane performance which in turn, leads to the deterioration of the membrane materials and a subsequent reduction in the membrane's lifespan [33]. Therefore, technological advances are needed to develop and produce membranes with fouling-resistant surfaces for prolonged use. Polymer-based membranes can be made to be highly selective and resistant to fouling through several surface modification techniques including polymer grafting and coating, polymer blending and through the incorporation of functional nanomaterials [22]. Conversely, most of the membrane surface modification strategies lead to the generation of highly permeable membranes which end up being subject to the permeability-selectivity trade-off, to the point of membrane separation becoming economically unviable.

In particular, the integration of nano-enabled materials into membrane-based technologies holds promise for the development of advanced nanocomposite membranes with superior properties; for possible application in sea and brackish water desalination [21]. Extensive research efforts has been done on the incorporation of different types of carbon nanotube (CNT) incorporated polymeric membranes for application in water remediation [33-39]. These CNT-based membranes take advantage of the infinitesimally small tube diameters and tubular structures of CNTs for enhancement of membranes' selectivity and water fluxes [40, 41]. Moreover, CNTs are well known for their highly adsorptive properties, atomically smooth inner walls, antimicrobial and self-cleaning properties[42], properties that can be instrumental in combating membrane fouling.

The atomically smooth inner walls of CNTs have been found particularly attractive for use in well-aligned carbon nanotube membranes fabrication for desalination processes [43]. This is due to the belief and understanding that the energy required to separate pure water molecules from a saline feed solution would be reduced as a result of high water fluxes through the CNT inner walls [20]. However, it has been demonstrated in several studies that the energy consumption of the desalination process is determined by the need to bring feed saline solution to a pressure that is equal to the osmotic pressure of the concentrate [44, 45]. As such, membrane permeability cannot reduce the applied pressure to be below the osmotic pressure of the concentrate. Whilst CNT-based membranes may not directly influence the energy efficiency of the desalination processes, they can significantly improve the selectivity of the membranes based on their “molecular sieving” or “molecular gating” separation mechanism rather than the conventional solution-diffusion mechanism [46, 47]. The molecular sieving mechanism of CNT membranes overcomes the selectivity-permeability trade-off that current polymeric membranes are prone to. This therefore

means that CNT membranes are able to filter out total dissolved solids (typically various salt compounds and minerals) from sea or brackish water sources while maintaining a high throughput rate [43]. Moreover, the multifaceted nature of CNT membranes enables for ample opportunities for use in water purification and treatment applications to improve the water quality to acceptable standards.

## **1.2. Justification of the study**

Nanostructured carbons alias nanocarbons such as graphene, carbon nanotubes (CNTs) and other shaped carbon nanomaterials that can be easily functionalised with oxygen-containing moieties, have the potential to mitigate the selectivity-permeability trade-off that is well-known in polymeric membranes, while reducing membrane fouling propensity to a large extent. In addition, CNT-incorporated membranes can contribute towards reducing the capital outlay for desalination plants and operating costs necessary to run the desalination process, due to the small membrane area required to achieve maximum flux. In the same light, the use of CNTs in membrane modification for large-scale applications is perceived as economically unfavourable due to the high manufacturing costs of CNTs with additional costs for their pre-treatment prior to their inclusion in polymer matrices [21]. These factors are envisaged to impose significant costs towards the overall desalination process, unless the initial capital cost can be offset by the savings from the enhanced membrane permeabilities and salt selectivity. However, as the number of industrial-scale facilities for low-cost, bulk production of carbon nanotubes continues to grow, the price of carbon nanotubes is expected to further decrease in the near future [48].

Over the years, a great deal of work has been carried out in the field of CNT mixed-matrix nanocomposite membranes as highlighted in subsequent chapters of this thesis. The studies have demonstrated amongst others, the ability of CNT-incorporated polymeric membranes to display high water fluxes, antifouling and antibiofouling membrane surfaces as a consequence of the enhanced hydrophilic character of the membrane upon incorporation of functional CNTs. Nonetheless, there have been conflicting findings with regards to reinforcing abilities of CNTs in polymer matrices. In this sense, some studies have reported on remarkable enhancement in mechanical strength properties of the mixed-matrix membrane upon inclusion of CNTs [39, 49, 50], while an opposite trend has been reported in others, particularly due to poor dispersion and lack of interfacial bonding between the CNTs and the polymer matrix [51-53]. Since CNTs are classified as one of the new generation nanomaterials for water reclamation and desalination [54], there is still a growing need for an in-depth probe and understanding of the role of CNTs in polymeric membrane matrices and how the enhancement or deterioration in modified membrane properties eventuates.

In this study, various types of catalytic chemical vapor deposition (CVD) prepared oxidized-multi walled carbon nanotube (O-MWCNT)-containing polymeric membranes were synthesized using facile and established procedures and these O-MWCNT-modified polymeric membranes were then investigated for their effectiveness in the removal of the natural hormone estrone, dissolved proteins and salt concentrations in the range of brackish waters. The study showcases the potentiality of O-MWCNT-modified polymeric membranes to be used as adsorptive membranes, molecular-sieving membranes and as support membrane substrates for the fabrication of polyamide thin-film composite nanofiltration membranes. The primary focus of the study was on

the effect of O-MWCNTs on the membrane microstructure, as it forms the heart from which membrane separation and permeability is regulated. The overall aim of the study was to provide an in-depth understanding of interfacial interactions between the incorporated O-MWCNTs and the polymer matrix, which leads to observed changes and enhancements in modified membrane performance behaviour. The ultimate goal of the study was to develop an understanding of the changes in membrane microstructure in the presence of O-MWCNTs and in the process, develop membranes with promising features for improving the quality of recycled water and brackish waters in order to bridge the widening gap between the increasing demand for water and the limited supply.

### **1.3. Aims and objectives**

This thesis aims to investigate the role of O-MWCNTs in regulating the microstructure of polymeric membranes and its effects on the removal of steroid hormones and soluble proteins and to prepare high flux thin-film composite nanofiltration (TFC NF) membranes with high monovalent/bivalent salt selectivity for low-pressure brackish water desalination.

#### **The study seeks to answer the following research questions:**

- Can O-MWCNT-containing ultrafiltration (UF) polymeric membranes be used for adsorptive removal of low molecular-weight steroid hormones?
- Does the incorporation of functional O-MWCNTs lead to the enhancement in pure water flux and other surface membrane properties as a consequence of increased membrane hydrophilicity?

- Which factor(s) govern the enhancement of mechanical properties of mixed-matrix polymeric membranes containing O-MWCNTs?
- Besides providing mechanical support, which other roles do O-MWCNTs play in the support membrane layer during the deposition of the polyamide layer for the fabrication of TFC NF membranes?
- Can a TFC NF membrane with high permeability and monovalent/bivalent salt selectivity than that reported in the literature be efficiently prepared?

**The research study objectives were as follows:**

- I. To synthesise and characterise O-MWCNTs via an efficient catalytic chemical vapor deposition (CCVD) method and incorporate them into polymeric membrane matrices via a non-solvent induced phase separation (NIPS) method.
- II. To demonstrate proof of concept for the inclusion of O-MWCNTs into polymeric membrane matrices for the removal of steroid hormones using the natural hormone estrone as a model.
- III. To model the steroid hormone adsorption process using kinetic and isotherm models, and to investigate the recyclability of O-MWCNT-modified polymeric membranes.
- IV. To control the formation of macrovoid-free polymeric UF membranes with high water permeability, mechanical strength and antifouling properties in the presence of hydrophilic O-MWCNTs.
- V. To compare the performance of macrovoid-free substrates (one containing O-MWCNTs and the other without) as support layers for TFC NF membranes.

VI. To evaluate the effectiveness of a mixed diamine monomer aqueous phase solution for fabrication of high performance (high flux and monovalent/bivalent salt selectivity) TFC NF membrane for low-pressure application.

#### **1.4. Thesis outline**

With the exception of Chapter 1, each chapter opens up with a separate introductory section that is relevant to the theme of the chapter. If similarities in the methodologies or characterisation data exist, a relevant section in the respective chapter is cross-referenced accordingly.

**Chapter 1** introduces the purpose of the study by highlighting pertinent issues with regards to the worldwide water crisis. The justification, aims and objectives of the study are also discussed in detail.

**Chapter 2** presents an overview of the manufacture, physicochemical properties, and effective application of carbon nanotube (CNT) membranes in desalination technologies. Moreover, an assessment on the sustainability of CNT membranes in desalination systems is made from a social, technological and commercial perspective. This chapter has been published as *Chapter 8 in a book entitled Hassan Arafat (Ed.), Desalination Sustainability: A Technical, Socioeconomic, and Environmental Approach, Elsevier, 2017, pp. 305-339.*

**Chapter 3** provides a detailed literature review on the work carried out to-date on polyethersulfone/carbon nanotube (PES/MWCNT) mixed-matrix membranes, with particular emphasis on their synthesis and modification methods, the different morphological structures

displayed by the membranes and their influence on the resultant membrane performance, surface and chemical properties as well as their application in water and wastewater treatment.

**Chapter 4** reports on the adsorptive removal of low molecular-weight hormone estrone by large pore size polyethersulfone/multi-walled carbon nanotube (PES/MWCNT) ultrafiltration (UF) membranes. The effect of the incorporation of O-MWCNTs on the adsorption capacity of the PES membranes is evaluated.

**Chapter 5** describes the controlled formation of macrovoid-free polymeric membrane substrates with high water permeability, mechanical strength, antifouling and antibiofouling properties, in the presence of hydrophilic O-MWCNTs. The chapter has been published in the *Journal of Membrane Science*, 566, (2018) 288-300.

In **Chapter 6**, a relation between sulfonated thin-film composite nanofiltration membrane performances and the structural properties of macrovoid-free polymeric support membranes is made. The use of mixed-diamine monomers for the fabrication of TFC NF is also investigated. Contrary to popular belief, it is demonstrated that sponge-like and macrovoid-free support membranes are able to generate TFC NF membranes with high-water permeability and high monovalent/bivalent salt selectivity. The chapter has been published in *Desalination*, 474, (2020) 114176.

**Chapter 7** presents overall conclusions and recommendations for future work. Perspectives on the future direction of research involving the use of MWCNTs for polymer membrane modification and their use in water treatment applications are also given.

**Appendices** section contains supplementary material and data to support findings from selected chapters.

## 1.5. References

- [1] M.A. Montgomery, J. Bartram, M. Elimelech, Increasing functional sustainability of water and sanitation supplies in rural sub-Saharan Africa, *Environmental Engineering Science*, 26 (2009) 1017-1023.
- [2] S. Kim, K.H. Chu, Y.A. Al-Hamadani, C.M. Park, M. Jang, D.-H. Kim, M. Yu, J. Heo, Y. Yoon, Removal of contaminants of emerging concern by membranes in water and wastewater: a review, *Chemical Engineering Journal*, 335 (2018) 896-914.
- [3] D. Lapworth, N. Baran, M. Stuart, R. Ward, Emerging organic contaminants in groundwater: a review of sources, fate and occurrence, *Environmental Pollution*, 163 (2012) 287-303.
- [4] J. Sorensen, D. Lapworth, D. Nkhuwa, M. Stuart, D. Gooddy, R. Bell, M. Chirwa, J. Kabika, M. Liemisa, M. Chibesa, Emerging contaminants in urban groundwater sources in Africa, *Water Research*, 72 (2015) 51-63.
- [5] J. Haarhoff, L. Coetzee, A. Ceronio, T. Msagati, B. Mamba, N. Gumbi, T. Nkambule, Status quo report on the state of knowledge on persistent organic pollutants and contaminants of emerging concern. Draft Final Report to the Water Research Commission for WRC Project No. K5/2509, Water Research Commission, Pretoria, South Africa (2015).
- [6] S.N. Kolle, T. Ramirez, H.G. Kamp, R. Buesen, B. Flick, V. Strauss, B. van Ravenzwaay, A testing strategy for the identification of mammalian, systemic endocrine disruptors with particular focus on steroids, *Regulatory Toxicology and Pharmacology*, 63 (2012) 259-278.
- [7] J.P. Sumpter, Endocrine disruptors in the aquatic environment: an overview, *Acta hydrochimica et hydrobiologica*, 33 (2005) 9-16.
- [8] A.P.A. da Silva, C.D.L. de Oliveira, A.M.S. Quirino, F.D.M. da Silva, R. de Aquino Saraiva, J.S. Silva-Cavalcanti, Endocrine Disruptors in Aquatic Environment: Effects and Consequences on the Biodiversity of Fish and Amphibian Species, *Aquatic Science and Technology*, 6 (2018) 35-51.
- [9] A.A. Weber, D.P. Moreira, R.M.C. Melo, Y.M. Ribeiro, N. Bazzoli, E. Rizzo, Environmental exposure to oestrogenic endocrine disruptors mixtures reflecting on gonadal sex steroids and gametogenesis of the neotropical fish *Astyanax rivularis*, *General and Comparative Endocrinology*, (2018).
- [10] N.H. Aneck-Hahn, M. Bornman, C. De Jager, Oestrogenic activity in drinking waters from a rural area in the Waterberg District, Limpopo Province, South Africa, *Water SA*, 35 (2009) 245-251.
- [11] S.I. Mahomed, K. Voyi, N.H. Aneck-Hahn, C. De Jager, Oestrogenicity and chemical target analysis of water from small-sized industries in Pretoria, South Africa, *Water SA*, 34 (2008) 357-364.
- [12] N. Swart, E. Pool, Rapid detection of selected steroid hormones from sewage effluents using an ELISA in the Kuils River water catchment area, South Africa, *Journal of Immunoassay & Immunochemistry*, 28 (2007) 395-408.

- [13] I. Barnhoorn, M. Bornman, G. Pieterse, J. Van Vuren, Histological evidence of intersex in feral sharptooth catfish (*Clarias gariepinus*) from an estrogen-polluted water source in Gauteng, South Africa, *Environmental Toxicology: An International Journal*, 19 (2004) 603-608.
- [14] G.-G. Ying, R.S. Kookana, Y.-J. Ru, Occurrence and fate of hormone steroids in the environment, *Environment International*, 28 (2002) 545-551.
- [15] T. Manickum, W. John, Occurrence, fate and environmental risk assessment of endocrine disrupting compounds at the wastewater treatment works in Pietermaritzburg (South Africa), *Science of the Total Environment*, 468 (2014) 584-597.
- [16] J. Legler, A. Jonas, J. Lahr, A.D. Vethaak, A. Brouwer, A.J. Murk, Biological measurement of estrogenic activity in urine and bile conjugates with the in vitro ER-CALUX reporter gene assay, *Environmental Toxicology and Chemistry*, 21 (2002) 473-479.
- [17] A.M. Soto, C. Sonnenschein, K.L. Chung, M.F. Fernandez, N. Olea, F.O. Serrano, The E-SCREEN assay as a tool to identify estrogens: an update on estrogenic environmental pollutants, *Environmental Health Perspectives*, 103 (1995) 113.
- [18] M.A. Shannon, P.W. Bohn, M. Elimelech, J.G. Georgiadis, B.J. Marinas, A.M. Mayes, Science and technology for water purification in the coming decades, in: *Nanoscience and technology: a collection of reviews from nature Journals*, World Scientific, 2010, pp. 337-346.
- [19] M. Elimelech, W.A. Phillip, The future of seawater desalination: energy, technology, and the environment, *Science*, 333 (2011) 712-717.
- [20] R. Das, M.E. Ali, S.B.A. Hamid, S. Ramakrishna, Z.Z. Chowdhury, Carbon nanotube membranes for water purification: a bright future in water desalination, *Desalination*, 336 (2014) 97-109.
- [21] P. Goh, A. Ismail, B. Ng, Carbon nanotubes for desalination: performance evaluation and current hurdles, *Desalination*, 308 (2013) 2-14.
- [22] Y. Baek, C. Kim, D.K. Seo, T. Kim, J.S. Lee, Y.H. Kim, K.H. Ahn, S.S. Bae, S.C. Lee, J. Lim, High performance and antifouling vertically aligned carbon nanotube membrane for water purification, *Journal of Membrane Science*, 460 (2014) 171-177.
- [23] V.I. Rich, R.M. Maier, Aquatic Environments, in: Ian L. Pepper, Charles P. Gerba, Terry J. Gentry (Eds.), *Environmental Microbiology*, Elsevier, 2014, pp. 111-138.
- [24] C.J. Gabelich, A. Rahardianto, C.R. Northrup, T.I. Yun, Y. Cohen, Process evaluation of intermediate chemical demineralization for water recovery enhancement in production-scale brackish water desalting, *Desalination*, 272 (2011) 36-45.
- [25] L. Katzir, Y. Volkmann, N. Daltrophe, E. Korngold, R. Mesalem, Y. Oren, J. Gilron, WAIV-Wind aided intensified evaporation for brine volume reduction and generating mineral byproducts, *Desalination and Water Treatment*, 13 (2010) 63-73.
- [26] F.L. Jordan, M. Yoklic, K. Morino, P. Brown, R. Seaman, E.P. Glenn, Consumptive water use and stomatal conductance of *Atriplex lentiformis* irrigated with industrial brine in a desert irrigation district, *Agricultural and Forest Meteorology*, 149 (2009) 899-912.

- [27] N. Hilal, H. Al-Zoubi, N. Darwish, A. Mohamma, M.A. Arabi, A comprehensive review of nanofiltration membranes: Treatment, pretreatment, modelling, and atomic force microscopy, *Desalination*, 170 (2004) 281-308.
- [28] J. Kaewsuk, D.Y. Lee, T.S. Lee, G.T. Seo, Effect of ion composition on nanofiltration rejection for desalination pretreatment, *Desalination and Water Treatment*, 43 (2012) 260-266.
- [29] A. Ismail, M. Padaki, N. Hilal, T. Matsuura, W. Lau, Thin film composite membrane—Recent development and future potential, *Desalination*, 356 (2015) 140-148.
- [30] B. Van der Bruggen, C. Vandecasteele, Distillation vs. membrane filtration: overview of process evolutions in seawater desalination, *Desalination*, 143 (2002) 207-218.
- [31] P. Goh, B. Ng, W. Lau, A. Ismail, Inorganic nanomaterials in polymeric ultrafiltration membranes for water treatment, *Separation & Purification Reviews*, 44 (2015) 216-249.
- [32] A. Matin, Z. Khan, S. Zaidi, M. Boyce, Biofouling in reverse osmosis membranes for seawater desalination: phenomena and prevention, *Desalination*, 281 (2011) 1-16.
- [33] E. Celik, L. Liu, H. Choi, Protein fouling behavior of carbon nanotube/polyethersulfone composite membranes during water filtration, *Water Research*, 45 (2011) 5287-5294.
- [34] E. Celik, H. Park, H. Choi, H. Choi, Carbon nanotube blended polyethersulfone membranes for fouling control in water treatment, *Water Research*, 45 (2011) 274-282.
- [35] M. Son, H.-g. Choi, L. Liu, E. Celik, H. Park, H. Choi, Efficacy of carbon nanotube positioning in the polyethersulfone support layer on the performance of thin-film composite membrane for desalination, *Chemical Engineering Journal*, 266 (2015) 376-384.
- [36] M.H.D.A. Farahani, V. Vatanpour, A comprehensive study on the performance and antifouling enhancement of the PVDF mixed-matrix membranes by embedding different nanoparticulates: Clay, functionalised carbon nanotube, SiO<sub>2</sub> and TiO<sub>2</sub>, *Separation and Purification Technology*, 197 (2018) 372-381.
- [37] E. Salehi, S. Madaeni, L. Rajabi, V. Vatanpour, A. Derakhshan, S. Zinadini, S. Ghorabi, H.A. Monfared, Novel chitosan/poly (vinyl) alcohol thin adsorptive membranes modified with amino functionalised multi-walled carbon nanotubes for Cu (II) removal from water: preparation, characterization, adsorption kinetics and thermodynamics, *Separation and Purification Technology*, 89 (2012) 309-319.
- [38] H. Zarrabi, M.E. Yekavalangi, V. Vatanpour, A. Shockravi, M. Safarpour, Improvement in desalination performance of thin film nanocomposite nanofiltration membrane using amine-functionalised multiwalled carbon nanotube, *Desalination*, 394 (2016) 83-90.
- [39] V. Vatanpour, M. Esmaili, M.H.D.A. Farahani, Fouling reduction and retention increment of polyethersulfone nanofiltration membranes embedded by amine-functionalised multi-walled carbon nanotubes, *Journal of Membrane Science*, 466 (2014) 70-81.
- [40] M.S. Mauter, M. Elimelech, Environmental applications of carbon-based nanomaterials, *Environmental Science & Technology*, 42 (2008) 5843-5859.
- [41] M. Majumder, N. Chopra, B.J. Hinds, Effect of tip functionalisation on transport through vertically oriented carbon nanotube membranes, *Journal of the American Chemical Society*, 127 (2005) 9062-9070.

- [42] E.-S. Kim, G. Hwang, M.G. El-Din, Y. Liu, Development of nanosilver and multi-walled carbon nanotubes thin-film nanocomposite membrane for enhanced water treatment, *Journal of Membrane Science*, 394 (2012) 37-48.
- [43] B. Corry, Designing carbon nanotube membranes for efficient water desalination, *The Journal of Physical Chemistry B*, 112 (2008) 1427-1434.
- [44] L. Song, J. Hu, S. Ong, W. Ng, M. Elimelech, M. Wilf, Emergence of thermodynamic restriction and its implications for full-scale reverse osmosis processes, *Desalination*, 155 (2003) 213-228.
- [45] A. Zhu, P.D. Christofides, Y. Cohen, Effect of thermodynamic restriction on energy cost optimization of RO membrane water desalination, *Industrial & Engineering Chemistry Research*, 48 (2008) 6010-6021.
- [46] B.J. Hinds, N. Chopra, T. Rantell, R. Andrews, V. Gavalas, L.G. Bachas, Aligned multiwalled carbon nanotube membranes, *Science*, 303 (2004) 62-65.
- [47] C.L. Cheung, A. Kurtz, H. Park, C.M. Lieber, Diameter-controlled synthesis of carbon nanotubes, *The Journal of Physical Chemistry B*, 106 (2002) 2429-2433.
- [48] K. Gong, F. Du, Z. Xia, M. Durstock, L. Dai, Nitrogen-doped carbon nanotube arrays with high electrocatalytic activity for oxygen reduction, *Science*, 323 (2009) 760-764.
- [49] S. Deng, X. Liu, J. Liao, H. Lin, F. Liu, PEI modified multiwalled carbon nanotube as a novel additive in PAN nanofiber membrane for enhanced removal of heavy metal ions, *Chemical Engineering Journal*, (2019) 122086.
- [50] H.A. Shawky, S.-R. Chae, S. Lin, M.R. Wiesner, Synthesis and characterisation of a carbon nanotube/polymer nanocomposite membrane for water treatment, *Desalination*, 272 (2011) 46-50.
- [51] B. Arash, Q. Wang, V. Varadan, Mechanical properties of carbon nanotube/polymer composites, *Scientific Reports*, 4 (2014) 6479.
- [52] J.N. Coleman, U. Khan, W.J. Blau, Y.K. Gun'ko, Small but strong: a review of the mechanical properties of carbon nanotube-polymer composites, *Carbon*, 44 (2006) 1624-1652.
- [53] S. Maphutha, K. Moothi, M. Meyyappan, S.E. Iyuke, A carbon nanotube-infused polysulfone membrane with polyvinyl alcohol layer for treating oil-containing waste water, *Scientific Reports*, 3 (2013) 1509.
- [54] Y.H. Teow, A.W. Mohammad, New generation nanomaterials for water desalination: a review, *Desalination*, 451 (2019) 2-17.

## CHAPTER 2

# PROSPECTS AND STATE-OF-THE-ART OF CARBON NANOTUBE MEMBRANES IN DESALINATION PROCESSES

---

### Summary of the chapter

This chapter presents an overview of the manufacture, physicochemical properties, and effective application of carbon nanotube (CNT) membranes in desalination technologies. A comprehensive discussion on the current knowledge pertinent to CNT exploitation in desalination is provided. It is demonstrated that considerable efforts have been made in the past decade towards the development of membranes incorporating nanocarbons, in particular CNTs, for desalination processes. Primary attention has been paid to the basic properties of CNT polymer mixed-matrix and vertically aligned CNT membranes. It is shown that solution transport properties and desirable chemical functionalities in CNTs necessitate high water fluxes as well as controllable salt rejection. Subsequently, the merits and challenges associated with these CNT membranes with regard to nanotoxicology and environmental remediation are analysed. Finally, an assessment of the sustainability of CNT membranes in desalination systems is made from a social, technological and commercial perspective.

**Keywords:** desalination, carbon nanotubes, reverse osmosis, SWCNT, MWCNT, VA-CNT<sup>1</sup>

---

<sup>1</sup> N.N. Gumbi, T.G. Tshabalala, S.D. Mhlanga, B.B. Mamba, A.I. Schäfer, E.N. Nxumalo, *Chapter 8 - Prospects and State-of-the-Art of Carbon Nanotube Membranes in Desalination Processes A2* - Arafat, Hassan A, in: *Desalination Sustainability*, Elsevier, 2017, pp. 305-339.

## 2.1. Introduction

Over the years, the world has witnessed a shift toward research efforts aimed at the exploitation of unconventional and untapped water sources such as wastewater, seawater, and brackish groundwater in order to meet the growing global water demand. By undergoing various treatment stages, these untapped water sources can be converted into potable water and are regarded as “new” water sources. Among all of these sources, seawater offers a very attractive alternative source for freshwater since it can potentially provide an abundant and unlimited supply for various human, agricultural, and industrial needs, provided the salt is removed in a sustainable manner.

Desalination technologies are used to convert undesirable and salty seawater into potable and usable water [1]. Seawater desalination using membrane-based processes, particularly reverse osmosis (RO) membranes, are highly favoured over thermally based processes, especially in energy-stressed countries, because of their lower energy consumption [2, 3]. Thermal desalination processes rely on the use of heat because of the need to evaporate water prior to condensation [4]. In contrast, in RO desalination technologies, pressure is applied to force water molecules to permeate through a semi-permeable membrane while preventing the passage of salts. Therefore, seawater desalination using RO membranes remains an energy-efficient reference point and a standard of comparison for newer or evolving desalination technologies [2]. One of the greatest issues existing in both seawater and brackish water desalination using currently available RO membranes is the lack of sustainable, robust, energy-efficient, and cost-effective membranes [5]. Indeed, this is a challenging task that requires innovative solutions with feasible implementations. Before attempting to correct these challenges, it is important to have adequate knowledge and understanding of the minimum amount of energy required to separate pure water from seawater.

For example, the theoretical minimum energy for desalination of seawater at 35 000 mg/L salt concentration and at a typical recovery rate of 50% was 1.06 kWh/m<sup>3</sup> in 2011 [2]. This figure provides a benchmark for comparison with recently crafted technologies and helps guide future efforts aimed at reducing the energy demand for desalination processes [2].

Nanotechnology-enabled or simply nano-enabled membranes are increasingly gaining popularity as promising candidates for desalination applications. These nano-enabled membranes rely on the incorporation of various types of nanomaterials into conventional polymeric membranes used in desalination or other processes such as ultrafiltration. The main aim of using nanomaterials is to overcome the challenges faced when using conventional membranes for water desalination, such as high fouling propensity, trade-off between their selectivity and permeability, as well their high energy consumption during the desalination process [5]. In particular, carbon nanotube (CNT)-incorporated polymeric membranes are one of the most widely studied nano-enabled membranes. Carbon nanotubes consist of single or multiple layers of graphene sheets rolled into a tubular structure and can have diameters ranging from 1 to 2 nm for single-walled CNTs (SWCNTs) or 2–25 nm for multiwalled CNTs (MWCNTs) [6]. They are known to possess a unique combination of structural and physicochemical properties owing to their nanoscale dimensions: high volume-to surface ratio, small inner diameters, antimicrobial properties, frictionless surfaces for rapid fluid flow, and many others [7]. The incorporation of CNTs into polymeric membranes has been shown to result in membranes with (i) improved mechanical and thermal stability, (ii) excellent hydrophilic and antifouling properties, (iii) controllable pore size diameters, and (iv) improved selectivity and permeability [8–10]. Currently, there are different views in the research area involving the use of newly emerging CNT-based membranes in desalination processes. These

diverse views are centred on whether CNT-based membranes, particularly the vertically aligned (VA) CNT membranes, are capable of reducing the energy needs of the desalination processes owing to their ultrahigh water permeabilities [3]. The ultrahigh water permeability of CNT membranes is believed to help reduce the amount of pressure or energy needed to drive pure water molecules across the semi-permeable membrane, whereas the energy consumption of a desalination process driven by the applied operational pressure that must be higher than the osmotic pressure of the concentrate [2]. This factor suggests that regardless of how permeable a membrane may be, the applied pressure cannot be reduced to below the osmotic pressure of the concentrate or, more precisely, the osmotic pressure of the boundary layer forming at the membrane surface. Furthermore, it should be emphasised that operating at high water fluxes generally leads to high membrane fouling; that is, at high fluxes, the effective concentration of the solutes or foulants near the membrane surface increases. Subsequently, the rate of foulant deposition on the membrane surface increases [11], which is a result of the greater permeation drag force that is experienced by the foulant toward the membrane surface [12, 13]. Therefore, the ultrahigh permeability characteristic of CNT membranes could assist in the reduction of capital costs needed to run the desalination process, because of the reduced membrane area that will be required to achieve maximum water flux while rejecting the transportation of salts. It is, however, important to emphasise that flux is not “everything” since there are many other membrane systems that function better when operated at lower fluxes.

The CNT-based membranes may be leveraged in RO membrane material modification to overcome the issue of fouling or biofouling. Biofouling, which is caused by growth of biofilm on the surface of a thin film composite (TFC) membrane, hinders the performance of the membrane,

thus limiting the membranes' prolonged use. Biological foulants such as bacteria, fungi, and algae grow in large quantities on the membrane surface, thereby inhibiting permeation through the membrane surface [14]. On the other hand, the use of strong oxidising agents such chlorine and ozone to remove the adsorbed biofilm may be detrimental to the membrane's structure as they are capable of degrading the polyamide layer on TFC membranes [1, 15]. Another limitation of conventional TFC RO membranes involves the ultimate trade-off between permeability and selectivity; i.e., it is practically impossible to further increase the membrane's selectivity without compromising permeability.

The CNT-based membranes possess antibacterial properties that are beneficial in combating biofouling upon direct contact with microorganisms. However, the antimicrobial mechanism of CNTs is not yet fully understood. Many authors present conflicting and diverse mechanistic models. For example, Vecitis et al. [16] proposed a three-step mechanism for SWCNTs that includes three sequential steps: (i) initial contact between SWCNTs and bacteria; (ii) perturbation of the membrane cell; and (iii) electronic structure-dependent bacterial oxidation. Several reports and reviews have been documented reporting on the use of CNTs in mitigating fouling in TFC RO membranes [17–20]. However, most of these studies were tested only on bench-scale systems. There is therefore still a need for further development and upscaling of CNT-based membrane processes to accurately determine their benefits. Furthermore, membrane scientists argue that biocidal properties alone do not demonstrate that a membrane has a low fouling propensity. For instance, in a staged array membrane configuration, the destroyed microbes may necessitate an additional step for membrane cleaning. The issue of selectivity-permeability trade-off could be avoided in CNT membranes due to the ability of selectively adding functional group moieties at

the CNT pore openings that are capable of rejecting salt ions while maintaining ultrafast water transport inside the nanotubes [21, 22]. Such gate-keeper-controlled chemical interactions are unique for CNT-based membranes, as first demonstrated by Hinds et al. [21]. For example, the addition of biotin functional groups at the CNT opening reduced the  $\text{Ru}(\text{NH}_3)_6^{3+}$  flux by a factor of 5.5, and this was further reduced by a factor of 15 when streptavidin was added to the biotin tether [21]. This result formed the basis for the separation or restriction of ionic flow from a solution containing an analyte of interest, and it can be used as a guiding tool for further control of pore dimensions.

A number of studies on the potentiality of VA-CNT membranes in desalination processes have been based on molecular dynamic (MD) simulations and only very few report on their experimental feasibility. This is particularly so because of the complexities encountered in synthesis procedures for aligned CNT membranes, which are the most promising candidates, rather than mixed-matrix CNT membranes, for desalination based on the findings from simulation studies. These issues are discussed in greater detail later in this chapter.

With such challenges, a great deal of work lies ahead before the full realisation and exploitation of CNT-based membranes for desalination applications can be achieved. This chapter presents an overview of the manufacture, physicochemical properties, and effective application of carbon nanotube (CNT) membranes in desalination technologies. Ultimately, this chapter seeks to summarise the current knowledge pertinent to CNT exploitation in desalination, explain the extent to which the fluid transport properties and chemical functionalities in CNTs necessitate high water fluxes, and describe the controllable salt rejection required for desalination. Factors that influence

the cost of CNT membranes, which ultimately translates to the cost of desalination using CNT membranes, are also discussed. Lastly and perhaps most importantly, the sustainability of CNT membranes as a solution to current desalination problems is evaluated.

## **2.2. Types of CNTs used in membrane fabrication**

### **2.2.1. CNT configurations**

Since their discovery in 1991 by Iijima [23], carbon nanotubes have been widely studied and applied in various disciplines, including in the water treatment field as adsorbent materials or in membrane modification for the removal of a wide range of organic and inorganic pollutants from water and wastewater [24–27]. This interest is due to a unique combination of the structural and physicochemical properties of carbon nanotubes: high volume-to-surface ratio; small inner diameters; antimicrobial properties; frictionless surfaces for rapid fluid flow; and many others [7]. The CNTs are commonly classified as SWCNTs or MWCNTs based on the number of cylindrical graphene sheets organised around the hollow nanotube core (Fig. 2.1). The SWCNTs consist of a single layer of graphene sheet rolled into a tubular structure and have diameters in the range of 1 to 2 nm, whereas MWCNTs consist of multiple layers of graphene sheets with diameter sizes in the range of 2 to 25 nm [6]. Most of the research on CNT-incorporated membranes focuses on MWCNTs and very rarely on SWCNTs, even though these possess the smallest outer diameters. This is because MWCNTs are generally easy to prepare and align using conventional chemical vapour deposition (CVD) methods, and their manufacturing costs are lower than those of SWCNTs. This means that MWCNTs can be produced in the large quantities necessary for industrial-scale applications.

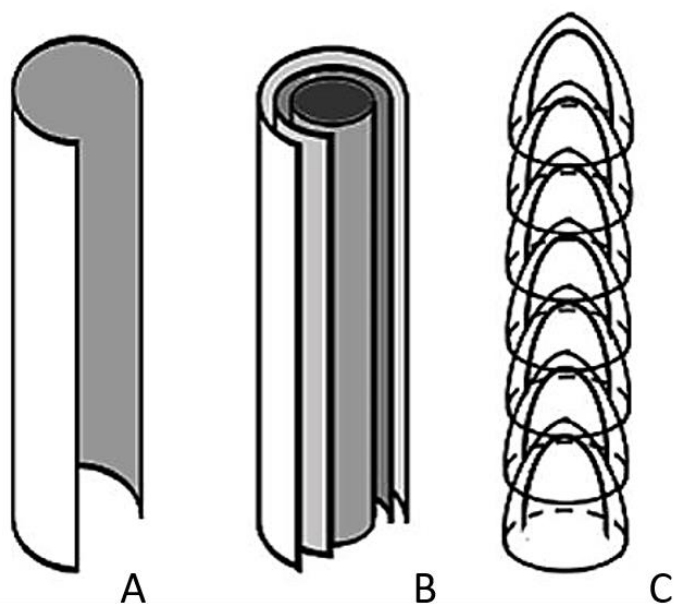


**Figure 2.1** Sketches depicting structures of (a) SWCNT, (b) MWCNT and (c) N-CNT (bamboo-shaped CNT). Reproduced with permission from [28].

Researchers have attempted to use heteroatom-doped CNTs in the form of nitrogen doped carbon nanotubes (N-CNTs) for polymer blend membrane modifications. These N-CNTs are typically produced by either post-synthesis modification of CNTs with a nitrogen-containing compound such as acetonitrile, melamine, and many others or by in situ incorporation of nitrogen during CNT growth [28]. The use of N-CNTs was intended to the compatibility and interaction between CNTs and the polymer material such as (PES) [29]. Performance results of this N-CNT/PES membrane revealed a superior compatibility between the N-CNTs and PES because of the high surface reactivity of N-CNTs compared with pristine CNTs. The differences in the structure of various forms of CNTs commonly used in membrane modification are shown in Fig.2.1. These include CNTs with typical tubular configurations and unique “bamboo-shaped” orientations.

Although the use of SWCNTs in membranes would be ideal for sea and brackish water desalination because of their intriguingly small inner diameters, the challenge of vertically aligning SWCNTs remains a serious hindrance [30, 31]. It is also less expensive to manufacture MWCNTs than their single-walled counterparts; therefore, MWCNTs can be produced in large quantities. However, the inner diameters of most MWCNTs range between 3 and 10 nm [32], which means that they fall short of molecular separation applications where extremely small diameters would be more beneficial in achieving effective and efficient separation of molecular species.

Park et al. [32] sought to substitute commercial UF membranes with VA-CNT membranes in water-purification applications. The authors discovered that the solute rejection of membranes was difficult to increase or control because it was difficult to further reduce the inner diameters of MWCNTs. Notwithstanding the concerns raised earlier, SWCNTs with diameters close to 1 nm were suggested as a probable solution for increasing salt rejection, provided that they undergo surface modifications to further reduce their pore size to just below 0.6 nm. This is because a hydrated Na<sup>+</sup> is about 0.716 nm and Cl<sup>-</sup> 0.664 nm in size.

### **2.2.2. CNT tip functionalisation and alignment**

Functional group moieties can be introduced with ease into the VA-CNT membranes. In particular, the CNT tips can be functionalised to reduce or control their pore size diameters. Park et al. [32] functionalised CNT tips of VA-CNT membranes with methacrylate groups by graft polymerisation to “gate” the transport of solute compounds [33]. The modified membranes showed better water flux and antifouling properties than the commercial UF membranes. In addition, the solute rejection potential was greatly improved vis-à-vis the control VA-CNT membranes. Consequently,

the use of SWCNTs as membranes is of great interest because of their intriguingly small inner diameters (1–2 nm) that can be useful for sea and brackish water desalination. However, as mentioned before, the challenge of aligning SWCNTs vertically remains a serious hindrance in their use as membrane filters. Filtration methods have previously been used successfully to align MWCNTs vertically. Recently, the same approach was adopted for the alignment of SWCNTs. Indeed, when shear forces are applied, they propagate the alignment of CNTs perpendicular to the filter substrate in the direction of flow [31]. Kim et al. [30] prepared VA-CNT membranes using a combination of methods, namely filtration and self-assembly of SWCNTs. In their study, functionalised SWCNTs were dispersed in tetrahydrofuran (THF) (Fig. 2.2, Step 1), and the suspension was filtered through a filtering media such as a polytetrafluoroethylene (PTFE) filter (in Step 2). Their findings showed that the filtration method used facilitated the vertical alignment of CNTs on a porous substrate and that the gas mixture transport through the prepared membranes was much faster than those predicted by Knudsen diffusion. As shown in Fig. 2.2, Step 3, the aligned SWCNT/filter is then spin-coated with a dilute solution of a high-mechanical-strength polymer to seal the structure, while allowing most of the nanotube ends to be slightly exposed above the polymer surface [30]. However, microscopic analyses of these membranes revealed that the SWCNTs are encapsulated with additional graphite layers, which signals that during the fabrication process, they are transformed from SWCNTs into MWCNTs. Alternatively, a polymer suspension containing CNTs can be injected into a mould cavity, a die, or a nano-channel to form a shape of interest. In this way, the CNTs will then change orientation by virtue of the flow that is induced by the shear forces applied [31].

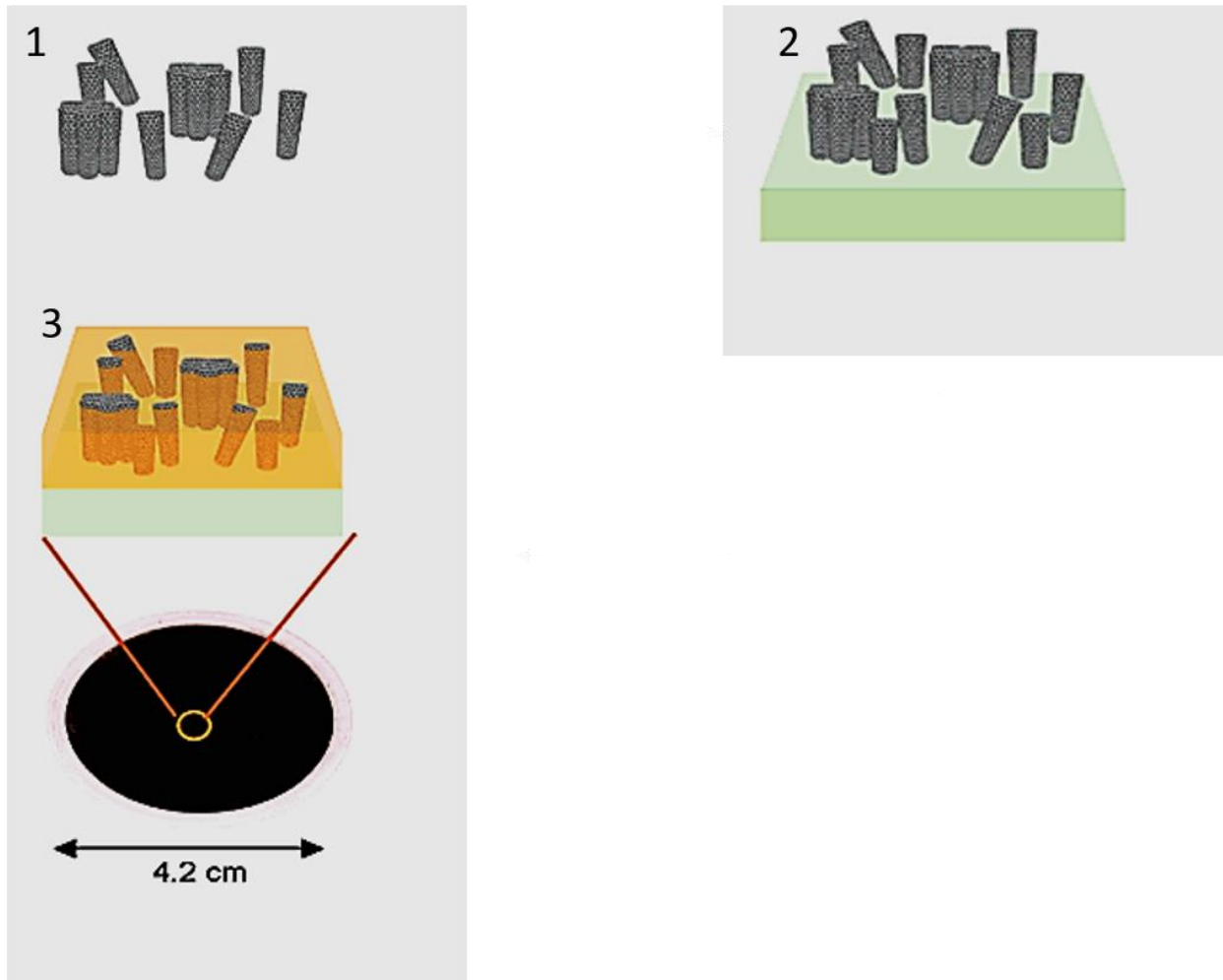


**Figure 2.2** Schematic representation of the fabrication of VA-CNT membranes by filtration method. Reproduced with permission from [30].

### 2.3. Types of CNT composite membranes

The CNT-incorporated membranes are promising tools for the treatment of conventional and emerging contaminants in water as well as for sea and brackish water desalination using RO systems. This option is due to the presence of nanoporous channels that allow for the passage of large volumes of water while rejecting the permeation of “unwanted” species/ions. These CNT-based membranes and in particular the VA-CNT membrane systems have an enormous potential

to improve the selectivity of RO membranes that are commonly used in seawater desalination processes, owing to their dynamic molecular sieving and separation mechanism [18]. There are two common types of CNT-based membranes: CNT mixed-matrix membranes (CNT MMMs), which are typically mixed matrices of CNTs and flexible polymers, and VA-CNT membranes, which could either be CNT “straws” protruding from a nonporous polymer or high-density, aligned CNT arrays. Fig. 2.3 shows the typical differences in the structures, water transport, and solute rejection of the two types of CNT membranes presented in this chapter. In the VA-CNT membranes, the CNTs are arranged in an upright position (perpendicular) to the membrane surface. On the contrary, for mixed composite CNT membranes, CNTs are dispersed in the matrix forming part of the membrane’s top layer, thereby contributing to the hydrophilic and surface properties. In latter sections, the differences of these CNT membrane types and the correlations between the morphological structures and permeation properties thereof will be probed and their water transport and solute rejection capacities investigated. We will also explore their environmental sustainability and commercial availability.

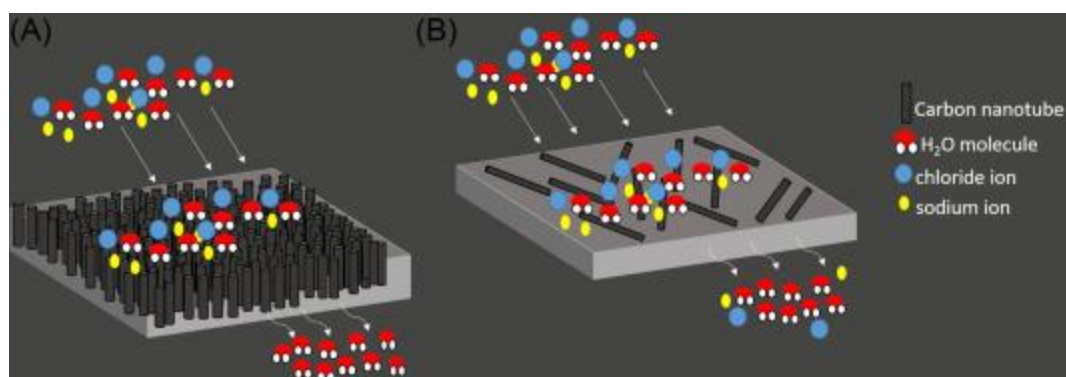


**Figure 2.3** Water transport and solute rejection of CNT membranes through (a) vertically aligned CNT membranes and (b) CNT mixed-matrix membranes.

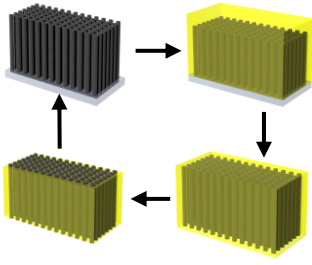
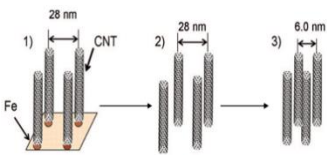
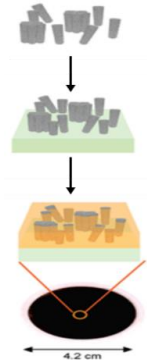
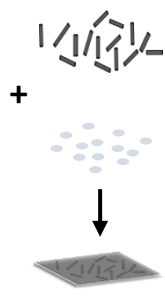
## 2.4. Fabrication processes for CNT membranes for desalination

Table 2.1 depicts the different fabrication techniques for CNT-based membranes normally utilised in a desalination process. Work carried out by different workers fabricating CNT membranes is compared and contrasted with respect to manufacturing process, support material used, CNT alignment or nonalignment, characterisation tools used, and performance properties. For the VA-CNT membranes, the process normally entails synthesis of VA-CNT arrays on a suitable substrate by making use of the conventional CVD method prior to the addition of an impermeable polymer such as polystyrene (as a support). On the other hand, the preparation of CNT MMMs involves the dispersion of CNTs in a solvent and mixing with a suitable polymer prior to casting the solution on a plate typically by a phase-inversion method [35]. Although tremendous progress has been made in the laboratory-scale production of CNT MMMs, experimental work involving the fabrication of VA-CNT membranes is still in its infancy because the production systems are challenging and onerous. These issues are dealt with appropriately in later sections of this chapter.

Several reviews dedicated to CNT-based membranes (MMMs and VA-CNT membranes) and their potentiality in desalination applications have been documented. For example, Das et al. [34] comprehensively reviewed the potential role of CNT membranes in seawater and brackish water desalination. The function of CNTs in the membrane technology arena was analysed by looking at the studies focusing on the fabrication and functionalisation of CNT membranes for desalination purposes and how CNT membranes compare in properties and performance behaviour with conventional membrane processes. These differences are tabulated in Table 2.2 and indicate that unlike CNT MMMs (in which CNTs are mixed in either a MF, UF, or NF membrane matrix), VA-CNT membranes are a unique membrane type because of their outstanding properties, including

among others, ultrafast water transport and self-cleaning properties. CNTs have the ability to be selectively functionalised at their pore openings to enhance their salt rejection capacities and their ability to remove various micropollutants present in water. Thus CNT membranes have been envisaged as potential candidates to replace both RO and NF membranes, because CNT membranes offer minimal energy consumption by lowering the applied pressure to drive desalting of solutions [34]. However, no single method is capable of alleviating the global water pollution problems on its own, which means that the existing water-treatment technologies are not sufficient to provide 100% pure water. Therefore, a combination of methods, including those that have advanced from nanotechnology through the use of carbon nanotube membranes, can be a more viable approach.

**Table 2.1** Different fabrication techniques for CNT membranes.

	<b>Polymer infiltration/ encapsulation</b> (Hinds et al., 2004)[21]	<b>Liquid-induced densification</b> (Yu et al., 2009) [24]	<b>Self-assembly and filtration method</b> (Kim et al., 2007) [30]	<b>Phase-inversion mixed-matrix method</b> (Celik et al., 2011) [8]
<b>CNT membrane type</b>	VA-CNT membrane	VA-CNT membrane	VA-CNT membrane	CNT MMM
<b>Manufacture</b>	<p>CNT arrays grown on a silicon wafer substrate                      Polystyrene infiltrated into the CNT array                      Spin-coating and removal of excess polymer                      HF acid used etch off CNT film from substrate                      Water-plasma oxidation to open CNT tips.</p> 	<p>CNT forest grown by water-assisted CVD method                      Water-etching to detach CNT arrays                      N-hexane introduced into as-grown CNT arrays and dried                      CNTs collapse near to packing into a rigid body upon liquid evaporation.</p> 	<p>SWCNTs prepared by arc discharge method and treated with H<sub>2</sub>SO<sub>4</sub>/HNO<sub>3</sub> acid mixture.                      Amine functionalised SWCNTs dispersed in THF.                      Dope solution filtered through a PTFE membrane filter.</p> 	<p>MWCNTs treated in H<sub>2</sub>SO<sub>4</sub>/HNO<sub>3</sub> acid mixture.                      MWCNTs sonicated and NMP followed by addition of PES                      Dope solution casted on glass plate and immersed in coagulation bath.</p> 
<b>Support</b>	Polystyrene	None	Polytetrafluoroethylene	None
<b>CNT configuration</b>	Vertically aligned	Vertically aligned	Partial alignment	Non-aligned
<b>Characterisation</b>	SEM, HRTEM, porometer and electrochemical measurements	TEM, SEM, N <sub>2</sub> desorption experiments	HRTEM, permeation of gas mixtures	SEM, FTIR, Contact angle goniometer, cross-flow filtration experiments
<b>Performance</b>	<p>The presence of CNTs increased conductivity of the membrane                      Attachment of biotin/streptavidin moiety on the CNT tip allowed for gating or sieving of Ru(NH<sub>3</sub>)<sub>6</sub><sup>3+</sup> ions.</p>	<p>Densely packed SWCNTs were observed from SEM                      N<sub>2</sub> gas diffusion is 2 orders of magnitude higher than predicted by Knudsen and 3-7 orders of magnitude higher than for composite membranes</p>	<p>Rapid gas transport through the CNT membranes that deviates from Knudsen diffusion.</p>	<p>Inclusion of CNTs into the PES membrane increased the membrane roughness, surface hydrophilicity, pure water flux and porosity.</p>

Although tremendous progress has been made in the lab-scale production of CNT MMMs, experimental work involving the fabrication of VA-CNT membranes is still in its infancy because the production systems are challenging and onerous. These issues are dealt with appropriately in later sections of this chapter.

Several reviews dedicated to CNT-based membranes (MMMs and VA-CNT membranes) and their potentiality in desalination applications have been documented. For example, Das et al. [34] comprehensively reviewed the potential role of CNT membranes in seawater and brackish water desalination. The function of CNTs in the membrane technology arena was analyzed by looking at the studies focusing on the fabrication and functionalisation of CNT membranes for desalination purposes and how CNT membranes compare in properties and performance behavior with conventional membrane processes. These differences are tabulated in Table 2.2 and indicate that unlike CNT MMMs (in which CNTs are mixed in either a MF, UF, or NF membrane matrix), VA-CNT membranes are a unique membrane type because of their outstanding properties, including among others, ultrafast water transport and self-cleaning properties.

**Table 2.2** Properties of different membrane processes used in water treatment (adapted from Das et al. [34]).

	MF	UF	NF	RO	VA-CNT	Ref
Pore size (nm)	> 50 – 500	2 – 50	< 2	0.3 – 0.6	0.6 – 10	[20], [34], [37]
Operating Pressure (bar)	0.1 – 2	< 5	3 – 15	29 – 100	0.7 – 2	[31], [39], [40]
Pure water permeability (L/(m <sup>2</sup> .h.bar))	> 1000	10 – 1000	1.5 – 30	0.05 – 15	>1000	[32], [39], [41]
MWCO (Da)	> 300 000	1000 – 1000, 000	100 – 1000	100	100	[32], [42], [43]
Membrane thickness (μm)	50 – 100	150 – 300	~0.05	0.1 – 0.2	0.6 – 10	[29], [44]
%NaCl rejection	-	-	20 - 80	95 - > 99	100	[45], [46]
Resistance to fouling and biofouling	Poor. Resistance to fouling can be improved through membrane surface modification with	Poor. Resistance to fouling can be improved through membrane surface modification with	Poor. Resistance to fouling can be improved through membrane surface modification with	Poor. Resistance to fouling can be improved through membrane surface modification with	Very good. CNTs possess antimicrobial properties. Resistance can be further enhanced with membrane surface	[24], [47]

Application	hydrophilic additives. Removal of solid particles, protozoa and bacteria.	hydrophilic additives. Removal of viruses and colloids.	hydrophilic additives. Removal of multivalent ions, proteins, dissolved organic matter and hardness.	hydrophilic additives. Removal of monovalent ions, desalination, water reuse, ultrapure water.	functionalisation. Removal of organic micropollutants and desalination application.	[8], [37], [39], [48], [49]
-------------	--	--	---	---	--	-----------------------------

The CNTs have the ability to be selectively functionalized at their pore openings to enhance their salt rejection capacities and their ability to remove various micropollutants present in water. Thus CNT membranes have been envisaged as potential candidates to replace both RO and NF membranes, because CNT membranes offer minimal energy consumption by lowering the applied pressure to drive desalting of solutions [34]. However, no single method is capable of alleviating the global water pollution problems on its own, which means that the existing water-treatment technologies are not sufficient to provide 100% pure water. Therefore a combination of methods, including those that have advanced from nanotechnology through the use of carbon nanotube membranes, can be a more viable approach.

Manawi and co-workers [36] recently assessed the potentiality of carbon-based nanomaterials (including CNTs, graphene, graphene oxide, carbon nanofibres, MXene, carbide-derived carbon, and fullerenes) in membrane fabrication for water treatment and desalination. Carbon nanotubes (CNTs), in particular, were identified as promising candidates to overcome the issues of fouling (and in particular biofouling) that membranes used in RO desalination processes are often faced with. This is due to the ability of CNTs to effectively destroy bacterial cells upon direct contact. Furthermore, VA-CNT membranes were highlighted to be potentially useful in water desalination because of their remarkably fast fluid transport properties. In as much as high salt rejection is

desired during seawater or brackish water desalination, the desalination process used must still be able to generate reasonably pure water flux on the other side of the semi-permeable membrane.

Indeed, Elimelech and Phillip [2] caution against the use of membranes with ultrahigh water permeability in seawater RO desalination processes because concentration polarisation as well as membrane fouling are exacerbated at high water fluxes [32]. (Author to check) For VA-CNT membranes to be effectively used for seawater desalination, a redesign of membrane modules will be required such that the preceding factors are taken into account. Goh et al. [5] wrote a comprehensive review that raises some important questions about the potentiality of nanomaterials in desalination membrane modifications. Questions about whether CNT polymeric membranes will be able to offer high performance and affordable desalination solutions were raised. Ultimately, this review encourages a thorough examination of all research areas and a priori focus points before commercialisation of this technology, such as considering economic and environmental concerns with regard to the use of nano-enabled or, better yet, CNT-based polymeric membranes. Toward the end of their review, the authors encouraged environmentalists to work closely with materials scientists in understanding and raising awareness of environmental hazards that these nano-enabled membranes may pose for humans.

Ahn et al. [3] documented the fabrication methods for CNT-based membranes and speculated on their potential use in desalination processes. The fundamental differences between the two CNT membrane types are presented in Table 2.3. Clearly, the limitations that hinder the popularity and commercialisation of VA-CNT membranes mainly include the complex fabrication processes used, which makes up-scaling of these membranes a challenge. For this reason, more efforts have

been directed toward the exploitation of mixed-matrix types of CNT membranes, even though they exhibit more moderate water fluxes than VA-CNT membranes. In addition, CNT MMMs are made using fabrication procedures that are relatively simple, and therefore CNT MMMs are more likely to be commercialised sooner [3].

**Table 2.3** Comparison of VA-CNT membranes and mixed-matrix CNT membranes (adapted from Ahn et al.[3]).

<b>VA-CNT membranes</b>	<b>Mixed-matrix CNT membrane</b>
CNTs are vertically aligned within the membrane	CNTs are irregularly arranged within the polymer matrix
CNTs are densely packed together	Composite layers with polymer membrane and non-woven support
Water flux through the membrane is extremely fast	Water flux through the membrane is reasonably fast
Functional groups can be conveniently attached at the CNT tips or on the membrane surface to prevent fouling	Low (or anti) fouling membranes
Complex fabrication procedures, less cost-effective	Fabrication processes are convenient, simple and readily commercialisable
May need specially adjusted operation system	Operation similar to that of conventional membrane processes

## 2.5. Solute transport properties of CNT membranes

Molecular dynamic (MD) simulation has been one of the fundamental tools used by researchers to gain insights into the transport behavior of water molecules inside confined CNT channels [37].

As mentioned earlier in this chapter, recent research work involving the use of CNT membranes for desalination has mainly been based on simulation studies. The properties and behaviour of fluids when confined at nano-length scales differ greatly from their behaviour in bulk form. For example, in the macroscopic world, it would be unexpected for water (a polar compound) to be able to enter and interact with the constricted and hydrophobic CNT pores [38]. However, the first MD simulation studies by Hummer and co-workers [39] showed that despite their hydrophobic nature, SWCNTs can be rapidly filled and emptied with water molecules (forming a column of five water molecules in length inside a nanotube). Furthermore, the filling and emptying of the CNTs with water molecules can be properly controlled such that water molecules do not remain constricted inside the tubes [39].

One other notable feature associated with CNT fluid transport, as reported by Hummer et al. [39], is that of the changes in the structural configuration of water molecules when inside a confined CNT channel. Inside the channel, the hydrogen-bonded and methodically linked water molecules or simply “water wires” are formed, as depicted in Fig. 2.4. The formation of these ordered one-dimensional hydrogen-bonded water wires inside the CNTs and at the CNT openings highly resembles those that are formed during water transport by biological channels such as transmembrane protein aquaporins [40, 41]. Other similarities between CNT channels and the biological aquaporin channels include their hydrophobic interiors or linings that enable near frictionless and fast water transport [40, 42]. Kalra et al. [43] used MD simulation to study molecular transport of water through CNT membranes under the influence of an osmotic gradient. The authors demonstrated that the flow rates within the CNT pores are extremely fast and independent of the length of the nanotubes. It was found that the flow inside these nanotubes was

almost frictionless and was restricted only by the events at the entry and exit points of the CNT pores. Nonetheless, the flow rates remain comparable with those of transmembrane aquaporins [43].

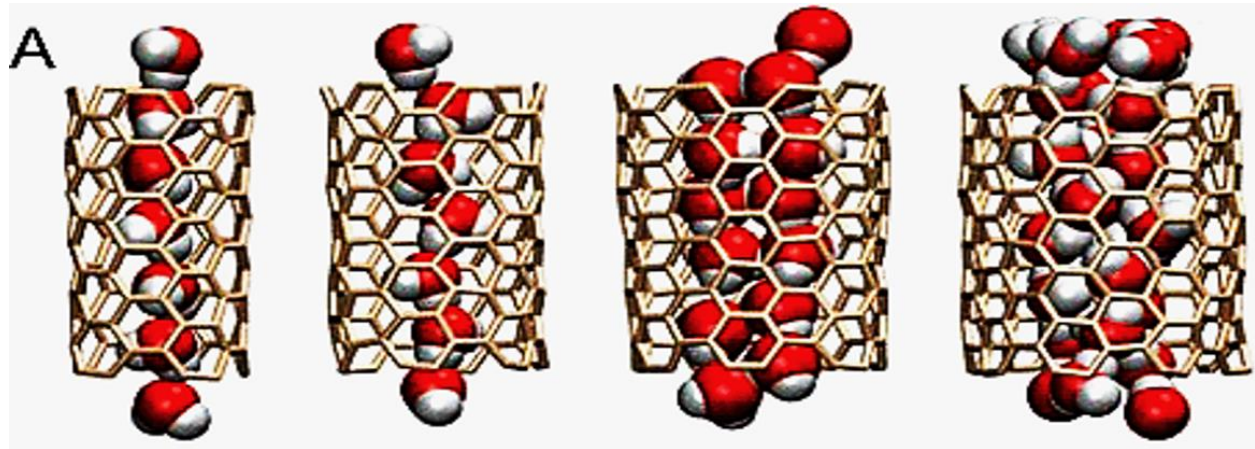


**Figure 2.4** Molecular dynamic simulation depicting water configuration or formation of “water wires” in differently sized armchair carbon nanotubes. Reproduced with permission from [42].

Several macroscopic equations have been used to explain the relationship between fluid flow or transport rate and the pore radius of the CNTs. One of these models is the non-slip Hagen Poiseuille equation which can be represented in Eq. 2.1 as follows:

$$Q_{\text{HP}} = \frac{\pi \left(\frac{d}{2}\right)^4}{8\mu L} \cdot \frac{\Delta P}{L} \quad (2.1)$$

where  $Q_{\text{HP}}$  represents the volumetric flow rate,  $\Delta P$  is the pressure difference across the tube length ( $L$ ),  $\mu$  is the viscosity of water and  $d$  is the pore diameter.

This equation assumes that fluid flow inside the CNT tubes is laminar and that there is no-slip at the boundary layer (*i.e.* the fluid velocity at the CNT walls is zero [46]). However, several studies on nanosized hydrophobic pores, such as those of CNT membranes have shown major deviations from this assumption, with flow enhancements that are orders of magnitude higher than predicted by the continuum Hagen Poiseuille model.

MD studies on CNT pores reveal that water molecules move freely with large slip inside the CNT walls due to the atomically smooth and hydrophobic interiors of CNTs [44]. The slip length which is merely the distance that the velocity profile can be extrapolated with to reach zero (Fig. 2.5), is normally used when describing the slip flow of molecules inside CNT walls

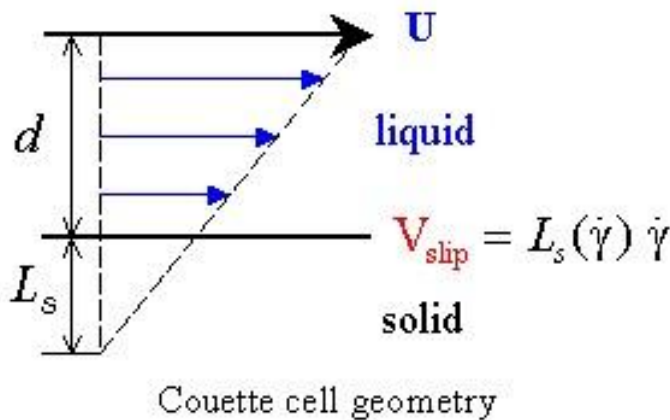


**Figure 2.5** Illustration of slip length at the liquid/solid interface. Reproduced from [1] of Further reading section.

When Hagen Poiseuille formalism in equation 1 is corrected to include slip-flow conditions, it can be represented in Eq. 2.2 as:

$$Q_{\text{slip}} = \frac{\pi \left(\frac{d}{2}\right)^4 + 4 \left(\frac{d}{2}\right)^3 \cdot L_S}{8\mu L} \cdot \frac{\Delta P}{L} \quad (2.2)$$

where  $L_S$  is the slip length and is given by Eq. (2.3) as follows:

$$L_S = \frac{U_{\text{wall}}}{dU/Dr} \quad (2.3)$$

and  $U_{\text{wall}}$  is the axial velocity at the wall and  $dU/dr$  is the radial velocity gradient at the wall.

Holt et al. [45] applied the slip-flow formalism (Eq. 2.2) to determine the flow through sub-2-nm CNT membranes. The slip lengths that were hundreds of nanometres larger than the pore sizes and were in the order of the overall size of the system were calculated [45]. When the same equation was used to calculate slip length for polycarbonate membranes with 15 nm pore sizes, the slip length was about 5 nm. These findings therefore suggest that slip-flow formalism cannot be used to describe flow through CNT pores in the 1 to 2 nm size regimes due to confinements in length and partial wetting of the CNT surface [9].

The extremely fast water transport of CNT membranes is therefore favourable for filtration purposes such as NF and RO. However, in the case of RO desalination, the efficiency of the process is determined by three critical factors, namely capital costs, energy costs, and the system operation costs [10]. Whilst there are many speculations on the potentiality of CNT membranes to greatly reduce the energy costs of RO desalination processes, the minimum energy required to pump water through a semi-permeable membrane is governed by the solution osmotic pressure, i.e. osmotic

pressure difference between seawater and freshwater [11]. Nonetheless, the high water fluxes of CNT membranes can greatly reduce the capital costs due to the small membrane area required to achieve maximum flux, without necessarily impacting on the energy consumption of the desalination process [11].

In an MD simulation study, Corry [42] simulated water conduction and suitability of differently sized CNTs with armchair type chirality (5,5), (6,6), (7,7) and (8,8) in water desalination applications. The CNT performance was evaluated by calculating salt rejection efficiency (see Table 2.4) [34]. The numbers denoted within parentheses describe the chirality and metallicity of the carbon nanotubes investigated; i.e. the manner in which the grapheme sheet has been rolled up to form a carbon nanotube [12]. The armchair configuration describes the shape of the hexagons making up the tube as one moves around the body of the nanotube and the metallic nature of SWCNTs. The calculations showed that the CNTs led to salt rejection ranging from 100% for (5,5 and 6,6) to 95% and 58% for the wider tube (7,7 and 8,8). Additionally, when the salt rejection efficiencies of the simulated CNT membranes and those of commonly used RO membranes were compared, the membrane comprising of (7,7) nanotubes could be expected to obtain 95% desalination at a flow rate that is over 1 500 times that of existing RO membranes [5]. Therefore, more in-depth studies on overcoming the energy costs of desalination processes using CNT membranes are crucial in order fully realise their applicability in water purification and desalination applications.

**Table 2.4** Water and ion conductance of nanotubes under 209 MPa Pressure at 250 mM ion concentration (reproduced from [42]).

Size	Diameter (Å)		Run lengths (ns)	conductance pt pns	
	C-C	Internal		H <sub>2</sub> O	Ions
(5,5)	6.6	3.2	10.00	10.4 ± 0.4	0.0
(6,6)	8.1	4.7	20.00	23.3 ± 0.3	0.0
(7,7)	9.3	5.9	25.00	43.7 ± 0.5	0.007 ± 0.005
(8,8)	10.9	7.5	17.00	81.5 ± 1.2	0.137 ± 0.025
(6,6) long	8.1	4.7	10.00	23.4 ± 0.5	0.0

From the discussions above, it is evident that the incorporation of VA-CNTs into polymeric membranes has important implications in terms of their transport and separation properties. This is because CNTs provide among others the ease of chemical functionalisation and doping, low friction, biocompatibility and controllable pore sizes necessary for rapid water transport and required solute rejection.

## 2.6. Characterisation tools for CNT-based membranes

### 2.6.1. Introduction to techniques used to probe CNT Membranes

Characterisation of CNT-based membranes is typically achieved using similar techniques to those that are normally used to characterise conventional polymer-based membranes. The techniques used include scanning electron microscopy (SEM), transmission electron microscopy (TEM), high-resolution TEM (HRTEM), atomic force microscopy (AFM), streaming potential and surface charge analysis, contact angle analysis, electrochemical impedance spectroscopy (EIS), thermal

gravimetric analysis (TGA), attenuated total reflection-Fourier transform infrared spectroscopy (ATR-FTIR), X-ray photoelectron spectroscopy, and many others [48]. It is of vital importance that the different techniques used for the analyses correlate with one another for effective clarification of the morphology and properties of the prepared membrane.

### **2.6.2. Microscopic Investigation of CNT membranes**

The incorporation of CNTs into membrane matrices is known to drastically transform the morphology of the membranes [49]. These changes can be detected easily by studying the surface properties as well as the internal structure of the membrane (Fig. 2.5) [50]. Depending on where the SEM image is taken on the membrane, it is possible to visualise and distinguish between the pores located on the top surface of the membrane and those located in the membrane sub-layer. Depending on the phase-inversion kinetics that occur during membrane formation, the membrane sub-layer may consist of large finger-like structures (referred to as macrovoids) or it can consist of a sponge-like structure made up of many small pores. For example, in order to effectively view the membranes' cross-sectional morphology (or internal structure), the membrane sample must be freeze-fractured in liquid nitrogen followed by coating with either gold or carbon in order to impart electrical conductivity [51]. The incorporation of CNTs into the polymer matrices is known to significantly affect a membrane's surface porosity. Celik et al. [8] reported that during the formation of CNT MMMs, the addition of small amounts of CNTs within the PES matrix enhanced the phase separation process, thus giving rise to the formation of larger membrane pore sizes. Furthermore, CNT inclusion has been reported to greatly influence the hydrophilicity, surface roughness, and mechanical strength of the MMMs [52, 53].

Transmission electron microscopy (TEM) is also a suitable technique for probing the internal structure of membranes containing nanomaterials such as CNTs. Therefore, information on the membrane thickness, pore sizes, and CNT density is obtainable from TEM analysis. Only a limited number of reports are available in which TEM has been used to structurally investigate the internal morphology of CNT/polymer membranes, particularly CNT MMMs. This is because the preparation of polymeric samples for TEM analysis tends to be significantly more complex because it involves preparing thin slices of the materials at cryogenic temperatures using a microtome [54]. However, the information obtained from TEM or HRTEM images is valuable and provides information about the dispersion of CNTs in the membrane matrices, their pore sizes, and distribution. Transmission electron microscopy could be used to study how chemical functionalisation or heteroatom doping (with either N or P) of CNTs affects dispersion in the membrane [55].

In the analyses of VA-CNT membranes, TEM analysis is commonly the first technique applied, in particular for the as-prepared CNT arrays, prior to polymer infiltration, as TEM is capable of probing the internal structure or morphology of these nano-based membranes and can also indicate whether vertical alignment of CNTs has been achieved. Scanning electron microscopy (SEM) is equally widely used to study the topography of VA-CNT membranes. Unlike TEM analysis, SEM examines the surface and produces an image that clearly establishes the alignment of CNTs within the membrane. The TEM and SEM images for VA-CNTs and VA-CNT membranes prepared using different methods are shown in Figs 2.6 and 2.7. In Fig. 2.6, SEM cross-sectional images of PSf membranes prepared from blending different amounts of MWCNTs are shown. All MWCNT/PSf membranes have similar substructures with finger-like internal pores. One noticeable difference

from their substructures is the amount of MWCNTs that have migrated to the top surface of the membrane, to make the membrane surface hydrophilic. Fig. 2.7(a) and (b) show SEM and TEM images for a CNT film with a height of about 2.2 mm (obtained under the CVD growth conditions: acetylene/argon composition ratio of 200/500 sccm, growth temperature of 810 °C, and ramp rate of 810 °C/min). The TEM micrographs presented in the figure show two graphene walls as well as patterned CNTs obtained via the nanotemplate method, in which a TEM grid was used as a mask [56]. The SEM images of VA-CNTs synthesised on stainless steel meshes are shown in Fig. 2.8.

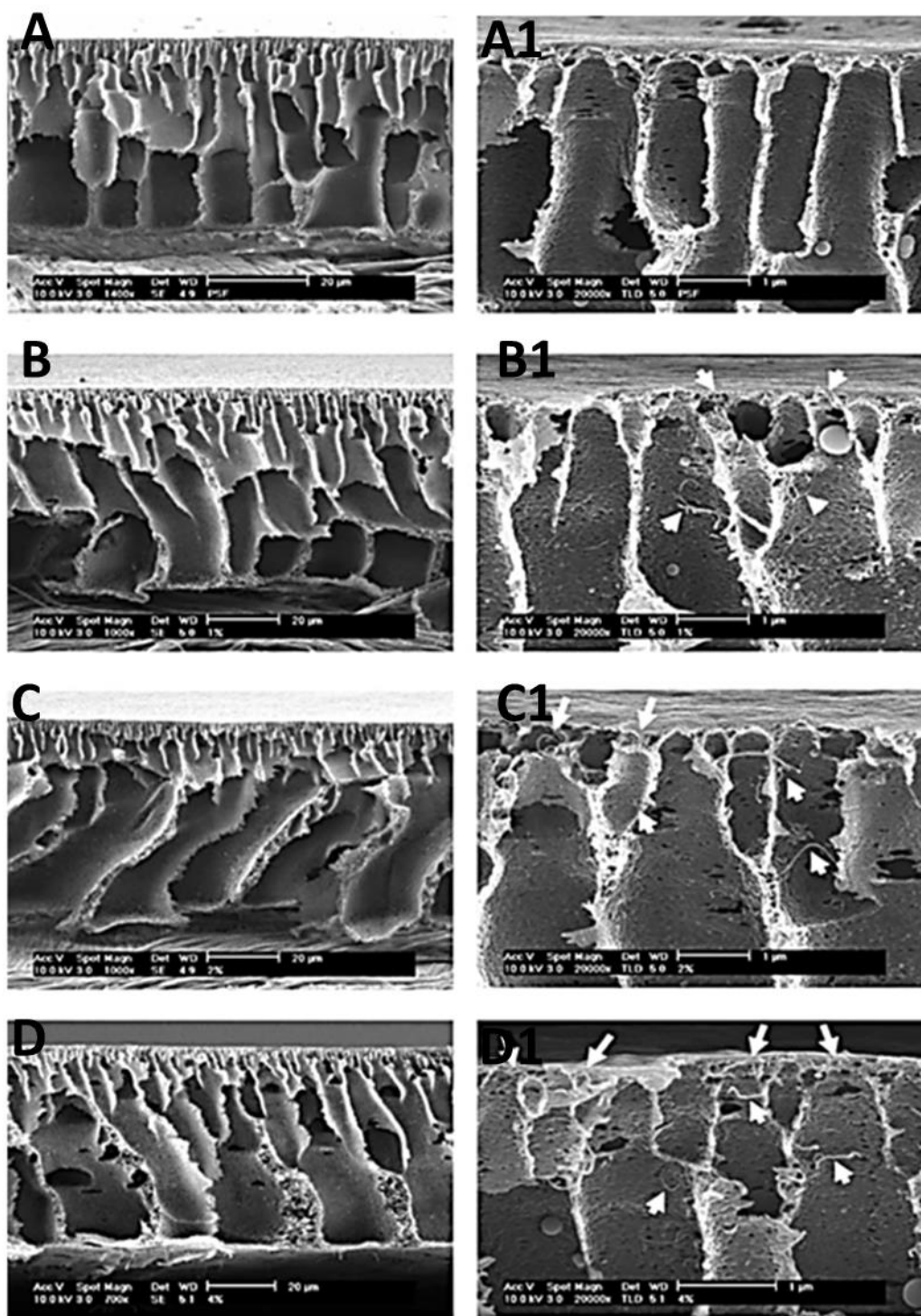


**Figure 2.6.** SEM cross-sectional images of MWCNT/PSf blend membranes with different loadings of MWCNTs; (A) 0 wt%, (B) 1.0 wt% (C) 2.0 wt%, and (D) 4.0 wt%. Images A1 to D1

are high magnification (20000 $\times$ ) images of A to D, showing the presence of MWCNTs in the surface layer of the membrane. Reproduced with permission from [50].

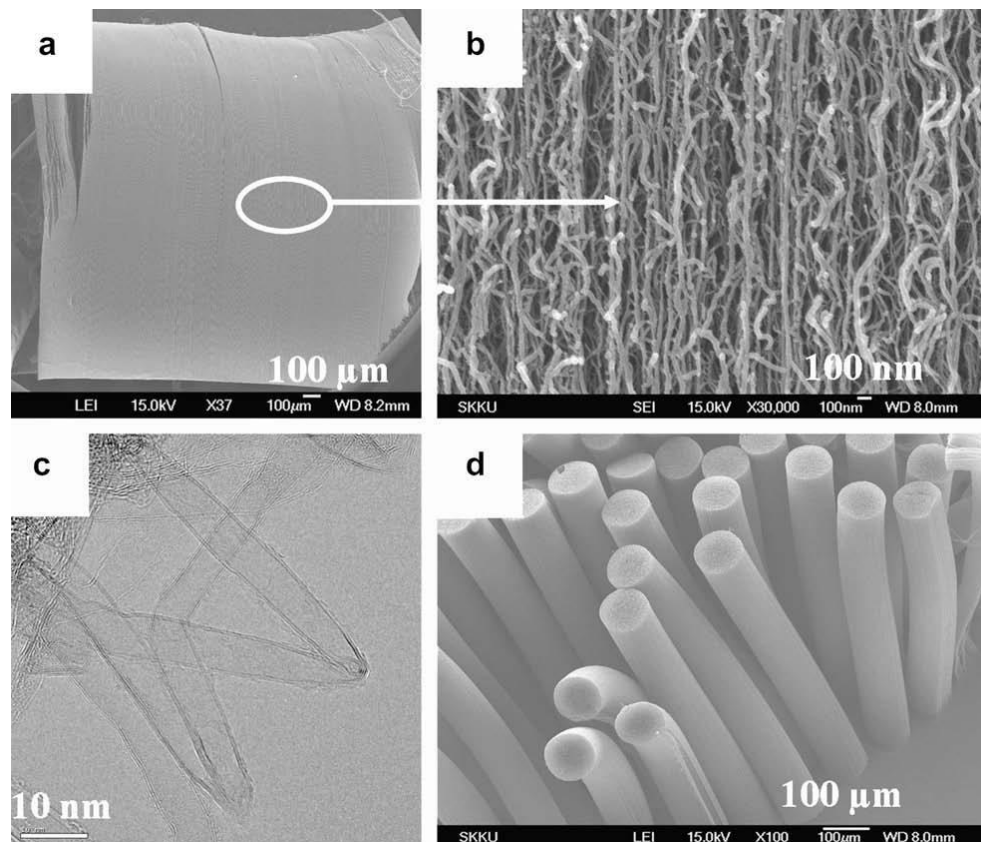


**Figure 2.7** SEM micrographs for (a) CNT film (b) the middle of the CNT film, (c) HR-TEM micrographs for CNTs, and (d) patterned CNTs using a TEM grid prepared using the nanotemplate method. Reproduced with permission from [56].

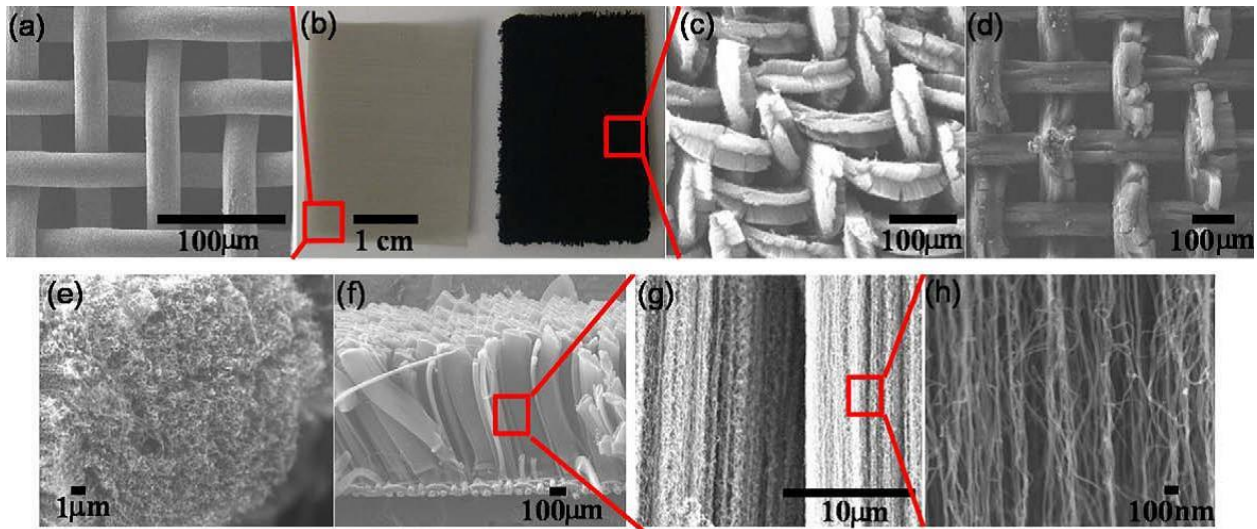


**Figure 2.8** SEM micrographs of VA-CNT membranes (in different forms) prepared using the filtration method. Reproduced with permission from [2, Further reading].

### 2.6.3. Mechanical strength analysis

The role of CNTs on improving the mechanical strength of MMMs polymeric membranes is widely documented [57, 58]. Inclusion of CNTs improves the mechanical strength of MMMs and as such increases the life span of the membranes. Membranes' mechanical strength properties are typically measured on a MicroStrain® analyser (LORD Sensing Systems, Williston, VT, USA) or Instron analyser (Instron, Massachusetts, USA). It is important for a membrane to have a sufficiently high mechanical strength in order to withstand transmembrane pressure during filtration. These measurements are very important particularly because CNT MMMs are tailor-made for pressure-driven processes. Maphutha et al. [59] showed that excellent mechanical properties can be obtained by the systematic incorporation of CNTs into a membrane material. A CNT composite membrane with polyvinyl alcohol used as a barrier layer was prepared for the purpose of removing oil from wastewater, and a 7.5% concentration of CNTs was found to produce a tensile strength of 119%, 77% in Young's modulus and 285% in toughness [59]. Other works

have also demonstrated the advantages resulting from the use of functionalised CNTs as additives (or fillers) in polymeric membranes. The ultimate tensile strength, mean modulus, and tensile strain were found to increase when small amounts of CNT particles (0.02–0.04 wt%) were added to suitable polymers [29].

#### **2.6.4. Contact angle analysis**

Surface contact angle analysis is used extensively in membrane technology to measure the hydrophilicity, surface energy, and surface tension of polymeric membranes containing CNTs. Contact angle measurements are usually recorded from 10 or more places on the membrane surface, and an average value is reported. This is done in order to obtain reproducible data representative of all the membrane surface properties. The ultimate goal is to fabricate membranes that are highly hydrophilic since they are generally desirable for desalination applications. Such membranes are less susceptible to fouling than their hydrophobic counterparts [50] because of the formation of a strong hydration layer on the membrane surface that prevents the attachment of foulants. Hydrophilicity is achieved by effectively mixing polymers with hydrophilic additives such as highly functionalised CNTs and/or heteroatom-doped CNTs such as N-doped CNTs [29] and can be predicted easily by a decrease in contact angle values. For example, when acid functionalised CNTs are incorporated into PES membranes, a decline in the contact angle from  $>71^\circ$  for bare PES membrane to  $<60^\circ$  for 4 wt% MWCNT/PES composite membranes is observed [50].

### **2.6.5. Atomic force microscopy (AFM) analysis**

Atomic force microscopy (AFM) analysis is a technique for analysing membrane surfaces and therefore provides information complementary to SEM and TEM analyses on the surface properties of carbon nanotube-based membranes. Atomic force microscopy generally probes the internal structure of the membrane and provides information on the surface roughness characteristics of the membrane and can also help measure membrane pore sizes. Fig. 2.9 shows that after the addition of surface-engineered CNTs into the cellulose acetate/polyethylene glycol polymer matrix (PM), the membrane surface roughness increased along with an increase in CNT loading up to 0.3 wt% (from PM-CNT 1 to PM-CNT 3). However, with further increments up to 0.4 wt% (PM-CNT 4), the membrane surface became smoother. The reason for the reduction in surface roughness is due to the reduced electrostatic interaction between the CNTs and the polymer matrix, thus leading to partial positioning of CNTs in the matrix, which then leads to smooth surfaces. As the loading was increased to 0.5 wt%, the surface roughness started to increase again because of the formation of CNT agglomerates and clusters within the membrane matrix. The major issue with very rough membrane surfaces is that they are prone to fouling because of the ease of attachment of foulants [50]. This is due to the increase in charged sites on the membrane surface.

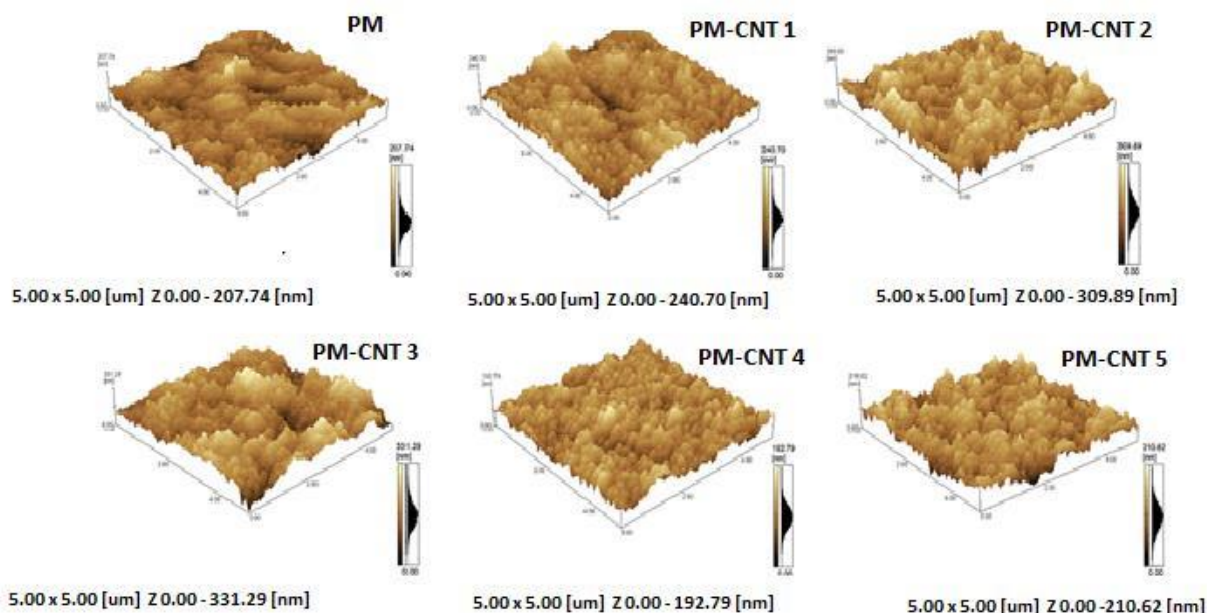


**Figure 2.9** AFM topographic images depicting changes in surface structure of cellulose acetate/polyethylene glycol polymer matrix (PM). Reproduced with permission from [3, Further reading].

### 2.6.6. Streaming potential and surface charge analysis

Information relating to the surface charge of CNT polymer membranes is important for understanding how a particular membrane will behave toward target pollutants in water, especially charged species/ions. The surface charge of a membrane can be determined via electrokinetic analysis [60]. Electrokinetic effects occur due to the interaction between a charged solid surface and the electrolyte rather than the inherent charge characteristics of the material [61]. In this measurement, zeta potential is measured as a function of pH. The inclusion of CNTs in membranes has a major effect on the surface charge of the membranes. However, the values obtained vary with the concentrations of CNTs added to the membrane and the type of chemical groups and/or heteroatom species attached to the CNTs. When the membrane charge is known, the behaviour of

the pollutants present in water or wastewater toward the membrane surface can be predicted. It has been shown that electrostatic repulsions between the membrane surface and pollutants prevent the occurrence of fouling on the membrane surface [62] suggesting that CNTs can be used as materials for manufacturing membranes that have outstanding antifouling properties.

### **2.6.7. Other characterisation techniques**

Other characterisation techniques used for membrane analysis include XPS and XRD spectroscopy. X-ray photoelectron spectroscopy (XPS) is normally used for surface chemical analysis of the CNT membranes and to study the chemical bonding environments within the CNTs and heteroatoms; XPS is most useful for studying the stability of the incorporated functionalised CNTs into the membrane surface and matrix. The change in ratio of elemental concentrations can be monitored before membrane operation and several days of operation. A large change in elemental ratio is indicative of the fact that some of the elements may have been washed off during operation and that they are not stably attached or incorporated into the membrane surface. X-ray powder diffraction (XRD), on the other hand, provides information on the crystallinity, atomic structure, and crystallite size determination of membranes. Other conventional and unconventional instrumental techniques used to study membranes in general are presented elsewhere [49, 50].

## **2.7. Environmental sustainability of CNT membranes**

### **2.7.1. Energy demand**

The energy demand for a desalination process is set up by the need to bring feed water to a pressure that is equal to the osmotic pressure of the concentrate. Currently, the energy consumed by RO

desalination stands at 2 kWh/m<sup>3</sup> at 50% recovery and is far greater than the theoretical minimum energy required for desalination of 1.06 kWh/m<sup>3</sup> [2,33]. The minimum amount of energy required to separate pure water from salty water is equal in magnitude but has an opposite sign to the free energy of mixing, and can be calculated in Eq. (4) as:

$$d(\Delta G_{\text{mix}}) = -RT \ln a_w dn_w = \pi_s V_w dn_w \quad (2.4)$$

where  $\Delta G_{\text{mix}}$  is the free energy of mixing,  $R$  is the ideal gas constant,  $T$  is the absolute temperature,  $a_w$  is the activity of water,  $n_w$  is number of moles of water,  $\pi_s$  is the osmotic pressure of seawater, and  $V_w$  is the molar volume of water.

The minimum energy can then be calculated from the integration of (2.4) as follows:

$$W_o = (-d(\Delta G_{\text{mix}})/dn_w)_{P, T} = -RT \ln a_w \quad (2.5)$$

Although the energy consumption of the RO desalination process has not yet reached the theoretical limit, the use of highly permeable membranes such as CNT-based membranes is expected to alleviate this problem. However, this will not directly influence the reduction of the energy necessary for desalination processes to occur [2]. Nonetheless, fouling-resistant membranes such as CNT-based membranes are beneficial in overcoming the high energy costs associated with high-pressure requirements essential in order to drive pure water molecules through a fouled membrane.

### 2.7.2. Disposal

As with other nanoparticles, disposal of CNTs and/or CNT-based membranes is not widely documented, because these materials are relatively new, and most researchers and environmentalists are still trying to study their impact on human health and the environment as well as their disposal issues. According to the UK Environmental Agency, “any CNT containing waste is considered as hazardous waste unless evidence suggests otherwise” [63]. This signals that the fabrication costs of CNT-based membranes could potentially be driven up (when environmentally benign processes are sought) and especially if these membranes are scaled up for manufacturing. For example, currently the cost of 1.0 g of pristine MWCNTs is greater than \$100. Although this seems high, because of their high surface area, very small amounts of CNTs are used as additives in CNT MMM fabrication processes. Furthermore, as newer methods of production are being developed, the price of CNTs is expected to gradually decrease. However, Brehm (2008) at the Massachusetts Institute of Technology (MIT) suggested that incorporating environmental objectives during the synthesis stage of novel materials (such as CNTs) can bring about a drastic change in both industrial and environmental practices, that is, preventing problems rather than reacting to them [64]. This is a viable approach to minimising CNT toxicity at the source prior to their incorporation into other materials such as membranes [64] or point-of-use systems such as filters. Methods that have been suggested for CNT disposal include high-temperature incineration [65] and vitrification or the encapsulation of CNTs into glass or ceramic structures [63]. Vitrification is a relatively new method that is still under development and is therefore considered as an alternative disposal technique for the future [63]. Clearly, more efforts are needed in this area in order to create better solutions for the disposal of CNTs or CNT-based membranes in a sustainable manner. These efforts will require active collaboration among materials scientists,

industrialists, academics, and environmentalists in order to pinpoint the potential risks associated with these new materials and to come up with better disposal methods [66].

### **2.7.3. Toxicity of CNT membranes**

Although desalination processes have been identified as a potential solution to global water scarcity [80], the economic implications associated with these processes, in general, are too high for underdeveloped and developing countries. The typical construction of desalination plants requires a massive capital expenditure. In addition, a huge amount of energy is required for pumping water from the sea into a desalination plant, leading to high daily operating costs. Since seawater desalination is a highly specialised field, personnel working on these projects are usually highly skilled engineers who are remunerated competitively. As such, input costs in these projects are astronomical. Over the past decade, attempts to lower the cost of desalination in developed countries have proved successful, with the price of desalinated water reaching \$2.10/m<sup>3</sup> [81]. According to a review by Ghaffour et al. (2013), the parameters that influence the total capital and operational costs of a desalination plant include electric power availability, desalination process configuration, plant size and its component design, raw water quality and required water quality and other consumables [81]. In a CNT membrane desalination plant, the parameters are expected to be similar. However, the CNT cost parameter is factored in separately. Therefore, in order for CNT membranes to be fully adopted in desalination processes, the cost per volume of saline water treated by these membranes would need to be the same or even lower than the current costs of desalination processes. In the end, cost is always the dominating and deciding factor. Polymeric membranes used for seawater desalination have evolved over time. By 1969, cellulose acetate (CA) membranes had emerged as the best membranes for desalination purposes [82]. However,

the quest for desalination membranes with high flux and high rejection capacities has been a continuous endeavour. Indeed, the incorporation of carbon nanomaterials, in particular CNTs or the fabrication of VA-CNT membranes, is being applied to lower the cost of seawater desalination. The incorporation of CNTs into polymeric membranes has been shown to produce remarkably enhanced membrane properties such as flux, recovery, antifouling, and salt rejection [5]. It is expected that CNTs will lead to lower energy requirements when pumping seawater across a membrane in order to obtain freshwater. Fouling of membranes is reported to drive up the energy costs, as a result of the requirements of high pressures necessary to drive pure water molecules across a fouled membrane. Therefore, the inclusion of carbon nanomaterials in membranes to be used for desalination processes is envisaged to eliminate the deposition of microorganisms on the membrane surfaces which can contribute to membrane fouling [83]. As such, the presence of CNTs in polymeric membranes brings about properties that can render the membranes energy-efficient. The schematic diagram given in Fig. 2.10 illustrates the potential performance and commercial viability of CNT membranes with reference to other nano-enabled membranes such as inorganic nanomaterials incorporating membranes, aquaporins, ceramics, and other nanostructured membranes [45]. Indeed, VA-CNT membranes have highly enhanced performance prediction (closer to aquaporins), yet commercialisation is still a long way off.

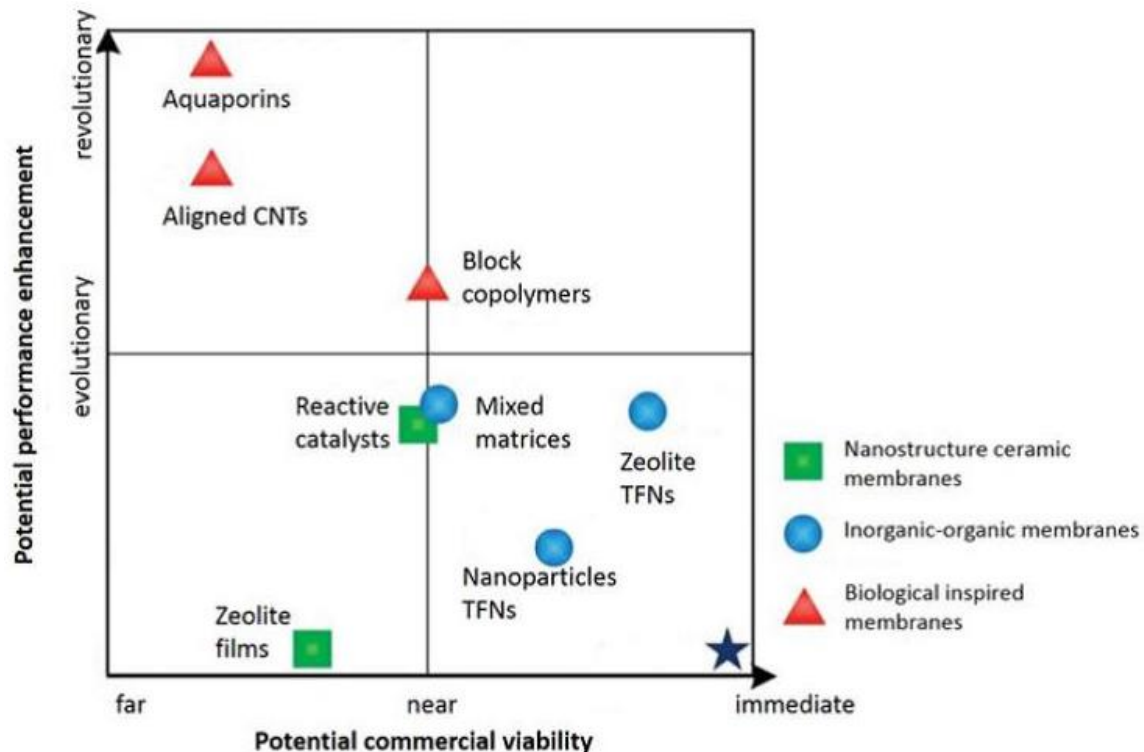


**Figure 2.10** Potential performance versus commercial viability of nanotechnology-enabled membrane. Reproduced with permission from [4, Further reading].

The use of integrated systems has been shown to be one of the ways by which energy costs can be minimised. Seawater has high osmotic pressure because of the presence of divalent ions, for example. By subjecting the seawater feed through a pre-filtration stage, the effect of lowering the osmotic pressure of the feed can be explored [84, 85]. The ability to fabricate membranes with improved surface properties by incorporating CNTs will further reduce the capital expenditure required for the running of desalination plants. Researchers have already projected that the use of CNT membranes in a desalination plant would offer a significant cost reduction of up to 22% and chemical cost savings of up to 76% [86]. Therefore, the use of CNT technologies to bring down costs will be at the centre stage of cutting-edge research until the scientific community considers the safety measures discussed in previous sections or provides proof that the potable water generated using CNT membranes is safe and acceptable.

## 2.8. Challenges and future perspectives

The CNT-based membranes are perceived as robust and ideal materials for the generation of freshwater during filtration and desalination processes. This perception is based on the advances made in the synthesis of CNTs of various morphologies (e.g., size, shape, and geometry). The millimetre-long VA-CNTs provide new openings for the transportation of water molecules through tubes. However, CNT-based membranes exhibit several obstacles that must first be addressed before they can be utilised effectively in desalination processes. The conventional methods for the production of CNTs (such as CVD) have insurmountable shortcomings [50]. One such disadvantage is that CNT manufacturing processes and in particular those for producing VA-CNTs have not yet been scaled up [35]. In addition, when alternative methods such as arc-discharge and laser ablation are utilised in CNT synthesis on an industrial scale, the process becomes very costly. The distinctive properties of CNTs can be useful when these nanomaterials have been homogeneously dispersed in a polymer solution [87]. Inherently, CNTs tend to cluster into bundles or agglomerates because of the presence of van der Waals interactions within the CNT lattice, which can further compromise the mechanical strength of CNT membranes [88]. However, the “unbundling” of CNTs can be achieved through (i) covalent modifications via the attachment of functional substituents, for example  $-\text{COOH}$ ,  $-\text{OH}$ , and  $-\text{NH}_2$ , (ii) non-covalent modification via wrapping of water-soluble linear polymers around the CNTs [89], and (iii) by mixing CNTs under shear force such as ultrasonication [90]. Although CNT functionalisation is a challenging and laborious exercise, it leads to more stable surface modification, which is vital in attaining CNTs that can be dispersed with ease in the membrane matrices [10]. The tendency of CNTs to agglomerate during solution-casting processes remains another overarching obstacle. The practice of chemically functionalising CNTs or substitutional doping of CNTs assists in obtaining

membranes with excellent surface properties [86]. To keep the fabrication costs of CNT membranes to a minimum, further research is needed to seek low-cost, simple, and efficient ways of functionalising and/or dispersing CNTs in membrane matrices. Therefore, further research to find ways of simplifying the engineering processes and to understand the membrane science should continue to be pursued. Membrane fouling is an inevitable occurrence where the application of CNT polymer membranes in water treatment is concerned. The degree of fouling is further influenced by the conditions of the feed water that is undergoing treatment [10]. Even though CNTs possess antimicrobial properties that may be beneficial in averting biofilm formation on a membrane surface, the big issue still remains the staged array membrane configurations and the influence of the destroyed microorganisms on subsequent membrane filtration steps. Furthermore, having CNTs in mixed-matrix membrane configuration remains questionable and is said to render all the attractive and desirable features of CNTs useless because the majority of the CNT mass is buried in the bulk polymer matrix [17]. The probability of CNTs leaching out from a polymer membrane is another issue requiring attention, especially in cases where dispersion and chemical bonding has not been achieved [46]. Therefore, if CNT polymer membranes are to be endorsed for future large-scale operations in water-treatment processes, the issue of nanomaterials leaching into the water source must be thoroughly addressed and attempts must be made to prevent leaching. As mentioned in the previous sections, VA-CNT membranes have better prospects than CNT MMMs when it comes to their performance in desalination processes and the diversity of application. However, their fabrication processes may be a limiting factor in that they hinder widespread exploitation as a result of the complexities in the process and thus incapability of producing reproducible membrane samples. Even though fluxes through the individual nanotube are high, fluxes per square centimetre are limited because of the low porosity of CNTs. This is a serious

limitation for their applications. Another great challenge in VA-CNT membranes is the alignment of large numbers of CNTs with well-controlled morphology and geometry across the entire membrane structure. For instance, during the polymer infiltration step, it is difficult to find a deposition process that will be able to conform to the spaces between the VA-CNT arrays and adequately fill these spaces, without tampering with the alignment of CNTs. Researchers need to design an etching process that will selectively open the nanotube ends without producing voids in the membrane structure. The challenge is to remove impurities within the VA-CNTs while maintaining the original integrity of the nanotubes. Because they are tiny particles instead of ions or molecules for which a system of risk assessment already exists, CNTs pose distinctive challenges for risk assessment and management [91]. A deep understanding of these nanomaterials is still required in order to prevent and eliminate the probability of hazards emanating from these nanomaterials in water treatment [91]. This level of understanding will be of significant help to exponentially increase research and development activities of composite membranes containing CNTs.

The VA-CNT membranes provide new prospects for the transportation of liquids and the separation of unwanted species. Clearly, the potential for CNT membranes is enormous. The key question that remains is: can these CNT materials be commercialised for large-scale applications? Commercialisation of these materials is important because CNT polymer membranes possess enhanced selectivities. In contrast to conventional polymeric membranes, CNT polymer membranes have outstanding advantages, such as higher flux and higher salt rejection [86]. In view of these outstanding properties, a drive toward commercialisation of these materials (which are energy-efficient and less susceptible to fouling) should be undertaken. Over the past decade,

challenges pertaining to the application of CNTs revolved around the high cost of CNTs. However, the cost has since dropped from \$200 per gram in 1999 to between \$50 and \$100 per gram in 2013, making it affordable to use CNTs in different materials [92]. The affordability of CNTs would make the scaling up of CNT polymer membranes a possible task [93]. The realisation of the ultrafast transport of molecules within tubes of CNT membranes is critical at this stage.

## **2.9. Conclusions**

The merits and challenges associated with the use of CNTs in membrane systems in desalination were systematically analysed. During the past decade considerable efforts have been made towards the development of membranes containing carbon nanomaterials to overcome the fouling, high energy demand, unselective separation of dissolved contaminants and low permeation. There is clear evidence that the use of CNTs in membrane systems is on the rise and will continue to be investigated and attempted to be implemented at industrial scale for the foreseeable future, provided that the health concerns can be resolved adequately. There are also issues regarding the hazards of nanomaterials in the workplace, i.e. research laboratory, production facility, or operation in which nanomaterials are processed, used, disposed of, or recycled. In the absence of scientific clarity about the potential health effects of occupational exposure to nanoparticles, a need exists for guidance in decision-making about hazards, risks, and controls.

## 2.10. References

- [1] N. Misdan, W.J. Lau, A.F. Ismail, Seawater reverse osmosis (SWRO) desalination by thin-film composite membrane—current development, challenges and future prospects, *Desalination*, 287 (2012) 228–237.
- [2] M. Elimelech, W.A. Phillip, The future of seawater desalination: Energy, technology, and the environment, *Science*, 333 (2011) 712–717.
- [3] C.H. Ahn, Y. Baek, C. Lee, S.O. Kim, S. Kim, S. Lee, S.-H. Kim, S.S. Bae, J. Park, J. Yoon, Carbon nanotube-based membranes: Fabrication and application to desalination, *Journal of Industrial and Engineering Chemistry*, 18 (2012) 1551–1559.
- [4] National Research Council (NRC) Committee on Advancing Desalination Technology, *Desalination: A National Perspective*, National Academies Press, Washington, DC, 2008. 312 pp.
- [5] P.S. Goh, A.F. Ismail, B.C. Ng, Carbon nanotubes for desalination—an innovative material with enormous potential, *Membrane Technology*, 2013 (2013) 7–10.
- [6] A.F. Ismail, P.S. Goh, S.M. Sanip, M. Aziz, Transport and separation properties of carbon nanotube mixed-matrix membrane, *Separation and Purification Technology*, 70 (2009) 12–26.
- [7] E. Drioli, L. Giorno (Eds.), *Comprehensive Membrane Science and Engineering*, Elsevier Science, 2010, 1570 pp. ISBN: 9780080932507.
- [8] E. Celik, H. Park, H. Choi, H. Choi, Carbon nanotube blended polyethersulfone membranes for fouling control in water treatment, *Water Research*, 45 (2011) 274–282.
- [9] V. Vatanpour, S.S. Madaeni, R. Moradian, S. Zinadini, B. Astinchap, Fabrication and characterisation of novel antifouling nanofiltration membrane prepared from oxidised multiwalled carbon nanotube/polyethersulfone nanocomposite, *Journal of Membrane Science*, 375 (2011) 284–294.
- [10] S. Kar, R. Bindal, P. Tewari, Carbon nanotube membranes for desalination and water purification: challenges and opportunities, *Nano Today*, 7 (2012) 385–389.
- [11] C. Tang, Q. Zhang, K. Wang, Q. Fu, C. Zhang, Water transport behavior of chitosan porous membranes containing multi-walled carbon nanotubes (MWNTs), *Journal of Membrane Science*, 337 (2009) 240–247.
- [12] S. Zou, Y. Gu, D. Xiao, C.Y. Tang, The role of physical and chemical parameters on forward osmosis membrane fouling during algae separation, *Journal of Membrane Science*, 366 (2011) 356–362.
- [13] P. Bacchin, P. Aimar, R.W. Field, Critical and sustainable fluxes: theory, experiments and applications, *Journal of Membrane Science*, 281 (2006) 42–69.
- [14] M.F. Goosen, S. Al-Obeidani, H. Al-Hinai, S. Sablani, Y. Taniguchi, H. Okamura, Membrane fouling and cleaning in treatment of contaminated water, in: E. Laboy-Nieves, F. Schaffner, A. Abdelhadi, M. Goosen (Eds.), *Environmental Management, Sustainable Development and Human Health*, 2009, CRC Press/Balkema; AK Leiden, The Netherlands, pp. 503.

- [15] K.R. Zodrow, M.E. Tousley, M. Elimelech, Mitigating biofouling on thin-film composite polyamide membranes using a controlled-release platform, *Journal of Membrane Science*, 453 (2014) 84–91.
- [16] C.D. Vecitis, K.R. Zodrow, S. Kang, M. Elimelech, Electronic-structure-dependent bacterial cytotoxicity of single-walled carbon nanotubes, *ACS Nano*, 4 (2010) 5471–5479.
- [17] A. Tiraferri, C.D. Vecitis, M. Elimelech, Covalent binding of single-walled carbon nanotubes to polyamide membranes for antimicrobial surface properties, *ACS Applied Materials & Interfaces*, 3 (2011) 2869–2877.
- [18] M.S. Mauter, M. Elimelech, Environmental applications of carbon-based nanomaterials, *Environmental Science & Technology*, 42 (2008) 5843–5859.
- [19] A. Matin, Z. Khan, S. Zaidi, M. Boyce, Biofouling in reverse osmosis membranes for seawater desalination: phenomena and prevention, *Desalination*, 281 (2011) 1–16.
- [20] S. Kang, M. Herzberg, D.F. Rodrigues, and M. Elimelech, Antibacterial effects of carbon nanotubes: size does matter! *Langmuir*, 24 (2008) 6409–6413.
- [21] B.J. Hinds, N. Chopra, T. Rantell, R. Andrews, V. Gavalas, L.G. Bachas, Aligned multiwalled carbon nanotube membranes, *Science*, 303 (2004) 62–65.
- [22] M. Majumder, N. Chopra, B.J. Hinds, Effect of tip functionalisation on transport through vertically oriented carbon nanotube membranes, *Journal of the American Chemical Society*, 127 (2005) 9062–9070.
- [23] S. Iijima, Helical microtubules of graphitic carbon, *Nature*, 354 (1991) 56–58.
- [24] J.-G. Yu, X.-H. Zhao, H. Yang, X.-H. Chen, Q. Yang, L.-Y. Yu, J.-H. Jiang, X.-Q. Chen, Aqueous adsorption and removal of organic contaminants by carbon nanotubes, *Science of the Total Environment*, 482 (2014) 241–251.
- [25] R.H. Baughman, A.A. Zakhidov, W.A. de Heer, Carbon nanotubes – the route toward applications, *Science*, 297 (2002) 787–792.
- [26] R. Andrews, M. Weisenberger, Carbon nanotube polymer composites, *Current Opinion in Solid State & Materials Science*, 8 (2004) 31–37.
- [27] L. Brunet, D.Y. Lyon, K. Zodrow, J.-C. Rouch, B. Caussat, P. Serp, J.-C. Remigy, M.R. Wiesner, P. J. Alvarez, Properties of membranes containing semi-dispersed carbon nanotubes, *Environmental Engineering Science*, 25 (2008) 565–576.
- [28] S. van Dommele, Nitrogen Doped Carbon Nanotubes: Synthesis, Characterisation and Catalysis, Doctoral Thesis, Utrecht University, Netherlands, 2008.
- [29] N. Phao, E.N. Nxumalo, B.B. Mamba, S.D. Mhlanga, A nitrogen-doped carbon nanotube enhanced polyethersulfone membrane system for water treatment, *Physics and Chemistry of the Earth A/B/C*, 66 (2013) 148–156.
- [30] S. Kim, J.R. Jinschek, H. Chen, D.S. Sholl, E. Marand, Scalable fabrication of carbon nanotube/polymer nanocomposite membranes for high flux gas transport, *Nano Letters*, 7 (2007) 2806–2811.
- [31] Z. Fan, S.G. Advani, Characterisation of orientation state of carbon nanotubes in shear flow, *Polymer*, 46 (2005) 5232–5240.

- [32] S.-M. Park, J. Jung, S. Lee, Y. Baek, J. Yoon, D.K. Seo, Y.H. Kim, Fouling and rejection behavior of carbon nanotube membranes, *Desalination*, 343 (2014) 180–186.
- [33] Y. Baek, C. Kim, D.K. Seo, T. Kim, J.S. Lee, Y.H. Kim, K.H. Ahn, S.S. Bae, S.C. Lee, J. Lim, High performance and antifouling vertically aligned carbon nanotube membrane for water purification, *Journal of Membrane Science*, 460 (2014) 171–177.
- [34] R. Das, M.E. Ali, S.B.A. Hamid, S. Ramakrishna, Z.Z. Chowdhury, Carbon nanotube membranes for water purification: a bright future in water desalination, *Desalination*, 336 (2014) 97–109.
- [35] R. Das, S.B.A. Hamid, M.E. Ali, A.F. Ismail, M. Annuar, S. Ramakrishna, Multifunctional carbon nanotubes in water treatment: the present, past and future, *Desalination*, 354 (2014) 160–179.
- [36] Y. Manawi, V. Kochkodan, M.A. Hussein, M.A. Khaleel, M. Khraisheh, N. Hilal, Can carbon-based nanomaterials revolutionize membrane fabrication for water treatment and desalination? *Desalination*, 391 (2016) 69–88.
- [37] J.K. Holt, Carbon nanotubes and nanofluidic transport, *Advanced Materials*, 21 (2009) 3542–3550.
- [38] M.S. Sansom, P.C. Biggin, Biophysics: water at the nanoscale, *Nature*, 414 (2001) 156–159.
- [39] G. Hummer, J.C. Rasaiah, J.P. Noworyta, Water conduction through the hydrophobic channel of a carbon nanotube, *Nature*, 414 (2001) 188–190.
- [40] O. Bakajin, A. Noy, F. Fornasiero, C.P. Grigoropoulos, J.K. Holt, J.B. In, S. Kim, H.G. Park, Nanofluidic carbon nanotube membranes: Applications for water purification and desalination, in: M. Diallo, J. Duncan, N. Savage, A. Street and R. Sustich (Eds.), *Nanotechnology Applications for Clean Water*, Elsevier Inc., Philadelphia, USA, 2014.
- [41] F. Fornasiero, H.G. Park, J.K. Holt, M. Stadermann, C.P. Grigoropoulos, A. Noy, O. Bakajin, Ion exclusion by sub-2-nm carbon nanotube pores, *Proceedings of the National Academy of Sciences of the United States of America*, 105 (2008) 17250–17255.
- [42] B. Corry, Designing carbon nanotube membranes for efficient water desalination, *Journal of Physical Chemistry B*, 112 (2008) 1427–1434.
- [43] A. Kalra, S. Garde, G. Hummer, Osmotic water transport through carbon nanotube membranes, *Proceedings of the National Academy of Sciences of the United States of America*, 100 (2003) 10175–10180.
- [44] M. Majumder, N. Chopra, B.J. Hinds, Mass transport through carbon nanotube membranes in three different regimes: ionic diffusion and gas and liquid flow, *ACS Nano*, 5 (2011) 3867–3877.
- [45] J.K. Holt, H.G. Park, Y. Wang, M. Stadermann, A.B. Artyukhin, C.P. Grigoropoulos, A. Noy, O. Bakajin, Fast mass transport through sub-2-nanometer carbon nanotubes, *Science*, 312 (2006) 1034–1037.
- [46] D. Mattia, H. Leese, K.P. Lee, Carbon nanotube membranes: from flow enhancement to permeability, *Journal of Membrane Science*, 475 (2015) 266–272.

- [47] P.J.F. Harris, *Carbon Nanotube Science: Synthesis, Properties and Applications*, Cambridge University Press, NY, USA, 2009.
- [48] O. Agboola, J. Maree, R. Mbaya, Characterisation and performance of nanofiltration membranes, *Environmental Chemistry Letters*, 12 (2014) 241–255.
- [49] P. Daraei, S.S. Madaeni, N. Ghaemi, H.A. Monfared, M.A. Khadivi, Fabrication of PES nanofiltration membrane by simultaneous use of multi-walled carbon nanotube and surface graft polymerization method: Comparison of MWCNT and PAA modified MWCNT, *Separation and Purification Technology*, 104 (2013) 32–44.
- [50] J.-H. Choi, J. Jegal, W.-N. Kim, Fabrication and characterisation of multi-walled carbon nanotubes/ polymer blend membranes, *Journal of Membrane Science*, 284 (2006) 406–415.
- [51] G.D. Vilakati, E.M. Hoek, B.B. Mamba, Probing the mechanical and thermal properties of polysulfone membranes modified with synthetic and natural polymer additives, *Polymer Testing*, 34 (2014) 202–210.
- [52] E. Celik, L. Liu, H. Choi, Protein fouling behavior of carbon nanotube/polyethersulfone composite membranes during water filtration, *Water Research*, 45 (2011) 5287–5294.
- [53] V. Vatanpour, M. Esmaceli, M.H.D.A. Farahani, Fouling reduction and retention increment of polyethersulfone nanofiltration membranes embedded by amine-functionalized multi-walled carbon nanotubes, *Journal of Membrane Science*, 466 (2014) 70–81.
- [54] E.-S. Kim, G. Hwang, M.G. El-Din, Y. Liu, Development of nanosilver and multi-walled carbon nanotubes thin-film nanocomposite membrane for enhanced water treatment, *Journal of Membrane Science*, 394 (2012) 37–48.
- [55] K. Yokwana, N. Gumbi, F. Adams, S. Mhlanga, E. Nxumalo, B. Mamba, Development of functionalized doped carbon nanotube/polysulfone nanofiltration membranes for fouling control, *Journal of Applied Polymer Science*, 132 (2015) 41835.
- [56] S. Patole, P. Alegaonkar, H.-C. Lee, J.-B. Yoo, Optimization of water assisted chemical vapor deposition parameters for super growth of carbon nanotubes, *Carbon*, 46 (2008) 1987–1993.
- [57] R. Sen, B. Zhao, D. Perea, M.E. Itkis, H. Hu, J. Love, E. Bekyarova, R.C. Haddon, Preparation of single-walled carbon nanotube reinforced polystyrene and polyurethane nanofibers and membranes by electrospinning, *Nano Letters*, 4 (2004) 459–464.
- [58] J.N. Coleman, U. Khan, W.J. Blau, Y.K. Gun'ko, Small but strong: A review of the mechanical properties of carbon nanotube–polymer composites, *Carbon*, 44 (2006) 1624–1652.
- [59] S. Maphutha, K. Moothi, M. Meyyappan, S.E. Iyuke, A carbon nanotube-infused polysulfone membrane with polyvinyl alcohol layer for treating oil-containing waste water, *Scientific Reports*, 3 (2013) 1509.
- [60] M.D. Afonso, G. Hagemeyer, R. Gimbel, Streaming potential measurements to assess the variation of nanofiltration membranes surface charge with the concentration of salt solutions, *Separation and Purification Technology*, 22 (2001) 529–541.
- [61] G. Hurwitz, G.R. Guillen, E.M. Hoek, Probing polyamide membrane surface charge, zeta potential, wettability, and hydrophilicity with contact angle measurements, *Journal of Membrane Science*, 349 (2010) 349–357.

- [62] B.S. Lalia, V. Kochkodan, R. Hashaikeh, N. Hilal, A review on membrane fabrication: Structure, properties and performance relationship, *Desalination*, 326 (2013) 77–95.
- [63] H. Greg, Safe Handling and Use of Carbon Nanotubes, Information Sheet, Safe Work Australia, 2012, <http://www.safeworkaustralia.gov.au> (accessed 20 March 2016).
- [64] D. Brehm, Minimizing the Environmental Impacts of CNTs, Massachusetts Institute of Technology, Cambridge, USA, 2008.
- [65] The Health and Safety Executive Annual Report and Accounts 2011/12, 2012, Health and Safety Executive (HSE), Bootle, UK. <http://www.hse.gov.uk/aboutus/reports/1112/ar1112.pdf> (accessed 30 March 2016).
- [66] P.S. Goh, A.F. Ismail, Review: Is interplay between nanomaterial and membrane technology the way forward for desalination? *Journal of Chemical Technology & Biotechnology*, 90 (2015) 971–980.
- [67] S.Y. Madani, A. Mandel, A.M. Seifalian, A concise review of carbon nanotube's toxicology, *Nano Reviews*, 4 (2013) 1–14.
- [68] K. Donaldson, F.A. Murphy, R. Duffin, C.A. Poland, Asbestos, carbon nanotubes and the pleural mesothelium: A review of the hypothesis regarding the role of long fibre retention in the parietal pleura, inflammation and mesothelioma, *Particle and Fibre Toxicology*, 7 (2010) 5.
- [69] C.-W. Lam, J.T. James, R. McCluskey, S. Arepalli, R.L. Hunter, A review of carbon nanotube toxicity and assessment of potential occupational and environmental health risks, *Critical Reviews in Toxicology*, 36 (2006) 189–217.
- [70] M.S. Boyles, L. Young, D.M. Brown, L. MacCalman, H. Cowie, A. Moisala, F. Smail, P. J. Smith, L. Proudfoot, A.H. Windle, Multi-walled carbon nanotube induced frustrated phagocytosis, cytotoxicity and pro-inflammatory conditions in macrophages are length dependent and greater than that of asbestos, *Toxicology in Vitro*, 29 (2015) 1513–1528.
- [71] K. Kostarelos, The long and short of carbon nanotube toxicity, *Nature Biotechnology*, 26 (2008) 774–776.
- [72] P. Sanpui, X. Zheng, J.C. Loeb, J.H. Bisesi Jr., I.A. Khan, A.N. Afrooz, K. Liu, A.R. Badireddy, M.R. Wiesner, P.L. Ferguson, et al. Single-walled carbon nanotubes increase pandemic influenza A H1N1 virus infectivity of lung epithelial cells, *Particle and Fibre Toxicology*, 11(2014) 66.
- [73] C.P. Firme, P.R. Bandaru, Toxicity issues in the application of carbon nanotubes to biological systems, *Nanomedicine: Nanotechnology, Biology and Medicine*, 6 (2010) 245–256.
- [74] J. Du, S. Wang, H. You, X. Zhao, Understanding the toxicity of carbon nanotubes in the environment is crucial to the control of nanomaterials in producing and processing and the assessment of health risk for human: A review, *Environmental Toxicology and Pharmacology*, 36 (2013) 451–462.
- [75] S. Lanone, P. Andujar, A. Kermanizadeh, J. Boczkowski, Determinants of carbon nanotube toxicity, *Advanced Drug Delivery Reviews*, 65 (2013) 2063–2069.

- [76] P. Jackson, N.R. Jacobsen, A. Baun, R. Birkedal, D. Kühnel, K.A. Jensen, U. Vogel, H. Wallin, Bioaccumulation and ecotoxicity of carbon nanotubes, *Chemistry Central Journal*, 7 (2013) 154.
- [77] J.N. Mwangi, N. Wang, C.G. Ingersoll, D.K. Hardesty, E.L. Brunson, H. Li, B. Deng, Toxicity of carbon nanotubes to freshwater aquatic invertebrates, *Environmental Toxicology and Chemistry*, 31 (2012) 1823–1830.
- [78] H. Ali-Boucetta, A. Nunes, R. Sainz, M.A. Herrero, B. Tian, M. Prato, A. Bianco, K. Kostarelos, Asbestos-like pathogenicity of long carbon nanotubes alleviated by chemical functionalisation, *Angewandte Chemie International Edition*, 52 (2013) 2274–2278.
- [79] O. Renn, M.C. Roco, Nanotechnology and the need for risk governance, *Journal of Nanoparticle Research*, 8 (2006) 153–191.
- [80] A.W. Mohammad, Y. Teow, W. Ang, Y. Chung, D. Oatley-Radcliffe, N. Hilal, Nanofiltration membranes review: recent advances and future prospects, *Desalination*, 356 (2015) 226–254.
- [81] N. Ghaffour, T.M. Missimer, G.L. Amy, Technical review and evaluation of the economics of water desalination: current and future challenges for better water supply sustainability, *Desalination*, 309 (2013) 197–207.
- [82] K.P. Lee, T.C. Arnot, D. Mattia, A review of reverse osmosis membrane materials for desalination—development to date and future potential, *Journal of Membrane Science*, 370 (2011) 1–22.
- [83] V.K. Upadhyayula, S. Deng, M.C. Mitchell, G.B. Smith, Application of carbon nanotube technology for removal of contaminants in drinking water: A review, *Science of the Total Environment*, 408 (2009) 1–13.
- [84] D. Zhou, L. Zhu, Y. Fu, M. Zhu, L. Xue, Development of lower cost seawater desalination processes using nanofiltration technologies—a review, *Desalination*, 376 (2015) 109–116.
- [85] V.G. Gude, Desalination and sustainability – an appraisal and current perspective, *Water Research*, 89 (2016) 87–106.
- [86] E.M.V. Hoek, A.K. Ghosh, Nanotechnology-based membranes for water purification, in: Anita Street, Richard Sustich, Jeremiah Duncan, Nora Savage (Eds.), *Nanotechnology Applications for Clean Water*, 1st edition, William Andrew Books, Norwich, NY, USA, imprint of Elsevier (2008), pp. 47-58.
- [87] C.-F. de Lannoy, E. Soyer, M.R. Wiesner, Optimizing carbon nanotube-reinforced polysulfone ultrafiltration membranes through carboxylic acid functionalisation, *Journal of Membrane Science*, 447 (2013) 395–402.
- [88] H.A. Shawky, S.-R. Chae, S. Lin, M.R. Wiesner, Synthesis and characterisation of a carbon nanotube/polymer nanocomposite membrane for water treatment, *Desalination*, 272 (2011) 46–50.
- [89] M.J. O’Connell, P. Boul, L.M. Ericson, C. Huffman, Y. Wang, E. Haroz, C. Kuper, J. Tour, K. D. Ausman, R.E. Smalley, Reversible water-solubilization of single-walled carbon nanotubes by polymer wrapping, *Chemical Physics Letters*, 342 (2001) 265–271.

- [90] T. Fujigaya, N. Nakashima, Non-covalent polymer wrapping of carbon nanotubes and the role of wrapped polymers as functional dispersants, *Science and Technology of Advanced Materials*, 16 (2016) 1–21.
- [91] X. Qu, P.J. Alvarez, Q. Li, Applications of nanotechnology in water and wastewater treatment, *Water Research*, 47 (2013) 3931–3946.
- [92] L. Dumeé, J. Lee, K. Sears, B. Tardy, M. Duke, S. Gray, Fabrication of thin film composite poly (amide)-carbon-nanotube supported membranes for enhanced performance in osmotically driven desalination systems, *Journal of Membrane Science*, 427 (2013) 422–430.
- [93] A.W. Thornton, A. Ahmed, M. Mainak, H.B. Park, A.J. Hill, Ultrafast transport in nanotubes and nanosheets, in: Ying (Ian) Chen (Ed.), *Nanotubes and Nanosheets: Functionalisation and Applications of Boron Nitride and Other Nanomaterials*, CRC Press, Boca Raton, FL, USA, 2015, p. 271.

### **FURTHER READING**

- [1] N.V. Priezjev, A.A. Darhuber, S.M. Troian, Slip behavior in liquid films on surfaces of patterned wettability: comparison between continuum and molecular dynamics simulations, *Phys. Rev. E* 71 (2005) 041608.
- [2] C. Lee, S. Baik, Vertically-aligned carbon nano-tube membrane filters with superhydrophobicity and superoleophilicity, *Carbon* 48 (2010) 2192–2197.
- [3] A. Sabir, M. Shafiq, A. Islam, A. Sarwar, M.R. Dilshad, A. Shafeeq, M.T.Z. Butt, T. Jamil, Fabrication of tethered carbon nanotubes in cellulose acetate/polyethylene glycol-400 composite membranes for reverse osmosis, *Carbohydr. Polym.* 132 (2015) 589–597.
- [4] M.M. Pendergast, E.M.V. Hoek, A review of water treatment membrane nanotechnologies, *Energy Environ. Sci.* 4 (2011) 1946–1971.
- [5] P.A. Schulte and F. Salamanca-Buentello, Ethical and scientific issues of nanotechnology in the workplace, *Environmental Health Perspectives* 115 (2007) 5–12).

**CHAPTER 3**  
**POLYETHERSULFONE/CARBON NANOTUBE MIXED-MATRIX MEMBRANES FOR**  
**WATER TREATMENT: CURRENT STATUS AND FUTURE PROSPECTS**

---

**Summary of the chapter**

This review discusses in great detail the scope of the work carried to date on PES/MWCNT membranes over the past 8 years, with particular emphasis on their synthesis and modification methods, different morphological structures displayed by the membranes and how they impact the resultant membrane performance, as well as their use in water and wastewater treatment. Furthermore, the review aims to provide the reader with useful insights on the different roles played by MWCNTs in the modification of PES-based MMM physicochemical properties; that is, the inclusion of MWCNTs into the PES matrices does not; in all cases yield significant improvements in membrane performance and structural properties. Summary remarks and future perspectives conclude the review.

**Keywords:** polyethersulfone, carbon nanotubes, mixed-matrix membranes, ultrafiltration, modification strategies, morphological structure, surface properties

### 3.1. Introduction

Membrane separation technology has emerged as a promising technological solution for addressing the worldwide water crisis, which includes both water shortage and deteriorating water quality. Owing to their wide pore size range (2 – 50  $\mu\text{m}$ ), ultrafiltration (UF) membranes particularly find use in the fractionation and pre-treatment stages of wastewater and seawater desalination [1]. Membrane are used as a support substrates for the production of thin film composite (TFC) nanofiltration (NF) and reverse osmosis (RO) membranes, which are consequently used in the removal of smaller-sized contaminants [2]. In addition, the larger pore sizes of UF membranes allow for high water permeability and low operational pressure thus bringing a further reduction in the operating costs [3].

Amongst the several currently available polymers, polyethersulfone (PES) has become the polymer of choice for the fabrication of laboratory-scale and industrial-scale UF membranes and other membrane types. This is due to its excellent mechanical properties, good thermal stability, operation over a broad range of temperature and pH values, as well as good chemical resistance to aliphatic hydrocarbons, alcohols and acids [4, 5]. Furthermore, PES can be easily processed into various configurations and modules. Despite possessing several advantages and benefits, the hydrophobic nature of PES makes it prone to fouling, thus limiting the long-term application of PES-based UF membranes in water filtration. Fouling of UF membranes is typically caused by hydrophobic interactions between the foulants present in the feed solution and the membrane surface, which leads to adsorption of proteins and particulate matter on the membrane surface and within the membrane pores (Fig. 3.1)[6].

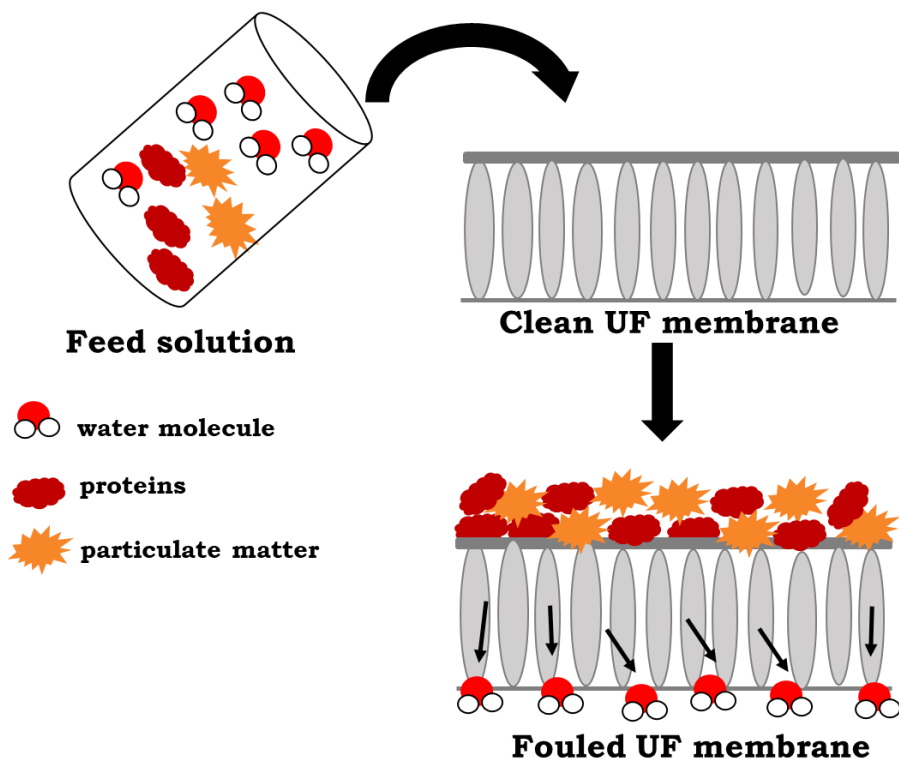


**Figure 3.1** Schematic depiction of membrane fouling in UF membranes.

It is well known that the attachment of the foulants into the membrane (the foulants are commonly hydrophobic) can be greatly reduced by making the surface of the membrane hydrophilic [7]. To this end, several research strategies have been directed towards the improvement of the hydrophilic properties of PES. These strategies, which are detailed in the latter section of this chapter, include but are not limited to, hydrophilic polymer blending, plasma oxidation and incorporation of nanomaterial additives (also called nanoadditives) [8-13]. Examples of nanomaterials that have been used as additives include carbon nanotubes (CNTs), graphene, graphene oxide (GO) as well as inorganic nanoparticles (e.g. titanium dioxide ( $\text{TiO}_2$ ), silicon dioxide ( $\text{SiO}_2$ ), iron oxide ( $\text{Fe}_2\text{O}_3$ ) and silver (Ag) nanoparticles).

The incorporation of nanoadditives into conventional polymeric materials provides an efficient alternative approach for the enhancement of the functionalities, surface properties and overall performance of these polymers. Modification of PES-based membranes with nanoadditives has been shown to produce membranes possessing the dual physicochemical properties of the nanoadditive and polymeric PES components [14]. For example, the incorporation of CNTs possessing different surface functionalities into PES polymeric membrane matrices has been widely employed in the production of PES/CNT mixed-matrix membranes (MMMs), with the aim of improving the structural and performance properties of the PES UF membrane such as hydrophilicity, mechanical strength, permeability, selectivity as well as antifouling properties [9, 15-22].

The use of CNTs in the modification of PES membranes and many other polymer-based membranes is driven largely by their excellent physicochemical properties such as high aspect ratio, low density, high mechanical strength and stiffness, superior adsorptive property and high flexibility [23, 24]. Additionally, the use of CNTs as nanofillers in PES membrane matrices has specifically been demonstrated to address the two challenges related to: (i) permeability-selectivity trade-off; and (ii) fouling encountered during membrane filtration applications [25]. However, it is important to note that intrinsically, CNT surfaces are chemically inert and likely to form agglomerates or clusters due to van der Waals interaction forces between the nanotubes. Ultimately, the existence of van der Waals forces results in inherently weak interactions and poor interfacial adhesion between the CNTs and the polymeric membrane materials. In addition, the hydrophobic nature of the CNTs makes it difficult for the CNTs to adequately disperse in the solvent and membrane matrix. Such a non-compatible dispersion process gives rise to intra-CNT

agglomeration, which ultimately leads to a decline in the overall compatibility between the CNT and the membrane structural matrix.

The resultant PES/CNT MMM sub-layer structure prepared from CNT bundles will therefore consist of non-selective voids in the sub-layer, which leads to a reduction in the mechanical strength of the membrane brought about by an inefficient stress transfer to individual nanotubes [26, 27]. Therefore, surface functionalisation of CNTs with functional group moieties or hyper-branched polymers, which could potentially transform the hydrophobicity of CNTs in a significant way and thus carry over the desired hydrophobicity property into the target hydrophilic structure, is necessary. The adoption of such a strategy has an added benefit of addressing other unintended and undesirable challenges associated with the entanglement and agglomeration of the CNTs [25, 28].

The hydrophilic or polar characteristic associated with the CNT surface is responsible for facilitating interfacial binding between the polar CNTs and the polar organic solvents [29]. Moreover, the hydrophilic properties brought about by the surface oxidation of CNTs reduces the trade-off between permeability and selectivity resulting from the electrostatic repulsion [25]. A reduction in the electrostatic repulsion implies that a negatively charged contaminant in feed water will be prevented from attaching into a membrane surface by electrostatic repulsion forces while water will be strongly attracted and efficiently transported through the PES/CNT mixed-matrix membrane [25].

From the discussion above, it is evident that the uniform dispersion of CNTs in organic solvents and polymer matrices is a critical issue that cannot be overlooked if high-performance MMMs containing these cylindrical carbons are to be prepared. In the majority of studies where functionalised or oxidised CNTs are used for the modification of PES membranes, multi-walled carbon nanotubes (MWCNTs) using chemical vapour deposition (CVD) are used instead of single-walled carbon nanotubes (SWCNTs). This is because CVD-synthesised MWCNTs can be produced in very large quantities and relatively cheaply when compared with their SWCNTs counterparts. In addition, MWCNTs retain some of the desirable characteristics of CNTs that are required for membrane modification [27], [30]. Recent advances in the scale-up of MWCNTs have also lowered the prices of MWCNTs by a factor of 2 or 3 over the past decade [31].

For reasons mentioned above, an approach involving the use of MWCNTs (instead of SWCNTs) in the modification of PES-based membranes has been adopted for this research study. Such an approach forms part of a research strategy predicating that carbon nanomaterials and other nanotechnology-based products have the potential to significantly transform and improve conventional water treatment technologies and systems such as membrane technologies. This research is therefore anchored on the various applications of MWCNTs in the modification of membranes.

In the previous chapter, the different carbon nanotube-based membrane types (*i.e.* vertically aligned CNT membranes *vis-à-vis* MMM CNT membranes), their prospects and sustainability as a solution towards addressing some of the current problems associated with water desalination, were discussed in detailed. The current knowledge pertaining to CNT exploitation in desalination

was summarised and the extent to which the fluid transport properties and chemical functionalities in CNTs necessitate high water fluxes and controllable salt rejection required for desalination were discussed. In order to build on what was discussed in the previous chapter, this literature review is focused on any progress made in the research work relating to the fabrication, functionalisation and applications in water treatment of PES/MWCNT-based MMMs. Specifically, the review commences with a detailed discussion of aspects relating to synthetic procedures for accessing the target membranes, with special attention being paid to how the morphological structures affect the properties and performance of the resultant target membranes. A further important objective of this literature review was to show the current state of knowledge in relation to the underlying theme of this study, namely how the competitive effect of the two important membrane properties (i.e. hydrophilicity and morphological structure of membranes) impacts on the performance of the PES/MWCNT membrane. The review concludes with a discussion on the various applications of PES/MWCNT based MMMs from a water treatment perspective.

### **3.2. Synthesis procedures for preparing PES/MWCNT mixed-matrix membranes**

The main purpose of the adaptation of nanotechnologies in membrane fabrication and modification is to control the membrane microstructure and performance properties so that the membrane is tailor-made for a particular purpose. For example, the UF membranes fabricated using the phase-inversion process generally have an asymmetric structure comprising of a skin layer, a porous sub-layer and support structure. On the other hand, the interfacial polymerisation method used for the fabrication of NF and RO membranes allows for the addition of an active thin film on top of the asymmetric structure. Each of the layers (i.e. the thin-film and support layers) comprising the thin-film composite membrane structure can be independently optimised to control the resultant

membrane performance [32]. Moreover, the nanomaterials can be added either in the support layer or thin-film layer or in both layers in order to induce an improvement of the structural and performance properties of the membrane. The structural differences between an asymmetric and thin-film composite membrane are illustrated in Fig. 3.2.

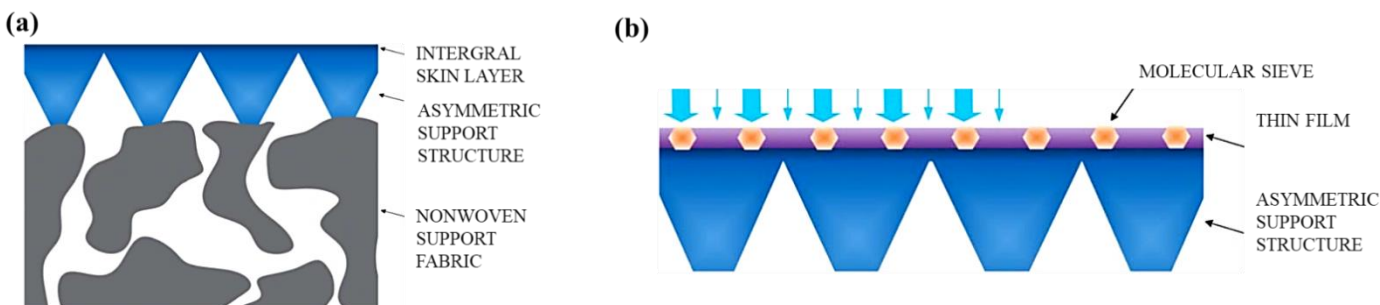


**Figure 3.2** Cross-sectional depiction of: (a) an asymmetric structure; and (b) thin-film composite membrane structure. Reproduced with permission from [33].

This section details the synthesis and modification procedures that are generally adopted for the fabrication of PES/MWCNT MMMs and how the membrane structure obtained in the presence of functionalised MWCNTs influences the physicochemical properties and performance behavior of the target membrane. The most commonly employed procedures for the fabrication of PES/MWCNT fabrication (i.e. phase-inversion method, interfacial polymerisation and spray-assisted layer-by-layer assembly) are discussed in detail in the following sub-sections.

### 3.2.1. Phase-inversion by immersion precipitation

The phase-inversion method has become a useful technique for the preparation of various types of membranes with desired configurations, morphological structures and performance properties.

The phase-inversion process can be induced by a non-solvent, vapour or temperature change [34]. The non-solvent induced phase separation (NIPS) method (also called immersion precipitation method) is commonly used for the fabrication of PES-based MMMs that contain functionalised MWCNTs [13, 16]. The various steps involved in the phase-inversion process are depicted in Fig. 3.3.

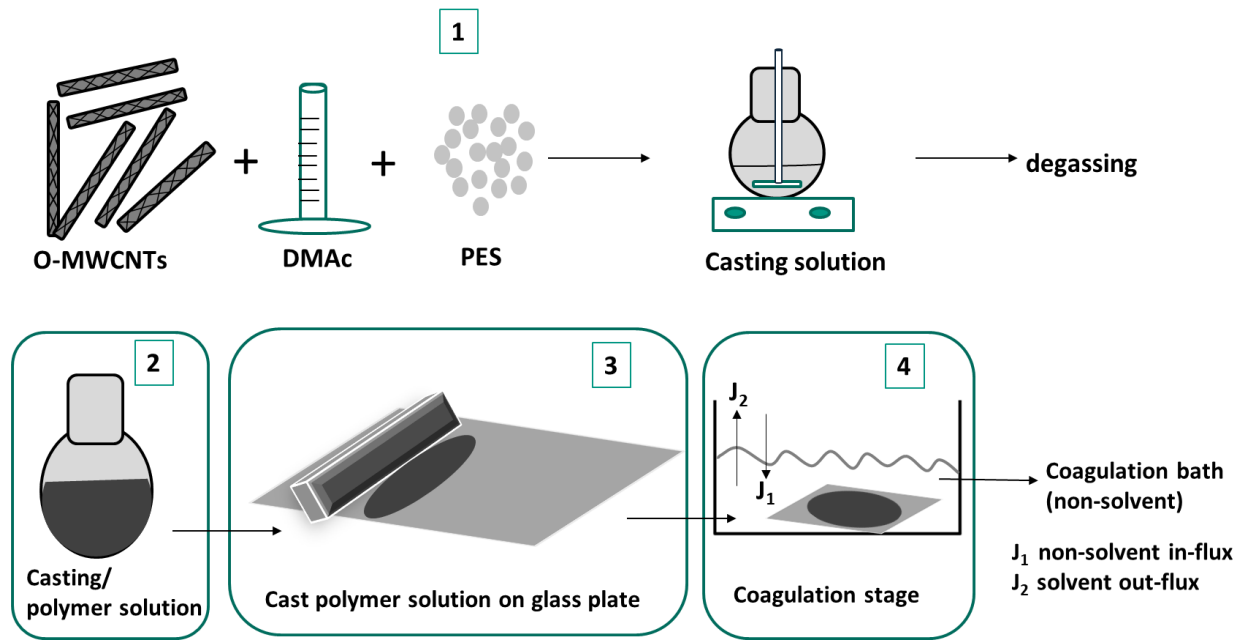


**Figure 3.3** Phase-inversion by immersion precipitation process for preparation of UF membranes.

In the first step, the target polymer such as PES is first dissolved in a solvent possessing good polymer miscibility; good miscibility basically means that the difference between the solubility parameters of the polymer and solvent should be negligible to ensure strong polymer-solvent interaction [35]. Based on the polymer type and the desired membrane morphology, different temperatures are used when dissolving the polymer in the selected solvent. In some cases, the polymer is dissolved at room temperature [36]. Typical temperatures used for complete dissolution of the PES range from 60 to 80 °C [16, 28].

For Step 2, the prepared polymer solution is allowed to settle under vacuum conditions to allow the removal of any gas bubbles produced during the dissolution stage. Ultrasonication over a predetermined duration is usually employed as an alternative method for degassing the casting solution. The degassing step is crucial in order to avoid the formation of pinholes and defects on the membrane. Step 3 involves coating the degassed solution on a support fabric or directly into a glass substrate using a casting knife that has been set at a predetermined thickness. The coating process is followed by immersion of the polymer into a non-solvent coagulation bath. A non-solvent that is miscible with the solvent but immiscible with the polymer should be used. Contact between the polymer solution and the non-solvent (as shown in Step 4) will cause the polymer to precipitate due to solvent–non-solvent exchange (Fig. 3.3.) [37]. During this process, two types of phase transitions take place, namely:

- (i) liquid-liquid phase separation, in which the completely miscible polymer solution crosses the binodal boundary layer to enter the two-phase region in the phase diagram; and
- (ii) solidification, as a result of the increase in viscosity of the polymer solution to a certain value, thereby restricting the movement of polymer chains.

At this point, the polymer solution solidifies in order to fix the membrane microstructure [38]. Since the polymer film solidifies during the solvent-non-solvent exchange, the miscibility of the solvent and non-solvent is important [39]. The key factors that influence the phase separation kinetics and the resultant membrane structure include the polymer concentration, the choice of solvent-non-solvent system, the composition of the polymer solution (i.e. the presence of non-

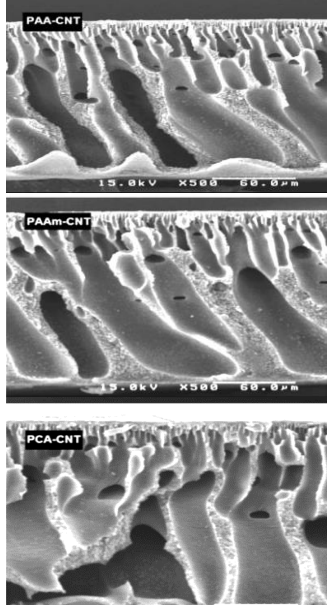
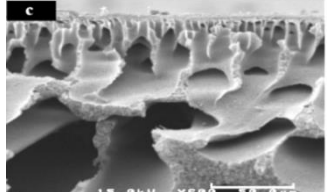
solvent additives in the dope solution), the coagulation bath temperature and the conditions under which the solution is cast (*i.e.* relative humidity and solvent evaporation prior to immersion) [40]. A comprehensive review on how each of these factors influences the phase-inversion process has been undertaken by Guillen et al. [39].

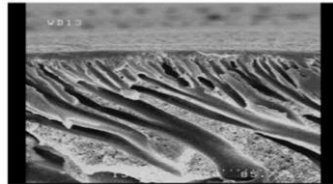
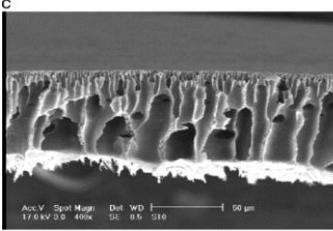
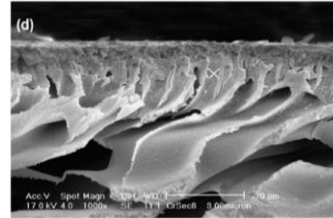
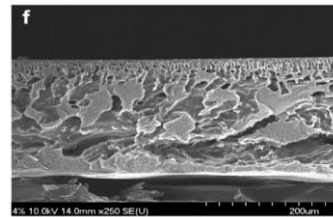
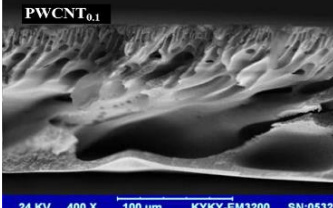
As previously mentioned, the phase-inversion method is also used for the preparation of PES UF membranes containing nanomaterial additives such as MWCNTs. In this method, the MWCNTs are first dispersed in an appropriate solvent by ultrasonication prior to addition of the polymer [29]. During the coagulation step, the hydrophilic functionalised MWCNTs enhance the rate of exchange between the solvent and non-solvent (non-solvent influx and solvent outflux expressed as  $J_1$  and  $J_2$ , respectively, in Step 4 in Fig. 3.3 [13, 18, 25] while forming part of the solidified polymer membrane film. Therefore, the presence of these functionalised MWCNTs as non-solvent additives in the PES casting solution has a major influence on the kinetics of the phase-separation process and the resultant membrane morphology. The increased demixing rate results in: (i) the formation of sub-layer with finger-like structures and macrovoids; (ii) reduced skin layer thickness; and (iii) large surface pores [13, 16, 20, 29]. The mechanism of formation and evolution of finger-like structures during the coagulation process are discussed in detail in subsequent sections. In this regard and as shown in Fig. 3.3.a, PES/MWCNT membranes prepared using the phase-inversion method have an asymmetric structure consisting of two layers, namely: a dense or thin skin layer and a porous sub-layer with macropores [16]. The top layer is formed first at the interface where the casting solution and non-solvent come into contact. The ratio of non-solvent inflow to solvent outflow is fundamental for the structural formation of the top layer [38].

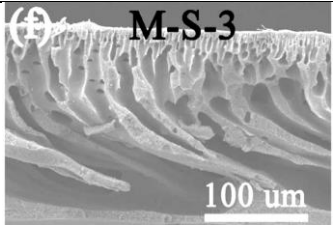
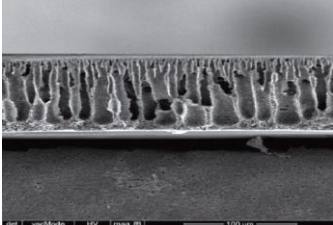
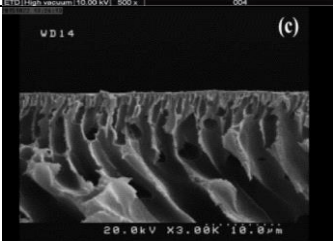
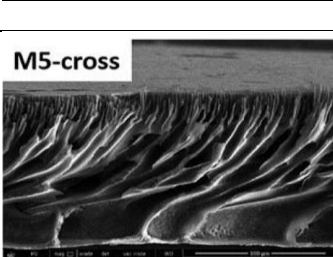
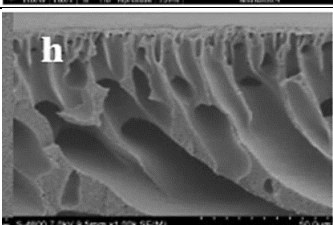
The presence of long finger-like and macrovoid structures in the membrane sub-layer is viewed as ideal as they act as microchannels, which allow the free flow of water molecules. Therefore, the presence of long finger-like and macrovoid structures effectively reduces flow resistance across the membrane. In the majority of studies where MWCNTs have been used as additives or nanofillers, the finger-like morphology of macrovoids is almost inevitable. Whereas this morphology is preferable since it offers low resistance to water flow, the macrovoids and finger-like structures are mechanically weak points and lead to reduced mechanical strength of the membrane. Nonetheless, the issue of low mechanical strength is normally combated through the use of support fabrics during the polymer solution coating stage of membrane formation. Therefore, it is still possible to generate a macrovoid-free PES membrane structure in the presence of MWCNTs by: (i) allowing the solvent to evaporate prior to immersion of the coated glass plate into the coagulation medium; (ii) addition of solvents such as propanol or isopropanol (which have a low affinity for the solvent of choice to dissolve the polymer) in the coagulation bath; and (iii) use of extremely high polymer concentrations. Although all of these strategies can be carried out in the absence of support fabrics, they can yield high mechanical strength of the fabricated membranes. However, the adoption of only one of these strategies would make the resultant membrane substructure very dense thus leading to extremely low fluxes. We have previously demonstrated the possibility of creating self-supporting, macrovoid-free PES membrane substructures in the presence of oxidised MWCNTs with reasonably high water fluxes and high mechanical strength [28]. The formation of such macrovoid-free PES membrane substructures is ascribed to the existence of hydrogen bonding interactions amongst the high molecular-weight polyethylene glycol, water and oxidised non-solvent MWCNTs additives in the PES/sulfonated

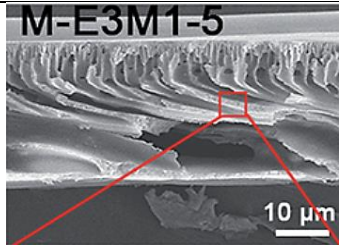
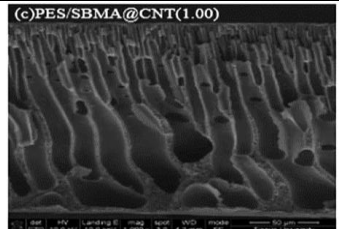
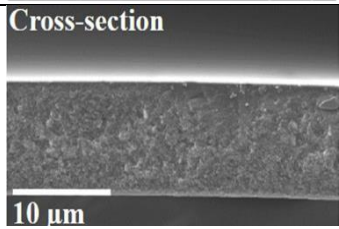
polysulfone casting solution, which result in the formation of an open porous sponge-like cross-sectional structure.

**Table 3.1** A summary of the structural properties and performance of PES/MWCNT membranes prepared via phase-inversion method for water treatment applications

Base polymer + solvent, coagulation bath temperature	Polymer concentration	Nanoadditive	Membrane type/process	*Membrane sub-layer structure	**Membrane performance	Ref
PES + DMAc, DI H <sub>2</sub> O @ 20 °C	20 wt. %	PAA-MWCNTs, PAAm-MWCNTs, PAC-MWCNTs	UF		PWF = all modified membranes had higher water flux than bare PES (25 – 31 L/m <sup>2</sup> .h) @ 4 bar Rejection of whey proteins = 97% FRR = 95%	[19]
PES + DMAc, DI H <sub>2</sub> O @ room temp.	20 wt. %	PAA-MWCNTs	NF		PWF = 40 L/m <sup>2</sup> .h @ 4 bar Rejection Na <sub>2</sub> SO <sub>4</sub> = 80%, NaCl = ~52% FRR = 97%	[20]

PES + DMAc, DI H <sub>2</sub> O (temp. not specified)	18 wt.%	PCL-MWCNTs	UF		PWF = 61 L/m <sup>2</sup> .h @ 8 bar Rejection Cd <sup>2+</sup> = 27% R <sub>ir</sub> (%) = 88.9%	[22]
PES + DMAc, DI H <sub>2</sub> O @ 25 °C	16 wt.%	NH <sub>2</sub> -MWCNTs	UF		PWF = 184 L/m <sup>2</sup> .h @ 3 bar Rejection BSA = ~86.5% FRR = 46%, R <sub>t</sub> = 90.2%	[41]
PES + DMAc, DI H <sub>2</sub> O @ 20 °C	18 wt.%	COOH-MWCNTs	NF		PWF = ~7 L/m <sup>2</sup> .h @ 4 bar Rejection Na <sub>2</sub> SO <sub>4</sub> = 80% FRR = 87.7%, R <sub>ir</sub> (%) = 12%	[13]
PES + NMP, DI H <sub>2</sub> O (temp. not specified)	20 wt.%	COOH-MWCNTs	UF		PWF = ~ 40 L/m <sup>2</sup> .h @ 3.5 bar Rejection NOM = ~50%	[16]
PES +DMAc	18 wt.%	PSS-MWCNTs	NF		PWF = ~ 14.5 L/m <sup>2</sup> .h @ 3.5 bar Rejection dye = ~99% at 800mg/l dye feed solution	[42]

PES + DMAc, DI H <sub>2</sub> O @ 10 °C	19 wt.%	SLS-MWCNTs	UF		PWF = 500 L/m <sup>2</sup> .h @ 1 bar Rejection BSA = ~97.5% FRR = 89.9%	[43]
PES + DMAc, DI H <sub>2</sub> O @ room temp.	15 wt.%	Pb (II) imprinted-MWCNTs	UF		PWF = ~320 L/m <sup>2</sup> .h @ 1 bar Adsorption Pb <sup>2+</sup> = 14.15 mg/g FRR = 93% (adsorption), 96% (desorption)	[44]
PES + DMF, DI H <sub>2</sub> O @ 25 °C	16 wt.%	COOH-MWCNTs, OH-MWCNTs	UF		OWF = 115 L/m <sup>2</sup> .h @ 2 bar, for COOH-MWCNTs OWF = 93.8 L/m <sup>2</sup> .h @ 2 bar for OH-MWCNTs	[21]
PES + DMF, DI H <sub>2</sub> O (temp. not specified)	17 wt.%	PVP-MWCNTs	UF		PWF = 270 L/m <sup>2</sup> .h @ 1 bar Rejection BSA = 96.4%, FRR = 95%, Rir (%) = 4.8%	[45]
PES + DMAc, DI H <sub>2</sub> O (temp. not specified)	18 wt.%	COOH-MWCNTs	NF		PWF = 42.7 L/m <sup>2</sup> .h @ 4 bar Rejection Na <sub>2</sub> SO <sub>4</sub> = 87.2%, Rejection MgSO <sub>4</sub> = 72.7%, Rejection NaCl = 24.7%	[46]

PES + DMAc, DI H <sub>2</sub> O (temp. not specified)	16 wt.%	PMTAC- MWCNTs, PEGMA-MWCNTs	UF		PWF = 464.6 L/m <sup>2</sup> .h @0.5 bar Rejection BSA = 96.2%, FRR = 91.4% Bacterial killing: <i>E. coli</i> = 99%, <i>S. aureus</i> = 99%	[47]
PES + DMF, DI H <sub>2</sub> O (temp. not specified)	16 wt.%	SBMA-MWCNT	UF		PWF = ~150 L/m <sup>2</sup> .h @1 bar Rejection BSA = ~100%, FRR = 98.9%	[48]
PES/SPSf + DMAc, DI H <sub>2</sub> O @ 25 °C	22 wt.%	COOH-MWCNTs	UF		PWF = 560 L/m <sup>2</sup> .h @1 bar Rejection BSA = 99.9%, FRR = 92%	[28]

\*All figures used in the Table 3.1 have been reproduced with permission from cited references.

\*\*Membrane performance results are based on the best performing composite membrane in the series.

### 3.2.1.1. Phase diagrams for predicting the structural properties of membranes

Phase diagrams and thermodynamic expressions for the chemical potentials in the system are necessary for proper description of the diffusion process when a coated glass plate is immersed in a non-solvent bath [49]. The structure of membranes prepared *via* a phase-inversion method results from a phase change of an initially stable polymer solution that has been brought to an unstable state. To this end, the state and equilibrium composition of polymer solutions can be well depicted using ternary phase diagrams [50]. Phase diagrams are constructed in order to study the thermodynamics of membrane formation.

As shown in Fig. 3.4, a phase diagram is represented by a triangle [39]. Whereas each corner of the triangle represents one of three components (polymer, solvent, and non-solvent), any point within the triangle is representative of a mixture of the three components [39]. Furthermore, phase diagrams can be divided into three regions (Fig. 3.4) namely: (I) one-phase region where all components are miscible; (II) two-phase region, where the system separates into a polymer-rich (polymer matrix) and polymer-poor phase (pores); and (III) a solidification region where solid-liquid demixing occurs [51]. The mutual affinity between solvent and non-solvent affects the position of the binodal curve in the phase diagram. If the affinity between the solvent and non-solvent is very high, the binodal curve will gravitate towards the polymer-solvent axis in the phase diagram, and less non-solvent will be required to induce liquid-liquid phase separation for pore formation [37, 39]. In a ternary phase diagram, the binodal curve is fixed at a constant temperature. However, in the presence of a non-solvent additive such as polyethylene glycol (PEG) in the polymer solution, the binodal curve moves toward the polymer/solvent axis [52]. This means that the precipitation rate increases, and instantaneous demixing is as a result accompanied by the formation of finger-like pores and macrovoids.

Therefore, the final membrane morphology is strongly related to the initial casting solution composition, the position of the binodal curve and the precipitation path [53].

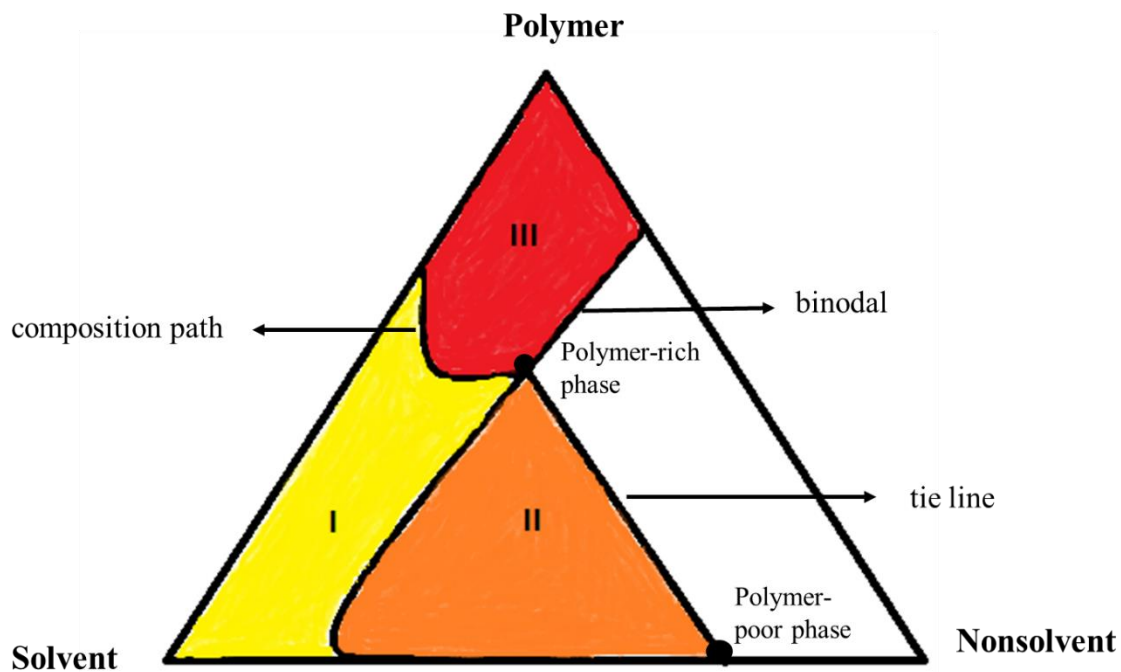


**Figure 3.4** Schematic representation of a ternary phase diagram.

In order to construct a phase diagram, cloud-point determination experiments are conducted whereby a polymer solution is titrated against a non-solvent for the system; the end-point of which is determined visually based on the formation of a turbid/cloudy solution [54]. The more non-solvent (water) needed for the end-point to be reached, the greater the shift of the binodal curve towards the polymer/non-solvent axis on the phase diagram. The opposite is true when less amount of non-solvent is required for the titration end-point. As already stipulated, the closeness of the binodal curve to the polymer-solvent axis is associated with instantaneous demixing and the formation of finger-like membrane morphology. On the other hand, delayed demixing results due to binodal curve shifting farther away from the polymer-solvent axis

The membrane formation process is governed by both thermodynamic and kinetic factors. The use of additives in polymeric solutions changes the dope solution composition and therefore affects its thermodynamic stability. Moreover, the dope solution rheology is affected, and this in turn changes the precipitation kinetics during phase-inversion [55]. In this regard, the effect of non-solvent additives on the thermodynamic stability of the polymeric casting solution can then be predicted from the cloud point experiments. However, cloud-point determination experiments cannot be used to predict the effect of functionalised MWCNTs on the resultant membrane morphology of PES-based polymer solutions since the polymeric casting solutions that contains the MWCNTs are dark coloured, which makes it impossible to visually observe the formation of a turbid solution, (i.e. when the end-point of the titration has been reached). However, it is possible to carry out cloud-point titrations and construct ternary phase diagrams for other metal nanoparticle incorporated PES membranes [56].

#### **3.2.1.2. PES/MWCNT membrane configurations: Flat-sheet versus hollow fibre**

The phase-inversion process mentioned in the preceding section can be adapted for preparation of modified PES based membranes possessing both flat-sheet and hollow fibre configurations. The images of MWCNT polymer composite membranes with flat-sheet and hollow fibre configurations are shown in Fig. 3.5.

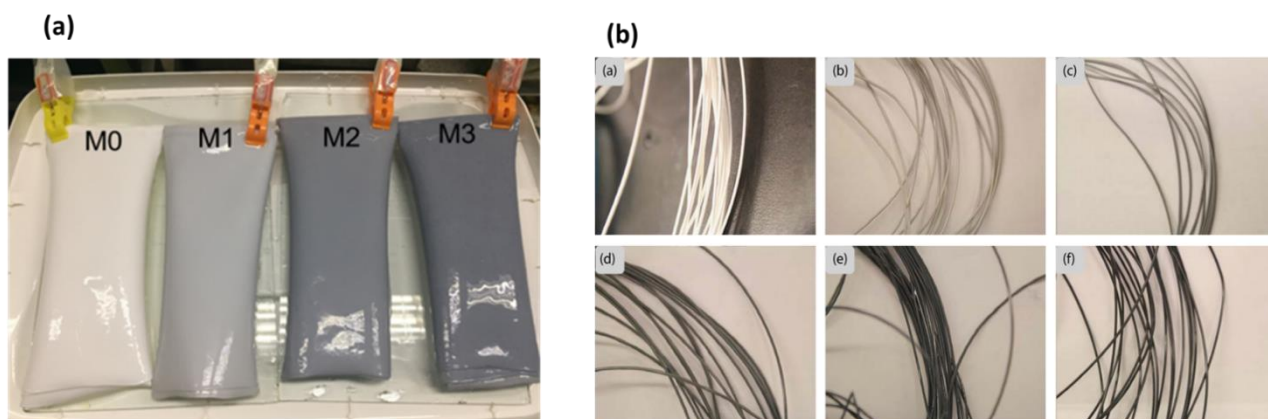


**Figure 3.5** Photographic images of O-MWCNT containing polymer composite membranes with different configurations (a) flat-sheet and (b) hollow fiber membrane. Reproduced with permission from [28, 57].

In both configurations, an increase in the intensity of the greyish colour of the membranes is observed when the MWCNT content is increased. Usually, the flat-sheet configuration is suitable for lab-scale applications and optimisation of the casting solution composition that is necessary to generate a particular membrane structure suitable for a specific use. From this optimised composition, hollow fibre membranes can then be prepared [58]. Compared to flat-sheet membranes, these hollow fibre membranes are more desirable for large-scale applications owing to their large module area or volume and high resistance to pressure [58].

As shown in Fig. 3.3, the procedure for the fabrication of flat-sheet membranes using the phase-inversion process is quite straightforward and requires minimal operation, space and apparatus (casting knife with adjustable gap height, glass support substrate and coagulation bath). In contrast, numerous factors need to be considered for the fabrication of hollow fibre membranes. These factors include the rapid phase-inversion kinetics and the interfacial mass transfer during the spinning process [59]. Other additional spinning parameters that need to be taken into account for the fabrication of hollow fibre membranes include: (i) the structure and dimension

of the spinneret; (ii) polymer dope viscosity; (iii) flow rate of the bore fluid; (iv) the dope extrusion rate; (v) the length of the air-gap; and (vi) take-up speed [4]. However, the fundamental thermodynamic and kinetic rules of polymeric casting solutions hold for both membrane configurations. For example, when MWCNT incorporated alumina/PES hollow fibre membranes were prepared by Feng et al. [60], it was established that an increase in the MWCNTs content led to an increase in the casting solution viscosity which was subsequently accompanied by a reduction in the number of large macrovoids in the membrane cross-sectional structure. Although configurations were different, the surface and cross-sectional morphologies of PES/MWCNT membranes were found to be the same.

### **3.2.2. Interfacial polymerisation**

The interfacial polymerisation (IP) process is generally used for the deposition of an active thin-film polyamide layer on top of a support membrane substrate (usually polysulfone or PES membrane) in order to generate thin-film composite (TFC) membranes. The IP process generally involves the immersion of a microporous support membrane into an aqueous polyamine solution for a specific period of time followed by an immersion into an organic phase polyacid solution. The organic phase solution selected should be immiscible with the aqueous phase solution so that the reaction occurs at the interface between the two solutions [33]. A thin polyamide film layer is then deposited on the surface of the support substrate within a few minutes of the reaction. The heating or curing step following thin-film deposition is necessary to complete the interfacial reaction and to ensure adequate cross-linking of the polyamide film, which subsequently influences the permeability, selectivity and stability of the membrane [51]. A schematic depiction of the entire IP procedure is shown in Fig. 3.6.

The polyamide film is synthesised by reacting the amine and acyl chloride functionalities of the diamine and diacid monomers, as shown in Fig. 3.7.

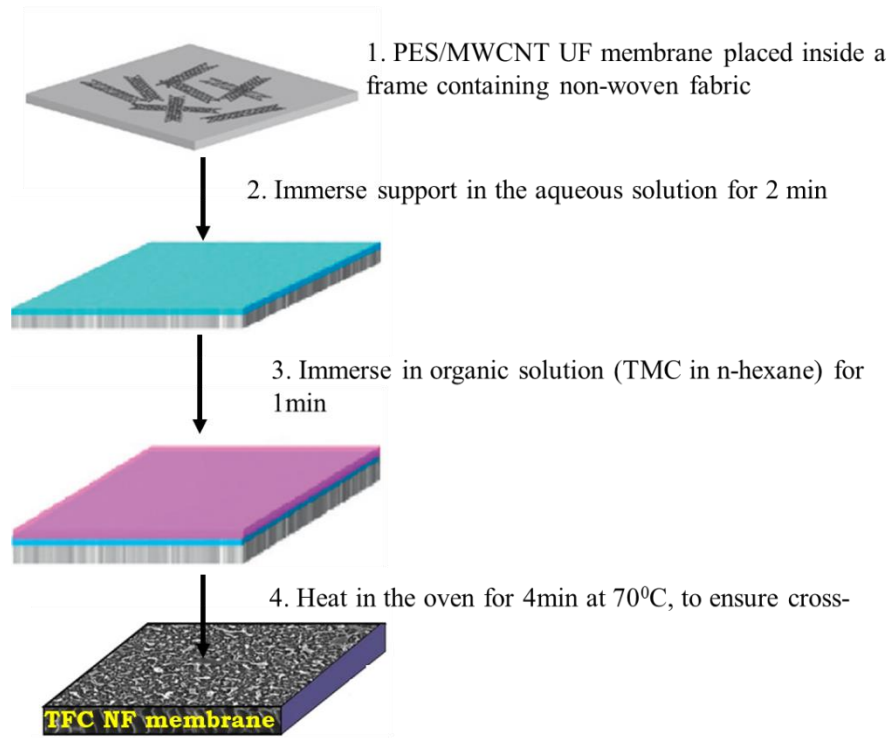


**Figure 3.6** Schematic diagram of the interfacial polymerisation method.

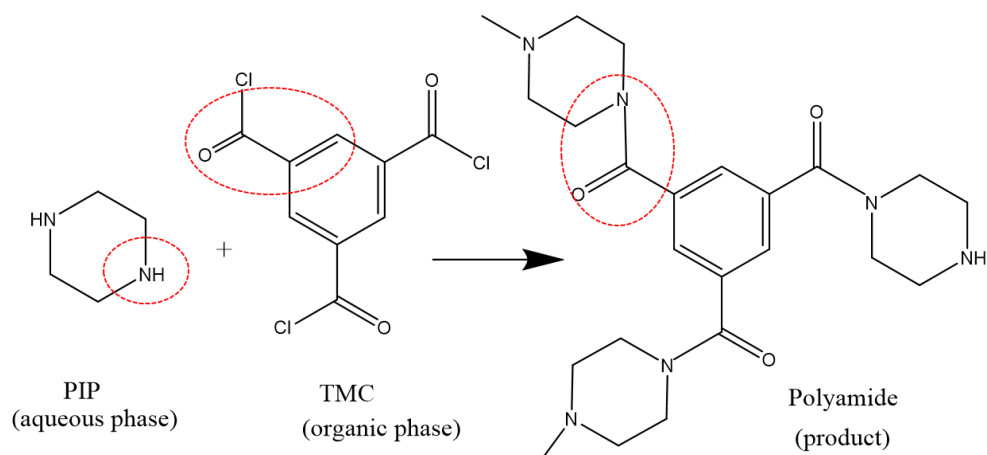


**Figure 3.7** Interfacial polymerisation reaction between TMC and PIP for the formation of the polyamide film.

The type of the aqueous and organic phase monomers that react at the top of the support substrate is important as it determines whether the final TFC membrane will be used for NF or RO applications. For example, the standard IP reaction between piperazine (PIP) in the aqueous phase with trimesoyl chloride (TMC) in the organic phase is commonly used for the formation of TFC NF membranes, while the TFC RO membrane is prepared using *m*-phenylenediamine (MPD) and TMC [61]. The TFC FO membranes can be prepared using either PIP or MPD as aqueous monomers and TMC as the organic phase monomer.

One of the key advantages of TFC membranes prepared *via* the IP process is that each layer (support layer and active polyamide layer) can be individually optimised to achieve a membrane with the desired selectivity and permeability properties while providing good mechanical strength and compression resistance [62]. To this end, functionalised MWCNTs typically find application in the modification of the active polyamide layer (dispersed in either aqueous or organic phase) [63] or in the enhancement of the mechanical strength and permeability of the support substrate. A comparative study on the effect of the PES/MWCNT substrate with neat PES substrates on the performance of the resultant TFC FO membrane fabricated *via* the IP process was undertaken by Wang et al. [64]. That study established that the TFC FO membrane prepared from the PES/MWCNT UF substrate displayed a superior performance in terms of water permeability and salt rejection (97% NaCl rejection) compared to the membrane fabricated using neat PES substrates (78% NaCl rejection) and the commercial HTI-derived TFC FO membrane (89% NaCl rejection). The superior performance of the PES/MWCNT UF derived membrane was ascribed to the porous structure of MWCNT that was incorporated into the PES support, which resulted in significantly decreased internal concentration polarisation and higher water flux [64].

A similar study by Son et al. [65] compared the performance of TFC RO membranes fabricated on PES/MWCNTs substrates to that fabricated on pristine PES substrates, and found that the functionalised TFC membranes showed enhanced water permeability (90% enhanced water flux in the brackish water reverse osmosis process) and higher organic fouling resistance compared to the bare TFC membrane. The enhanced performance was attributed to the increased hydrophilicity, enhanced pore properties and more negatively charged surface of the PES/MWCNT substrates (Fig. 3.8) [65].

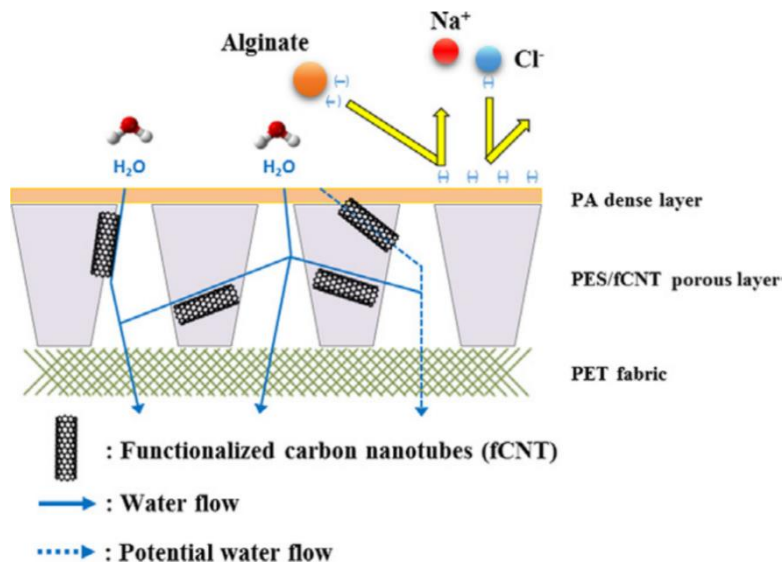


**Figure 3.8** Schematic diagram of TFC RO membrane fabricated on PES/fMWCNT substrate. Reproduced with permission from [65].

Choi et al. [66] investigated how functionalisation of TFC membrane with a PES/MWCNT substrate affects the performance of the resultant TFC membrane towards seawater desalination and wastewater reclamation using the forward osmosis process. Relative to the pristine TFC membrane, the study reported a 72% increase in the water flux of the PES/MWCNT-functionalised TFC membrane, which was attributed to the enhanced hydrophilicity of the PES/MWCNT substrate. Moreover, an 8% decline in the water flux of the PES/MWCNT

functionalised TFC membrane, emanating from the electrostatic repulsive effects caused by the negatively charged membrane surface, was recorded during the organic matter fouling test [66].

### **3.2.3. Spray-assisted layer-by-layer assembly**

Spray-assisted layer-by-layer (LbL) is a membrane surface modification technique in which polyelectrolyte (cationic and anionic) solutions are alternatively deposited on the membrane substrate to create multi-layers on the membrane surface. The spray-assisted LbL procedure allows for the deposition of highly-ordered and densely-packed multilayers into a large substrate area, while maintaining light transmittance [67].

Liu et al. [68] has fabricated PES/CNT membranes with improved antifouling properties using the LbL technique. Briefly, an anionic solution consisting of poly(sodium 4-styrenesulfonate) (PSS) and oxidised MWCNTs and a cationic solution consisting exclusively of poly(diallyl-dimethyl ammonium chloride) (PDDA) were prepared individually in deionised water by means of ultrasonication. Commercial PES membranes were then vertically positioned and their surface alternatively spray-deposited with anionic and cationic solution polyelectrolyte multilayers. Between each deposition step, the PES substrate was rinsed with DI water before the assembly of the next layer. The PSS/MWCNT layer served both as the initiating and terminating layer. Furthermore, the PSS/MWCNTs were attached into the PES substrate via hydrogen bonding, while the cationic PDDA layer interacted with the PSS/MWCNTs layer via electrostatic and van der Waals forces [69]. The configuration of spray-assisted layer-by-layer for the modification of PES membrane is shown in Fig. 3.9.

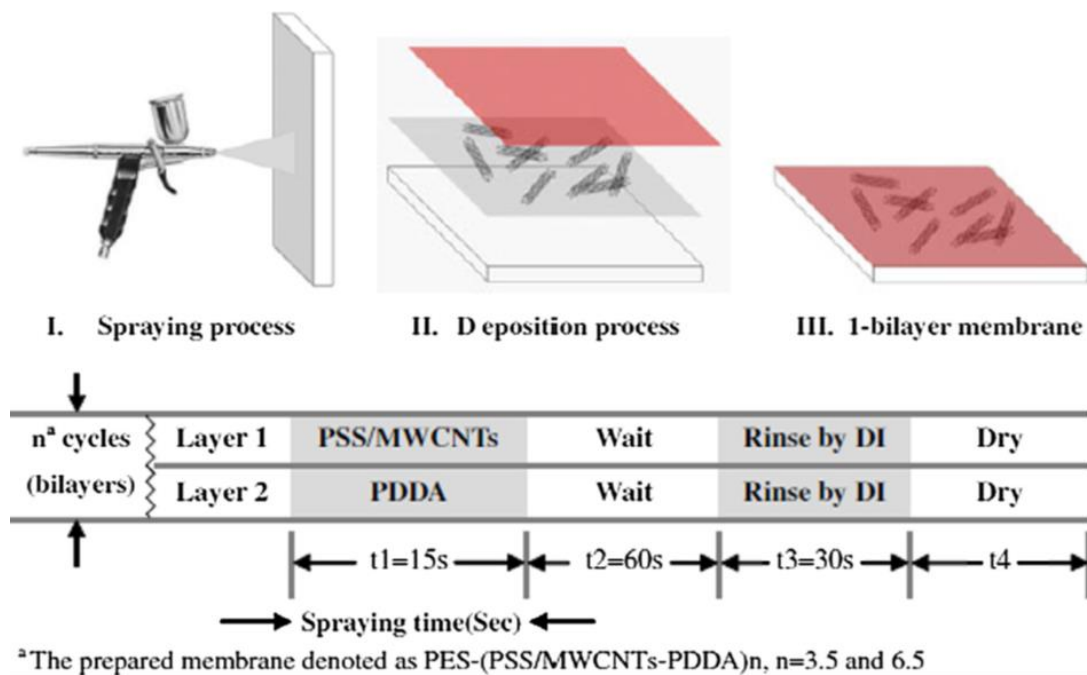


**Figure 3.9** Spray-assisted layer-by-layer deposition method used for the preparation of polyelectrolyte multilayer PES/MWCNT membranes. Reproduced with permission from [69].

### 3.3. Morphological structures of PES/MWCNT membranes

During the phase-inversion process, a one-phase polymer solution is separated into two phases; a solid polymer-rich phase (from which the membrane structure is formed) and a liquid polymer-poor phase (from which the membrane pores are generated) [70]. There are two classical cross-sectional membrane morphologies that PES/MWCNT MMMs fabricated via phase-inversion methods may possess, namely: (i) finger-like structures with macrovoids; or (ii) sponge-like morphology (discussed briefly in Section 3.1). Whereas low precipitation rates during the coagulation process generally yield membranes with sponge-like structures (known as type I membranes), high or fast precipitation rates give rise to membranes with finger-like structures or macrovoids (known as type II membranes). Type II membranes generally have low salt rejection rates but high fluxes by virtue of their finger-like sub-layer structure [71]. The finger-like morphology is commonly achieved for asymmetric PES based MMMs

membranes fabricated in the presence of MWCNTs via the phase-inversion process while the sponge-like morphology is seldom achieved. In the section that follows, the formation mechanism and the factors that influence the formation of each of the mentioned cross-sectional structures will be discussed.

### **3.3.1. Finger-like structures with macrovoids versus sponge-like structure**

#### **3.3.1.1. Evolution of finger-like structure and macrovoids**

Reuvers et al. [71] classified two possible types of cross-sectional membrane morphologies as type I membranes (*i.e.* membrane structures that are formed from delayed onset of liquid-liquid demixing), and type II membranes (membrane structures that are formed from instantaneous liquid-liquid demixing). Whereas no macrovoids are formed for type I membranes, macrovoids are always formed for type II membranes except in cases where the polymer concentration or non-solvent concentration in the casting solution exceed a certain minimum value [71]. The cross-sectional sub-layer of membranes formed by immersion precipitation is generally made up of finger-like structures or macrovoids.

Apparently, no uniform view exists within the research community on the presence of finger-like structures and macrovoids in the membrane sub-layer. Some researchers are of the opinion that their presence makes a positive contribution towards the ultrafiltration processes since the finger-like channels limit the flow resistance thus resulting in improved permeability of the membrane [39]. On the other hand, the presence of macrovoids in the membranes substructure is thought to be an undesirable structural irregularity that results in the weakening of the membrane and skin rupture, particularly under high pressure operations [34, 72]. Most published studies on the incorporation of functionalised MWCNTs into polymeric membrane

matrices, especially PES based membrane systems aimed at improving structural properties and performance of the membrane, have reported on the formation of finger-like structures and macrovoids in the membrane sub-layer (Table 3.1). The improvement in the structural properties and performance of the membranes is attributed to the hydrophilic nature of oxidised MWCNTs; that is, the rate of exchange between solvent and non-solvent is increased during the phase-separation process. As already stated, the presence of these finger-like structures and macrovoids tends to limit the mechanical strength properties of the MWCNT modified PES MMMs, more specifically for membranes fabricated in the absence of a support fabric, even though the incorporated O-MWCNTs may possess reinforcement properties. Therefore, the presence of finger-like structures and macrovoids may lead to membrane failure when the membranes are operated under high pressures. To this end, in the absence of support fabrics, an open, porous, spongy membrane structure that is macrovoid-free is highly desirable since it is mechanically stable and allows for good water permeability. The initiation of macrovoids in the membrane substructure has been linked to the nucleation of droplets of the polymer-poor phase in the immersed polymer solution. Based on this assumption, macrovoids are formed when some or all of the nucleated droplets expand to very large dimensions; however, the growth of droplets in the sponge-like substructure is stopped rapidly upon immersion of the polymer solution in the non-solvent coagulation bath[73].

### **3.3.1.2. Mechanisms of macrovoid formation**

According to Guillen et al. [37], finger-like macrovoids in the membrane substructure are formed by convective flow of non-solvent into the polymer–solvent solution. This convective flow arises from interfacial energy gradients at the polymer solution–non-solvent interface. Furthermore, convective non-solvent flow into the polymer solution is hindered by the

formation of a surface skin layer or viscous gel layer within the polymer solution film, which gives rise to the formation of a membrane layer with shorter or no finger-like structures and macrovoids. On the other hand, large finger-like macrovoids propagate the membrane cross-section only when non-solvent convective flow into the polymer solution film exceeds viscous hindrance forces, that is, when a good solvent, ample supply of good non-solvent and polymer solution of relatively lower viscosity are used [37]. Therefore, the state of the polymer solution prior to immersion in the coagulation bath is critical for determining the final membrane morphology. Therefore, determining or measuring the rheological properties of the casting solutions, particularly the viscosity prior to casting membrane and immersion into coagulation bath, is vital.

As proposed by Matz [74], a further understanding of the kinetics and membrane formation mechanisms taking place during the phase-inversion process can be attained through direct film observation with the assistance of a light transmission microscope. For analysis with light transmission microscope, a drop of polymer solution is thinly spread between glass slides and contacted with a non-solvent coagulant (usually water). Thereafter, the rate of precipitation is monitored under an optical microscope and recorded photographically. Carbon black particles or phenolphthalein are sometimes added to the casting solution, to enhance the visualisation of the currents and movements in the casting solutions and precipitation media [70]. Feng et al. [75] used the same technique to study the formation mechanisms leading to the morphological structure of sulfonated polyphenylenesulfone UF membranes possessing various compositions of the polyethylene glycol (PEG 400 Da). The sPPSU polymer solutions containing PEG displayed slower precipitation rates than polymer solutions without PEG (PEG0) (Fig. 3.10). The initiation of macrovoids was also found to be delayed by the addition of PEG into the polymer solutions.

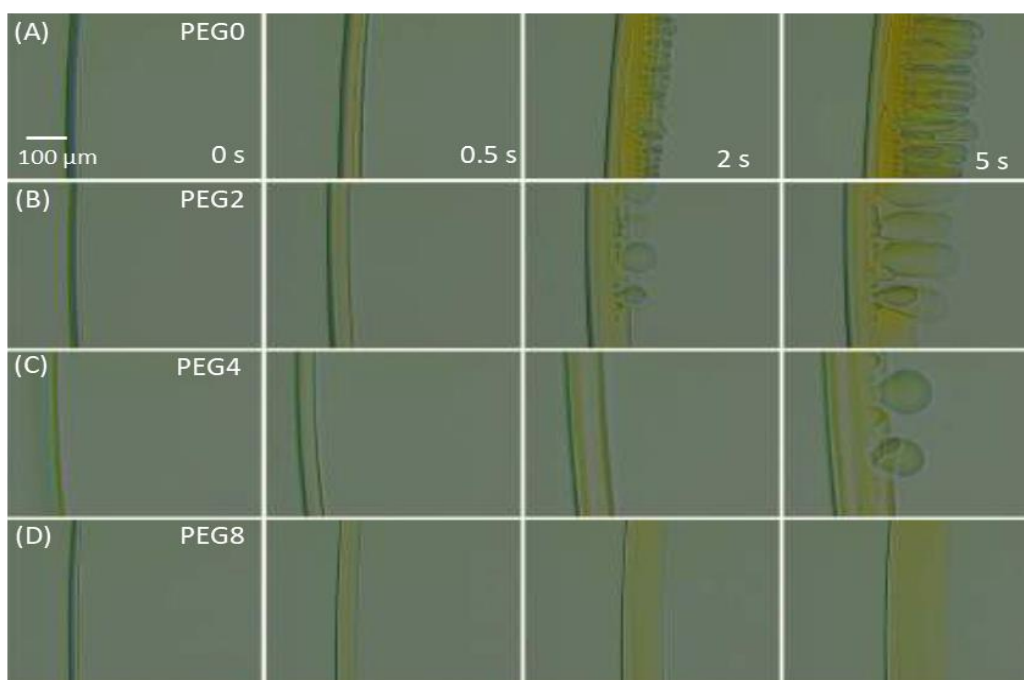


**Figure 3.10** Phase-inversion phenomena of sPPSU/NMP dope solutions modified with various compositional contents of PEG 400 Da: (A) 0 wt.% (PEG0), (B) 2 wt.% (PEG2), (C) 4 wt.% (PEG4) and (D) 8 wt.% (PEG8) in water. Reproduced with permission from [68].

The delay in the macrovoid initiation for various compositions of PEG was attributed to slower phase separation resulting from high solution viscosity, which effectively hinders the diffusional exchange between the solvent and non-solvent. At sufficiently high PEG composition (*i.e.* PEG8 in Fig. 3.10), an increase in the viscosity was found to facilitate the formation of the macrovoid-free structure [75]. It is important to note that the microscope visualisation technique enables real time measurement of void formation to be undertaken. Other than using only a small amount of material, this technique can also be used for the rapid evaluation of novel polymer-solvent-additive-non-solvent combinations. However, similar to cloud-point determination experiments, it is difficult to observe film formation in opaque polymer solutions (such as PES/MWCNT polymer solution) when using the microscope visualisation technique [37]. An alternative technique for measuring the precipitation rate has been suggested by Noel and Monnerie [76]. It involves measurement of the time from when

the polymer-coated glass plate is immersed in the coagulation bath to the time when the solution turns opaque or separates from the glass plate [76].

### **3.3.1.3. Formation of sponge-like structures**

As mentioned in the earlier sections, membrane cross-sectional morphology is determined by the polymer precipitation kinetics; rapid precipitation produces finger-like pores while a slow precipitation rate produces sponge-like structure. When the in-flux of the non-solvent from the coagulation bath and the out flux of solvent are nearly equal in magnitude, the net flux becomes small, and the polymer solution is slowly exposed to the non-solvent. Slow exposure of the polymer solution to non-solvents results in a slow precipitation rate and the formation of sponge-like pores. However, rapid precipitation is achieved when the magnitude of in-flux of the non-solvent far exceeds that of the net flux, thus leading to the production of finger-like pores [77].

Hollow fibre membranes and sometimes flat-sheet membranes possessing sponge-like cross-sectional structures are highly preferable in order to withstand the vigorous stretch and vibration occurring during the operation and chemical backwashing of the membrane [52]. According to Peng et al. [78], factors that may potentially aid macrovoid formation include non-solvent moving front, precipitation front, surface weakness, flow instability, capillary flow, moisture sorption and low viscosity. With such knowledge in mind, several strategies involving the suppression of macrovoid formation in the membrane sub-layer have been proposed. These strategies include:

- I. **Selection of solvent-non-solvent pair with low miscibility** – solvent-non-solvent pairs with very good miscibility such as DMAc and water or n-propanol are most likely to form membranes with large macrovoids. The difference in solubility parameters between the solvent and non-solvent pair can give an indication of the type of microstructure that the membrane will assume. If the difference between solubility parameters of the solvent and non-solvent is high, the non-solvent diffuses more easily into the polymer solution, leading to an increase in the exchange rate between solvent and non-solvent [79].
- II. **Increasing polymer concentration in the casting solution** – increasing the polymer concentration leads to an increase in casting solution viscosity thereby delaying the exchange rate between solvent and non-solvent during the coagulation stage and thus leading to the suppression of macrovoids.
- III. **Increasing solvent evaporation time** – increasing the evaporation time prior to immersion of coated glass plate into the coagulation bath leads to the formation of a more concentrated polymer region near the air–polymer solution interface, thus resulting in the formation of a dense skin layer with fewer macrovoid structures [80].
- IV. **Adding a non-solvent to the polymeric casting solution** or introducing organic additives such as poly(vinyl pyrrolidone) (PVP), PEG, or nanomaterial additives such as MWCNTs [37] - the presence of the non-solvent additives in the casting solution increases the viscosity of the casting solution, and other additives (e.g. high molecular-weight PEG) have the ability to improve pore interconnectivity thus leading to the elimination of macrovoids.

The factors described above seem to suggest that the elimination of macrovoid formation is necessary for a reduction in the fluidity of the casting solution, which leads to the inhibition of the diffusion exchange between solvent and non-solvent in the coagulation bath and ultimately the lowering of the phase-inversion rate [81]. However, any substantial increase in the polymer concentration as a means of increasing the viscosity of the dope solution may lead to operational difficulties because high polymer concentrations tend to give rise to other issues such as increased dense layer thickness and substructure resistance, which subsequently reduce membrane flux [82, 83]. Therefore, a sole increase in the polymer solution viscosity may not be an appropriate and cost-effective approach for eliminating macrovoids in the membrane sub-layer. In other words, other factors such as decreasing the casting knife gap height (to decrease polymer solution thickness) and using different casting solutions or coagulation bath temperatures should be considered for the suppression of macrovoids.

It should be noted that the effect of the above-mentioned processing variables on the resultant membrane structure supersede those of the added nanoadditive. For example, Farahani et al. [84] investigated the effect of the polymer concentration on the structure of the PES membrane in the presence of several nanoadditives including OH-MWCNTs and COOH-MWCNTs. It was found that PES nanocomposite membranes fabricated using 15 wt.% polymer concentration displayed higher porosity and macrovoid formation in their substructure compared to membranes fabricated using 18 wt.% [84]. The observed results were attributed to the occurrence of a faster exchange rate between solvent and non-solvent at lower polymer solution viscosity. Furthermore, an additional increase in the loading of the nanoadditive at the two polymer concentrations evaluated failed to change the morphology of the membrane to sponge-like structure. On account of this, membrane synthesis conditions are usually optimised prior to the inclusion of MWCNTs or other nanoadditives. Thereafter, the functionalised

MWCNTs are incorporated into the optimised bare PES membrane in order to enhance the membrane performance. The processing variables that impact on the suppression of macrovoids and membrane structure are discussed in more detail in the following section.

#### **3.3.1.3.1. Effect of casting solution thickness on membrane structure**

The membrane cross-sectional morphology, especially the formation of macrovoids, is also dependent on the thickness of the cast solution. Vogrin et al. [85] established that macrovoids only appeared when the casting knife was set at a gap height thickness of 500  $\mu\text{m}$ ; compared to no macrovoids forming at lower gap height thicknesses of 150  $\mu\text{m}$  and 300  $\mu\text{m}$ . Li et al. [86] suggested that this occurrence is linked to the critical structure-transition thickness ( $L_c$ ) of the membranes; *i.e.*, the membrane structure possesses a macrovoid-free structure at gap height thickness levels that are lower than the  $L_c$ .

The  $L_c$  indicates a transition of the membrane morphology from a sponge-like to a finger-like structure when the membrane thickness is increased. This means that for a given dope solution there exists an  $L_c$  below which the membranes will show a fully sponge-like cross-sectional structure as well as an  $L_c$  above which the membranes exhibit mainly finger-like macrovoid structure [86]. Similar findings have also been reported by Feng et al. [86], whereby the sulfonated polyphenylenesulfone (sPPSU) polymer solutions were casted by varying the casting knife gap height from 100  $\mu\text{m}$  to 200  $\mu\text{m}$  [87]. The membrane morphology transitioned from a fully spongy structure to a combination of sponge and finger-like structures when the thickness of the cast solution was increased (Fig. 3.11). These results suggest that, apart from increasing the casting solution viscosity by merely keeping all other membrane formation parameters unchanged and reducing the thickness of the cast film of a given polymeric solution

to below the critical structure-transition thickness of the system, a sponge-like morphology can be obtained.

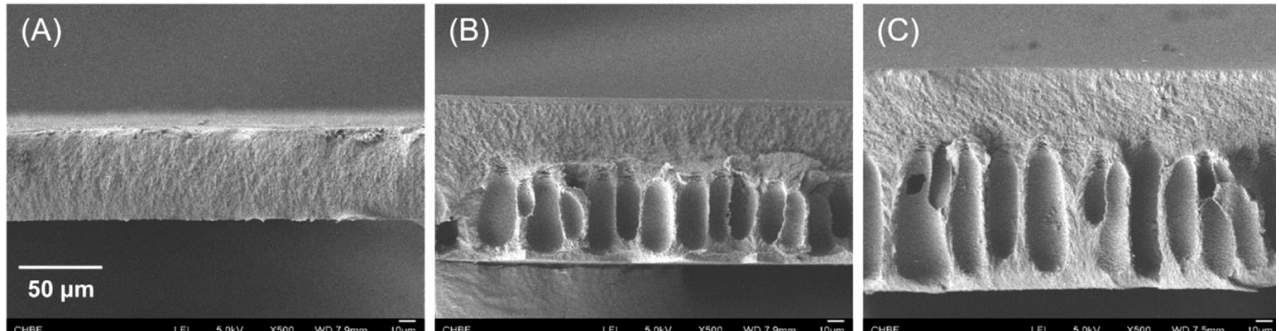


**Figure 3.11** SEM images of the flat-sheet membranes cast from 26% 2.5sPPSU polymer solution with the casting gap height of (A) 100  $\mu\text{m}$  (B) 150  $\mu\text{m}$  and (C) 200  $\mu\text{m}$ . Reproduced with permission from [87].

### 3.3.1.3.2. Addition of solvent into the coagulation bath

Careful selection of a coagulant for use in a particular polymer/additive/solvent system during phase separation process can yield an asymmetric membrane with or without macrovoids. Mulder [51] has reported that the selection of solvent/non-solvent system with low miscibility generally leads to the formation of a dense membrane structure with no macrovoids. Wang et al. [52, 88] have observed that finger-like membranes were transformed into sponge-like structures upon replacement of the water coagulant with alcohols. In order to obtain delayed onset of liquid-liquid demixing (to form type I membranes, without macrovoids) for casting solution with increased non-solvent content, the amount of the solvent in the coagulation bath will have to be increased [50]. According to Smolders et al. [49], for a ternary phase system consisting of cellulose acetate/acetone/water, a slight increase in the amount of water (non-solvent) added to the dope solution resulted in the transition from delayed onset of demixing

(with no macrovoids in the substructure) to instantaneous demixing that is accompanied by the formation of macrovoids. The addition of a specific minimum amount of non-solvent to the dope solution was sufficient to induce instantaneous demixing (the formation of type II membranes). On the other hand, in the ternary system of cellulose acetate/dioxane/water, an increase in the amount of solvent (dioxane) added to the coagulation bath led to the suppression of macrovoids (transition from type II to type I membranes) [49].

#### **3.3.1.3.3. Addition of non-solvent additives**

The addition of non-solvent additives to the dope solution has been shown to play an important role in the formation of a membrane structure that possesses improved separation performance [89]. In fact, the use of non-solvent additives in polymeric casting solutions is considered to be one of the most important parameters that controls the overall membrane morphology [52]. Xu et al. [52] investigated the individual influences of ethanol, methanol, *n*-propanol and water as non-solvent additives in the PES/NMP polymer solution. It was found that the morphology of the PES UF hollow fibre membrane changes slowly from long and wide finger-like structure through a thin finger-like structure to the sponge-like structure when the ethanol concentration in the dope solution was increased to 25 wt.% [4]. An appropriate amount of non-solvent additive in the dope solution apparently enhances the formation of macrovoids whereas a high loading of the non-solvent additive suppresses their formation due to a delayed demixing that occurs during membrane growth process [71, 90]. This suggests that, in addition to the presence of non-solvent in the dope solution, membrane morphology is strongly influenced by the amount of non-solvent used. PEG and PES are some of the most commonly used additives in polymeric casting solutions due to their ability to form pores during phase separation process. Since PEG is a weak non-solvent for polymers, its addition to the dope solution

reduces the solvency of the solvent while the ratio of polymer to solvent increases thus affecting the membrane formation process [55, 91]. An investigation by Arthanareeswaran et al. [92] of the effect of varying the concentrations of PEG 600 Da on the performance of PSf/sulfonated poly(ether ketone) (SPEEK) blend membrane has revealed that the addition of PEG 600 Da enhances the rate of exchange between the additive and non-solvent, which in turn leads to the formation of large macrovoids in the membrane sub-layer [92]. In addition, whereas pure water flux and MWCO of the membrane were found to increase with the content of the PEG 600 Da, the hydrolytic permeability was affected in a negative way (i.e. it decreased) [92]. Due to their lower mobility in the coagulation bath, Ma et al. [91] assert that an increase in the molecular weight of PEG leads to a higher number of PEG molecules being permanently trapped in the membrane matrix upon successful completion of the solvent and non-solvent exchange process. As a consequence, contact angles measured for the membrane were found to be smaller thus improving the membranes' hydrophilicity [91]. The addition of hydrophilic additives, such as PEG, to the casting solution has a dual effect on the membrane morphology. Therefore, not only does PEG facilitate the formation of macrovoids brought about by the intensification of thermodynamic instability of the casting solution, it also aids the suppression of macrovoids arising from increasing viscosity of the casting solution and improving pore interconnectivity [93].

As already discussed, in instances where functionalised MWCNTs were used as non-solvent additives in PES casting solutions, a preponderance of finger-like structures in the membrane sub-layer with macrovoids was noticeable [13, 15, 16, 94]. The formation of finger-like structures in the membrane sub-layer has been strongly linked to the hydrophilic nature of functionalised MWCNTs, which leads to a rapid exchange between the solvent and non-solvent during the coagulation stage. However, any further increases in the MWCNT loading lead to

the casting solutions becoming viscous, thus favouring a delay in the phase separation process that results in a reduction in the number of finger-like structures. This phenomenon concurs with results first reported over 30 years ago by Reuvers [71] and Smolders et al. [49], which propounded that the resultant membrane morphology is composed of either finger-like structures, a fully sponge-like structure or a combination of both membrane morphologies, depending on the loading of non-solvent additive in the casting solution.

#### **3.3.1.3.4. Coagulation bath temperature**

When a polymeric dope solution that is cast at high temperatures ( $\sim 60 - 80$  °C) is cooled down to room temperature prior to immersion into the non-solvent coagulation bath, liquid-liquid phase separation is induced prior to immersion in the non-solvent coagulation. This means that a decrease in the temperature of the casting solution leads to the formation of many nuclei, which cause phase separation before the non-solvent influx and thus inhibiting the formation of finger-like membrane morphology [38]. It has already been established that the formation of macrovoids occurs under rapid precipitation conditions, and the precipitation is often more rapid at high temperatures [93]. This means that the temperature of the coagulation bath also plays a significant role in determining the final membrane morphology. Furthermore, it is common knowledge that any increase in the temperature is accompanied by a decrease in the solution viscosity (as a consequence of the increase in kinetic energy of molecules). If the same notion is applied to the membrane formation processes, a decrease in the casting solution viscosity would most likely lead to instantaneous demixing, thus promoting the formation of membranes with finger-like structures and macrovoids. This phenomenon has also been confirmed by Zheng and co-workers [95] after studying how the viscosity of the polysulfone casting solution and the resultant membrane structure is influenced by casting solution and

coagulation bath temperatures. In that study [95], it was reported that an increase in the casting solution or coagulation bath temperatures led to a decrease in the viscosity of the casting solution; such a decrease in the viscosity subsequently led to the generation of large finger-like structures in the membrane sub-layer.

### **3.4. Influence of PES/MWCNT cross-sectional structure on membrane performance as measured by permeability and selectivity**

An enhancement of pure water flux and permeability of most PES/MWCNT MMMs is associated with the presence of finger-like structures in the membrane sub-layer [13, 16, 19]. Based on 3D simulation results generated by Shi et al. [96], finger-like macrovoids in UF and NF membranes have the lowest tortuosity and therefore exhibit the lowest flow resistivity. Moreover, it has been experimentally proven that the water permeance for the sponge-like membrane was much lower than that of finger-like membranes [96]. According to Lee et al. [97], the water flow velocity through finger-like macrovoids is nearly ten-fold higher than through the sponge-like regions, which exist between finger-like macrovoids. It has also been demonstrated that when the dense sponge-like regions constitute a larger portion of the support layer volume, a high pressure drop across a support layer is likely to occur, resulting in low water fluxes across the membrane [97]. During the fabrication of TFC membranes, when the sponge-like structure and closed macrovoid become predominant in the support layer, the overall water flux of the membrane can be reduced [97].

Yip et al. [77, 98] and Wang et al. [77, 98] suggested that an ideal support substrate for a TFC-FO membranes should be comprised of a combination of sponge-like and finger-like structures; that is, a thin layer of sponge-like structure near the top edge of membrane cross-section with

a fully finger-like structure underneath. Nevertheless, FO tests undertaken by Widjojo et al. [77, 98] have proven that the degree of hydrophilicity of membrane substrates is in fact a much stronger contributor to the enhancement of the water flux. Although the TFC membrane tested in the study by Widjojo and coworkers consisted of a fully sponge-like morphology, it displayed highest water flux (33.0 L/m<sup>2</sup>.h) reported in literature and salt flux (15 L/m<sup>2</sup>.h) compared to the TFC membrane with part finger-like structures in the membrane sublayer.

It is worth highlighting that a fully sponge-like structure with anti-fouling properties is desirable for long-term membrane stability. In contrast, Ghosh and Hoek investigated the impact of membrane support structure on the performance of TFC membranes and reported that more permeable and hydrophilic supports produced low permeability TFC membranes, whereas the highly porous and relatively hydrophobic supports produced more permeable TFC membrane [2]. However, Widjojo and co-workers [120] reported contradictory results; showing that porous, hydrophilic supports yield highly permeable TFC membranes.

It is quite clear that a big question still remains unanswered: is it the membrane hydrophilicity or presence of finger-like structures in the support layer that drives the improvement of the permeability of the TFC membranes? We are of the view that, as opposed to a dense sponge-like structure, a fabric-free support membrane structure with an open porous sponge-like morphology is beneficial for the enhancement of TFC membrane permeability and long-term performance stability.

### **3.5. Modification strategies for PES/MWCNT mixed-matrix membranes**

Surface modification or outer-wall functionalisation of MWCNTs with different functional groups such as  $-\text{CO}_2\text{H}$ ,  $-\text{OH}$ ,  $-\text{NH}_2$ ,  $-\text{SO}_3\text{H}$ , or  $-\text{CONH}_2$  is conducted to aid their dispersion as well as their interaction and compatibility with the solvent and the polymer. Such modification strategies facilitate the transformation of ordinary MWCNTs into multifunctional materials capable of being used in various reactions and processes. To this end, the incorporation of modified MWCNTs or the blending of PES polymeric matrix with hydrophilic polymers enable the surface properties of the resultant PES membrane to be altered with the aim of bestowing hydrophilic properties on this PES membrane that reduce its susceptibility to fouling. All of the surface modification strategies discussed in the following sub-sections share a common approach and goal namely incorporation of hydrophilic materials in the hydrophobic PES membrane matrix.

#### **3.5.1. Functionalisation of MWCNTs prior to inclusion in the PES matrix**

##### **3.5.1.1. Oxidation of MWCNTs to MWCNT-COOH and MWCNT-OH**

Oxidation of raw MWCNTs with strong acids or other oxidative media, allows for their purification and rids them of residual metal catalyst particles, amorphous carbon, and hydrocarbon gases used in their preparation. The oxidation process simultaneously introduces carboxyl ( $-\text{CO}_2\text{H}$ ) and hydroxyl ( $-\text{OH}$ ) functional groups into the outer walls of the MWCNTs [99, 100]. Not only does the presence of  $-\text{CO}_2\text{H}$  and  $-\text{OH}$  moieties endow the MWCNTs and ultimately the PES membrane with hydrophilic properties, but under alkaline conditions, they undergo deprotonation, become negatively charged and also impart the same negative charges into the membrane surface. During the coagulation stage of membrane formation,

functionalised MWCNTs migrate spontaneously to the membrane-water interface to alter the membrane surface properties such as hydrophilicity, surface charge and roughness [13, 16]. A negatively charged membrane surface has an added advantage in terms of solute retention mechanism in addition to size-exclusion mechanism; that is, negatively charged solutes or contaminants are prevented from settling into a negatively charged membrane surface based on electrostatic repulsion interactions, thus leading to high solute retention. Furthermore, in the case of salt retention, the Donnan exclusion mechanism comes into play, whereby a negatively charged membrane surface will have higher rejection values for divalent anions and monovalent cations than monovalent anions and divalent cations; the opposite is true for positively charged membranes [101].

Acid functionalisation is usually carried out under reflux conditions, whereby the desired amount of MWCNTs is refluxed (130 °C in a silicone oil bath) in a mixture of H<sub>2</sub>SO<sub>4</sub> and HNO<sub>3</sub> with mass ratio of around 3:1. Thereafter, the resultant acid functionalised MWCNTs are washed with plenty of distilled water until a neutral pH of the washing solution is obtained (equal to distilled water pH). Finally, the washed functionalised MWCNTs are dried in an oven at 120 °C [102, 103].

Generally, acid functionalisation of MWCNTs with oxygen-containing functional groups form the basis of which other subsequent functionalisation strategies such as amination (functionalisation with amine groups) or polymer grafting stem from. In essence, the new functional group or polymeric moiety is simply attached to the MWCNT via the reactive sites such as the carboxyl (–COOH) and hydroxyl (–OH) functional groups present on the side-walls of the MWCNT (Fig. 3.12). The acid treatment process opens up the nanotube end caps, and

shortens the nanotube length. Shorter nanotubes have an advantage of being uniformly dispersed in the membrane matrix and along the membrane surface.

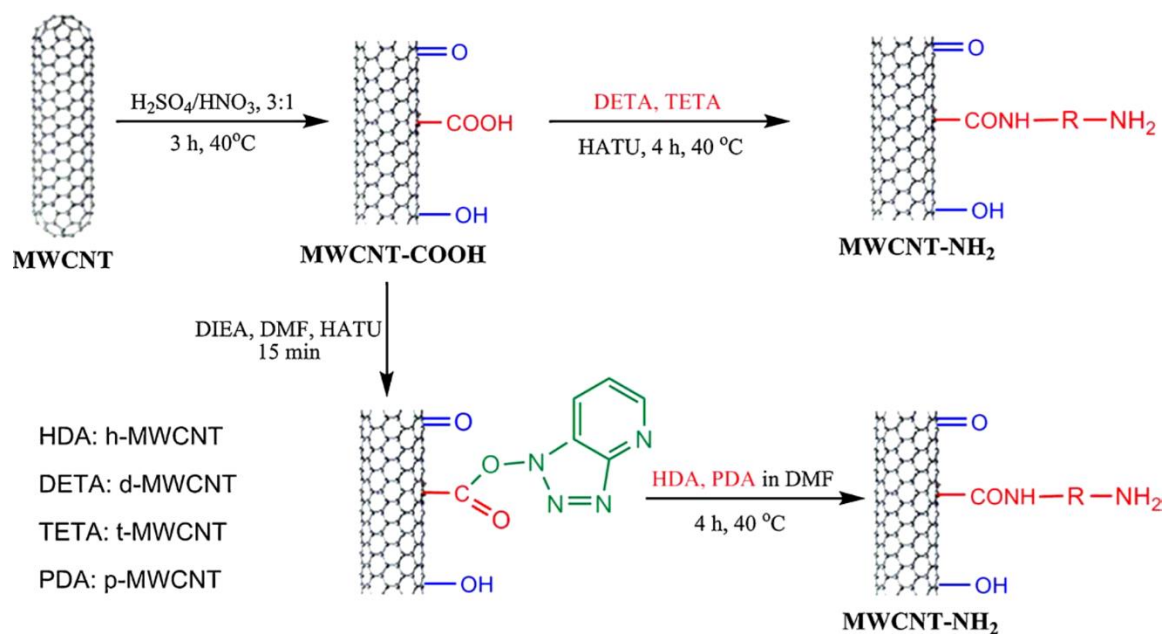


**Figure 3.12** Schematic representation for functionalisation of MWCNTs. Reproduced with permission from [104].

Using hydrothermal treatment of pristine MWCNTs in a potassium hydroxide solution, it is also possible to exclusively prepare hydroxyl functionalised MWCNTs (MWCNT-OH) that do not possess  $\text{-CO}_2\text{H}$  groups [105]. Briefly, following ultrasonication of pristine MWCNTs in a potassium hydroxide solution, the resultant suspension was autoclaved and heated at  $180^\circ\text{C}$  for 2 h. Thereafter, the resultant MWCNT-OH was purified by washing with deionised water until a neutral pH of the washings was obtained. As far as the modification of the PES membrane is concerned, a comparative performance analysis of MWCNT- $\text{CO}_2\text{H}$  incorporated and MWCNT-OH incorporated PES membranes was undertaken by Dehkordi et al. [21]. The study revealed that, at a low nanoadditive content, the  $\text{-CO}_2\text{H}$ -MWCNT/PES membrane displayed higher permeability compared to its MWCNT-OH counterpart [21]. The difference

in permeability was attributed to the difference in structural the geometries of the two functional groups (i.e.  $-\text{CO}_2\text{H}$  and  $-\text{OH}$ ) present in the membranes. Unlike the linear geometry of the  $-\text{OH}$  groups, the bent molecular geometry associated with the  $-\text{CO}_2\text{H}$  groups allows for the formation of cavities between the PES polymeric chains and  $-\text{CO}_2\text{H}$ -MWCNTs where the solvent is initially trapped. Outward diffusion of solvent during phase-separation process leaves behind empty spaces thus forming a porous  $-\text{CO}_2\text{H}$ -MWCNT/PES membrane structure with high permeability.

### **3.5.1.2. Amination of MWCNTs to $\text{NH}_2$ -MWCNTs**

Amine ( $-\text{NH}_2$ ) functionalisation of MWCNTs offers a wide range of reaction applications since the  $-\text{NH}_2$  functional group is highly reactive, possesses a wealth of chemistry and can therefore be reacted with many chemicals and polymers [104]. As already highlighted in section 4.1.1., acid functionalisation of MWCNTs with  $-\text{OH}$  and  $-\text{CO}_2\text{H}$  groups forms the basis from which other forms of MWCNTs modification stem from. This also holds true for amine functionalisation of MWCNTs. As shown in Fig. 3.13a, the initial step in the  $-\text{NH}_2$  modification of MWCNTs involves acid treatment of MWCNTs to introduce the carboxylic acid group moieties ( $-\text{CO}_2\text{H}$ ). Upon attachment of the  $-\text{CO}_2\text{H}$  into the MWCNTs, the  $-\text{CO}_2\text{H}$  is reacted with an amine-containing precursor (in this case polydopamine (PDA) dissolved in DMF solvent was used as a precursor) to produce the desired  $-\text{NH}_2$ -MWCNTs. The exact mechanism for the amination reaction, which is depicted in Fig. 3.13b, involves a transfer of electrons between an  $-\text{NH}_2$  and  $-\text{CO}_2\text{H}$ . Another commonly used strategy for the amination of MWCNTs is the acetylation of the carboxylic acid group of the of the MWCNT- $\text{CO}_2\text{H}$  using thionyl chloride ( $\text{SOCl}_2$ ) followed by reaction with a diamine [18, 106]. The  $\text{NH}_2$ -MWCNTs functionalised PES membranes prepared by Vatanpour et al. [18] displayed a significant

improvement in the antifouling properties of the membranes, which was ascribed to the generation of a more negatively charged surface possessing high hydrophilicity and lower surface roughness. Similar results involving higher BSA rejection, reduced surface roughness and improved antifouling properties compared to the neat membrane have been reported by Rahimpour et al. [41] following incorporation of the NH<sub>2</sub>-MWCNTs into the PES matrix.

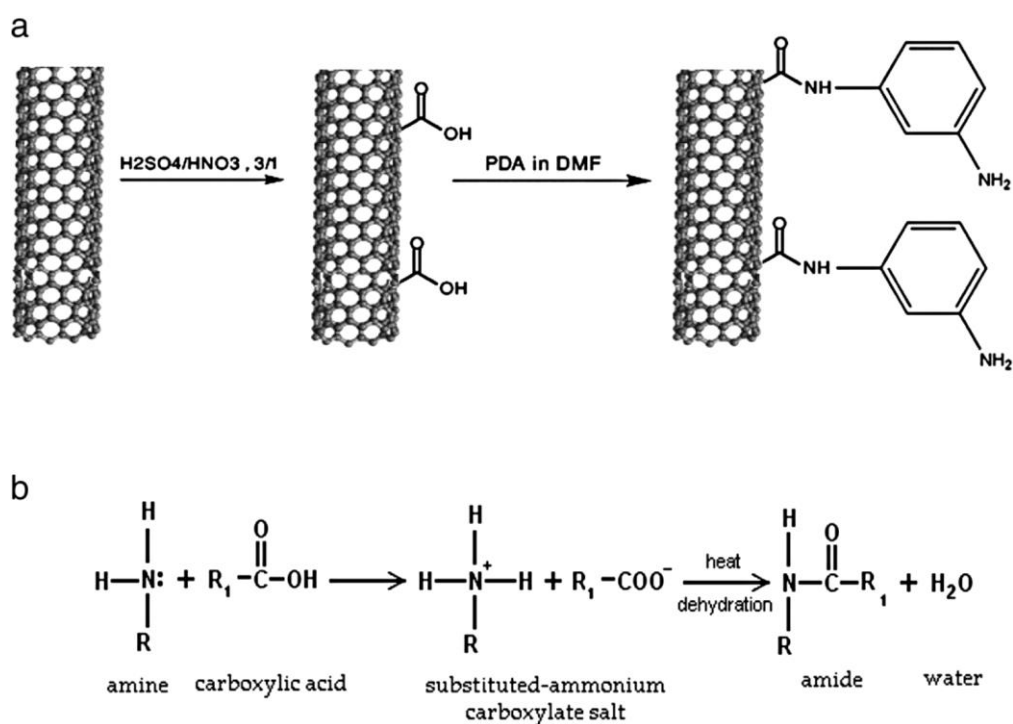


**Figure 3.13** (a) Procedure for amine functionalisation of MWCNTs; and (b) mechanism for amine functionalisation of MWCNTs. Reproduced with permission from [41].

### 3.5.1.3. Polymer-functionalised MWCNTs (by polymer grafting and polymer wrapping)

An ideal mixed-matrix nanocomposite membrane should be agglomeration-free. To fulfil this requirement, several types of MWCNT surface modification strategies (apart from acid functionalisation) have been adopted. One of these strategies involves the introduction of hyper-branched polymers into the outer walls of the MWCNT. Choi et al. [107] have reported

that the grafting of carboxylic acid-terminated hyperbranched poly(ether-ketone) into the MWCNT surface enables their dispersion in polar solvents even at a low degree of functionalisation. Daraei et al. [20] has conducted a water dispersibility test between raw MWCNTs and polyacrylic acid (PAA) modified MWCNTs by ultrasonication in water. Fig. 3.14 shows that the PAA modified MWCNTs remained dispersed in the solution one week following ultrasonication, whereas the raw MWCNTs began to separate and precipitate out of solution within 30 mins following ultrasonication. These results provide evidence that the presence of polar functional groups of PAA attached to the outer walls of the MWCNT improves the dispersibility and hydrophilic properties of MWCNTs in water as a hydrophilic medium.

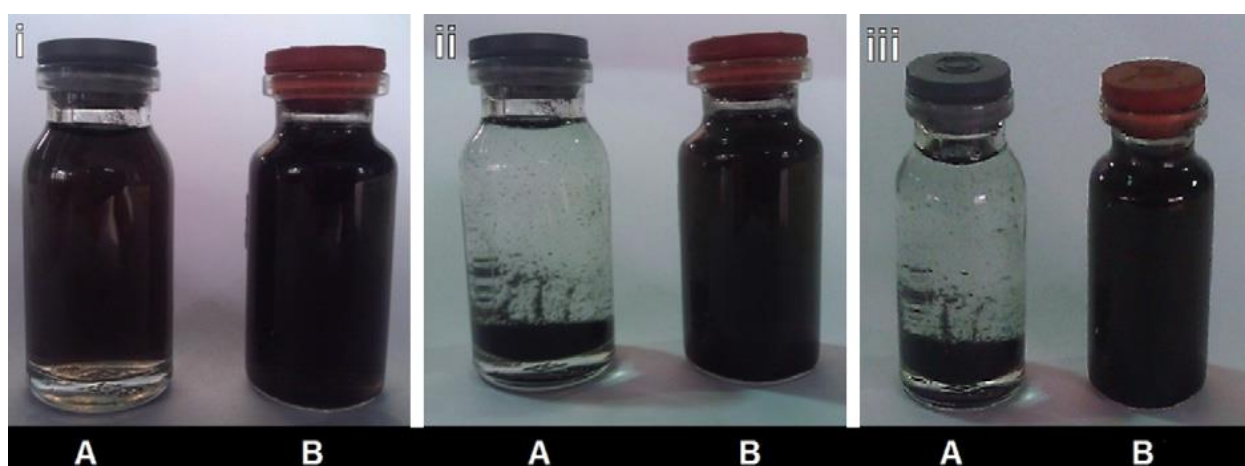


**Figure 3.14** Digital photographs showing the appearance of (A) raw MWCNTs and (B) PAA modified MWCNTs in water: (i) 30 min; (ii) 1 day; and (iii) 1 week after ultrasonication. Reproduced with permission from [20].

Although incorporated into a different polymer than PES, similar results (Fig. 15) have also been reported by Zhao and co-workers [14] when hyper-branched poly(amine ester) (HPAE) functionalised MWCNTs were used as hydrophilic nanoadditives for the modification of the PVDF UF membranes. It was established from the study that the PVDF casting solutions

containing either MWCNT-HPAE or raw MWCNTs are homogenous when flasks were placed vertically on the bench. However, only the MWCNT-HPAE was homogeneously dispersed in solution at the bottom of the flasks when both flasks were tilted. The raw MWCNTs on the other hand precipitated out of solution within one day (Fig. 3.15) [14]. The observed results were attributed to the hydrophilic side chains of HPAAE being stretched out into the solvent thus providing homogenous dispersion of MWCNTs in the membrane matrix [14].

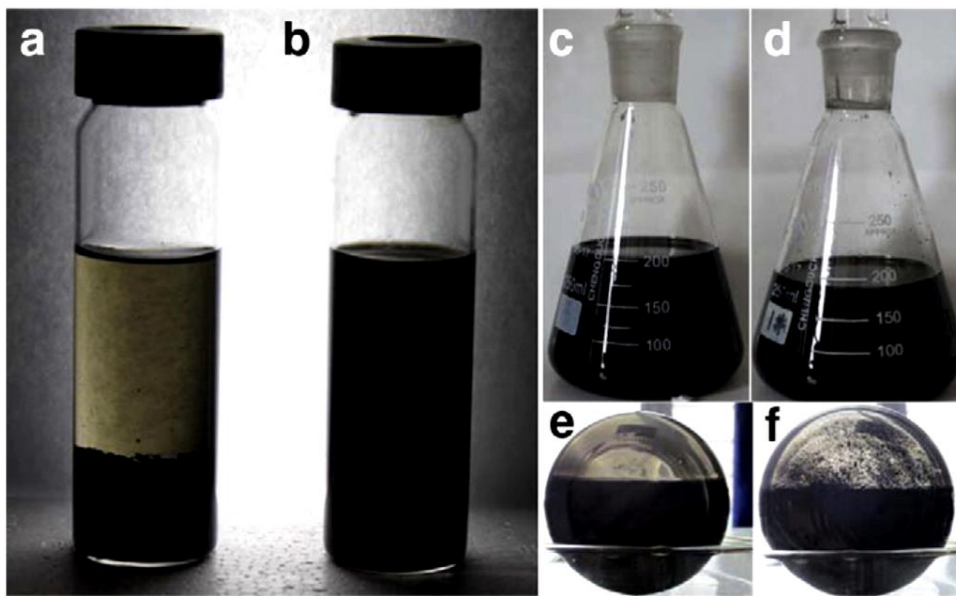


**Figure 3.15** Digital photographs showing the dispersion of MWNTs and MWNT-HPAE in DMF (a and b) and in PVDF casting solutions: (c and e) MWCNT-HPAE dispersion and (d and f) raw MWCNT dispersion. Reproduced with permission from [14].

#### **3.5.1.4. MWCNT/hybrid nanocomposites as new generation materials for PES modification**

Nanohybrid materials formed between MWCNTs and other nanomaterials have features that promise to make these nanohybrids the next generation of materials for membrane modification. This is because of the existence of the synergy between the two types of

nanomaterials, which allows the structural and performance properties of the resultant membrane to be improved upon inclusion of the nanohybrid in the membrane matrix. Individual nanomaterials may sometimes not possess or fully exude the desired properties for promising next-generation anode material that the target nanohybrid materials possess due to agglomeration resulting from the Van der Waals forces of interaction between the individual nanomaterials. For example, in the case of a nanohybrid formed between O-MWCNTs and GO, the introduction of O-MWCNTs has been shown to prevent the stacking of individual GO sheets, thus preventing their agglomeration. As previously discussed elsewhere in this chapter, the improvement in nanoadditive dispersion within the polymer matrix is accompanied by effective enhancements in the structural and performance properties of the membrane. In the next sub-sections, progress made on the use of MWCNT nanohybrids in PES-based UF membrane modification for various applications is explored.

#### **3.5.1.4.5. MWCNT/GO or MWCNT/graphene**

It is known that nanohybrid formation between MWCNTs and GO allows for a cost-effective and environmentally friendly solution towards solution-phase processing of both nanomaterials [108]. The method for synthesis of MWCNT/GO is relatively simple and straight forward and involves ultrasonication of MWCNT powder in diluted GO dispersion in water [108]. To study the stability and dispersion of the nanohybrid material, ultraviolet–visible (UV–Vis) spectroscopy and zeta potential analyses are amongst the characterisation techniques that are generally employed. The more negative the zeta potential value becomes, the higher the stability of the mixed hybrid solution [109]. Moreover, higher zeta potential values indicate higher electrostatic repulsion between charged particles in the dispersion and reduced overlapping areas [109]. Chatterjee et al. [110] investigated the effect of MWCNT/graphene

nanohybrid on the mechanical properties of an epoxy composite, and established that the resultant improvement in mechanical strength was due to the combination of high aspect ratio of MWCNTs and larger surface area of the graphene nanoplatelets. Additionally, for the full realisation of the reinforcing capabilities in the composites, it was established that the ratio of the nanomaterials consisting the hybrid nanofiller mixture is an important factor to consider. Homogenous distribution of the MWCNTs and GnP consisting the nanohybrids can be observed from the TEM image in Fig. 3.16.

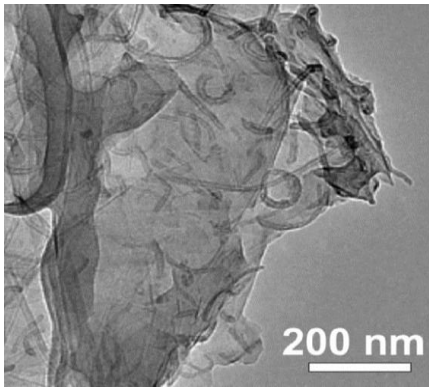


**Figure 3.16** TEM image showing the distribution of MWCNT/GnP nanohybrids for a MWCNT:GnP ratio of 9:1. Reproduced with permission from [110].

Zhang et al. [111] investigated the synergistic effects of the different ratios of O-MWCNT/GO nanofiller on the fouling control capacity of PVDF UF membranes. The UV–Vis results showed that the suspension of OMWCNTs can be effectively stabilised using GO sheets. At an O-MWCNT/GO ratio of 5:5 in the PVDF matrix, the membrane hydrophilic properties were greatly enhanced due to the homogeneous dispersion of GO and OMWCNTS in the casting solution. Moreover, the increase in dispersion of both nanomaterials facilitated an increase in the affinity between the castings solution and coagulant thus leading to an enhancement of the solvent–non-solvent exchange rate, which ultimately resulted in the formation of large

macrovoids in the membrane substructure [111]. The increased permeability observed for the membrane is associated with the presence of the reported large macrovoids in the substructure. Zhang et al. [112] prepared nanohybrids from functionalised graphene (f-G) and functionalised MWCNTs (f-MWCNTs) and investigated the effect of the nanohybrid on the electrical conductivity and tensile modulus of PES composites membranes. The results showed that the tensile strength modulus of the 5 wt.% (f-G:f-MWCNT)/PES composite membrane (nanohybrid ratio of 1:1) increased by 16.5% from that of 5 wt.% f-G/PES composite membrane and by 50.6% from that of 5 wt.% f-MWCNTs/PES composite membrane, respectively [112]. Moreover, the electrical conductivity of the 5 wt.% f-G:f-MWCNT/PES composite membrane (nanohybrid ratio of 1:1) was found to be 2.2 times higher than that of the 5 wt.% f-G/PES composite membrane and 8.9 times higher than that of 5 wt.% f-CNTs/PES composite membrane. It is evident from the studies discussed above that the incorporation of MWCNT/GO or MWCNT/graphene nanohybrids in polymeric membrane matrices especially PES, PSf and PVDF leads to enhanced dispersion in the polymer matrix, thus enabling further enhancement in the structural and performance properties of the membrane compared to when individual nanoparticles are used.

#### **3.5.1.4.6. MWCNT/TiO<sub>2</sub> polymer membranes**

In their respective individual capacities, MWCNTs and TiO<sub>2</sub> nanoparticles have proven to be additives of choice for the enhancement of polymeric membrane properties such as hydrophilicity, permeability and antibacterial activity. However, nanohybrid formed between TiO<sub>2</sub> and MWCNTs enables the joint photocatalytic properties of TiO<sub>2</sub>, reinforcing abilities of MWCNTs and the compatibility of functionalised MWCNTs with polymer matrices as well as

good hydrophilicity of both nanomaterials to be exploited and applied in the modification of the properties membrane.

Recently, the effect of TiO<sub>2</sub> nanoribbons/multi-walled carbon nanotubes (TNRs/MWCNTs) on the physicochemical and performance properties of the PES membranes during the desalination of brackish water was investigated by Shaban et al. [113]. Following preparation using the hydrothermal method, the TNRs were then used as catalysts for the growth of MWCNTs using the CVD method. The fabricated TNR/MWCNT nanohybrids displayed superior reinforcing capabilities in the PES matrix as well as salt retentions greater than 90% in synthetic brackish water solutions when compared with individual nanomaterials. In another study, MWCNTs coated with TiO<sub>2</sub> nanoparticles were prepared and embedded in a PES membrane matrix by Vatanpour et al. [94] with the view to bolster performance and anti-biofouling properties of the membrane. The TiO<sub>2</sub> nanoparticles were synthesized by precipitation of the TiCl<sub>4</sub> precursor on the acid oxidised MWCNTs prior to incorporation into the PES matrix. The results showed that the addition of TiO<sub>2</sub>/MWCNTs led to significant improvements in the pure water flux of the PES blend membranes. Interestingly, although the PES membrane modified exclusively with TiO<sub>2</sub> nanoparticles displayed a lower pure water flux, they displayed higher hydrophilicity relative to the PES membrane containing the TiO<sub>2</sub>/MWCNTs. This behaviour can be associated with agglomeration of TiO<sub>2</sub> nanoparticles, which causes plugging of the membrane pores [94]. The coating of TiO<sub>2</sub> nanoparticles on the surface of oxidised MWCNTs apparently prevents their agglomeration due to compatibility of functionalised MWCNTs with the polymer matrix. Similarly, ZnO-coated MWCNTs for the modification of the performance and antibiofouling properties of PES membrane were prepared by the same research group [114]. In addition to the incorporation of the ZnO/MWCNT into the nanocomposite leading to marked improvements in membrane hydrophilicity and pure water flux, the antibiofouling properties

of the membrane tested against activated sludge were also greatly enhanced. Such improvements were attributed to the effectiveness of the ZnO nanoparticles to destroy the cell membrane and damage the cell morphology, which consequently leads to a reduction in biofouling. Additionally, upon irradiation with UV light, the protein fouled ZnO/MWCNT/PES membranes were able to photocatalytically destroy organic contaminants thereby reducing fouling [114]. The photocatalytic mechanism of degradation involving the ZnO/MWCNT is shown in Fig. 3.17. The ZnO/MWCNT/PES membrane prepared in this study are promising candidates for application in membrane bioreactors (MBR).

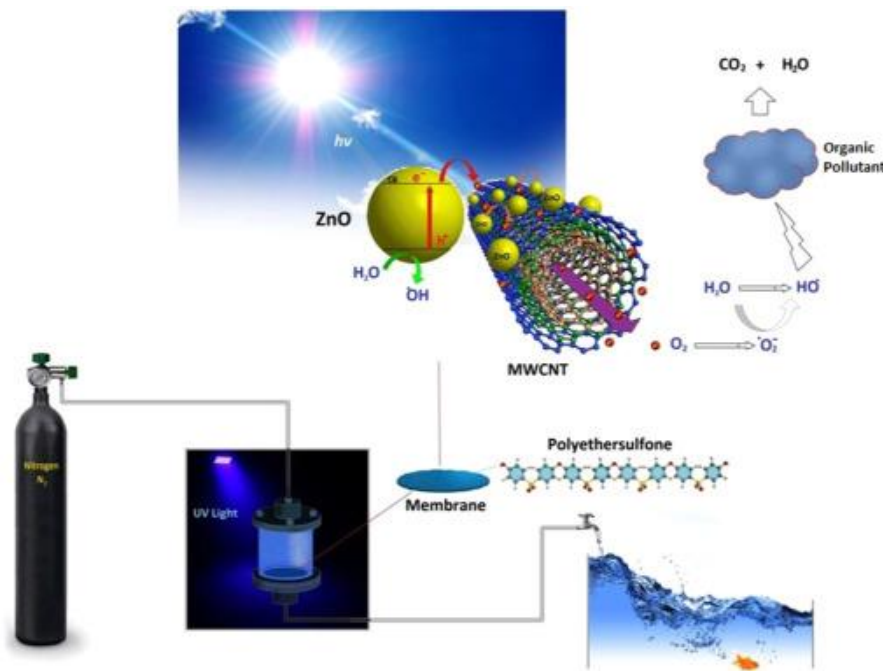


**Figure 3.17** Schematic illustration of photocatalytic activity of ZnO coated MWCNTs. Reproduced with permission from [114].

### 3.5.1.5. Polymer grafting and polymer blending of PES

Surface graft polymerisation is an efficient method for increasing the hydrophilicity and selectivity of PES membranes. The graft polymerisation technique has also been demonstrated

to be capable of converting a UF membrane into an NF membrane owing to the formation of a membrane surface with small pore sizes and high salt rejection [20, 115]. The grafting process involves a chemical attachment of either hydrophilic or water-soluble polymers into the membrane surface. For the grafting process to take place, the membrane surface should already possess polymerisation sites to which a stable graft layer can be attached. These reactive sites can be generated by treatment of the membrane surface with UV or gamma ray irradiation. However, such treatment methods may be detrimental to the structural integrity of the membrane support system, especially under weakly controlled conditions. In this regard, several researchers have explored the use of milder and gentler methods for creating these reactive sites on the surface of the PES membrane. For example, Daraei et al. [19, 20] investigated the combined effect of the inclusion nanoadditives (PAA-g-MWCNTs) on the PES membrane matrix and surface grafting of polyacrylic acid (PAA). The results showed that grafting of the PAA into PAA-g-MWCNT/PES mixed-matrix membrane support, led to superior water fluxes, improved reusability, high antifouling properties and efficient salt rejections relative to the PAA-g-MWCNT/PES produced without grafting [20]. This suggests that modified MWCNTs located within the PES membrane matrix offers reactive sites for the attachment of PAA. In addition to the presence of the hydrophilic additive (PAA-g-MWCNT) in the PES membrane support, the grafting of the PES membrane surface leads to more enhanced hydrophilicity.

Polymer blending as a means of improving the hydrophilic properties of hydrophobic membrane matrices has an advantage over the use of nanomaterial additives as it is relatively simple and capable of being applied on an industrial or commercial scale. Over the years, blending of PES with sulfonated polymers has become popular since it is aimed at improving the hydrophilic properties of membranes and, subsequently, the membrane performance

properties relating to permeability and selectivity. Sulfonated polymers such as sulfonated polysulfone (SPSf), sulfonated polyetheretherketone (SPEEK), sulfonated polyethersulfone (SPES), sulfonated polyphenylsulfone (sPPSU) have all been used for blending with PES [116-120]. Before blending the polymers, an important aspect that needs to be taken into consideration is the inter-miscibility or -compatibility of the polymers. According to Ng and MacKnight [121], poor compatibility between the polymers generally leads an irregular membrane surface as well as a membrane structural defects resulting from the self-assembly of the individual polymers. It is noteworthy that the presence of sulfonic acid groups (-SO<sub>3</sub>H) in sulfonated polymers allows for the hydrogen bonding interaction with the sulfonyl groups (-SO<sub>2</sub>) of the PES chains thus improving their compatibility.

In order to evaluate the compatibility between two polymers, the Schneier theory and differential scanning calorimetry (DSC) analysis were adopted. According to the Schneier theory (Eq. 3.1), the compatibility between polymers is evaluated based on the calculation of the mixing enthalpy ( $\Delta H_m$ ) from Flory–Huggins theory. An  $\Delta H_m$  value that is above 0.01 cal/mol suggests that the blend system is incompatible, while an  $\Delta H_m$  value lower than 0.01 cal/mol is indicative of a compatible blend system.

$$\Delta H_m = \left[ X_1 M_1 \rho_1 (\delta_1 - \delta_2)^2 \frac{X_2}{X_1 M_2 \rho_2 + X_2 M_1 \rho_1} \right]^{1/2} \quad (3.1)$$

where  $\Delta H_m$  is the enthalpy of mixing, subscripts 1 and 2 denote polymers 1 and 2, respectively; X is the weight fraction of the polymer in the blend (therefore,  $X_1 + X_2 = 1$ ); M is the molecular weight of the repeating monomer unit (g/mol);  $\rho$  and  $\delta$  are the respective density (g/cm<sup>3</sup>) and solubility parameters ((cal/cm<sup>3</sup>)<sup>1/2</sup>) of polymers 1 and 2.

Li et al.[117] used the Schneier theory to evaluate the compatibility between PES and PSf versus PES and SPSf. Based on the  $\Delta H_m$  values calculated for various weight ratios, the results showed) that the PES/SPSf system was compatible at all the evaluated ratios (i.e. all the  $\Delta H_m$  values were below  $10 \times 10^{-3}$  cal/mol) (Fig. 3.18). On the other hand, the PES/PSf system on the other hand, was found to be only compatible at specific weight ratios (i.e. when PES/PSf mass ratio was less than 95:5wt/ wt or higher than 22:78 wt/wt). It was therefore concluded that the PES/PSf blend system is partly compatible. These findings seem to suggest that blending of the two hydrophobic polymers (PES and PSf) leads to partial compatibility between the polymers and the formation of a heterogeneous solution [117]. On the other hand, the strong inter-molecular hydrogen bonding interaction between the SPSf and PES chains are thought to lead to better phase mixing and system compatibility between SPSf and PES [117].

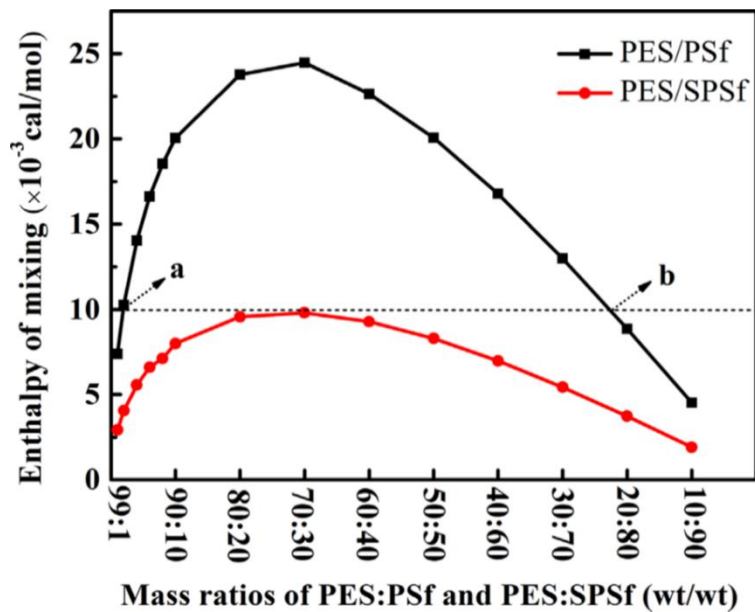


**Figure 3.18.** Mixing enthalpies of PES/PSf and PES/SPSf blend systems. Reproduced with permission from [117].

Experimentally, the compatibility or miscibility of polymers can be evaluated by DSC analysis; the appearance of a single thermal glass transition ( $T_g$ ) peak at a temperature that is intermediate between those of pure components suggests that the polymer system is miscible [122]. As shown in Fig. 3.19(a), for the majority of weight ratios tested for the PES/PSf system, more than one  $T_g$  peak appeared at  $\sim 185$  and  $\sim 228$  °C. In contrast, only a single  $T_g$  peak was detected at  $\sim 228$  °C for all the weight ratios tested for the PES/SPSf system. Therefore, the DSC results provided further evidence that the PES/SPSf system was indeed compatible at the majority of weight ratios tested. Furthermore, it is also evident from the DSC results that the hydrophobic PES/PSf system undergoes phase separation resulting from the strong repulsion between the two hydrophobic polymers thus making them partially compatible.

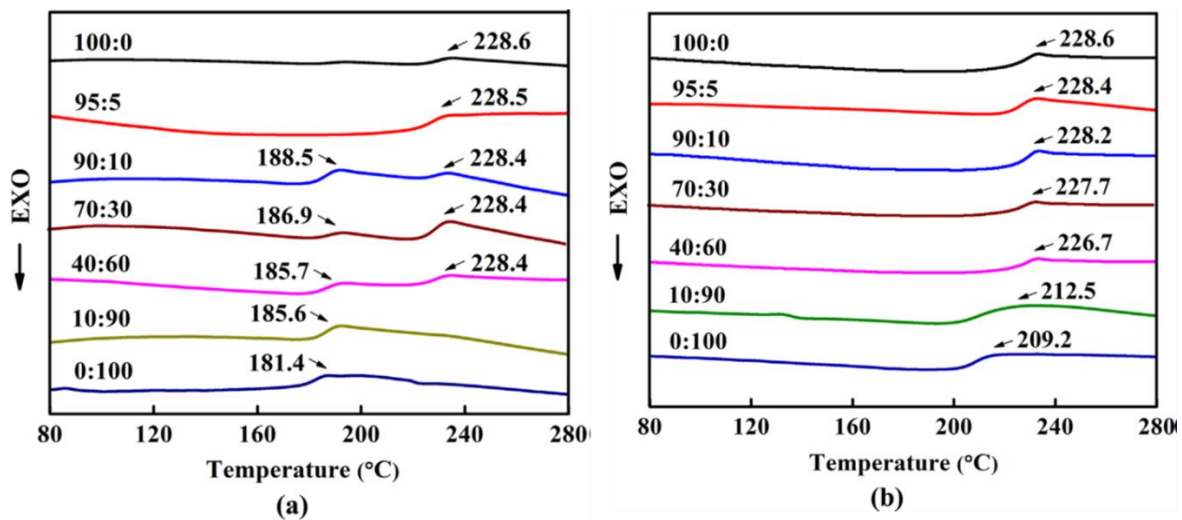


**Figure 3.19** DSC thermograms of (a) PES/PSf and (b) PES/SPSf at different weight ratios. Reproduced with permission from [117].

### **3.6. Properties of PES/MWCNT membrane**

#### **3.6.1. Surface roughness**

Rough membrane surfaces are prone to fouling due to the increased availability of sites for the attachment of foulants on the membrane surface [7]. The addition of functionalised MWCNTs into PES membranes affects surface roughness and ultimately the antifouling properties of the membrane. The addition of NH<sub>2</sub>-MWCNTs into the PES matrix has been reported to initially increase the surface roughness of the membrane; however, further 1 wt.% loadings of the NH<sub>2</sub>-MWCNTs decreased the surface roughness of the membrane [41]. Reasons behind the observed results are based on the fact that the introduction of hydrophilic NH<sub>2</sub>-MWCNTs initially enhances the phase-separation process during membrane formation leading to the generation of large pore sizes and high porosity; i.e. high porosity and large pore sizes of the membrane increase the membrane surface roughness. However, any further increases in the loading of the NH<sub>2</sub>-MWCNTs promote increases in the viscosity of the casting solution. This viscosity increase results in a delay in the demixing process during membrane formation and the formation of small surface pores, which in turn give rise to smoother surfaces. Similar results have also been reported by Daraei et al. [20].

In contrast, Vatanpour et al. [13] reported an initial reduction in the surface roughness when the oxidised MWCNTs were incorporated into the PES. However, this decrease in the surface area was accompanied by a drastic increase in the surface area when with further increments in the nanoparticle loading were effected. Interestingly, another reduction of the surface roughness was observed at the highest MWCNTs loading of 0.4%. The initial reduction in the surface roughness was linked to regular collocation of MWCNTs in the membrane matrix at low nanoparticle loading, which is due to low electrostatic interactions among the MWCNTs

that led to the generation of a smooth membrane surface. However, at higher nanoparticles loading, the observed increase in roughness was due to the formation of large surface pore sizes and the agglomeration of MWCNTs.

Although the studies discussed above [20, 41 vs 13] reported opposing trends in surface roughness upon the inclusion of functionalised MWCNTs, a marked improvement in the antifouling properties of PES membranes containing functionalised MWCNTs was reported (*i.e.* relative to the pristine PES membrane). A possible explanation for the observed behaviour is that membrane surface hydrophilicity seems to be contributing hugely towards antifouling properties compared to surface roughness. This explanation can be substantiated by the fact, although the PES membrane generally has a smooth surface that makes it less prone to fouling, its hydrophobic nature (water contact angle  $\sim 70^\circ$ ) counteracts the fouling effect and critically reduces the flux recovery ratio of the membrane [19]. Therefore, it suffices to conclude that a combination of increased hydrophilicity and decrease in surface roughness for MWCNT-modified PES membranes increases reversible fouling.

### **3.6.2. Surface charge**

The influence of membrane surface charge on the antifouling properties of the membrane is dependent on the charge state of foulants in the feed solution. This is because the electrostatic repulsive forces that exist between the like-charged membrane surface and foulants prevent the deposition of the foulants on the membrane surface thus leading to a reduction in the fouling of the membrane [7]. Therefore, for neutral solutes or foulants, the membrane surface charge will have a minimal effect on the overall antifouling properties of the membrane.

When hydrophilic-modified PES-based membranes come into contact with aqueous solutions over a wide pH range (particularly from neutral to basic pH), they acquire a negative surface charge due to the dissociation of ionisable surface functional groups or the adsorption of ions from the solution. Although protein molecules such as bovine serum albumin (BSA), which are generally responsible for PES membrane fouling, have an isoelectric point at pH 4.9, they become negatively charged at neutral pH ( $\sim 7$ ) [123]. Therefore, when antifouling filtration experiments are conducted under neutral conditions, a strong electrostatic repulsion force between both negatively charged BSA molecules and MWCNT-functionalised PES membrane surface is responsible for preventing proteins adsorption on the surfaces of the blended membranes, thus improving the antifouling properties of the membrane [13, 15, 18].

Surface modification of PES-based membranes with zwitterion functionalised MWCNTs or hydrophilic polymers is much more favourable for the enhancement of antifouling properties of the PES membrane compared to the use of conventional negatively charged membrane surface. Shi et al. [124] prepared tertiary amine-modified PES (TA-PES) from cationic amine and anionic sulfonic groups to fabricate a TA-PES UF membrane via phase-inversion method, and found that the resultant membrane displayed superior anti-protein-fouling properties and desirable ultrafiltration performance. Compared to MWCNTs functionalised with singly charged moieties, which only target pollutants possessing a specific charge, incorporation of zwitterion-functionalised MWCNTs into a polyamide nanocomposite membrane yielded a membrane that is capable of rejecting both negatively and positively charged ions during the water desalination process [125]. Zwitterion-functionalised membrane surfaces have also been found to promote the prevention of cell adhesion and biofouling [126]. The incorporation of zwitterionic poly(sulfobetaine methacrylate) (PSBMA) modified MWCNTs into the PES matrix via the phase-inversion method produced a modified membrane with superior

antifouling properties towards BSA [48]. A measurement of the interaction force between the membrane surface and the BSA-immobilized AFM tip revealed an interaction force for the unmodified PES membrane (16 nN) that is higher compared to that of the SBMA-CNT/PES membrane surface (10 nN). The high interaction force was attributed to hydrophobic properties of the PES; the formation of a strong hydration layer by the PSBMA functional groups limits the interaction of the membrane with the foulant.

### **3.6.3. Surface hydrophilicity in relation to pure water flux in PES/MWCNT membranes**

As already mentioned in the previous section, membrane surface hydrophilicity is one of the highly desired properties in membranes for combating fouling and enhancing the pure water flux of the membrane. The concept of the improvement of antifouling properties arising from the hydrophilic surfaces is based on the fact that a strong hydration layer is created on the membrane surface, which drives off the settlement of foulants on the membrane surface [127] (Fig. 3.20). In a nutshell, the hydration layer acts as a protective screen for minimising the chances of the foulant attaching on the membrane surface. Contact angle measurements are generally conducted to evaluate the hydrophilicity of membrane surface. Whereas a decline in the contact angle of a modified membrane is indicative of improvements in membrane surface hydrophilicity, an increase in the contact angle suggests that the membrane surface is becoming hydrophobic [7]. Other than the membrane surface chemistry, the contact angle values are also affected by surface roughness, porosity and pore size [84].

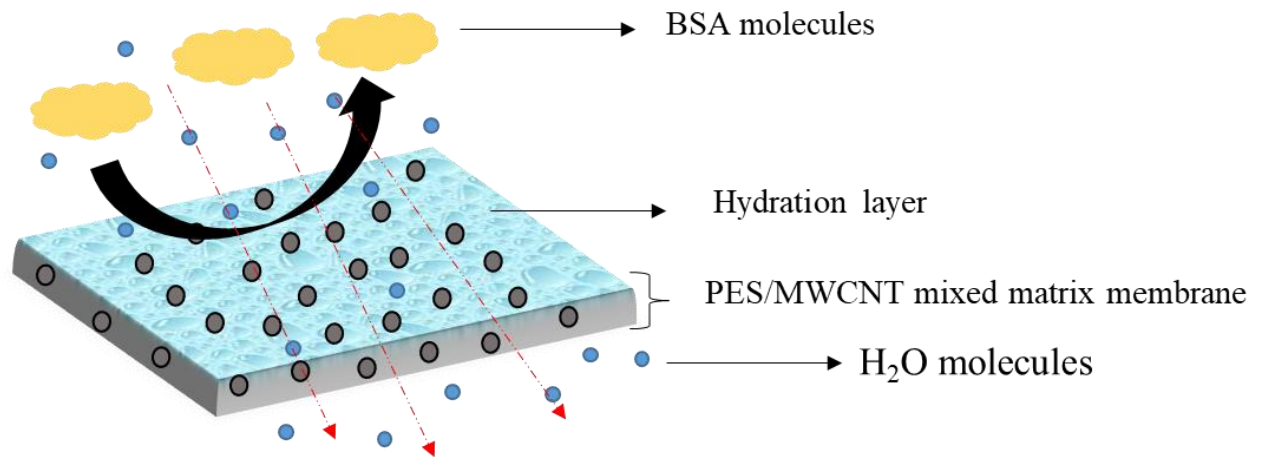


**Figure 3.20** Schematic representation of a hydrophilic PES/MWCNT membrane surface.

It has aptly been demonstrated that the incorporation of functionalised MWCNTs or polymer blending of PES leads to significant improvements in the surface hydrophilicity of an otherwise hydrophobic PES-based polymer membranes thereby improving its pure water flux. Surface hydrophilicity and membrane morphology have a strong influence on the membrane performance, particularly on the pure water flux. Both properties have similar but sometimes different effects on the membrane water flux; they impart similar effects in the sense that an increase in hydrophilicity and/or membrane pore size leads to an increase in the pure water flux. However, a hydrophilic membrane that consists of small-size surface pores, with a dense or thick skin layer will have low pure water flux or permeability [14, 41]. According to the Hagen-Poiseuille equation (Eq. 3.2), pure water flux is directly proportional to the pore size. The ultimate membrane structural parameter that has a dominating influence of on pure water flux of the membrane is its membrane pore size or pore size distribution.

$$Q_{HP} = \frac{\Pi \left(\frac{d}{2}\right)^4 \Delta P}{8\eta} \quad (3.2)$$

where  $Q_{HP}$  represents the volumetric flow rate (L/s);  $\Delta P$  is the pressure difference (Pa); across the  $L$  is tube length ( $m^2$ );  $\eta$  is the viscosity of water (Pa.s); and  $d$  is the pore diameter (m).

Whilst hydrophilicity and membrane structure are major drivers of the pure water flux enhancement, pore plugging is an important aspect that is seldom addressed. Pore plugging has a major influence on the membrane pure water flux when nanoadditives such as functionalised MWCNTs are incorporated into polymer matrices. It occurs as a consequence of the presence of functionalised MWCNTs at higher loadings in the membrane matrix leading to agglomeration. It has already been established from previous research works that the presence of hydrophilic MWCNTs in the polymeric casting solution enhances the phase-separation process leading to the generation of larger pore sizes; MWCNTs migrate spontaneously to the membrane/ water interface to improve the membrane surface properties, including surface hydrophilicity.

However, while surface hydrophilicity is improving, an additive material occupying certain locations or pores within the membrane surface and matrix is now present; pores that were otherwise vacant in the pristine and unmodified membrane. Pore plugging becomes severe and greatly impacts the membrane performance when high loadings of nanoadditives or MWCNTs are incorporated into the membrane matrix [41, 128]. In a study undertaken by Bai et al. [129], whereby different surface functionalised MWCNTs (-COOH-MWCNTs and PEG-MWCNTs) were incorporated into the PES UF membrane, it was shown that the pure water flux of all the modified membranes was always slightly below that of the pristine PES regardless of the nanoadditive content used (Fig. 3.21). The observed reduction in pure water flux was attributed to membrane pore plugging and constrictions of the water channels in the membrane substructure by the presence of MWCNTs.

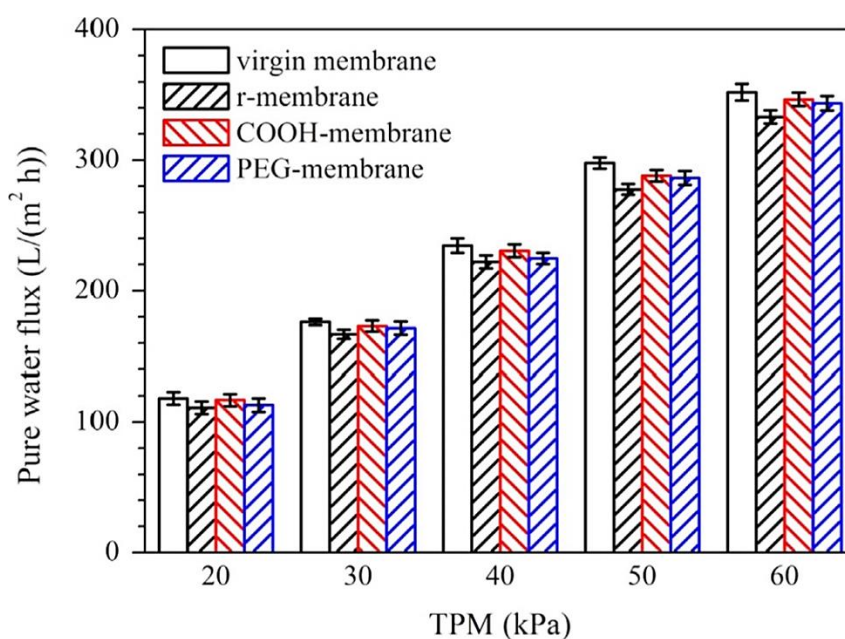


**Figure 3.21** Pure water flux of pristine and modified PES UF membranes at different trans-membrane pressures. Reproduced with permission from [129].

### 3.6.4. Antifouling and antimicrobial properties

Apart from the selectivity/permeability trade-off issue that limits membranes, membrane fouling is another major hindrance that limits long-term applicability of membranes due to permeate flux reduction, diminished selectivity and frequent chemical cleaning that ultimately destroys the membrane material. Membrane fouling in UF membranes can be either reversible or irreversible. Whereas reversible fouling involves loose adsorption of foulants or proteins molecules on the membrane surface that can be easily removed by hydraulic cleaning, irreversible fouling is caused by firm entrapment of foulants on the membrane surface pores and it cannot be remediated by simple cleaning methods [130, 131]. The hydrophobic interaction between the membrane surface and foulant provides the basis for the irreversible type of membrane fouling [132]. The desirable characteristics for all membrane processes and

membranes is to have maximum flow rate, maximum solute rejection, minimal fouling and minimum operating costs [133]. When irreversible fouling has taken place, the membrane can no longer be used and has to be discarded. This therefore increases the process operating costs.

In an effort to combat the escalation of operating costs emanating from fouling, several research efforts have been aimed at the development of PES-based membranes with less fouling propensity. Various modification strategies have been adopted for this purpose. Being a hydrophobic membrane material, PES is prone to irreversible fouling; therefore, the incorporation of hydrophilic MWCNTs into PES membrane matrices or the polymer blending of PES has become necessary in order to combat fouling. In addition to hydrophilicity, other membrane parameters that influence the propensity for membrane fouling include surface roughness and surface charge [7]. All these parameters and factors that influence membrane fouling have been discussed in detail in the previous sections.

Silver nanoparticles (AgNPs) are some of the most widely used nanomaterial additives for modifying the antimicrobial properties of the membrane owing to their relatively low cost and robust antibacterial characterisation [134]. Moreover, AgNPs are capable of enhancing surface hydrophilicity of membranes due to their strong affinity for water molecules [47]. Despite the advantages associated with AgNPs, their tendency to be corroded by oxygen reduces their antibacterial efficiency, thus limiting their long-term antibacterial applications. In this regard, research on the use of alternative nanomaterials with antimicrobial properties (e.g. functionalised MWCNTs) has been undertaken [47]. Yang et al. [47] prepared PMTAC modified MWCNTs and PEGMA modified MWCNTs and incorporated them into PES UF membrane matrix at different weight ratios with a view to improve the antibacterial properties of the membrane. The modified PES membranes were reportedly very effective against 99%

of both *Escherichia coli* and *Staphylococcus aureus* bacteria, while limiting adhesion of dead bacteria on the membrane surface [47]. When antibacterial hybrid nanoadditives consisting of AgNP-decorated MWCNTs were incorporated into the PES UF membrane matrix via phase-inversion method, an increase in the AgNP/MWCNT content resulted in an increase in the antibacterial activity of the composite membrane against *Escherichia coli* and *Staphylococcus aureus* bacteria [135]. It appears that the mechanism of the observed antibacterial activity is linked to the release  $\text{Ag}^+$  from the membrane, which led to the deformation of the bacterial cell membrane and structure [135]. The SLS-MWCNTs prepared by Wang et al. [43] for inclusion into the PES matrix produced a modified membrane that did not initially display excellent antibacterial properties against *Escherichia coli*. It was reasoned that the SLS-MWCNTs were buried in the membrane matrix and could not appear on the membrane surface to make direct contact with bacterial cells [43]. However, the antibacterial properties were significantly improved upon application of an electric field (Fig. 3.22). The improved antibacterial activity is ascribed to bacterial cell damage induced by  $\text{H}_2\text{O}_2$  that was formed from the two-electron oxygen reduction reaction. Apparently, MWCNTs have large specific surface areas that facilitate electron transfer and diffusion, thus promoting the oxygen reduction reaction that produces large amounts of  $\text{H}_2\text{O}_2$  [136].

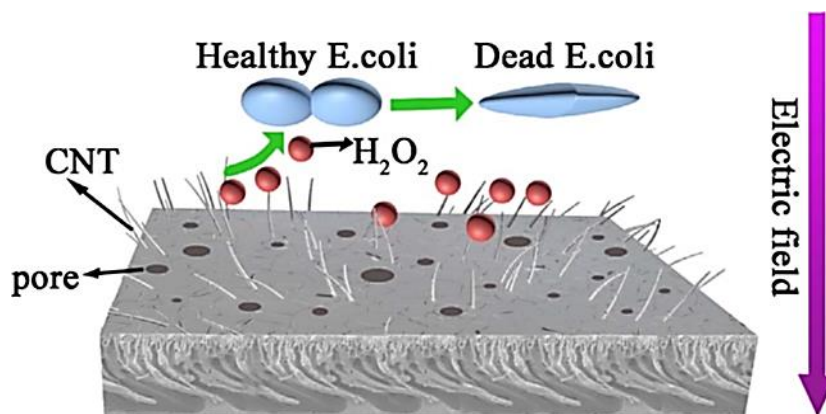


**Figure 3.22** Synergistic antibacterial effect between hybrid SLS-PES membrane and electric field against *E. coli*. Reproduced with permission from [43].

### 3.6.5. Porosity and pore size

Before discussing the effect of the addition of functionalised MWCNTs into PES-based membrane matrices, it is important to first distinguish between porosity and pore size in membranes, as both terms are sometimes wrongly used. Membrane porosity refers to a fraction of the total volume that is taken up by the pore space; membrane pore size on the other hand refers to the size or diameter of the pores (with regards to surface pores) or the ratio of pore length to diameter (for internal pores). In Fig. 3.23, the difference between both membrane morphological properties is further explained by means of sketches, and their influence on membrane performance indicators is also depicted. Ideally, a membrane that is best suited for water treatment applications should have high porosity and small pore sizes, i.e., large number of pores that are relatively small in size [92]. Such a membrane is capable of avoiding to a large extent the permeability-selectivity trade-off that applies to membranes. This is because the small pore sizes favour the rejection of solutes while the large number of pores is beneficial for the improvement of flux. While an enhancement in membrane porosity contributes towards the improvements of membrane permeability, it has been shown that membranes with comparable

porosities can have widely different performances, depending on their cross-sectional morphologies [96].

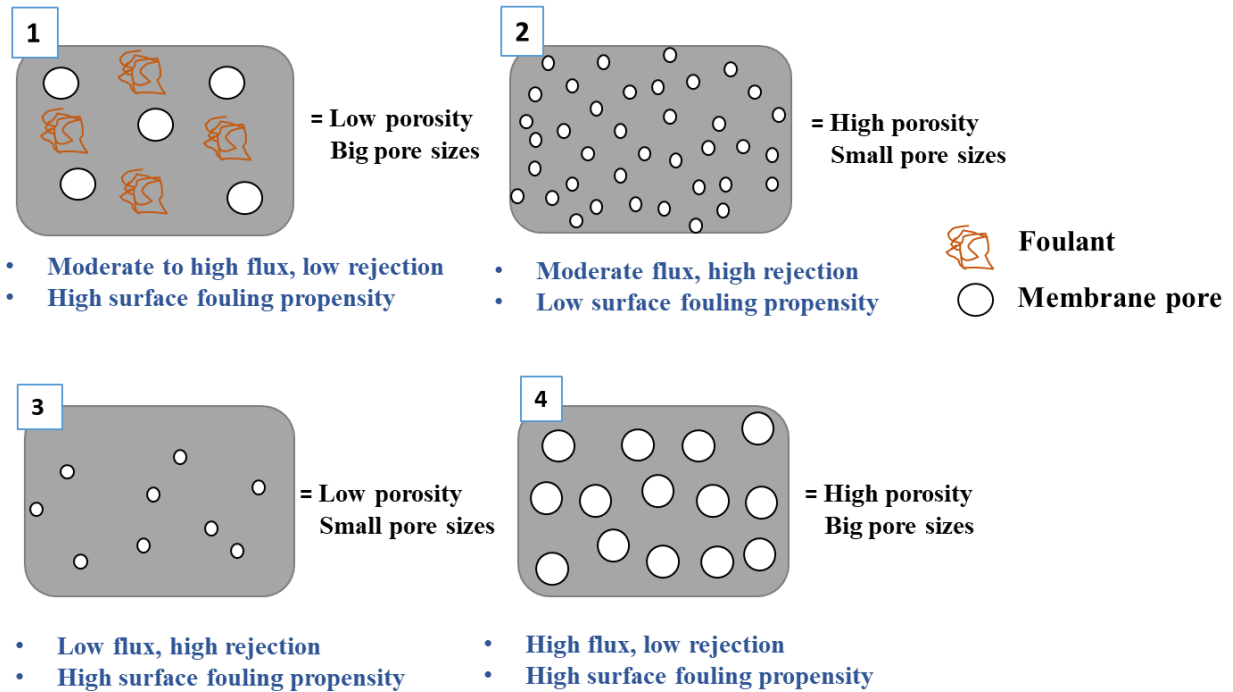


**Figure 3.23.** Schematic diagram of membrane porosity versus membrane pore size and their effect on membrane performance indicators.

The overall bulk porosity of the membrane can be determined by measuring the mass of wet and dry membrane samples and the thickness of the wet membrane. Excess water droplets on the surface of the wet membrane are carefully removed by a light dabbing of the membrane pieces with filter paper prior to weighing the membrane. Thereafter, the membrane samples are dried under vacuum and weighed again. To obtain reliable and reproducible membrane porosity results, measurements can be performed with at least three different pieces of the membrane type. The porosity  $\varepsilon$  of the membrane (%) can be calculated using Eq. 3.3 as follows:

$$\varepsilon(\%) = \frac{W_w - W_d}{\rho_w A \delta} \times 100\% \quad (3.3)$$

where  $\varepsilon$  is the porosity of membrane,  $W_w$  is the weight (g) of the wet membrane,  $W_d$  is the weight (g) of dry the membrane,  $\rho_w$  is the density of pure water ( $\text{g}/\text{cm}^3$ ),  $A$  is the membrane area ( $\text{cm}^2$ ) and  $\delta$  is the thickness of membrane (cm).

The addition of polymeric additives such as PVP or PEG as pore-forming agents in the PES polymeric casting solutions has been shown to promote the formation of surface pores in the membrane, the size of which increases proportionally with the molecular weight and concentration of the incorporated nanoadditive [137-139]. In principle, large surface pore sizes lead to enhanced membrane permeability, which is accompanied by reduced solute rejection.

In the majority of studies where functionalised MWCNTs have been incorporated into hybrid PES membranes, water flux has been found to increase in proportion to the amount of MWCNTs up to a certain point in terms of a specific concentration added. This is because the hydrophilic additive is capable of increasing bulk membrane porosity and membrane pore sizes during the membrane formation process. Nevertheless, the agglomeration of MWCNTs at higher loadings is always deemed a limiting factor with regards to the extent to which porosity and pore sizes of the membrane are increased; this is as a consequence of counteracting pore-formation process [45].

Both the separation performance and the permeate flux are affected by the membrane pore size. The effect of pore size on separation performance is obvious, in that solutes larger than the pore size are prevented from passing through while solutes of smaller size than the membrane pores simply pass through the membrane. It is important to note that membranes do not have

pores of a single size range but rather a distribution of pore sizes. Therefore, rejection of a solute will depend on whether the solute approaches a small or a large pore. Nonetheless, even if the pores were of uniform size, there would still not be a sharp cut-off or rejection since the hydrodynamic and shape effects would ensure that some particles, which are smaller than the pore size, would still be rejected by the membrane.

### **3.6.6. Mechanical properties**

One of the major aims of incorporating MWCNTs into PES-based membrane matrices is to improve the mechanical strength properties of the composite membrane so that the structural integrity of the membrane remains intact when the membrane is subjected to various pressures during hydraulic cleaning. Using tensile strength, Young's modulus and elongation at break (fracture strain) measurements, several studies have demonstrated an enhancement of the mechanical strength of polymeric membranes when specific weight ratios of MWCNTs have been incorporated within the PES-based membrane matrix [28, 60, 64, 140]. The well-dispersed MWCNTs intertwined within the polymer matrix act as bridges, thereby improving interfacial interactions amongst polymeric chains and those between the MWCNTs and the polymer matrix. There are four main requirements for effective reinforcement of the polymer composite by the nanofiller, and these include: (a) large aspect ratio; (b) good dispersion; (c) alignment; and (d) interfacial stress transfer [27]. Therefore, the dispersion of MWCNTs is a critical factor that needs to be addressed in order to realize a significant improvement in the reinforcement properties of the composite membrane. Poor dispersion and agglomeration of MCNTs in the polymer matrix has been shown to result in a reduction of mechanical strength and modulus of the composite membrane. Moreover, the mechanical properties of the composites are significantly influenced by interfacial interactions between MWCNTs and

polymer matrices [141]. The role of the MWCNTs in the composites is that when external stress is applied on the composite as a whole, part of those stresses can be transferred to the MWCNTs thus allowing the nanoparticles to take a larger part of the load (Fig. 3.24).

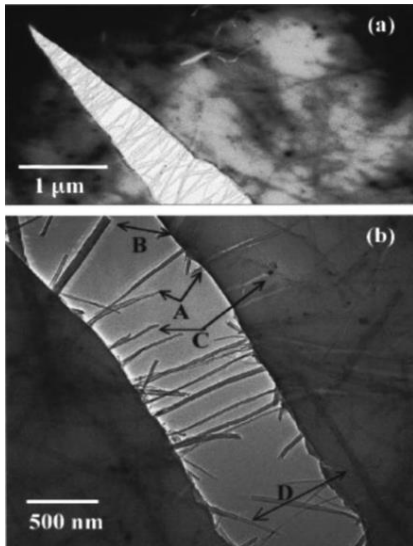


**Figure 3.24** TEM observation of crack nucleation and propagation in MWCNT-polystyrene thin films as induced by thermal stresses. Reproduced with permission from [142].

The presence of defects in the structure of functionalised MWCNTs reduces the mechanical strength of these nanoparticles. The defects in the structure of MWCNTs originate from the oxidation process that occurs during surface functionalisation of the particles to introduce the  $-OH$ ,  $-CO_2^-$  and  $-CO_2H$  groups. Unfortunately, these defects inducing functional groups, which are located on the surface of MWCNTs, are essential to aid interaction of the MWCNTs with the polymer. The aspect ratio is another factor that plays a major role in increasing the critical threshold necessary to establish a percolated particle network in the polymer matrix [143]. A 1 nm thick layer of graphene, graphene and GO nanoparticles has an aspect ratio in the range of 20 – 40, when compared with that of MWCNTs which is above 1 000. Such a low aspect ratio for GO requires relatively high levels of the nanoparticles to be added to the

polymer matrix in order to realise a percolated network structure with prominent mechanical reinforcement [144].

While the presence of MWCNTs in PES-based membrane matrices bestows improved mechanical strength properties on the membrane with improved mechanical strength properties, the membrane morphology plays an equally important role in determining the resultant mechanical strength of the membrane. For example, the sponge-like morphology is likely enhance the mechanical strength of the membrane when compared with the finger-like substructure. It has already been pointed out in earlier sections that finger-like structures and macrovoids are mechanically weak points in the membrane structure, which reduce the overall mechanical strength of the membrane. Previous studies have reported that the incorporation of MWCNTs into the membrane matrix generally leads to the formation of a finger-like cross-sectional structure with macrovoids (the size of which increases with an increase in the composition of MWCNT) [13, 16, 20, 29, 145]. Therefore, in order to fully realise significant enhancements in the mechanical strength properties of the PES-based membranes, a combination of sponge-like morphology with homogeneously distributed MWCNTs in the matrix is, as reported by Gumbi et al. [28], is necessary.

### **3.7. PES/MWCNT membrane performance indicators**

Apart from membrane surface characteristics, other factors that influence the fouling propensity of a membrane system include feed composition, pre-treatment process used and proper adjustment of operating conditions that produce least fouling [4, 19]. In addition, hydrodynamic parameters such as cross-flow velocity, transmembrane pressure and operating below critical flux of the membrane should be taken into account so as to reduce the permeation

drag forces experienced by the membrane surface leading to the deposition of a cake-layer [4, 19]. According to Field et al. [146], critical flux for the membrane filtration process can be considered as the flux just below which deposition into the membrane begins to occur leading to the formation of a cake layer [146]. It has been found that an increase in transmembrane pressure encourages the formation of irreversible fouling due to an increase in the amount of protein transported to the membrane surface by convection [147, 148]. It is known that the protein deposit formed under high pressure operation becomes tightly bound into the membrane surface making it as a result difficult to remove and thus contributing towards irreversible fouling [149]. Therefore, correct selection of the initial transmembrane pressure can greatly contribute towards minimising membrane fouling because the critical flux will not be exceeded. To this end, it is more ideal to work under constant-flux rather than a constant-pressure for antifouling experiments of PES based membranes [146].

Parameters that are generally used for assessing fouling include flux recovery ratio (*FRR*), the degree of total flux loss caused by total fouling (*R<sub>t</sub>*), reversible fouling ratio (*R<sub>r</sub>*), irreversible fouling ratio (*R<sub>ir</sub>*). The flux recovery ratio can be calculated using the following equation.

$$FRR (\%) = \frac{J_{wc}}{J_{w1}} * 100 \quad (3.4)$$

where  $J_{w1}$  is the initial pure water flux and  $J_{wc}$  is pure water flux of the cleaned membrane.

The fouling resistance capability of the membrane can be described in terms of the total fouling ratio (*R<sub>t</sub>*), reversible fouling ratio (*R<sub>r</sub>*) and irreversible fouling ratio (*R<sub>ir</sub>*) as follows:

$$R_t (\%) = \frac{J_{w1} - J_p}{J_{w1}} \quad (3.5)$$

$$R_r (\%) = \frac{J_{wc} - J_p}{J_{w1}} \quad (3.6)$$

$$R_{ir} (\%) = \frac{J_{w1} - J_{wc}}{J_{w1}} \quad (3.7)$$

$$R_t = R_r + R_{ir} \quad (3.8)$$

where  $J_{w1}$  is the initial pure water flux;  $J_{wc}$  is pure water flux of cleaned membrane; and  $J_p$  is the solution flux of the foulant.

The FRR is an important indicator of membrane reusability after fouling and cleaning had taken place. Therefore, an excellent antifouling membrane has high FRR and low  $R_t$  values.

Flux decline during fouling tests in the dead-end filtration setup, can be caused by several factors, including adsorption between the membrane and foulants in the feed solutions, cake or gel formation, concentration polarisation, and membrane hydraulic resistance. The resistance-in-series model is useful for the analysis of flux decline [150] and can be described by the following equation as:

$$J = \frac{TMP}{\mu R_{tot}} \quad (3.9)$$

where  $J$  is the flux ( $L/m^2 \cdot h$ );  $TMP$  is the transmembrane pressure (MPa);  $\mu$  is the viscosity of water at room temperature ( $1.005 \times 10^{-3}$  Pas); and  $R_{tot}$  is the total filtration resistance.

The resistance-in-series model combines various resistances that cause flux decline as follows:

$$R_{tot} = R_m + R_g + R_c + R_a \quad (3.10)$$

where  $R_m$  is the membrane hydraulic resistance;  $R_g$  is the cake layer resistance;  $R_c$  is the concentration polarisation resistance; and  $R_a$  is the adsorption resistance. The following equations can be used to calculate these various types of resistances:

$$R_m = \frac{\text{TMP}}{\mu J_{mem}} \quad (3.11)$$

$$R_g = \frac{\text{TMP}}{\mu J_{pore}} - R_m - R_a \quad (3.12)$$

$$R_a = \frac{\text{TMP}}{\mu J_{irr}} - R_m \quad (3.13)$$

where  $J_{mem}$  is pure water flux measured through a clean membrane;  $J_{pore}$  water flux measured after the fouling stage; and  $J_{irr}$  is water flux measured after the fouling stage and cleaning off the gel layer.

### 3.8. Performance of PES/MWCNT membranes in water treatment applications

The PES/MWCNT-based membranes have found use in various applications in the water treatment sector such as: (i) membranes for the pretreatment of wastewater and seawater for the removal of dissolved proteins and organic matter; (ii) adsorptive membranes for the removal of heavy metals and emerging pollutants from water; and (iii) supports membranes for the fabrication of TFC RO for application in brackish or seawater desalination.

The potential application of various carbon nanotube based membranes including PES/MWCNT MMMs in water desalination has been discussed in detail elsewhere [151] and in preceding chapters. The pre-treatment of seawater and the water produced during the shale drilling both make use of UF membrane technology [43]. In addition to desalination applications, PES/MWCNT membranes have found use in the removal of emerging pollutants and heavy metal ions from water, oil/water separation and in many other applications [152].

Lee et al. [1] investigated the application of PANI-MWCNT/PES membranes in the pre-treatment stage of seawater reverse osmosis (SWRO) process in the removal of low molecular-weight dissolved organic matter (LMW-DOMs). Results of their study revealed that the PANI-MWCNT/PES membranes displayed a superior permeability ( $321.3 \text{ L/m}^2\cdot\text{h}\cdot\text{bar}$ ), which was four times higher than that of the pristine PES membrane [1]. Moreover, a 66% removal percentage rate of LMW-DOM was reported when 0.5 g/L of PAC was used in combination with a PANI-MWCNT/PES membrane possessing a high permeate flux of  $600 \text{ L/m}^2\cdot\text{h}\cdot\text{bar}$ .

The application of nitrogen-doped MWCNTs (N-CNTs) incorporated into PES membranes in the removal of emerging pollutants from water sources (EMPs) has been reported by Wanda et al. [153]. The fabricated N-CNT/PES blend membranes displayed superior and effective removal capabilities towards a selection of EMPs, with the highest (99.20 – 99.92%) and lowest (84.61–87.21%) percentage removal rates being achieved for galaxolide and caffeine, respectively. The high percentage removal rates for galaxolide was ascribed to the large surface area ( $94.3 \pm 0.60 \text{ m}^2/\text{g}$ ) and high porosity  $0.37 \pm 0.03 \text{ cm}^3/\text{g}$  of the 0.01 wt.% N-CNT/PES blend membrane, which subsequently led to a substantial increase in the number of sorption sites for the target pollutants.

The application of SWCNT-COOH/PES UF membranes in the adsorptive removal of bisphenol A (BPA) and nonylphenol (NP) has been investigated by Kaminska et al. [154]. Using filtration experiments, the pore sizes of the fabricated SWCNT/PES UF membranes were found to be considerably large for the retention of the targeted pollutants; however, both static and dynamic adsorption experiments were still carried out. The study revealed that by increasing the SWCNT-COOH loading on the PES membranes, the membrane became more hydrophobic thus enabling high adsorptive removal of BPA (~ 78% removal) and NP (~85% removal) via hydrophobic-hydrophobic interactions. However, very high SWCNT contents (0.5 wt.% SWCNT-COOH of relative to the PES concentration) lead to a decreased efficiency rate in the removal pollutants due to an increase in the porosity, which reduces the number of adsorption sites available on the membrane surface [154]. In another study, the ability of commercial PES membranes towards the adsorption and retention of BPA and 17 $\beta$ -estradiol (E2) was investigated [155]. The retention experiments were carried out in the presence and absence of natural organic matter (NOM) and SWCNTs (experimental set-up used is shown in (Fig. 3.25)). Results of this study have shown that the adsorption of hydrophobic pollutants in the feed tank prior to membrane filtration was responsible for their overall retention. Furthermore, depending on the membrane area, the adsorption of BPA increased by 10–40% in the exclusive presence of SWCNTs when a contact time of 3 h was used [155].

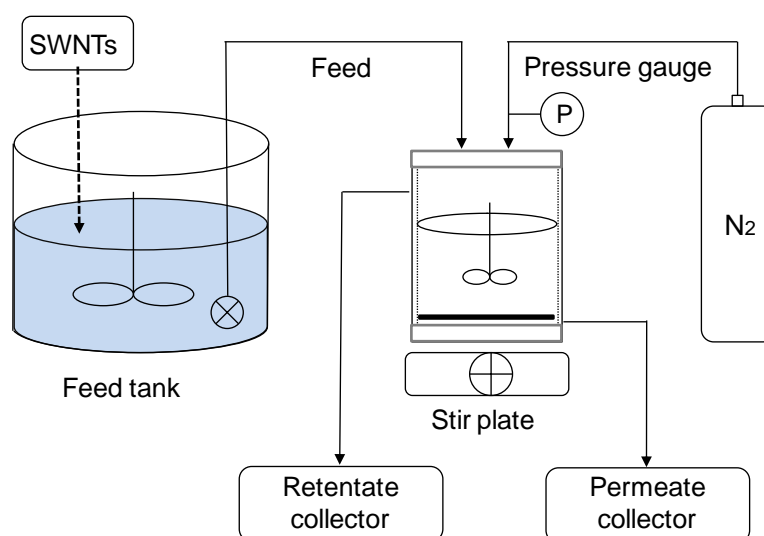


**Figure 3.25** Experimental set-up of SWCNTs-UF membrane testing unit used by Heo et al. Reproduced with permission from [155].

Investigated. When the use of MWCNT/PES membranes as substrates for the fabrication of TFC FO membranes was investigated, Wang et al. [64] found that the PES composite substrate containing MWCNTs displayed excellent FO performance (high salt rejection and high water permeability) compared to the commercial PES membrane substrate. Additionally, the presence of MWCNTs led to an improvement in the mechanical strength properties of the composite membrane. The fabricated membrane displayed promising features for practical use in FO applications. Although slightly different from PES, PSf membranes containing acid treated MWCNTs were prepared by Kim and coworkers [134] and used as support substrates for TFN membranes with AgNPs in polyamide layer. It was found that TFN membranes containing 5.0 wt.% of MWCNTs in the support layer displayed a 23% improvement in the pure water permeability compared to the TFN membrane that did not have MWCNTs as part of their composition. The improvement in the permeability was attributable to the diffusive

channel effects of MWNTs [134]. Other properties such as surface hydrophilicity and antibacterial and antibiofouling properties were accordingly enhanced.

The studies discussed in this section highlight some of the important applications of PES/MWCNT membranes in water treatment. With currently used polymeric membranes seemingly having reached a point where it is challenging to improve the separation performance by mere optimisation of the synthesis parameters, the incorporation of functionalised MWCNTs offers new possibilities and enhancement in the properties of membranes.

### **3.9. Outlook and future perspectives**

The use of PES/MWCNT MMMs in water treatment applications is steadily gaining popularity due the promising features that these membranes display. These features include enhanced permeabilities, high mechanical strength, improved adsorptive capacities as well as antifouling and antibiofouling properties that allows for membrane recyclability. Progress on work undertaken on PES/MWCNT composite membranes for water treatment applications in over the past eight years can be is illustrated in Fig. 3.26 which shows an increase in the number of papers published annually. The fabricated PES/MWCNT membranes have been mainly used in wastewater treatment applications, including oil-water separation as well as the removal of soluble proteins, organic dyes and targeted micropollutants and other pollutants during water desalination.

This review has demonstrated that the cross-sectional structure of PES/MWCNT membranes is at the heart of the enhancement of membrane performance and structural properties.

However, the debate is ongoing regarding the desired membrane morphology required for the enhancement of the properties associated with the performance of PES/MWCNT MMMs. Generally, membranes formed by phase-inversion processes in the presence of hydrophilic additives such as functionalised MWCNTs possess a finger-like morphology with macrovoids located in the membrane sub-layer. While other applications require the presence of finger-like channels to limit the resistance to water flow, the presence of these finger-like channels in the membrane substructure reduces mechanical strength properties and long-term stability of the membrane. Support fabrics (woven and non-woven) are commonly used for the restoration of the mechanical integrity of the membranes; however, the use of support fabrics is known to induce resistivity to water flow in osmotically driven membrane processes [156, 157].

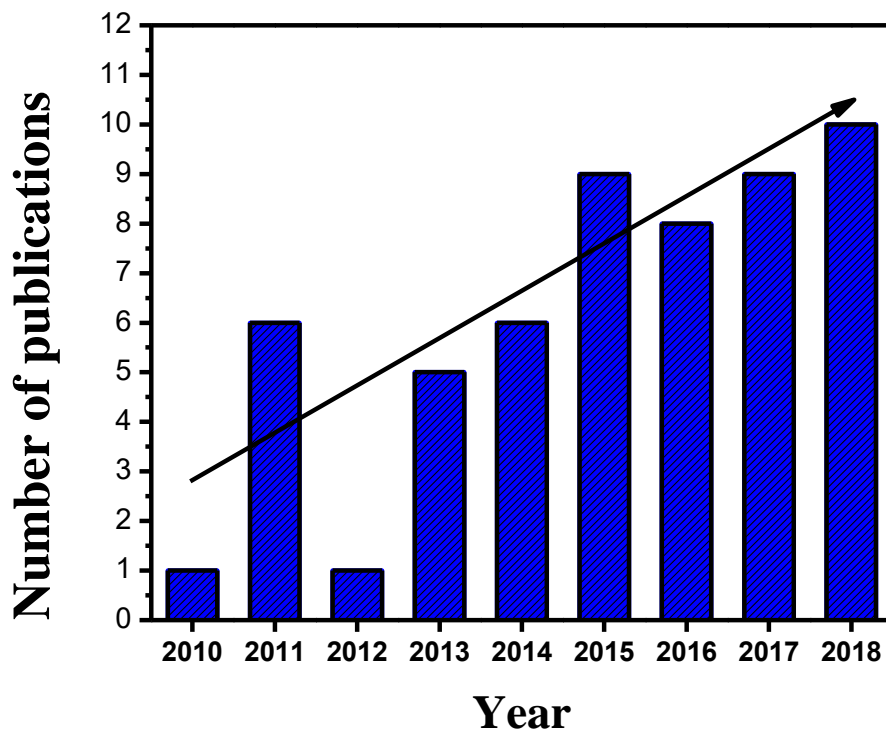


**Figure 3.26** Number of research papers published between the years 2010 – 2018 on the subject of PES/MWCNT MMMs for various water treatment applications (Search results obtained upon entering the following keywords on Web of Science and Scopus: “carbon nanotube polyethersulfone composite membranes for water treatment”).

Phase-inversion and interfacial polymerisation methods, which are discussed in detail in this, review remain the methods of choice in all studies cited due to simplicity of operation and the ease of incorporation of MWCNTs into the PES membrane matrices. Modification strategies of PES membranes involving either the incorporation of functionalised MWCNTs or MWCNT nanohybrids or polymer blending processes have been thoroughly reviewed. It has been reiterated throughout this review that nanoadditive dispersion in the PES matrix is crucial for the realisation of maximum enhancement of the properties of the membrane. As far as polymer blending with PES is concerned, compatibility of the polymers is essential. The Schneier theory enables first-hand evaluation of polymer compatibility prior to synthesis. To date, exciting results relating to the improvement of the structural and performance properties of PES-based membranes have been obtained through the adoption of the mentioned strategies. However, there is still ample room for improvements to the existing modification strategies and/or the development of other surface modification strategies which is anticipated in the near future.

Toxicity concerns which pertain to the use of MWCNTs in water treatment applications cannot be overlooked. While the addition of MWCNTs yields incredible physicochemical properties in membranes, there is still this fear that their presence is likely to cause more harm than good particularly because their toxic effects in the environment are not fully understood. Perceptions of MWCNTs leaching into the water sources during filtration thereby causing secondary contamination are continuing. However, the few toxicity studies that have been carried out have demonstrated that the toxicity of MWCNTs depends upon the type of MWCNTs, size or dimension, presence of impurities, synthetic method used and physical state (*i.e.* dispersed or agglomerated) [158, 159]. In general, agglomerated MWCNTs are viewed as being more toxic compared to well-dispersed MWCNTs. It has been reiterated throughout the review that pristine MWCNTs tend to agglomerate easily via van der Waals forces of interaction and are,

therefore, likely to be more toxic than functionalised MWCNTs. Therefore, controlling the dispersion of MWCNTs in polymer matrices through the adaptation of various methods of functionalisation discussed in this review and/or incorporating them at very low contents could be a step towards reducing their toxic effects. Another major hurdle that limits large-scale applications of MWCNTs is the costs associated with MWCNTs. When choosing to use MWCNTs as nanoadditives for membrane modification, researchers are often faced with the challenging task of justifying their use since the high costs of MWCNTs have the potential to increase the overall operating costs of membrane filtration. Nonetheless, it is envisaged that the attractive features and physicochemical properties of MWCNTs modified with various surface moieties will continue to drive up the demand for MWCNTs which will propel the need for more research into cost-effective methods of producing MWCNTs. The high cost of implications of MWCNTs are currently driven by the fact that the manufacturing processes employed are only capable of producing a few grams in quantity of MWCNTs per single run which requires about 800 °C to operate. As such, much research focused on developing economical processes for the mass production of MWCNTs at lower costs currently being undertaken.

Based on their attractive structural and performance features, the future of PES/MWCNT membranes looks promising. Nonetheless, even better improvements in membrane properties could be realised if the alignment of functionalised MWCNTs within the PES membrane matrix can be effectively controlled. Vertically aligned MWCNTs can provide an additional pathway for the transport of water molecules, thereby increasing membrane permeability and subsequently reducing the required operating pressure. Therefore, more research into scalable and cost-effective fabrication methods of aligned functionalised MWCNT/PES membranes is needed. Multi-walled carbon nanotube membranes possessing the aligned geometry have the

potential to introduce new structural and performance properties thereby introducing another dimension to the way in which water is treated.

### 3.10. References

- [1] J. Lee, S. Jeong, G. Naidu, Y. Ye, V. Chen, Z. Liu, S. Vigneswaran, Performance evaluation of carbon nanotube enhanced membranes for SWRO pretreatment application, *Journal of Industrial and Engineering Chemistry*, 38 (2016) 123-131.
- [2] A.K. Ghosh, E.M. Hoek, Impacts of support membrane structure and chemistry on polyamide-polysulfone interfacial composite membranes, *Journal of Membrane Science*, 336 (2009) 140-148.
- [3] P.J. Westgate, C. Park, Evaluation of proteins and organic nitrogen in wastewater treatment effluents, *Environmental Science & Technology*, 44 (2010) 5352-5357.
- [4] Z.-L. Xu, F.A. Qusay, Polyethersulfone (PES) hollow fiber ultrafiltration membranes prepared by PES/non-solvent/NMP solution, *Journal of Membrane Science*, 233 (2004) 101-111.
- [5] M.T. Tsehaye, S. Velizarov, B. Van der Bruggen, Stability of polyethersulfone membranes to oxidative agents: A review, *Polymer Degradation and Stability*, (2018).
- [6] R.J. Gohari, E. Halakoo, N. Nazri, W. Lau, T. Matsuura, A. Ismail, Improving performance and antifouling capability of PES UF membranes via blending with highly hydrophilic hydrous manganese dioxide nanoparticles, *Desalination*, 335 (2014) 87-95.
- [7] D. Rana, T. Matsuura, Surface modifications for antifouling membranes, *Chemical Reviews*, 110 (2010) 2448-2471.
- [8] A. Razmjou, J. Mansouri, V. Chen, The effects of mechanical and chemical modification of TiO<sub>2</sub> nanoparticles on the surface chemistry, structure and fouling performance of PES ultrafiltration membranes, *Journal of Membrane Science*, 378 (2011) 73-84.
- [9] N. Ghaemi, S.S. Madaeni, P. Daraei, H. Rajabi, S. Zinadini, A. Alizadeh, R. Heydari, M. Beygzadeh, S. Ghouzivad, Polyethersulfone membrane enhanced with iron oxide nanoparticles for copper removal from water: application of new functionalised Fe<sub>3</sub>O<sub>4</sub> nanoparticles, *Chemical Engineering Journal*, 263 (2015) 101-112.
- [10] J.-n. Shen, H.-m. Ruan, L.-g. Wu, C.-j. Gao, Preparation and characterisation of PES-SiO<sub>2</sub> organic-inorganic composite ultrafiltration membrane for raw water pretreatment, *Chemical Engineering Journal*, 168 (2011) 1272-1278.
- [11] N. Maximous, G. Nakhla, W. Wan, K. Wong, Preparation, characterisation and performance of Al<sub>2</sub>O<sub>3</sub>/PES membrane for wastewater filtration, *Journal of Membrane Science*, 341 (2009) 67-75.
- [12] S. Zinadini, A.A. Zinatizadeh, M. Rahimi, V. Vatanpour, H. Zangeneh, Preparation of a novel antifouling mixed-matrix PES membrane by embedding graphene oxide nanoplates, *Journal of Membrane Science*, 453 (2014) 292-301.
- [13] V. Vatanpour, S.S. Madaeni, R. Moradian, S. Zinadini, B. Astinchap, Fabrication and characterisation of novel antifouling nanofiltration membrane prepared from oxidised multiwalled carbon nanotube/polyethersulfone nanocomposite, *Journal of Membrane Science*, 375 (2011) 284-294.

- [14] X. Zhao, J. Ma, Z. Wang, G. Wen, J. Jiang, F. Shi, L. Sheng, Hyperbranched-polymer functionalised multi-walled carbon nanotubes for poly (vinylidene fluoride) membranes: From dispersion to blended fouling-control membrane, *Desalination*, 303 (2012) 29-38.
- [15] E. Celik, L. Liu, H. Choi, Protein fouling behavior of carbon nanotube/polyethersulfone composite membranes during water filtration, *Water Research*, 45 (2011) 5287-5294.
- [16] E. Celik, H. Park, H. Choi, H. Choi, Carbon nanotube blended polyethersulfone membranes for fouling control in water treatment, *Water Research*, 45 (2011) 274-282.
- [17] A. Ismail, P. Goh, S. Sanip, M. Aziz, Transport and separation properties of carbon nanotube-mixed-matrix membrane, *Separation and Purification Technology*, 70 (2009) 12-26.
- [18] V. Vatanpour, M. Esmaili, M.H.D.A. Farahani, Fouling reduction and retention increment of polyethersulfone nanofiltration membranes embedded by amine-functionalised multi-walled carbon nanotubes, *Journal of Membrane Science*, 466 (2014) 70-81.
- [19] P. Daraei, S.S. Madaeni, N. Ghaemi, M.A. Khadivi, B. Astinchap, R. Moradian, Enhancing antifouling capability of PES membrane via mixing with various types of polymer modified multi-walled carbon nanotube, *Journal of Membrane Science*, 444 (2013) 184-191.
- [20] P. Daraei, S.S. Madaeni, N. Ghaemi, H.A. Monfared, M.A. Khadivi, Fabrication of PES nanofiltration membrane by simultaneous use of multi-walled carbon nanotube and surface graft polymerisation method: comparison of MWCNT and PAA modified MWCNT, *Separation and Purification Technology*, 104 (2013) 32-44.
- [21] S.A. Dehkordi, F.Z. Ashtiani, A. Fouladitajar, High performance functionalised MWCNT/PES membrane for oil-in-water treatment, *European Water*, 58 (2017).
- [22] Y. Mansourpanah, S. Madaeni, A. Rahimpour, M. Adeli, M. Hashemi, M. Moradian, Fabrication new PES-based mixed-matrix nanocomposite membranes using polycaprolactone modified carbon nanotubes as the additive: property changes and morphological studies, *Desalination*, 277 (2011) 171-177.
- [23] F. Gojny, M. Wichmann, U. Köpke, B. Fiedler, K. Schulte, Carbon nanotube-reinforced epoxy-composites: enhanced stiffness and fracture toughness at low nanotube content, *Composites Science and Technology*, 64 (2004) 2363-2371.
- [24] L. Joseph, J. Heo, Y.-G. Park, J.R.V. Flora, Y. Yoon, Adsorption of bisphenol A and 17 $\alpha$ -ethinyl estradiol on single walled carbon nanotubes from seawater and brackish water, *Desalination*, 281 (2011) 68-74.
- [25] M. Sianipar, S.H. Kim, F. Iskandar, I.G. Wenten, Functionalised carbon nanotube (CNT) membrane: progress and challenges, *RSC Advances*, 7 (2017) 51175-51198.
- [26] C. Chen, X. Chen, L. Xu, Z. Yang, W. Li, Modification of multi-walled carbon nanotubes with fatty acid and their tribological properties as lubricant additive, *Carbon*, 43 (2005) 1660-1666.
- [27] J.N. Coleman, U. Khan, W.J. Blau, Y.K. Gun'ko, Small but strong: a review of the mechanical properties of carbon nanotube-polymer composites, *Carbon*, 44 (2006) 1624-1652.
- [28] N.N. Gumbi, M. Hu, B.B. Mamba, J. Li, E.N. Nxumalo, Macrovoid-free PES/SPSf/O-MWCNT ultrafiltration membranes with improved mechanical strength, antifouling and antibacterial properties, *Journal of Membrane Science*, 566 (2018) 288-300.

- [29] J.-H. Choi, J. Jegal, W.-N. Kim, Fabrication and characterisation of multi-walled carbon nanotubes/polymer blend membranes, *Journal of Membrane Science*, 284 (2006) 406-415.
- [30] Sigma-Aldrich, Carbon Nanotubes, in: <https://www.sigmaaldrich.com/materials-science/material-science-products.html?TablePage=16376687>, Sigma-Aldrich, owned by Merck KGaA, Darmstadt, Germany, 2018..
- [31] Nanocyl, The Carbon Nanotube Specialist, in: <http://www.nanocyl.com/>, Nanocyl SA, 2018.
- [32] A.P. Rao, N. Desai, R. Rangarajan, Interfacially synthesized thin film composite RO membranes for seawater desalination, *Journal of Membrane Science*, 124 (1997) 263-272.
- [33] M.M. Pendergast, E.M. Hoek, A review of water treatment membrane nanotechnologies, *Energy & Environmental Science*, 4 (2011) 1946-1971.
- [34] N. Peng, N. Widjojo, P. Sukitpaneenit, M.M. Teoh, G.G. Lipscomb, T.-S. Chung, J.-Y. Lai, Evolution of polymeric hollow fibers as sustainable technologies: past, present, and future, *Progress in Polymer Science*, 37 (2012) 1401-1424.
- [35] A.K. Shukla, J. Alam, M. Alhoshan, L.A. Dass, M. Muthumareeswaran, Development of a nanocomposite ultrafiltration membrane based on polyphenylsulfone blended with graphene oxide, *Scientific Reports*, 7 (2017).
- [36] G. Arthanareeswaran, V.M. Starov, Effect of solvents on performance of polyethersulfone ultrafiltration membranes: Investigation of metal ion separations, *Desalination*, 267 (2011) 57-63.
- [37] G.R. Guillen, G.Z. Ramon, H.P. Kavehpour, R.B. Kaner, E.M. Hoek, Direct microscopic observation of membrane formation by non-solvent induced phase separation, *Journal of Membrane Science*, 431 (2013) 212-220.
- [38] T.-H. Young, L.-W. Chen, Pore formation mechanism of membranes from phase-inversion process, *Desalination*, 103 (1995) 233-247.
- [39] G.R. Guillen, Y. Pan, M. Li, E.M. Hoek, Preparation and characterisation of membranes formed by non-solvent induced phase separation: a review, *Industrial & Engineering Chemistry Research*, 50 (2011) 3798-3817.
- [40] D. Wu, L. Zhao, V.K. Vakharia, W. Salim, W.W. Ho, Synthesis and characterisation of nanoporous polyethersulfone membrane as support for composite membrane in CO<sub>2</sub> separation: From lab to pilot scale, *Journal of Membrane Science*, 510 (2016) 58-71.
- [41] A. Rahimpour, M. Jahanshahi, S. Khalili, A. Mollahosseini, A. Zirepour, B. Rajaeian, Novel functionalised carbon nanotubes for improving the surface properties and performance of polyethersulfone (PES) membrane, *Desalination*, 286 (2012) 99-107.
- [42] N. Ghaemi, S.S. Madaeni, P. Daraei, H. Rajabi, T. Shojaeimehr, F. Rahimpour, B. Shirvani, PES mixed-matrix nanofiltration membrane embedded with polymer wrapped MWCNT: Fabrication and performance optimization in dye removal by RSM, *Journal of hazardous materials*, 298 (2015) 111-121.
- [43] W. Wang, L. Zhu, B. Shan, C. Xie, C. Liu, F. Cui, G. Li, Preparation and characterisation of SLS-CNT/PES ultrafiltration membrane with antifouling and antibacterial properties, *Journal of Membrane Science*, 548 (2018) 459-469.

- [44] J. Sun, L. Wu, Y. Li, Removal of lead ions from polyether sulfone/Pb (II)-imprinted multi-walled carbon nanotubes, mixed-matrix membrane, *Journal of the Taiwan Institute of Chemical Engineers*, 78 (2017) 219-229.
- [45] K. Zhu, G. Wang, S. Zhang, Y. Du, Y. Lu, R. Na, Y. Mu, Y. Zhang, Preparation of organic–inorganic hybrid membranes with superior antifouling property by incorporating polymer-modified multiwall carbon nanotubes, *RSC Advances*, 7 (2017) 30564-30572.
- [46] L. Wang, X. Song, T. Wang, S. Wang, Z. Wang, C. Gao, Fabrication and characterisation of polyethersulfone/carbon nanotubes (PES/CNTs) based mixed-matrix membranes (MMMs) for nanofiltration application, *Applied Surface Science*, 330 (2015) 118-125.
- [47] Y. Yang, C. Nie, Y. Deng, C. Cheng, C. He, L. Ma, C. Zhao, Improved antifouling and antimicrobial efficiency of ultrafiltration membranes with functional carbon nanotubes, *RSC Advances*, 6 (2016) 88265-88276.
- [48] Q. Zhang, Y. Liu, Y. Su, R. Zhang, L. Fan, Y. Liu, T. Ma, Z. Jiang, Fabrication and characterisation of antifouling carbon nanotube/polyethersulfone ultrafiltration membranes, *RSC Advances*, 6 (2016) 35532-35538.
- [49] C. Smolders, A. Reuvers, R. Boom, I. Wienk, Microstructures in phase-inversion membranes. Part 1. Formation of macrovoids, *Journal of Membrane Science*, 73 (1992) 259-275.
- [50] I. Wienk, R. Boom, M. Beerlage, A. Bulte, C. Smolders, H. Strathmann, Recent advances in the formation of phase-inversion membranes made from amorphous or semi-crystalline polymers, *Journal of Membrane Science*, 113 (1996) 361-371.
- [51] J. Mulder, *Basic principles of membrane technology*, Springer Science & Business Media, 2012.
- [52] D. Wang, K. Li, W. Teo, Relationship between mass ratio of non-solvent-additive to solvent in membrane casting solution and its coagulation value, *Journal of Membrane Science*, 98 (1995) 233-240.
- [53] M. Sadrzadeh, S. Bhattacharjee, Rational design of phase-inversion membranes by tailoring thermodynamics and kinetics of casting solution using polymer additives, *Journal of Membrane Science*, 441 (2013) 31-44.
- [54] G.D. Vilakati, E.M. Hoek, B.B. Mamba, Investigating the usability of alkali lignin as an additive in polysulfone ultrafiltration membranes, *BioResources*, 10 (2015) 3079-3096.
- [55] Y. Feng, G. Han, T.-S. Chung, M. Weber, N. Widjojo, C. Maletzko, Effects of polyethylene glycol on membrane formation and properties of hydrophilic sulfonated polyphenylenesulfone (sPPSU) membranes, *Journal of Membrane Science*, (2017).
- [56] J. Garcia-Ivars, M.-I. Iborra-Clar, M.-I. Alcaina-Miranda, B. Van der Bruggen, Comparison between hydrophilic and hydrophobic metal nanoparticles on the phase separation phenomena during formation of asymmetric polyethersulphone membranes, *Journal of Membrane Science*, 493 (2015) 709-722.
- [57] J. Yin, G. Zhu, B. Deng, Multi-walled carbon nanotubes (MWNTs)/polysulfone (PSU) mixed-matrix hollow fiber membranes for enhanced water treatment, *Journal of Membrane Science*, 437 (2013) 237-248.

- [58] P. Machado, A. Habert, C. Borges, Membrane formation mechanism based on precipitation kinetics and membrane morphology: flat and hollow fiber polysulfone membranes, *Journal of Membrane Science*, 155 (1999) 171-183.
- [59] D. Wang, K. Li, W. Teo, Preparation of poly (ether sulfone) and poly (ether imide) hollow fiber membranes for gas separation: Effect of internal coagulant, in: *ACS Symposium Series 744* (1999) 96-109, ScholarBank@NUS Repository (1999).
- [60] Y. Feng, K. Wang, C.H. Davies, H. Wang, Carbon nanotube/alumina/polyethersulfone hybrid hollow fiber membranes with enhanced mechanical and anti-fouling properties, *Nanomaterials*, 5 (2015) 1366-1378.
- [61] J. Schaep, C. Vandecasteele, Evaluating the charge of nanofiltration membranes, *Journal of membrane science*, 188 (2001) 129-136.
- [62] W. Lau, A. Ismail, N. Misdan, M. Kassim, A recent progress in thin film composite membrane: a review, *Desalination*, 287 (2012) 190-199.
- [63] F.-Y. Zhao, Y.-L. Ji, X.-D. Weng, Y.-F. Mi, C.-C. Ye, Q.-F. An, C.-J. Gao, High-flux positively charged nanocomposite nanofiltration membranes filled with poly (dopamine) modified multiwall carbon nanotubes, *ACS Applied Materials & Interfaces*, 8 (2016) 6693-6700.
- [64] Y. Wang, R. Ou, Q. Ge, H. Wang, T. Xu, Preparation of polyethersulfone/carbon nanotube substrate for high-performance forward osmosis membrane, *Desalination*, 330 (2013) 70-78.
- [65] M. Son, H.-g. Choi, L. Liu, E. Celik, H. Park, H. Choi, Efficacy of carbon nanotube positioning in the polyethersulfone support layer on the performance of thin-film composite membrane for desalination, *Chemical Engineering Journal*, 266 (2015) 376-384.
- [66] H.-g. Choi, M. Son, H. Choi, Integrating seawater desalination and wastewater reclamation forward osmosis process using thin-film composite mixed-matrix membrane with functionalised carbon nanotube blended polyethersulfone support layer, *Chemosphere*, 185 (2017) 1181-1188.
- [67] J. Heo, M. Choi, J. Hong, Facile Surface Modification of Polyethylene Film via Spray-Assisted Layer-by-Layer Self-Assembly of Graphene Oxide for Oxygen Barrier Properties, *Scientific Reports*, 9 (2019).
- [68] L. Liu, D.Y. Di, H. Park, M. Son, H.-G. Hur, H. Choi, Improved antifouling performance of polyethersulfone (PES) membrane via surface modification by CNTs bound polyelectrolyte multilayers, *RSC Advances*, 5 (2015) 7340-7348.
- [69] L. Liu, M. Son, S. Chakraborty, C. Bhattacharjee, H. Choi, Fabrication of ultra-thin polyelectrolyte/carbon nanotube membrane by spray-assisted layer-by-layer technique: characterisation and its anti-protein fouling properties for water treatment, *Desalination and Water Treatment*, 51 (2013) 6194-6200.
- [70] H. Strathmann, K. Kock, P. Amar, R. Baker, The formation mechanism of asymmetric membranes, *Desalination*, 16 (1975) 179-203.
- [71] A.J. Reuvers, Membrane formation: diffusion induced demixing processes in ternary polymeric systems, in, University of Twente, 1987.
- [72] J. Craig, J. Knudsen, V. Holland, Characterisation of acrylic fiber structure, *Textile Research Journal*, 32 (1962) 435-448.

- [73] Y. Liu, G. Koops, H. Strathmann, Characterisation of morphology controlled polyethersulfone hollow fiber membranes by the addition of polyethylene glycol to the dope and bore liquid solution, *Journal of Membrane Science*, 223 (2003) 187-199.
- [74] R. Matz, The structure of cellulose acetate membranes 1. The development of porous structures in anisotropic membranes, *Desalination*, 10 (1972) 1-15.
- [75] L.-F. Fang, H.-Y. Yang, L. Cheng, N. Kato, S. Jeon, R. Takagi, H. Matsuyama, Effect of Molecular Weight of Sulfonated Poly (ether sulfone)(SPES) on the Mechanical Strength and Antifouling Properties of Poly (ether sulfone)/SPES Blend Membranes, *Industrial & Engineering Chemistry Research*, 56 (2017) 11302-11311.
- [76] M. Guillotin, C. Lemoyne, C. Noel, L. Monnerie, Physicochemical processes occurring during the formation of cellulose diacetate membranes. Research of criteria for optimizing membrane performance. IV. Cellulose diacetate-acetone-organic additive casting solutions, *Desalination*, 21 (1977) 165-181.
- [77] N.Y. Yip, A. Tiraferri, W.A. Phillip, J.D. Schiffman, M. Elimelech, High performance thin-film composite forward osmosis membrane, *Environmental Science & Technology*, 44 (2010) 3812-3818.
- [78] N. Peng, T.-S. Chung, K.Y. Wang, Macrovoid evolution and critical factors to form macrovoid-free hollow fiber membranes, *Journal of Membrane Science*, 318 (2008) 363-372.
- [79] S.S. Madaeni, A.H. Taheri, Effect of casting solution on morphology and performance of PVDF microfiltration membranes, *Chemical Engineering & Technology*, 34 (2011) 1328-1334.
- [80] M. Son, H. Park, L. Liu, H. Choi, J.H. Kim, H. Choi, Thin-film nanocomposite membrane with CNT positioning in support layer for energy harvesting from saline water, *Chemical Engineering Journal*, 284 (2016) 68-77.
- [81] Z.-G. Wang, Z.-K. Xu, L.-S. Wan, Modulation the morphologies and performance of polyacrylonitrile-based asymmetric membranes containing reactive groups: Effect of non-solvents in the dope solution, *Journal of Membrane Science*, 278 (2006) 447-456.
- [82] I. Cabasso, E. Klein, J.K. Smith, Polysulfone hollow fibers. I. Spinning and properties, *Journal of Applied Polymer Science*, 20 (1976) 2377-2394.
- [83] S. Gordeyev, S. Shilton, Forced convection spinning of gas separation hollow fibre membranes: some underlying factors, mechanisms and effects, *Journal of Membrane Science*, 229 (2004) 225-233.
- [84] M.H.D.A. Farahani, H. Rabiee, V. Vatanpour, Comparing the effect of incorporation of various nanoparticulate on the performance and antifouling properties of polyethersulfone nanocomposite membranes, *Journal of Water Process Engineering*, 27 (2019) 47-57.
- [85] N. Vogrin, Č. Stropnik, V. Musil, M. Brumen, The wet phase separation: the effect of cast solution thickness on the appearance of macrovoids in the membrane forming ternary cellulose acetate/acetone/water system, *Journal of Membrane Science*, 207 (2002) 139-141.
- [86] D. Li, T.-S. Chung, J. Ren, R. Wang, Thickness dependence of macrovoid evolution in wet phase-inversion asymmetric membranes, *Industrial & Engineering Chemistry Research*, 43 (2004) 1553-1556.

- [87] Y. Feng, G. Han, L. Zhang, S.-B. Chen, T.-S. Chung, M. Weber, C. Staudt, C. Maletzko, Rheology and phase-inversion behavior of polyphenylenesulfone (PPSU) and sulfonated PPSU for membrane formation, *Polymer*, 99 (2016) 72-82.
- [88] L.-W. Chen, T.-H. Young, Effect of non-solvents on the mechanism of wet-casting membrane formation from EVAL copolymers, *Journal of Membrane Science*, 59 (1991) 15-26.
- [89] C. Barth, M. Goncalves, A. Pires, J. Roeder, B. Wolf, Asymmetric polysulfone and polyethersulfone membranes: effects of thermodynamic conditions during formation on their performance, *Journal of Membrane Science*, 169 (2000) 287-299.
- [90] R. Boom, I. Wienk, T. Van den Boomgaard, C. Smolders, Microstructures in phase-inversion membranes. Part 2. The role of a polymeric additive, *Journal of Membrane Science*, 73 (1992) 277-292.
- [91] Y. Ma, F. Shi, J. Ma, M. Wu, J. Zhang, C. Gao, Effect of PEG additive on the morphology and performance of polysulfone ultrafiltration membranes, *Desalination*, 272 (2011) 51-58.
- [92] G. Arthanareeswaran, D. Mohan, M. Raajenthiren, Preparation, characterisation and performance studies of ultrafiltration membranes with polymeric additive, *Journal of Membrane Science*, 350 (2010) 130-138.
- [93] E. Saljoughi, M. Amirilargani, T. Mohammadi, Effect of PEG additive and coagulation bath temperature on the morphology, permeability and thermal/chemical stability of asymmetric CA membranes, *Desalination*, 262 (2010) 72-78.
- [94] V. Vatanpour, S.S. Madaeni, R. Moradian, S. Zinadini, B. Astinchap, Novel antibifouling nanofiltration polyethersulfone membrane fabricated from embedding TiO<sub>2</sub> coated multiwalled carbon nanotubes, *Separation and Purification Technology*, 90 (2012) 69-82.
- [95] Q.-Z. Zheng, P. Wang, Y.-N. Yang, D.-J. Cui, The relationship between porosity and kinetics parameter of membrane formation in PSF ultrafiltration membrane, *Journal of Membrane Science*, 286 (2006) 7-11.
- [96] M. Shi, G. Printsypar, O. Iliev, V.M. Calo, G.L. Amy, S.P. Nunes, Water flow prediction for membranes using 3D simulations with detailed morphology, *Journal of Membrane Science*, 487 (2015) 19-31.
- [97] J. Lee, H. Yoon, J.H. Yoo, D.-C. Choi, C.H. Nahm, S.H. Lee, H.-R. Chae, Y.H. Kim, C.-H. Lee, P.-K. Park, Influence of a sublayer structure of thin-film composite reverse osmosis membranes on the overall water flux, *Environmental Science: Water Research & Technology*, (2018).
- [98] R. Wang, L. Shi, C.Y. Tang, S. Chou, C. Qiu, A.G. Fane, Characterisation of novel forward osmosis hollow fiber membranes, *Journal of membrane science*, 355 (2010) 158-167.
- [99] K. Balasubramanian, M. Burghard, Chemically functionalised carbon nanotubes, small, 1 (2005) 180-192.
- [100] S. Tsang, Y. Chen, P. Harris, M. Green, A simple chemical method of opening and filling carbon nanotubes, *Nature*, 372 (1994) 159.
- [101] X.-X. Xu, C.-L. Zhou, B.-R. Zeng, H.-P. Xia, W.-G. Lan, X.-M. He, Structure and properties of polyamidoamine/polyacrylonitrile composite nanofiltration membrane prepared by interfacial polymerisation, *Separation and Purification Technology*, 96 (2012) 229-236.

- [102] R. Sepahvand, M. Adeli, B. Astinchap, R. Kabiri, New nanocomposites containing metal nanoparticles, carbon nanotube and polymer, *Journal of Nanoparticle Research*, 10 (2008) 1309.
- [103] R. Moradian, B. Astinchap, Synthesis and control size of SnS<sub>2</sub> nanoparticles on the surface multi-walled carbon nanotubes, *Nano*, 5 (2010) 139-142.
- [104] G. Vuković, A. Marinković, M. Obradović, V. Radmilović, M. Čolić, R. Aleksić, P.S. Uskoković, Synthesis, characterisation and cytotoxicity of surface amino-functionalised water-dispersible multi-walled carbon nanotubes, *Applied Surface Science*, 255 (2009) 8067-8075.
- [105] L. Chen, H. Xie, Y. Li, W. Yu, Carbon nanotubes with hydrophilic surfaces produced by a wet-mechanochemical reaction with potassium hydroxide using ethanol as solvent, *Materials Letters*, 63 (2009) 45-47.
- [106] E. Salehi, S. Madaeni, L. Rajabi, V. Vatanpour, A. Derakhshan, S. Zinadini, S. Ghorabi, H.A. Monfared, Novel chitosan/poly (vinyl) alcohol thin adsorptive membranes modified with amino functionalised multi-walled carbon nanotubes for Cu (II) removal from water: preparation, characterization, adsorption kinetics and thermodynamics, *Separation and Purification Technology*, 89 (2012) 309-319.
- [107] J.-Y. Choi, S.-W. Han, W.-S. Huh, L.-S. Tan, J.-B. Baek, In situ grafting of carboxylic acid-terminated hyperbranched poly (ether-ketone) to the surface of carbon nanotubes, *Polymer*, 48 (2007) 4034-4040.
- [108] L. Qiu, X. Yang, X. Gou, W. Yang, Z.F. Ma, G.G. Wallace, D. Li, Dispersing carbon nanotubes with graphene oxide in water and synergistic effects between graphene derivatives, *Chemistry—A European Journal*, 16 (2010) 10653-10658.
- [109] S.H. Aboutalebi, A.T. Chidembo, M. Salari, K. Konstantinov, D. Wexler, H.K. Liu, S.X. Dou, Comparison of GO, GO/MWCNTs composite and MWCNTs as potential electrode materials for supercapacitors, *Energy & Environmental Science*, 4 (2011) 1855-1865.
- [110] S. Chatterjee, F. Nafezarefi, N. Tai, L. Schlagenhauf, F. Nüesch, B. Chu, Size and synergy effects of nanofiller hybrids including graphene nanoplatelets and carbon nanotubes in mechanical properties of epoxy composites, *Carbon*, 50 (2012) 5380-5386.
- [111] J. Zhang, Z. Xu, M. Shan, B. Zhou, Y. Li, B. Li, J. Niu, X. Qian, Synergetic effects of oxidised carbon nanotubes and graphene oxide on fouling control and anti-fouling mechanism of polyvinylidene fluoride ultrafiltration membranes, *Journal of Membrane Science*, 448 (2013) 81-92.
- [112] S. Zhang, S. Yin, C. Rong, P. Huo, Z. Jiang, G. Wang, Synergistic effects of functionalised graphene and functionalised multi-walled carbon nanotubes on the electrical and mechanical properties of poly (ether sulfone) composites, *European Polymer Journal*, 49 (2013) 3125-3134.
- [113] M. Shaban, A.M. Ashraf, H. AbdAllah, H.A. El-Salam, Titanium dioxide nanoribbons/multi-walled carbon nanotube nanocomposite blended polyethersulfone membrane for brackish water desalination, *Desalination*, 444 (2018) 129-141.
- [114] S. Zinadini, S. Rostami, V. Vatanpour, E. Jalilian, Preparation of antibiofouling polyethersulfone mixed-matrix NF membrane using photocatalytic activity of ZnO/MWCNTs nanocomposite, *Journal of Membrane Science*, 529 (2017) 133-141.

- [115] M. Homayoonfal, A. Akbari, M.R. Mehrnia, Preparation of polysulfone nanofiltration membranes by UV-assisted grafting polymerisation for water softening, *Desalination*, 263 (2010) 217-225.
- [116] C. Manea, M. Mulder, Characterisation of polymer blends of polyethersulfone/sulfonated polysulfone and polyethersulfone/sulfonated polyetheretherketone for direct methanol fuel cell applications, *Journal of Membrane Science*, 206 (2002) 443-453.
- [117] S. Li, Z. Cui, L. Zhang, B. He, J. Li, The effect of sulfonated polysulfone on the compatibility and structure of polyethersulfone-based blend membranes, *Journal of Membrane Science*, 513 (2016) 1-11.
- [118] L. Zhang, Z. Cui, M. Hu, Y. Mo, S. Li, B. He, J. Li, Preparation of PES/SPSf blend ultrafiltration membranes with high performance via H<sub>2</sub>O-induced gelation phase separation, *Journal of Membrane Science*, 540 (2017) 136-145.
- [119] A. Rahimpour, S.S. Madaeni, S. Ghorbani, A. Shockravi, Y. Mansourpanah, The influence of sulfonated polyethersulfone (SPES) on surface nano-morphology and performance of polyethersulfone (PES) membrane, *Applied Surface Science*, 256 (2010) 1825-1831.
- [120] N. Widjojo, T.-S. Chung, M. Weber, C. Maletzko, V. Warzelhan, The role of sulphonated polymer and macrovoid-free structure in the support layer for thin-film composite (TFC) forward osmosis (FO) membranes, *Journal of Membrane Science*, 383 (2011) 214-223.
- [121] C.-W.A. Ng, W.J. MacKnight, Ionomeric blends of poly (ethyl acrylate-co-4-vinylpyridine) with zinc-neutralized sulfonated poly (ethylene terephthalate). 3. Effects of functionalisation level, *Macromolecules*, 29 (1996) 2412-2420.
- [122] K. Aouachria, N. Belhaneche-Bensemra, Miscibility of PVC/PMMA blends by vicat softening temperature, viscometry, DSC and FTIR analysis, *Polymer Testing*, 25 (2006) 1101-1108.
- [123] J. Li, R. Sanderson, G. Chai, D. Hallbauer, Development of an ultrasonic technique for in situ investigating the properties of deposited protein during crossflow ultrafiltration, *Journal of Colloid and Interface science*, 284 (2005) 228-238.
- [124] Q. Shi, Y. Su, W. Zhao, C. Li, Y. Hu, Z. Jiang, S. Zhu, Zwitterionic polyethersulfone ultrafiltration membrane with superior antifouling property, *Journal of Membrane Science*, 319 (2008) 271-278.
- [125] W.-F. Chan, H.-y. Chen, A. Surapathi, M.G. Taylor, X. Shao, E. Marand, J.K. Johnson, Zwitterion functionalised carbon nanotube/polyamide nanocomposite membranes for water desalination, *ACS Nano*, 7 (2013) 5308-5319.
- [126] G. Cheng, G. Li, H. Xue, S. Chen, J.D. Bryers, S. Jiang, Zwitterionic carboxybetaine polymer surfaces and their resistance to long-term biofilm formation, *Biomaterials*, 30 (2009) 5234-5240.
- [127] A. Tiraferri, Y. Kang, E.P. Giannelis, M. Elimelech, Superhydrophilic thin-film composite forward osmosis membranes for organic fouling control: fouling behavior and antifouling mechanisms, *Environmental Science & Technology*, 46 (2012) 11135-11144.
- [128] T.-H. Bae, T.-M. Tak, Effect of TiO<sub>2</sub> nanoparticles on fouling mitigation of ultrafiltration membranes for activated sludge filtration, *Journal of Membrane Science*, 249 (2005) 1-8.

- [129] L. Bai, H. Liang, J. Crittenden, F. Qu, A. Ding, J. Ma, X. Du, S. Guo, G. Li, Surface modification of UF membranes with functionalised MWCNTs to control membrane fouling by NOM fractions, *Journal of Membrane Science*, 492 (2015) 400-411.
- [130] J. Peng, Y. Su, Q. Shi, W. Chen, Z. Jiang, Protein fouling resistant membrane prepared by amphiphilic pegylated polyethersulfone, *Bioresource technology*, 102 (2011) 2289-2295.
- [131] J. Pieracci, J.V. Crivello, G. Belfort, Increasing membrane permeability of UV-modified poly (ether sulfone) ultrafiltration membranes, *Journal of Membrane Science*, 202 (2002) 1-16.
- [132] K. Xiao, X. Wang, X. Huang, T.D. Waite, X. Wen, Combined effect of membrane and foulant hydrophobicity and surface charge on adsorptive fouling during microfiltration, *Journal of Membrane Science*, 373 (2011) 140-151.
- [133] S. Sablani, M. Goosen, R. Al-Belushi, M. Wilf, Concentration polarization in ultrafiltration and reverse osmosis: a critical review, *Desalination*, 141 (2001) 269-289.
- [134] E.-S. Kim, G. Hwang, M.G. El-Din, Y. Liu, Development of nanosilver and multi-walled carbon nanotubes thin-film nanocomposite membrane for enhanced water treatment, *Journal of Membrane Science*, 394 (2012) 37-48.
- [135] S. Al Aani, V. Gomez, C.J. Wright, N. Hilal, Fabrication of antibacterial mixed-matrix nanocomposite membranes using hybrid nanostructure of silver coated multi-walled carbon nanotubes, *Chemical Engineering Journal*, 326 (2017) 721-736.
- [136] X. Wu, Z. Xie, H. Wang, C. Zhao, D. Ng, K. Zhang, Improved filtration performance and antifouling properties of polyethersulfone ultrafiltration membranes by blending with carboxylic acid functionalised polysulfone, *RSC Advances*, 8 (2018) 7774-7784.
- [137] A. Idris, N.M. Zain, M. Noordin, Synthesis, characterisation and performance of asymmetric polyethersulfone (PES) ultrafiltration membranes with polyethylene glycol of different molecular weights as additives, *Desalination*, 207 (2007) 324-339.
- [138] N. Ochoa, P. Pradanos, L. Palacio, C. Pagliero, J. Marchese, A. Hernández, Pore size distributions based on AFM imaging and retention of multidisperse polymer solutes: characterisation of polyethersulfone UF membranes with dopes containing different PVP, *Journal of Membrane Science*, 187 (2001) 227-237.
- [139] J. Marchese, M. Ponce, N. Ochoa, P. Prádanos, L. Palacio, A. Hernández, Fouling behaviour of polyethersulfone UF membranes made with different PVP, *Journal of Membrane Science*, 211 (2003) 1-11.
- [140] R. Sengur, C.F. de Lannoy, T. Turken, M. Wiesner, I. Koyuncu, Fabrication and characterisation of hydroxylated and carboxylated multiwalled carbon nanotube/polyethersulfone (PES) nanocomposite hollow fiber membranes, *Desalination*, 359 (2015) 123-140.
- [141] B. Arash, Q. Wang, V. Varadan, Mechanical properties of carbon nanotube/polymer composites, *Scientific Reports*, 4 (2014) 6479.
- [142] D. Qian, E.C. Dickey, R. Andrews, T. Rantell, Load transfer and deformation mechanisms in carbon nanotube-polystyrene composites, *Applied physics letters*, 76 (2000) 2868-2870.

- [143] L. An, Y. Pan, X. Shen, H. Lu, Y. Yang, Rod-like attapulgite/polyimide nanocomposites with simultaneously improved strength, toughness, thermal stability and related mechanisms, *Journal of Materials Chemistry*, 18 (2008) 4928-4941.
- [144] M. Fang, K. Wang, H. Lu, Y. Yang, S. Nutt, Covalent polymer functionalisation of graphene nanosheets and mechanical properties of composites, *Journal of Materials Chemistry*, 19 (2009) 7098-7105.
- [145] H. Zarrabi, M.E. Yekavalangi, V. Vatanpour, A. Shockravi, M. Safarpour, Improvement in desalination performance of thin film nanocomposite nanofiltration membrane using amine-functionalised multiwalled carbon nanotube, *Desalination*, 394 (2016) 83-90.
- [146] R.W. Field, D. Wu, J.A. Howell, B.B. Gupta, Critical flux concept for microfiltration fouling, *Journal of Membrane Science*, 100 (1995) 259-272.
- [147] H. Bauser, H. Chmiel, N. Stroh, E. Walitza, Control of concentration polarization and fouling of membranes in medical, food and biotechnical applications, *Journal of Membrane Science*, 27 (1986) 195-202.
- [148] A.S. Grandison, W. Youravong, M.J. Lewis, Hydrodynamic factors affecting flux and fouling during ultrafiltration of skimmed milk, *Le Lait*, 80 (2000) 165-174.
- [149] K. Jim, A. Fane, C. Fell, D. Joy] Fouling mechanisms of membranes during protein ultrafiltration, *Journal of Membrane Science*, 68 (1992) 79-91.
- [150] R.-S. Juang, H.-L. Chen, Y.-S. Chen, Membrane fouling and resistance analysis in dead-end ultrafiltration of *Bacillus subtilis* fermentation broths, *Separation and Purification Technology*, 63 (2008) 531-538.
- [151] N.N. Gumbi, T.G. Tshabalala, S.D. Mhlanga, B.B. Mamba, A.I. Schäfer, E.N. Nxumalo, Chapter 8 - Prospects and State-of-the-Art of Carbon Nanotube Membranes in Desalination Processes A2 - Arafat, Hassan A, in: *Desalination Sustainability*, Elsevier, 2017, pp. 305-339.
- [152] L. Ma, X. Dong, M. Chen, L. Zhu, C. Wang, F. Yang, Y. Dong, Fabrication and water treatment application of carbon nanotubes (CNTs)-based composite membranes: a review, *Membranes*, 7 (2017) 16.
- [153] E.M. Wanda, B.B. Mamba, T.A. Msagati, Nitrogen Doped Carbon Nanotubes/Polyethersulfone Blend Membranes for Removing Emerging Micropollutants, *CLEAN–Soil, Air, Water*, 45 (2017) 1500889.
- [154] G. Kaminska, J. Bohdziewicz, J. Calvo, P. Prádanos, L. Palacio, A. Hernández, Fabrication and characterisation of polyethersulfone nanocomposite membranes for the removal of endocrine disrupting micropollutants from wastewater. Mechanisms and performance, *Journal of Membrane Science*, 493 (2015) 66-79.
- [155] J. Heo, J.R. Flora, N. Her, Y.-G. Park, J. Cho, A. Son, Y. Yoon, Removal of bisphenol A and 17 $\beta$ -estradiol in single walled carbon nanotubes–ultrafiltration (SWNTs–UF) membrane systems, *Separation and Purification Technology*, 90 (2012) 39-52.
- [156] J.R. McCutcheon, M. Elimelech, Influence of membrane support layer hydrophobicity on water flux in osmotically driven membrane processes, *Journal of Membrane Science*, 318 (2008) 458-466.
- [157] J. Su, T.-S. Chung, Sublayer structure and reflection coefficient and their effects on concentration polarization and membrane performance in FO processes, *Journal of Membrane Science*, 376 (2011) 214-224.

[158] P. Wick, P. Manser, L.K. Limbach, U. Dettlaff-Weglikowska, F. Krumeich, S. Roth, W.J. Stark, A. Bruinink, The degree and kind of agglomeration affect carbon nanotube cytotoxicity, *Toxicology Letters*, 168 (2007) 121-131.

[159] A. Magrez, S. Kasas, V. Salicio, N. Pasquier, J.W. Seo, M. Celio, S. Catsicas, B. Schwaller, L. Forró, Cellular toxicity of carbon-based nanomaterials, *Nano Letters*, 6 (2006) 1121-1125.

**CHAPTER 4**  
**POLYETHERSULFONE/MULTI-WALLED CARBON NANOTUBE**  
**ULTRAFILTRATION (UF) MEMBRANES FOR ADSORPTIVE REMOVAL OF**  
**NATURAL HORMONE ESTRONE**

---

**Summary of the chapter**

This chapter reports on the adsorptive removal of natural hormone estrone (E1) by large pore-size polyethersulfone/multi-walled carbon nanotube (PES/MWCNT) ultrafiltration (UF) membranes. The PES/O-MWCNT membranes were prepared via conventional non-solvent induced phase-separation method, in which oxidised MWCNTs (O-MWCNTs) were homogeneously dispersed in the PES matrix. Membrane surface and morphological features presumed to have significant influence on E1 removal, were characterised using scanning electron microscopy (SEM), atomic force microscopy (AFM), zeta potential measurements and molecular weight cut-off (MWCO) experiments. The incorporation of O-MWCNTs resulted in a 20% increase in the membrane adsorption capacity; adsorption initially increased with an increase in O-MWCNT content followed by a decline upon further increments in O-MWCNT loading. Langmuir maximum adsorption capacity increased by 30% in the presence of 0.5 wt.% O-MWCNTs in PES membranes (31.25 mg/g) in comparison to bare PES UF membrane (23.81 mg/g). The adsorption kinetics followed the pseudo-second-order kinetic model and the Freundlich isotherm provided a better fit for the adsorption data. After five adsorption-regeneration cycles, the PES/O-MWCNT membranes maintained almost the same adsorption efficiency, a property that is ideal for repeated use. Results obtained in this study provided evidence that the right combination of membrane surface characteristics and adsorbate solution chemistry is necessary for an open UF membrane to display reasonable removal efficiencies for low molecular-weight solutes such as E1.

**Keywords:** estrone; multi-walled carbon nanotubes; mixed-matrix membrane; adsorptive interactions; hydrogen-bonding;  $\pi$ - $\pi$  interactions

## **4.1. Introduction**

### **4.1.1. Techniques for the removal of estrogenic EDCs from water systems**

As early as 1965, Stumm-Zollinger and Fair were among the first researchers to demonstrate that several steroid hormones are unlikely to be removed by conventional wastewater treatment processes and raised concerns regarding their possible adverse effects in municipal wastewater and receiving water bodies that eventually supply drinking water [1]. Since then, numerous studies have been carried out which have confirmed this fact, while advanced technologies such as ozonation, ultraviolet irradiation and membrane filtration have been shown to be capable of enhancing their removal [2-7]. Steroid hormones generally find their way into wastewater, natural surface waters and groundwater through excreted human urine [8]. The excreted hormones in urine are predominantly in an inactive form, and become reactivated by enzymes produced by bacteria present in water sources [9]. The problem with the presence of these estrogenic hormones and several other organic micropollutants in water bodies is that they are endocrine-disrupting compounds (EDCs) in humans and in animals [10]. This means that they are capable of interfering with the endocrine system by mimicking the natural body hormones and triggering responses by blocking receptors thus preventing hormone responses [11].

The difficulty in removing hormones from water sources lies in the fact that they occur at extremely low concentrations and that their sizes or molecular weights are very small (268 – 315 Da) [11]. Therefore, in pursuit of selecting a removal method for hormones in water

sources, their small sizes need to be taken into account. As such nanofiltration (NF) and reverse osmosis (RO) membranes are obvious candidates for the removal hormones, owing to their small membrane pore sizes. Numerous studies have since been carried out and have demonstrated the ability of high-pressure NF and RO membranes for the retention of hormones and other EDCs via size exclusion or adsorption mechanism or combination of both mechanisms [6, 12-15].

Apart from the characteristics of the membrane used, other physicochemical properties of hormones such as the magnitude of their octanol–water partition coefficients ( $\log K_{ow}$ ) also influences the extent of their removal by membranes [16]. The  $\log K_{ow}$  value is used to express the hydrophobicity of organic solutes. Organic solutes with  $\log K_{ow} > 2.5$  are expected to be hydrophobic, while those with  $\log K_{ow} < 2.5$  are presumably hydrophilic [13]. Seemingly,  $\log K_{ow}$  values can be correlated with hydrophobic-hydrophobic interactions as the most likely separation mechanism to take precedence when hydrophobic membranes are used. Yoon et al., investigated the removal of EDCs and pharmaceuticals and personal care products (PPCPs) of various physicochemical properties, by NF (thin-film aromatic polyamide) and UF (sulfonated PES) membranes [7]. It was reported by these authors that although bigger in pore size, UF membranes were capable of retaining mostly hydrophobic EDCs and PPCPs due to hydrophobic-hydrophobic adsorption, whereas retention by NF membranes occurred by a combination of both hydrophobic-hydrophobic adsorption and steric exclusion mechanisms. Another study by Sheng et al. [17], investigated the removal efficiencies of different water treatment technologies including UF membranes with MWCO = 100 kDa, powdered activated carbon (PAC) and coagulation (COA) and a combination of these technologies for various trace pharmaceuticals (e.g. acetaminophen, bezafibrate, caffeine, carbamazepine, etc.) of less than 0.4 kDa in size from water. The authors reported that when UF membrane filtration process

was used alone, the average removal of trace pharmaceuticals was about 29%, whereas the combination of UF and PAC, led to an increase in average removal efficiency up to 90.3%. The increase in observed retention after the combination of the two treatment technologies was attributed to the fact that trace pharmaceuticals were initially adsorbed into the surface PAC, thereby forming PAC clusters which could then be easily filtered by the UF membrane [17]. As such, by virtue of their porous nature, the key mechanism by which UF membranes are capable of removing organic micropollutants in water systems is predominantly by membrane surface adsorption, which is in turn associated with the solute compound hydrophobicity ( $\log K_{ow}$ ).

Powdered activated carbon (PAC) and granular activated carbon (GAC) are commonly used adsorbents during the pretreatment stages of wastewater and seawater desalination [18]. Nonetheless, several studies have compared the adsorption capacities of activated carbon for various organic micropollutants to those of single-walled carbon nanotubes (SWCNTs) and multi-walled carbon nanotubes (MWCNTs). It has been found that CNTs are more effective for the adsorption of pollutants than AC due to their fibrous shape, large surface area-to-volume ratio and shorter equilibrium times [19, 20]. Moreover, AC has low adsorption affinity for low molecular-weight organic compounds, while CNTs strongly adsorb the majority of these compounds due to the diverse CNT-contaminant interactions including hydrophobic effect,  $\pi - \pi$  interactions, hydrogen bonding, covalent bonding, and electrostatic interactions [21, 22]. Kumar and Mohan [23], investigated the removal of natural and synthetic steroid hormone estriol (E3) and 17 $\alpha$ -ethynylestradiol (EE2) by MWCNTs as adsorbents. It was reported that the adsorption of hormones was largely dependent on adsorbate concentration and pH of the solution. Whilst AC is capable of removing organic micropollutants to certain extents, large

amount of chemical sludge is generated due to the usage of relatively high adsorbent dosage. The sludge produced is deemed to be a serious environmental concern [24].

Therefore, an approach to reduce the chemical dosage of adsorbents by developing membrane material with enhanced removal capacity for organic micropollutants, and with low energy requirements must be investigated. The present study investigated the adsorptive removal of the natural hormone estrone (E1) by making use of an integrated system that combines polyethersulfone membranes with different loadings of O-MWCNTs (in order to prepare PES/O-MWCNT UF membranes). Polyethersulfone (PES) is a hydrophobic polymer with adsorptive capabilities for retaining hydrophobic steroid hormones [11]. However, the incorporation of O-MWCNTs was investigated for further enhancement of the adsorptive capacity of the PES UF membrane for hormones. Kaminska et al. [25], investigated the removal of micropollutants (bisphenol A and 4-Nonylphenol) in synthetic wastewater using PES NF nanocomposite membrane incorporated with carboxyl-functionalised SWCNTs. The authors reported that an increase in SWCNT content led to an increase in micropollutant removal due to the increase in membrane hydrophobicity. Although natural hormones generally occur at low concentrations in water sources compared to other micropollutants, the endocrine-disrupting potency of hormones is several orders of magnitudes higher than that of organic micropollutants such as pesticides and alkyl phenols [26, 27]. This fact alone makes it worthwhile to investigate other alternative methods by which hormones can be removed from contaminated water sources. The E1 hormone was selected as a target micropollutant in this study due to its high persistence, high potency and moderate concentrations in wastewaters [12]. Moreover, E1 is a degradation product of the  $17\beta$ -estradiol (E2) hormone [5], and will therefore give an indication on the potential removal of other estrogenic hormones alike. Very

little has been reported on the removal efficiencies of natural hormones such as E1 by UF membranes.

#### **4.1.2. Theory on membrane separation mechanisms**

The retention of solutes or organic micropollutants in contaminated water sources by membranes occurs by one or a combination of the following mechanisms; (i) steric hindrance (or size exclusion), (ii) electrostatic interaction and (iii) hydrophobic-hydrophobic interactions (or adsorption) [13] as depicted in Fig. 4.1. With the steric hindrance mechanism, solutes larger than the pore sizes of the membranes are prevented from passing through while those smaller than the membrane pore sizes, simply permeate through the membrane. The electrostatic interaction mechanisms take precedence when charged organic solutes are subjected to a charged membrane surfaces [11]. Here, the Coulomb's law of attraction is followed, whereby negatively charged organic solutes are highly rejected by negatively charged membrane surfaces as a consequence of electrostatic repulsion. Verliefde et al. [28], further demonstrated that the rejection of positively charged organic solutes by negatively charged membranes is lower than that of neutral organic solutes. This was attributable to electrostatic attraction between the negatively charged membrane and positively charged solute. On the other hand, hydrophobic-hydrophobic interactions, predicts that when hydrophobic membranes are used for solute separation, the hydrophilic solutes are better rejected than hydrophobic solutes as a consequence of hydrophobic solutes easily partitioning into the membrane matrix through the formation of H-bonds, thereby diffusing to the permeate side [13]. Initially, hydrophobic solutes easily adsorb into hydrophobic membrane surfaces which may lead to an overestimation of observed rejection values [10, 29]. It is therefore essential that saturation of the membrane with the solute of interest is carried out first, in order to obtain accurate

membrane retention capacity. Once membrane saturation has reached equilibrium, the rejection of hydrophobic solutes by hydrophobic membranes will be lower than that of hydrophilic solutes.

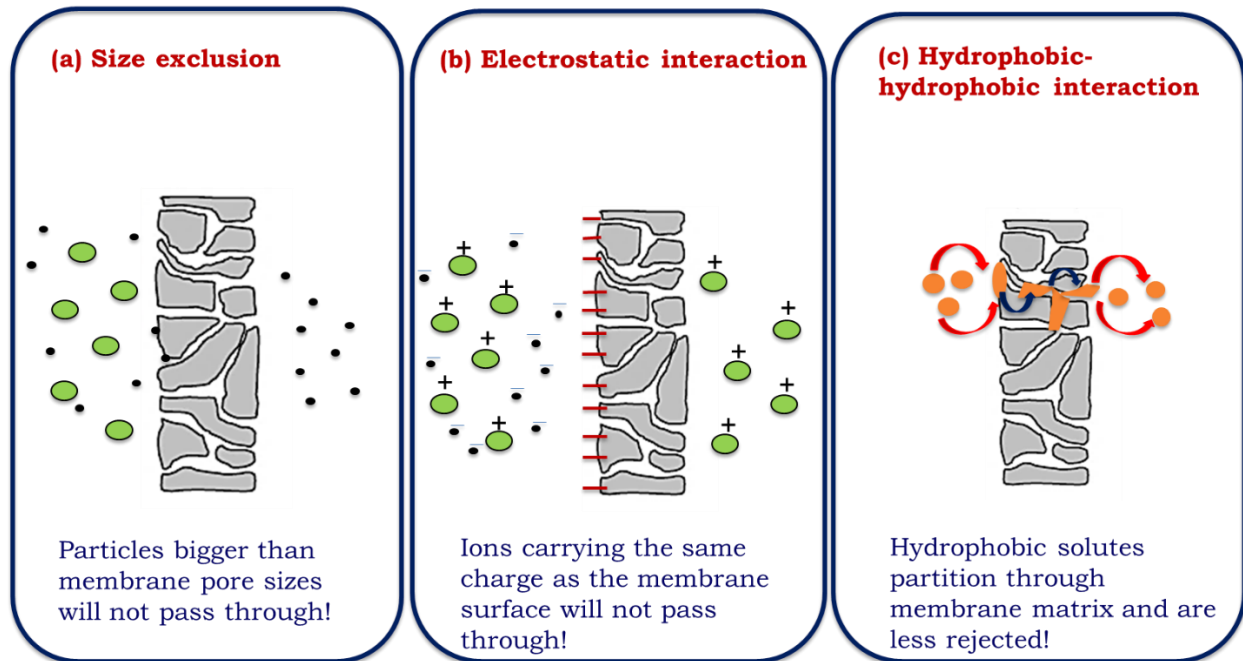


**Figure 4.1** Membrane separation mechanisms.

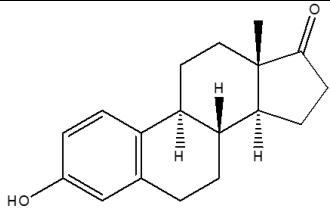
The purpose of the present study was to evaluate the E1 adsorption behaviour of O-MWCNTs and PES/O-MWCNT UF membranes using low-concentration E1 solutions. The main emphasis was on the development of adsorptive PES membranes as hosts for O-MWCNTs adsorbents. The effect of O-MWCNT content in the PES matrix, membrane surface characteristics, membrane area, contact time and solution pH on the E1 removal capacity was investigated.

## 4.2. Experimental

### 4.2.1. Materials

Polyethersulfone (PES) (Veradel 3000P) was kindly supplied by Solvay Advanced Chemicals (Belgium), while N-methyl-2-pyrrolidinone (NMP) and 55% nitric acid (HNO<sub>3</sub>) were purchased from Sigma-Aldrich, Germany. Multi-walled carbon nanotubes (O.D. x I.D. x L= 10 nm ± 1 nm × 4.5 nm ± 0.5nm × 3- ~6 μm) were produced in-house via a catalytic chemical vapour deposition (CVD) method (Appendix B. supplementary materials section). PEG (10, 20, 35 kDa) and PEO (100, 200 kDa) were purchased from Sigma-Aldrich, Germany. Radiolabelled [2,4,6,7-<sup>3</sup>H] estrone (E1) hormone solution (3.48 TBq/mmol) was purchased from PerkinElmer. The E1 stock solution concentration was 10 μg/L. MilliQ type 1 water (>18.2 MΩ/cm at 25 °C) was used for the dilution of the E1 stock solution to the required concentrations (0, 0.1, 1, 10, and 100 ng/L). Commercial Millipore Biomax® PES membrane (PBQK 50205) was supplied by Merck Millipore.

**Table 4.1** Physicochemical properties of estrone (E1)

Molecular structure	Molecular weight (g/mol)	Water solubility (mg/L)	Octanol-water partition coefficient (log <i>K<sub>ow</sub></i> ) <sup>[3, 30]</sup>	pKa <sup>[3]</sup>	Diameter (nm) <sup>[12]</sup>
	270.37	30	3.13	10.5	0.8

#### 4.2.2. Membrane preparation

Pristine PES and MWCNT modified PES membranes were synthesized using non-solvent induced phase separation method (NIPS). Briefly, weighed amounts of O-MWCNTs were ultrasonicated in NMP solvent until homogeneously dispersed. This was followed by the addition of 16 wt.% of PES in solution. The mixture was then stirred at 60 °C for 12 h to ensure complete dissolution. The polymer solution formed was then cooled and degassed overnight under vacuum conditions to remove of any bubbles formed during stirring. The polymer solution was then cast directly on a glass plate using an adjustable casting knife set at a film thickness of 150 µm, followed by immediate immersion into a water coagulation bath. The nascent membrane was then washed several times with deionised water at room temperature and stored in deionized water at 4 °C. Pristine PES membranes were labelled as M0, whilst PES membranes containing 0.1 wt.%, 0.5 wt.% and 1.0 wt.% of O-MWCNTs were marked as M1, M2 and M3 respectively (Table 4.2).

**Table 4.2** Composition of the casting solutions for the preparation of PES/O-MWCNT membranes.

Membrane	Concentration (wt.%)			Viscosity (MPa.s)
	PES	NMP	O-MWCNTs	
M0	15.0	85.0	0.0	1465 ± 1.05
M1	15.0	84.9	0.1	1615 ± 1.22
M2	15.0	84.5	0.5	1885 ± 1.13
M3	15.0	84.0	1.0	1945 ± 1.45

### 4.2.3. Membrane characterization

Attenuated total reflectance Fourier transform-infrared (ATR–FTIR) spectrometer (Perkin Elmer, Germany) was used to assess the functional groups present on the surface of PES blend membranes. Scanning electron microscopy (SEM) (JEOL JSM – IT300) was used to study the surface and cross-sectional morphology of the membranes. Dried membrane samples were sputter-coated with gold (5 nm coating) and freeze-fractured in liquid nitrogen (to avoid structure collapse) for viewing of the cross-sectional morphology. Coating of samples with a conductive layer of metal inhibits sample charging thus improving the imaging process. The size of the surface pores was analysed and processed using Image J software and the results are reported in Table 4.3. Atomic force microscopy (AFM WITec Alpha 300) was used to study the roughness parameters, namely roughness average ( $S_a$ ) and root mean square roughness ( $S_q$ ) of the dried composite membranes. Measurements were carried out in non-contact mode under a scan size of  $5\ \mu\text{m} \times 5\ \mu\text{m}$ . Water contact angle measurements were carried out using a Krüss Drop shape analyzer, (DSA30E, Krüss GmbH, German) for the evaluation of the hydrophilic/hydrophobic membrane properties based on the sessile-drop method. In total, six measurements were taken at different locations on the membrane surface and the average value is reported. The contact angle values reported were recorded within the first 3 s of the adherence of the water droplet on the membrane surface. The thickness of membranes was measured using a digital micrometer (Schut Geometrical Metrology, Trossingen, Germany). Thickness measurements were taken from at least five different positions on the membranes and the average result is reported.

The SurPASS Electrokinetic Analyser (Anton Paar GmbH, Austria) was used to determine the zeta potential and isoelectric point values of composite membranes at various pH values. A

background electrolyte solution of 10 mM KCl was used during measurements. The zeta potentials ( $\zeta$ ) were calculated using the Helmholtz-Smoluchowski Eq. 4. as:

$$\zeta = \frac{\Delta V \cdot \eta \delta}{\Delta P \cdot \epsilon} \quad (4.1)$$

where  $\Delta V$  is the measured streaming potential (V),  $\eta$  is the electrolyte viscosity (Pa.s),  $\delta$  is the electrolyte conductivity (S/m),  $\Delta P$  is the applied pressure (Pa), and  $\epsilon$  is the permittivity of water.

Filtration experiments were conducted using stainless steel stirred cells with an active membrane area of 38.48 cm<sup>2</sup>, internal diameter of 7 cm and a cell capacity of 900 mL. The feed pressure, solution temperature and mass of permeate were monitored continuously and data collected were recorded on the computer using LabVIEW Version 2014 software (National Instruments Corporation, Austin, Texas, USA). Membrane coupons were soaked in 10 mM NaCl solution for 1 h prior to use, followed by 1 h compaction with MilliQ water. Pure flux ( $J_w$ ) was calculated according to Eq. (4.2) as:

$$J_{w1} = \frac{V}{A \times t} \quad (4.2)$$

where  $V$  is the volume of permeate (L),  $A$  is the effective membrane area (m<sup>2</sup>) and  $t$  is the permeation time (h).

A minimum of three membrane coupons for each membrane type, were tested for pure water flux at different pressures and the average of the three values was expressed in the graph of pure water flux versus transmembrane pressure (Fig. 4.6).

Molecular weight cut-off (MWCO) is defined as the molecular weight of neutral solute for which the rejection of the membrane is 90% [31]. The experiments to determine the MWCO for the approximation of membrane pore sizes, were conducted using 20 mg/L of polyethylene glycol (PEG) and polyethylene oxide (PEO) solutes of different molecular weights. A new membrane coupon was used for each molecular weight of PEG tested. Membrane solute rejection  $R$  (%) was calculated using Eq. 4.3:

$$R(\%) = \left( 1 - \frac{C_p}{C_f} \right) \times 100 \quad (4.3)$$

where  $C_p$  and  $C_f$  are solute concentrations in the permeate and feed solution.

The flow rate was maintained at 0.4 g/L during the MWCO determination to ensure that all membranes were operated under the same flux of 114.94 L/m<sup>2</sup>. h. The MWCO results reported are based on 15% recovery of the permeate to avoid interferences from adsorption or fouling of tested solutes on the membrane surface at higher recoveries which could mask the true rejection of the membranes. The feed and permeate concentrations were measured using the Sievers M9 Total Organic Carbon (TOC) analyzer (GE Sievers M9 TOC Analytical Instruments Inc., Boulder, CO, USA). The relationship between Stokes radius and molecular weight of PEG [32] can be expressed according to Eq. 4.4 as:

$$r = 16.73 \times 10^{-3} M^{0.557} \quad (4.4)$$

#### 4.2.4. Static adsorption experiments

Static adsorption experiments were carried out in a New Brunswick™ Innova® 43R Incubator Shaker (Eppendorf Inc., Enfield, CT, USA) at an agitation speed of 260 rpm and a constant temperature of 20 °C. The PES/O-MWCNT membranes were rinsed with MilliQ water and placed in a conical flask containing 250 mL of E1 solution (100 ng/L) inside followed by agitation. Membrane areas evaluated ranged from 4 to 36 cm<sup>2</sup>. Sample aliquots of 2.5 mL were drawn using a 5 mL micropipette, at predetermined time intervals and stored in 20 mL glass vials. Thereafter, 1 mL of sample solution was drawn from each vial and mixed with 1 mL of liquid scintillation solvent (Ultima Gold™ LLT, Perkin Elmer, Inc., Shelton, CT USA) in a 10 mL scintillation glass vial. The concentration of hormones in each vial was then measured using Liquid scintillation counter (LSC; 2550 TR/AB, Packard, USA). A control solution of E1 solution (without any membrane) mixed with the scintillator solution was also analyzed. The concentration of hormones in each vial was then determined by liquid scintillation (LS) counting technology 10 min and measured in triplicate. The E1 concentration in each sample was calculated from a linear regression performed on calibration standards (0, 1, 10 and 100 ng/L). Sampling time intervals used were 0.25, 0.5, 1, 2, 6, 8, 24 h. The percentage of E1 removed was calculated using Eq. 4.5:

$$\% \text{ E1 removed} = \left(1 - \frac{C_t}{C_0}\right) \times 100 \quad (4.5)$$

where  $C_t$  is the sample concentration in ng/L at time  $t$  and  $C_0$  is the initial sample concentration (in ng/L).

In the case of E1 adsorption by O-MWCNTs, different amounts of O-MWCNTs (1, 2, 6, 8 and 10 mg) were added into the conical flasks containing the E1 solution, and sample aliquots drawn at predetermined time intervals were filtered through a commercial PES membrane (PBQK 50kDa, pore diameter  $\cong$  13.9 nm) prior to mixing with the scintillator solution. The commercial membrane was saturated with E1 solution prior to filtration of sample aliquots. The adsorbed amounts per unit membrane area ( $\text{ng}/\text{cm}^2$ ) were calculated through the difference between the initial and pseudo-equilibrium concentrations at 72 h.

The logarithm of the partition coefficient ( $\log K$ ) of E1 between the membrane and the bulk solution was evaluated per unit volume of membrane [33] using Eq 4.6:

$$\log K = \log \frac{Q}{C_b} \quad (4.6)$$

where  $K$  is the partition coefficient (dimensionless),  $Q$  is the amount of E1 adsorbed per unit membrane volume ( $\text{ng}/\text{L}$ ) and  $C_b$  is the concentration of E1 in the bulk solution ( $\text{ng}/\text{L}$ ). The Langmuir and Freundlich models were employed for data fitting of the membrane adsorption isotherms of E1 as shown in the equations below:

Langmuir equation:

$$\frac{C_e}{q_e} = \frac{C_e}{q_o} + \frac{1}{q_o b} \quad (4.7)$$

where  $C_e$  is the equilibrium concentration ( $\text{ng}/\text{L}$ ),  $q_e$  is the equilibrium adsorbed amount per unit membrane area ( $\text{ng}/\text{cm}^2$ ),  $q_o$  is the maximum adsorption capacity ( $\text{ng}/\text{L}$ ) and  $b$  is the binding energy constant ( $\text{L}/\text{ng}$ ). An essential characteristic of the Langmuir isotherm is the dimensionless separation factor ( $R_L$ ) which defines the favourability of an adsorption process

( $R_L = 0$  suggests that the process is irreversible,  $R_L < 1$  indicates a favourable adsorption process,  $R_L = 1$  indicates that the process is linear and  $R_L > 1$  indicates that the adsorption process is unfavourable) [34]. The dimensionless factor ( $R_L$ ) can be calculated using Eq. 4.8 as follows:

$$R_L = \frac{1}{1 + b C_0} \quad (4.8)$$

Freundlich equation (linearised form):

$$\log q_e = \log K_F + \frac{1}{n} \log C_e \quad (4.9)$$

where  $q_e$  is the equilibrium loading (mg/g),  $K_F$  is the Freundlich adsorption capacity parameter in relation to the adsorption capacity of the sorbent  $(\text{ng/cm}^2) (\text{ng/L})^{1/n}$  and  $1/n$  is an empirical constant indicating the Freundlich adsorption intensity (dimensionless).  $C_e$  is the equilibrium concentration (ng/L).

Data collected from the investigation of the effect of contact time on E1 adsorption were fitted using the pseudo-first-order and pseudo-second-order kinetic model using Eq. 4.10 and 4.11 as follows:

$$\ln(q_t - q_e) = \ln q_e - k_1 t \quad (4.10)$$

$$\frac{t}{qt} = \frac{1}{k_2 q_e^2} + \frac{t}{q_e} \quad (4.11)$$

where  $k_1$  (1/min) is the rate constant for pseudo-first-order and  $k_2$  (g/mg.min) is the rate constant for pseudo-second-order rate kinetic model,  $q_t$  is the amount of E1 adsorbed at a given time,  $t$  (mg/g) and  $q_e$  is equilibrium adsorption capacity (mg/g).

The study was conducted using an E1 solution at a concentration of 100 ng/L and optimum membrane area for each membrane sample. About 2.5 mL of aliquots were taken from the suspensions at different time intervals.

#### 4.2.5. Regeneration of PES/O-MWCNT membranes

To determine the reversibility of the adsorption process, a 25 cm<sup>2</sup> of each of the membranes after 72 h contact time with E1, were soaked in an ethanol/water mixture (1:1) and shaken for 30 min [35]. This was followed by rinsing with MilliQ water and drying at room temperature. Dried membrane samples were stored in the desiccator overnight. The E1 adsorption experiments were re-conducted in the incubator shaker at an agitation speed of 260 rpm and at a constant temperature of 20 °C. Sample aliquots were only drawn out of the flasks only after 72 h contact time with E1. The adsorption-regeneration process was repeated five times. The regeneration efficiency was calculated using Eq. 4.12 as:

$$\text{Regeneration efficiency (\%)} = \frac{q_e}{q_o} \times 100 \quad (4.12)$$

where  $q_e$  is the adsorption capacity of the regenerated membrane and  $q_o$  is initial adsorption capacity of membrane.

### 4.3. Results and discussion

#### 4.3.1. FTIR analysis of PES/O-MWCNT membranes

Fig. 4.2 shows the ATR-FTIR spectra of the PES blend membranes containing various loading of O-MWCNTs. All the membranes were found to exhibit the characteristic sulfonyl group bands in the regions  $\sim 1235$  and  $1136\text{ cm}^{-1}$  due to the asymmetric and symmetric stretching vibrations of the  $-\text{S}=\text{O}$  groups of the PES polymer chains [36]. The PES membranes containing O-MWCNTs have a broad band in the region  $\sim 3400\text{ cm}^{-1}$  due to the presence of  $-\text{OH}$  functional groups and an additional band at  $1643\text{ cm}^{-1}$  due to asymmetric stretching of the  $-\text{C}=\text{O}$  groups [37]. It can be also seen from the figure that the intensity of both  $-\text{OH}$  and  $-\text{C}=\text{O}$  bands is higher for membrane M3 containing the highest loading of O-MWCNTs. The appearance of these peaks suggests that O-MWCNTs were adequately incorporated into the PES matrix and did not leach out of the polymer solution during the coagulation process. Moreover, their presence is essential for enhancing the hydrophilic properties of the PES membrane.

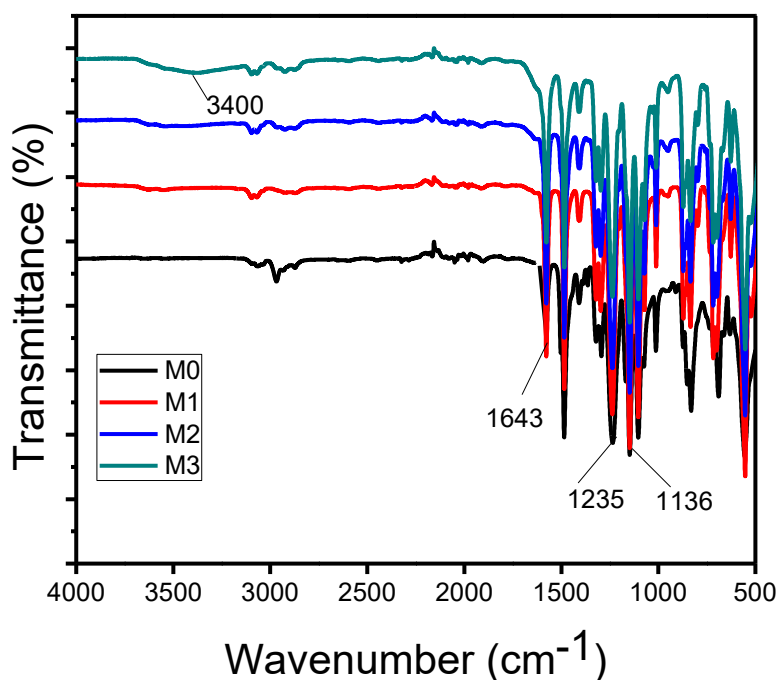


**Figure 4.2** FTIR spectra of PES/O-MWCNT membranes.

#### 4.3.2. Morphological characterisation of PES/O-MWCNT membranes

The SEM surface and cross-sectional images of PES/O-MWCNT membranes are shown in Fig. 4.3. It can be visually observed from the surface images that all the membranes studied have an open-porous surface morphology. It was found that the addition of O-MWCNTs led to a gradual decrease in membrane pore size from  $25.9 \pm 0.01$  nm for M0 to  $19.3 \pm 0.03$  nm for M1 and  $17.4 \pm 0.09$  nm for M2 (Table 4.3). However, upon further increments in O-MWCNT content, the surface pore sizes for M3 slightly increased to  $21.3 \pm 0.11$  nm, although still relatively below those of M0. The observed phenomenon from SEM surface images can be correlated with their corresponding cross-sectional images. Clearly, the finger-like macrovoid morphology of M0 undergoes a transition into a less open sub-layer morphology with fewer macrovoid structures in the membrane sublayer of M1, M2 and M3 upon increments in O-MWCNT content.

Generally, the incorporation of low amounts of hydrophilic O-MWCNTs into polymer matrices enhances the phase-separation kinetics during membrane formation, leading to the creation of finger-like and macrovoid structures in the membrane sublayer. The size and number of these unique structures reduces upon further increments in nanoadditive loading [36, 38]. However, an opposite trend was obtained in this study, whereby the inclusion of O-MWCNTs (at all loadings) in the PES matrix led to a reduction in pore sizes and suppressed the formation of macrovoid structures. This can be explained by the fact that although the presence of hydrophilic MWCNTs enhances phase separation, their presence also increases the polymer solution viscosity, leading to a delay in solvent/non-solvent demixing, thus leading to a generation of dense and less porous membrane structure. At high O-MWCNT loadings, membrane pore clogging occurs, thus reducing the surface pore size [39]. Expressing the O-MWCNT loading with respect to the polymer concentration can assist in further understanding the observed morphology. As such, the content of O-MWCNTs with respect to PES used in the study ranged from 0.66 – 6.67 wt.%. This is a relatively high nanoadditive loading compared to what has been previously used in other studies (0.03 – 0.09 wt.% by Sengur-Tasdemir et al.; 0.25 – 0.5 wt.% by Saranya et al.; and 0.22 – 0.55 wt.% by Vatanpour et al.) to modify structural and surface properties of PES/MWCNT membranes [36, 40, 41]. This demonstrates that the O-MWCNT content has a significant effect on the resultant membrane internal morphology and microstructure.

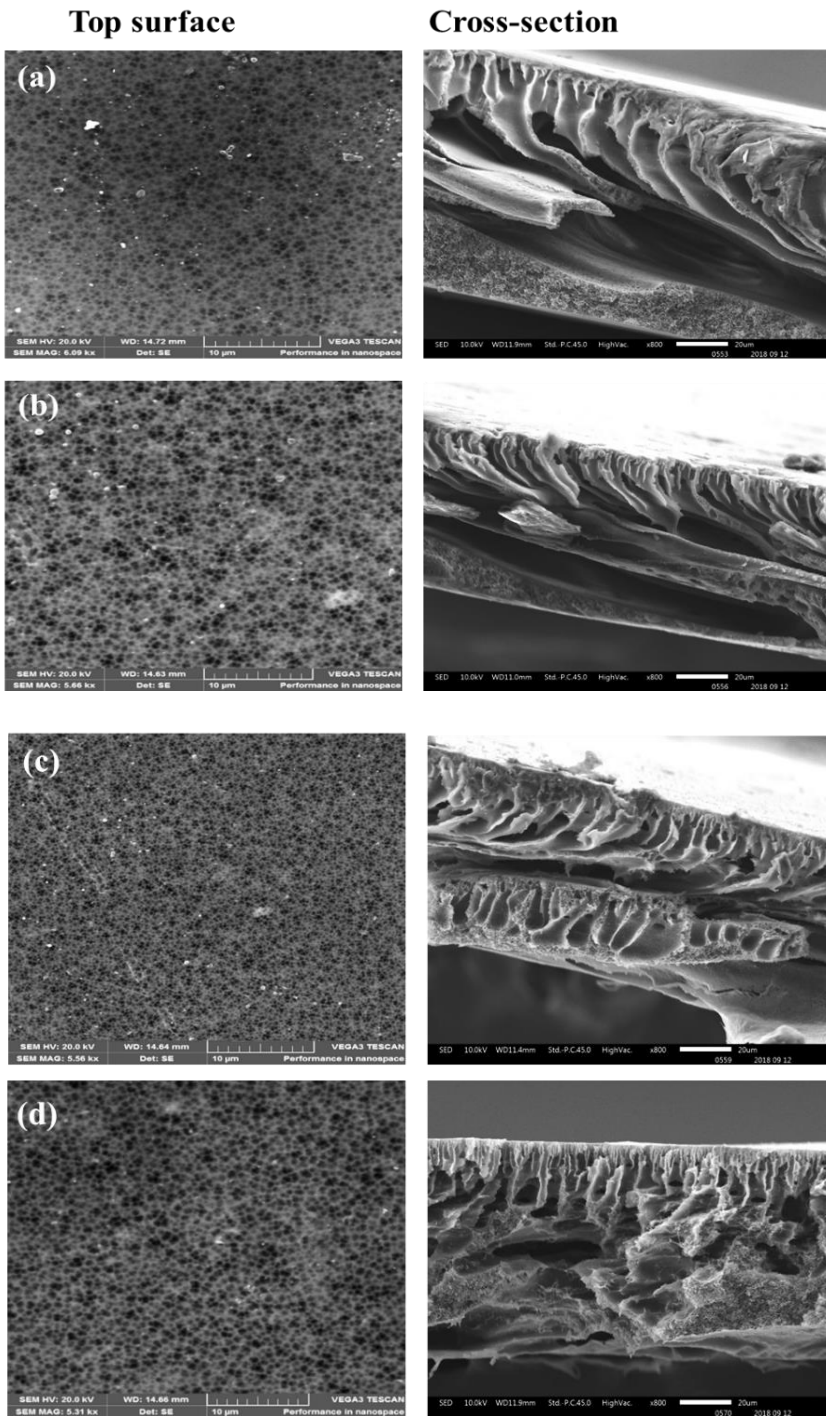


**Figure 4.3** SEM surface and cross-sectional images of PES/O-MWCNT membranes: (a) M0, (b) M1, (c) M2 and (d) M3.

Atomic force microscopy (AFM) was used to investigate the changes in membrane surface roughness upon inclusion of O-MWCNTs in the PES matrix. The average arithmetic roughness

(Sa) and root mean square roughness (Sq) values initially decreased upon the incorporation of O-MWCNTs for M1 and M2 followed by an increase for M3 containing the highest O-MWCNT loading (Table 4.3). This initial decline in surface roughness of membranes can be attributed to the increase in viscosity of the casting solution upon inclusion of O-MWCNTs, leading to the inhibition of the exchange rate between solvent and non-solvent, resulting in the formation of smoother membrane surface [38]. Moreover, the formation of smaller-size surface pores as established from SEM analysis, contributes towards the reduction in membrane surface roughness. However, at higher loadings, bundling and agglomeration of O-MWCNTs occurs due to increased van der Waals interactions leading to the formation of rougher membrane surface [36, 42].

Membrane thickness initially decreased by about 7% upon the inclusion of 0.1 wt.% of O-MWCNTs for membrane M1. However, with further increments in O-MWCNTs content, the membrane thickness was found to increase for membranes M2 and M3 compared to that of bare PES membrane (M0). This initial decline in membrane thickness can be attributed to the partial enhancement in phase-separation kinetics at lower O-MWCNT contents in the PES matrix, leading to reduced membrane thickness. However, at higher loadings of O-MWCNTs, the viscosity of the casting solutions increases leading to delayed demixing process (*i.e.* the rate of non-solvent influx into the polymer solution decreases) resulting in the formation of thicker membranes [43]. The membrane thickness results obtained are congruent with findings from SEM cross-sectional images of the membranes.

**Table 4.3** Roughness parameters, average surface pore size and thickness of PES/O-MWCNT membranes.

Membranes	Roughness parameters		Average surface pore size (nm)	Membrane thickness ( $\mu\text{m}$ )	MWCO (kDa)
	SA (nm)	SQ (nm)			
M0	$19.8 \pm 0.01$	$24.6 \pm 0.13$	$25.9 \pm 0.01$	$70.8 \pm 0.13$	95.8
M1	$12.0 \pm 0.05$	$17.2 \pm 0.02$	$19.3 \pm 0.03$	$66.0 \pm 0.21$	91.6
M2	$11.2 \pm 0.01$	$15.3 \pm 0.04$	$17.4 \pm 0.09$	$74.0 \pm 0.11$	88.1
M3	$24.2 \pm 0.08$	$32.2 \pm 0.11$	$21.3 \pm 0.11$	$77.0 \pm 0.19$	81.7

#### 4.3.3. MWCO characterisation of PES/O-MWCNT membranes

Molecular weight cut-off (MWCO) is a measure of the pore size of membranes and is defined as the molecular weight of a neutral solute that is retained at 90% by the membrane [44, 45]. In addition to the physical characterisation of membrane pores by microscopic evaluation, permeation and solute rejection studies in terms of the MWCO of membrane were conducted and the results are shown in Fig. 4.4. It can be seen that the addition of O-MWCNTs to the PES matrix led to a decrease in MWCO of the nanocomposite membranes. The MWCO of membranes progressively declined from ~96 kDa for M0 to ~82 kDa for M3. The decrease in MWCO of the membrane can be attributed to the formation of less open sublayer morphology as established from SEM analyses, due to the presence of high O-MWCNT loadings in the PES matrix. The presence of high (0.5 and 1.0 wt.%) O-MWCNT loadings increased the viscosity of PES casting solution, leading to delayed solvent/non-solvent demixing during the phase-

inversion process, thereby significantly reducing the surface pore size. As expected, the MWCO has a linear relationship with the pore size of the membrane. Similar findings were also reported by Saranya et al., whereby a decrease in MWCO of PES membranes containing functionalised MWCNTs was obtained as a consequence of selective transport channels being introduced by the presence of functionalised MWCNTs [40].

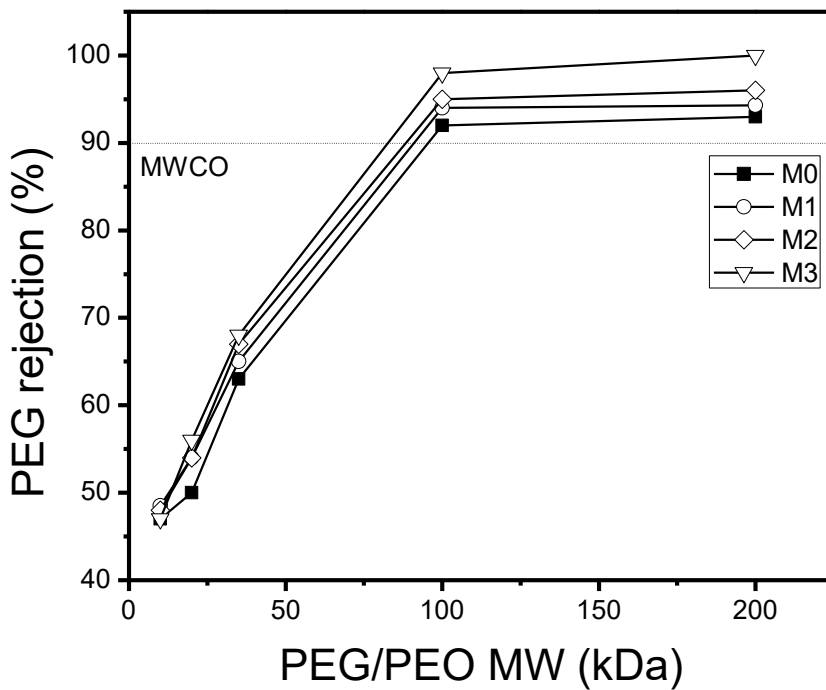


**Figure 4.4** Molecular weight cut-off profiles of PES/O-MWCNT membranes.

#### 4.3.4. Contact angle and pure water flux measurements of PES/O-MWCNT membranes

To study the changes in surface hydrophilicity upon inclusion of O-MWCNTs in the PES matrix, contact angle measurements were carried out. It is shown in Fig. 4.5 that the contact angle values initially decreased for membranes M1 and M2 followed by an increase for M3. A decline in contact angle value for M1 and M2 from that of M0 suggests that the hydrophilic properties of the membrane surface are enhanced by incorporation of hydrophilic O-MWCNTs

[46]. It is understood that during phase separation of the membrane formation process, hydrophilic O-MWCNTs migrate spontaneously to the membrane-water interface to reduce the interfacial energy, thereby making the membrane surface hydrophilic [38, 47]. Additionally, the contact angle values measured for M1 and M2 do not differ much (with only a 2° decline), suggesting that only a small amount of O-MWCNTs is sufficient to improve membrane surface hydrophilicity. The increase in contact angle at higher O-MWCNT loadings can be linked to the formation of agglomerates or clusters of O-MWCNTs, which become irregularly positioned in the PES matrix for M3, thus increasing membrane surface roughness. The increase in surface roughness leads to higher contact angle values measured. Therefore, contact angle measurement results are in agreement with the roughness data from the AFM analysis.

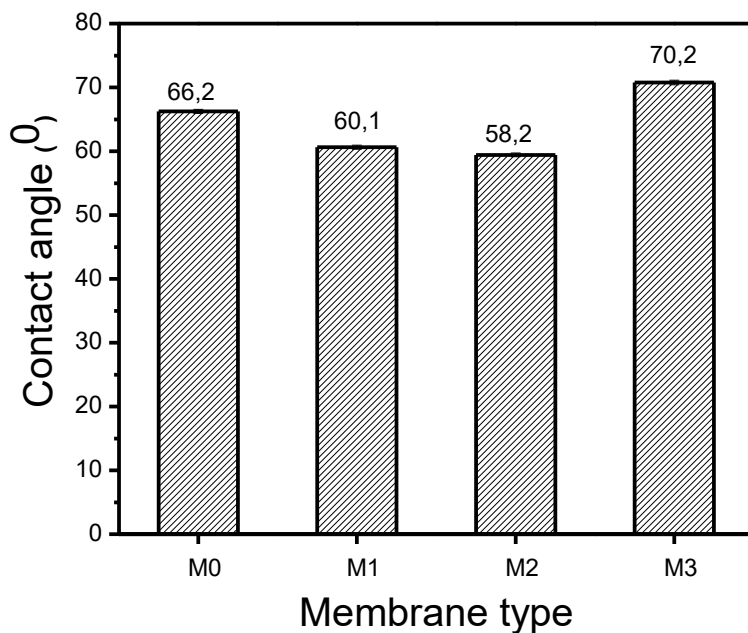


**Figure 4.5** Contact angles of PES/O-MWCNT membranes.

It is often reported that an increase in surface hydrophilicity of a membrane is desired and favourable for the improvement of membrane pure water flux [47-49]. This is because an increase in the hydrophilic character of the membrane helps to attracts water molecules closer

to the membrane surface and increases the thickness of the pure water layer deposited on the membrane surface [50, 51]. The effect of applied transmembrane pressure on pure water flux of PES/O-MWCNT membranes was evaluated (Fig. 4.6). The plot of the pure water flux versus pressure displayed a linear relationship, and the inverse of the slope is the intrinsic membrane hydraulic resistance ( $R_m$ ) [52]. The pure water fluxes of M1, M2 and M3 containing of O-MWCNTs were lower than that of M0 at all applied pressures. For example, at 1 bar, the pure water flux declined from 405.4 L/m<sup>2</sup>.h for M0 to 296.8 L/m<sup>2</sup>.h, 201.6 L/m<sup>2</sup>.h and 148.7 L/m<sup>2</sup>.h for M2, M3 and M4. The decline in pure water fluxes of membranes containing O-MWCNTs can be attributed to their smaller surface pore sizes, and low MWCO values compared to those of the pristine PES membrane. Although membranes containing O-MWCNTs displayed improved surface hydrophilicity, it is the membrane pore sizes that had a dominating effect on the resultant pure water flux or permeation properties of the membrane as predicted by the Hagen-Poiseuille theory [53]. Moreover, the higher  $R_m$  values of 0.03, 0.05 and 0.06 bar/l.m<sup>-2</sup>.h<sup>-1</sup> for M1, M2 and M3 compared to that of M0 (0.02 bar/l.m<sup>-2</sup>.h<sup>-1</sup>) are as a result of their compact, and less porous membrane structure. Therefore, PES membranes containing O-MWCNTs are likely to have higher stability under prolonged operation compared to the bare PES membrane as a consequence of their compact structure and higher hydraulic resistance.

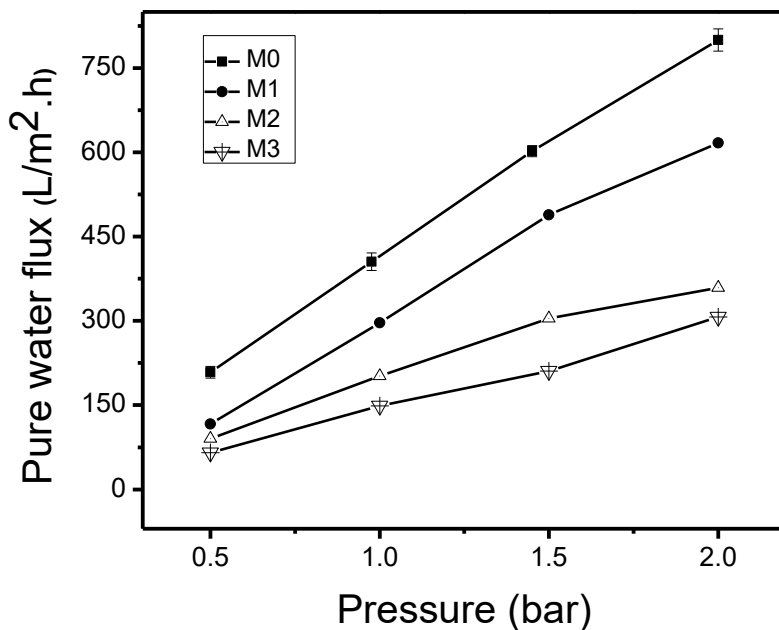


**Figure 4.6** Effect of transmembrane pressure on pure water flux of PES/O-MWCNT membranes.

#### 4.3.5. Zeta potential of PES/O-MWCNT membranes

The surface charge on the membrane is generated from the interaction of surface functional groups with the aqueous environment and therefore, the pH value of the electrolyte solution used plays a crucial role in determining the charge assumed by the membrane [54]. Measurement of the zeta potential of a membrane surface assist in the prediction of the electrostatic interaction between the membrane surface and the aqueous environment. Zeta potential values of prepared membranes as a function of electrolyte pH are presented in Fig. 4.7. All the membranes have positive surface charges at lower pH (< 2.5) and then assume a negative charge at higher pH values (> 3). This is because under alkaline conditions, sulfonic acid groups of the PES backbone and the carboxyl groups of incorporated O-MWCNTs undergo dissociation to generate negatively charged ions. At low pH values, adsorption of cations from the electrolyte solution into the membrane surface takes place [25]. Indeed,

membranes containing O-MWCNTs (M1, M2 and M3) have more negative zeta potentials than M0; the zeta potential values become more negative as the content of O-MWCNT is increased. For example, at pH of  $\sim 10$ , the zeta potential value is -49 mV for M0, -54 mV for M1, -56 mV for M2 and -61 mV for M3.

The isoelectric points (IEP), i.e., the pH at which the net charge of the membrane is zero, of the zeta potential curves is found to shift to lower pH values with an increase in O-MWCNT loading in the PES matrix *i.e.* from 2.80 for M0 to 2.58 for M1, 2.40 for M2 and 2.31 for M3. The increase in negative charge as well as the shift in IEPs to lower pH values for M1 – M3 can be attributed to the presence of acidic functional groups of O-MWCNTs on the surface of the PES membrane. It was established from contact angle measurements that during membrane formation, hydrophilic O-MWCNTs migrate to the membrane-water interface to improve surface properties of the membranes as reported in other studies [25, 55]. The shape of the zeta potential curves is characteristic of amphoteric surfaces with acidic and basic functional groups [56, 57].

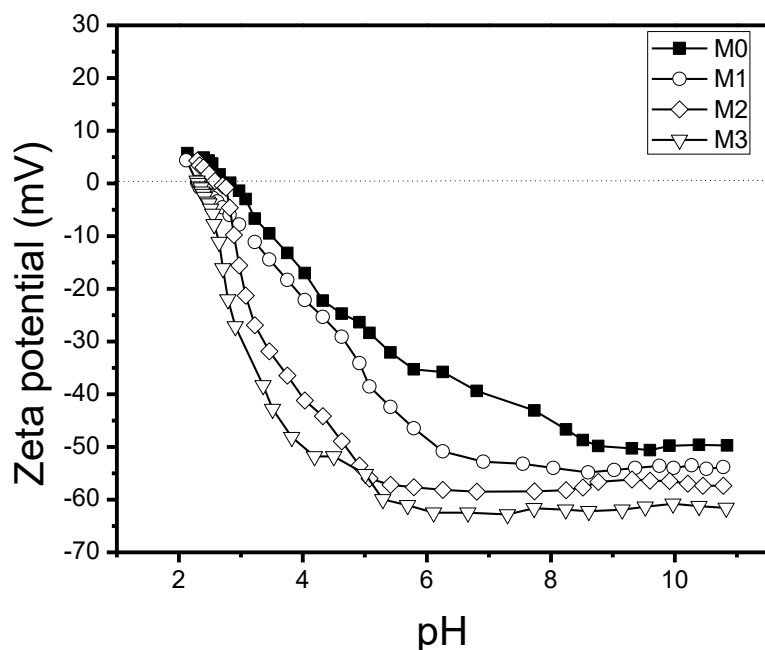


**Figure 4.7** Surface zeta potential as a function of electrolyte pH for PES/O-MWCNT membranes.

#### 4.3.6. Removal of natural hormone estrone (E1)

It has been established from SEM analysis and from MWCO determination experiments that the pore sizes of the prepared PES/O-MWCNT membranes are much larger (typically between 82 – 96 kDa) than the size or molecular weight of the target micropollutant E1 (which is 270 Da). As such, the removal of E1 molecules by size exclusion mechanism cannot be possible using the prepared UF nanocomposite membranes. The two other possible mechanisms to investigate are removal by hydrophobic interactions and electrostatic interactions. Nonetheless, when considering the log  $K_{ow}$  value for E1 which is above 2.5, it is expected that the hormone will interact with the membranes by hydrophobic-hydrophobic interactions. As such, the effect of O-MWCNT content on the PES matrix and the role of solution pH in the adsorption of E1 were studied.

#### 4.3.6.1. Effect of membrane area and O-MWCNT content on E1 adsorption

Batch adsorption experiments allow for rapid investigation of solute adsorption on membrane surface and/or pores without having to carry out filtration experiments [33]. Fig. 4.8 shows the adsorption of E1 by PES membranes containing various loadings of O-MWCNTs as a function of membrane area after 72 h contact time. Several generalisations can be drawn from the figure. Firstly, E1 adsorption increases with an increase in membrane area used, with optimum adsorption for each membrane type obtainable for the 25 cm<sup>2</sup> membrane area (Fig. 4.8). No significant increases in E1 adsorption were obtained above 25 cm<sup>2</sup>. This is due to the increase in the number of available sites for adsorption of hormones on larger membrane area. Secondly, E1 removal increased with an increase in O-MWCNT loading in the PES matrix. For example, as shown in Fig. 4.8, for 25 cm<sup>2</sup> of membrane used, E1 removal increased from 59% for M0 to 74% for M1, 80% for M2 and 68% for M3. It is important to note that pristine PES membrane (M0), displayed a reasonable adsorption capacity of 59% to due to the hydrophobic-hydrophobic interactions between the hydrophobic E1 (log  $K_{OW}$  value of E1 is above 2.5) and a hydrophobic PES membrane. The hydrophobic segments of E1 and PES interact in aqueous media and in the process, water molecules are displaced from the interacting surface (Fig. 4.9) [58]. In a separate experiment, E1 adsorption by PES based O-MWCNT membranes was compared to that of polysulfone (PSf) based O-MWCNT membranes. It was found that E1 adsorption by PES based membranes was higher than those achieved by PSf/O-MWCNT membranes (Fig. S4.1). Schäfer and coworkers [11] investigated the difference in estradiol (E2) sorption on variety of polymer materials including amongst others PES and PSf. It was reported that PES is a highly adsorbing polymer compared to PSf even though PSf is more hydrophobic (higher contact angle) than that of PES. The chemical structure of PSf consists of isopropylidene groups (-C(CH<sub>3</sub>)<sub>2</sub>) in addition to the sulfonyl (-SO<sub>2</sub>-) and the ether (-O-) groups

that PES also consist of, which causes the polymer to be nonpolar and hydrophobic (Fig S4.2). On the other hand, PES has the highest number of sulfonyl moieties in the repeating polymer chain compared to PSf hence the higher affinity for water. Therefore, the increase in adsorptive capacity of PES although less hydrophobic than PSf can be attributed to the likelihood of the formation of hydrogen bonds between  $-\text{SO}_2-$  groups of PES and  $-\text{OH}$  and  $-\text{C}=\text{O}$  groups of E1.

In the case of PES membranes containing O-MWCNTs (M1, M2 and M3), hydrophobic interactions are not the main mechanism for enhanced E1 adsorption as the FTIR analysis and contact angle measurements have already shown that the membranes have a hydrophilic character. Other workers have reported that the large surface area-to-volume ratio of O-MWCNTs enhances the adsorption of polyaromatic hydrocarbons, pesticides and natural organic matter [59]. The presence of O-MWCNTs with large surface areas in the active skin layer is also responsible for enhanced adsorption of E1 by membranes M1 and M2. However, at higher loadings (M3), O-MWCNTs form by agglomerations and clusters leading to a reduction in specific surface area available for adsorption. Similar results have also been reported by others [25, 60]. In addition, hydrogen bonding interactions between  $-\text{OH}$  and  $-\text{C}=\text{O}$  groups of E1 with  $-\text{COO}^-$  groups of O-MWCNTs also contribute towards the improvement in hormone adsorption of membranes M1, M2 and M3 under neutral conditions (Fig. 4.10). Moreover, the presence of O-MWCNTs in the PES matrix introduces an additional E1 adsorption mechanism; the  $\pi$ - $\pi$  electron-donor-acceptor interactions with E1, *i.e.*, aromatic rings of E1 containing the  $-\text{C}=\text{O}$  groups are electron acceptors, while graphene sheets of O-MWCNTs become electron donors (high  $\pi$ -system polarisability) [61]. According to Hunters and Sanders, it is in fact the properties of atoms in the regions of intermolecular contact between two materials that control the strength and geometry of the  $\pi$ - $\pi$  interactions, rather than the overall molecular oxidation or reduction potentials [62]. This suggests that the

resultant strong net  $\pi$ - $\pi$  interactions occur as a result of  $\pi$ -sigma attractions overcoming any possible  $\pi$ - $\pi$  repulsions. Moreover, the incorporation of O-MWCNTs in the PES matrix creates a compact membrane structure with smaller-size surface pores, which increases the surface area available for hormone adsorption.

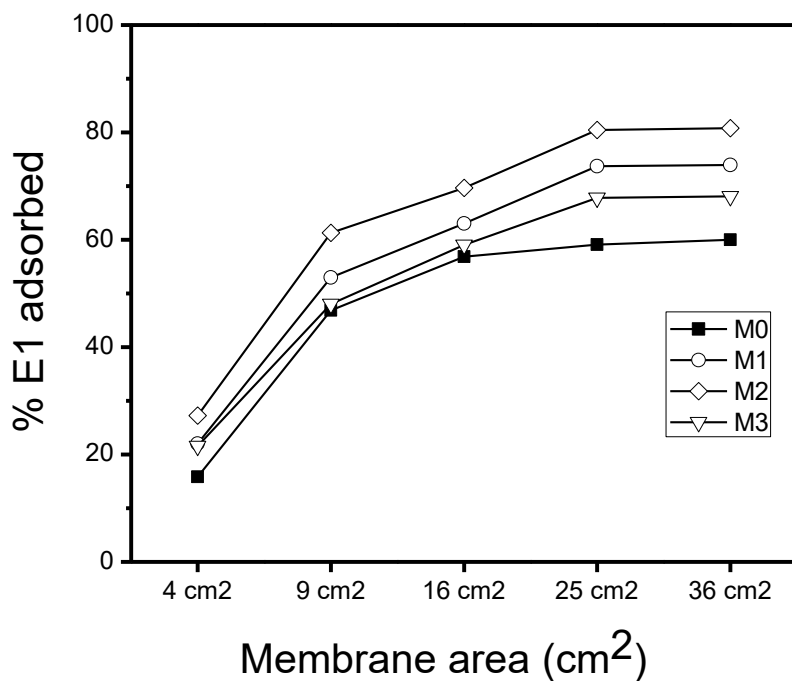


**Figure 4.8** E1 adsorption on PES membranes containing various loadings of O-MWCNTs after 72 h contact time as a function of membrane area. Experimental conditions: 100 ng/L solution of E1, pH ~6, at 20 °C, 260 rpm.

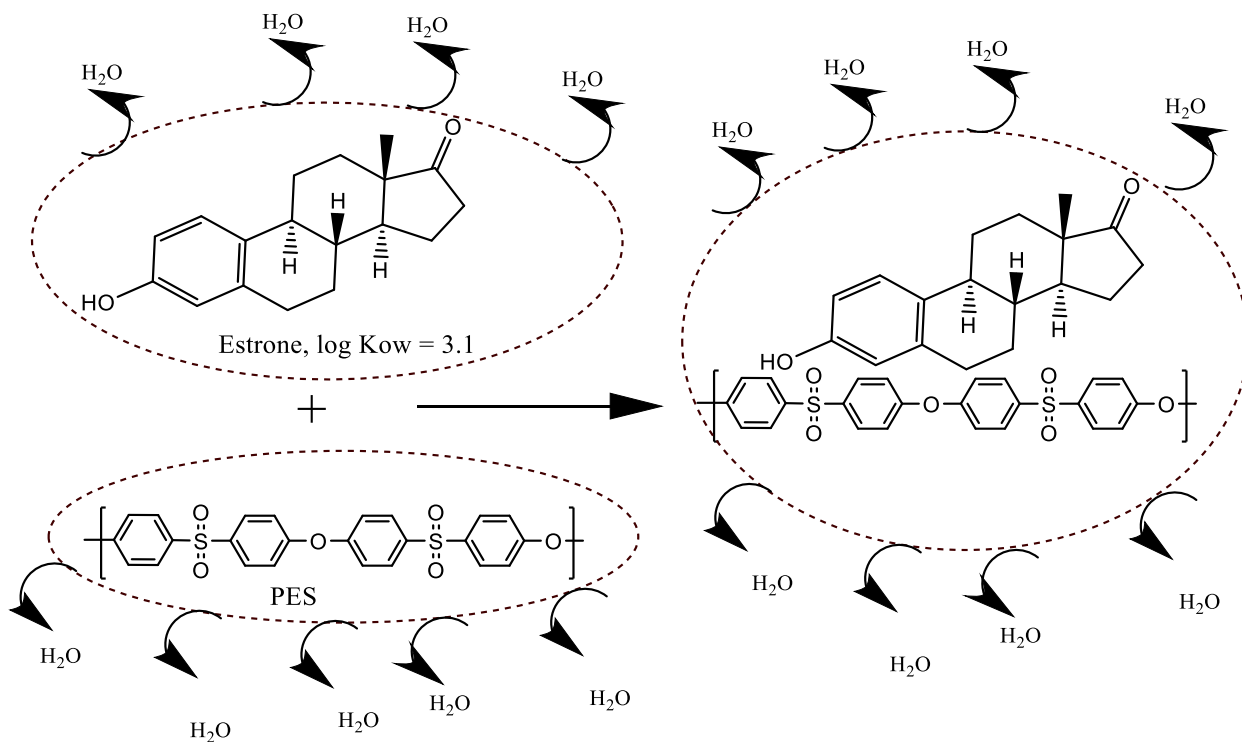


**Figure 4.9.** Hydrophobic interactions between E1 and PES membrane (M0).

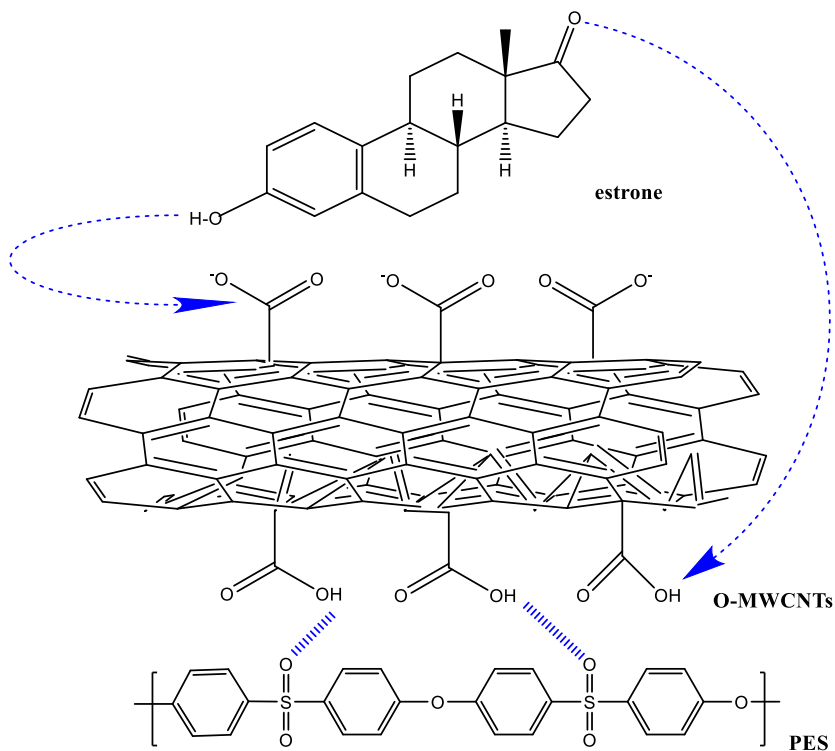


**Figure 4.10.** Hydrogen bonding interactions between E1 and PES/O-MWCNT membranes.

The partition coefficients ( $\log K$ ) of E1 between PES/O-MWCNT membranes and bulk solution as a function of membrane area are represented in Fig. 4.11. It can be seen that for all PES membrane types,  $\log K$  remains fairly constant as the membrane areas are increased from 4 – 36 cm<sup>2</sup>. This suggests that pseudo-equilibrium state was reached for all membrane types [33]. Moreover, the  $\log K$  values of M0 (59.10 – 104.91) were lower than those of PES membranes containing O-MWCNTs, M1 (73.43 – 141.82), M2 (100 – 179.56) and M3 (61.70 – 122.06). The increase in  $\log K$  values in the presence of O-MWCNTs is indicative of the favourable partitioning of E1 hormone between the solution and the modified PES membranes, thereby contributing towards the enhancement of E1 adsorption.

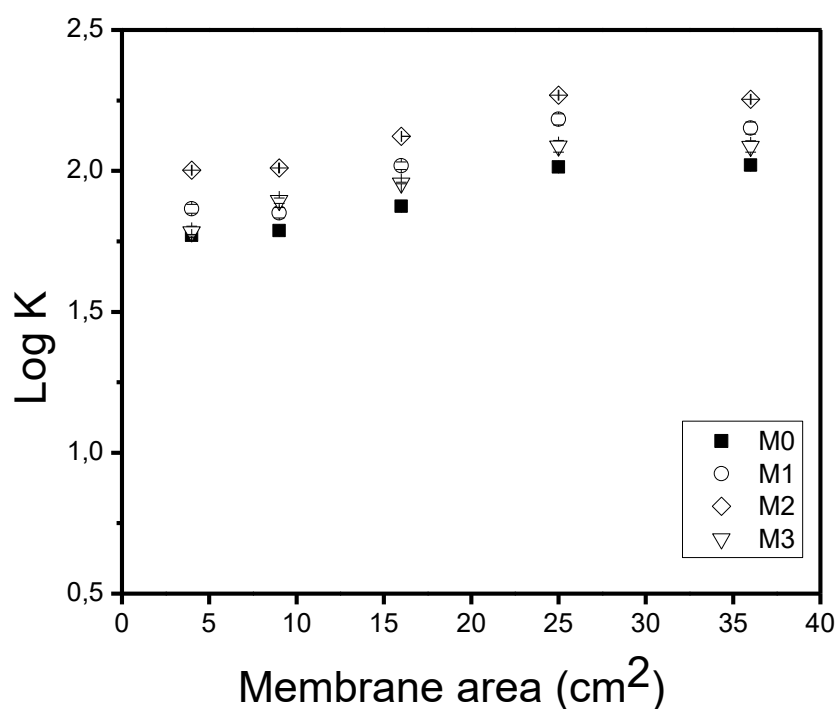


**Figure 4.11** Comparison of partition coefficients of E1 between the PES/O-MWCNT membranes and the bulk E1 solution. Experimental conditions: 72 h contact time, 100ng/L E1 solution, pH ~6, at 20 °C, 260 rpm.

#### 4.3.6.2. Effect of contact time on E1 adsorption

Over the course of time, the mass of E1 adsorbed into the membranes increased until a steady state was reached after 72 h (Fig. 4.12). The E1 adsorption was found to increase by 39% for M0 and 59% for M2 with the increase in contact time from 0.5 h to 24 h. This is due to an increase in continued adsorption of E1 hormone into the membranes with time and the presence of highly adsorbing O-MWCNTs with large-surface area, in the skin layer of PES/O-MWCNT membranes. However, compared to the adsorption into free-standing O-MWCNTs, the rate of E1 adsorption was much faster on free-standing O-MWCNTs, with the equilibrium reached after a contact time of 6 h. Moreover, a higher adsorption efficiency ( $96 \pm 1.7\%$ ) was achieved with O-MWCNTs. This is because with free-standing O-MWCNTs, a large surface-area of O-MWCNTs is available for contact and adsorption of E1 molecules, whereas in a mixed-matrix membrane configuration, fewer O-MWCNTs become available for contact with E1 molecules. This means that a portion of the O-MWCNTs migrate to the PES membrane skin layer to enhance the membrane surface properties while some remain in the membrane sublayer and matrix. As such, further research on increasing the availability of O-MWCNTs through spatial localisation of O-MWCNTs in the membrane active layer, while minimising leaching, is necessary, in an effort to make full use of the highly adsorptive properties of O-MWCNTs.

Pseudo-first-order and second-order kinetic models were used to study the adsorption kinetics followed by PES/O-MWCNT membranes during the adsorption of E1 from aqueous solutions. Based on the linear correlation coefficients ( $R^2$ ) of both models given in Table 4.4, pseudo-second-order kinetic model provided a better fit for the adsorption data (higher  $R^2$  values compared to those of pseudo-first-order model). Moreover, the rate constant values obtained for the pseudo-second-order kinetics were higher than those of pseudo-first-order kinetics,

further confirming that the adsorption of E1 by PES membranes containing different loadings of O-MWCNTs favoured pseudo-second order kinetics. This suggests that chemisorption of E1 onto evaluated membranes is the rate limiting step [34].

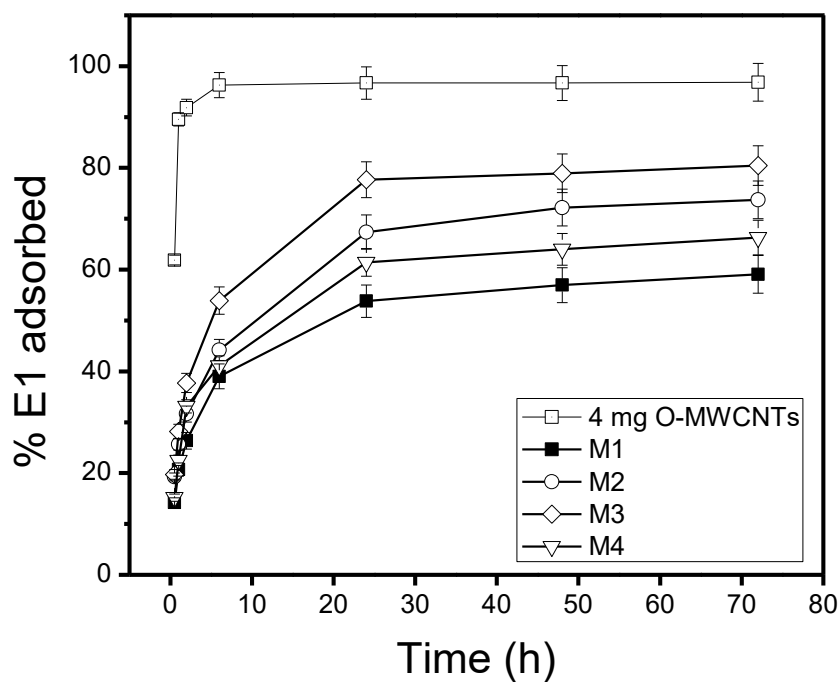


**Figure 4.12** Time-dependent E1 removal by O-MWCNTs and by PES membranes containing various loadings of O-MWCNTs. Experimental conditions: 25 cm<sup>2</sup> membrane area, initial E1 concentration of 100 ng/L, pH ~6, at 20 °C, 260 rpm.

**Table 4.4** Kinetic model parameters for E1 adsorption by PES/O-MWCNT membranes.

Kinetic model	Parameters	Membrane type			
		M0	M1	M2	M3
Pseudo-first-order	$k_1$ ( $\text{min}^{-1}$ )	8.40E-4	7.73E-4	4.98E-4	8.65E-4
	$q_e$ (mg/g)	0.298	0.458	0.470	0.432
	$R^2$	0.974	0.951	0.959	0.929
Pseudo-second-order	$k_2$ (g/mg.min)	0.018	0.007	0.008	0.006
	$q_e$ (mg/g)	0.578	0.746	0.828	0.716
	$R^2$	0.999	0.998	0.998	0.984

Fig. 4.13 shows isotherm data fittings of E1 adsorption by PES/O-MWCNT UF membranes using Langmuir and Freundlich isotherms. The Langmuir isotherm is based on the assumption that a monolayer of adsorbate molecules is formed on active sites of the adsorbent and no other molecules can adsorb into the monolayer while Freundlich model is based on multilayer adsorption of solutes [63]. The fitting parameters of Langmuir and Freundlich isotherm model used are listed in Table 4.5. It can be seen from Table 4.5 that the maximum adsorption capacity ( $q_0$ ) increased by 30% in the presence of O-MWCNTs in the PES matrix, i.e. from 23.81 mg/g for M0 to 31.25 mg/g for M2. Evaluation of the dimensionless separation factor values suggests that the adsorption process was favourable for all PES-based membranes evaluated ( $R_L$  values  $< 1$ ). Based on the linear correlation coefficient ( $R^2$ ) values obtained from both models, the Freundlich isotherm gives a better correlation since the  $R^2$  values for all membranes are  $\geq 0.9$ . As such, adsorption of E1 hormone follows the Freundlich isotherm suggesting that more than one layer of hormone attaches on the membrane active sites, and that the already adsorbed layers interacts with incoming hormones. Moreover, the Freundlich adsorption capacity

parameter ( $K_F$ ) for membranes containing O-MWCNTs is higher than that of pristine PES membrane (M0), indicating a greater affinity of E1 hormone for PES/O-MWCNT membranes. A higher  $K_F$  value is indicative of greater hormone adsorption capacity [64]. Heterogeneous adsorption on the prepared membranes can be further substantiated by the fact the  $1/n$  values are  $> 1$  which suggests that the more E1 hormone present on the polymeric membrane material, the greater the enhancement of free-energy of further sorption (Table 4.5) [64].

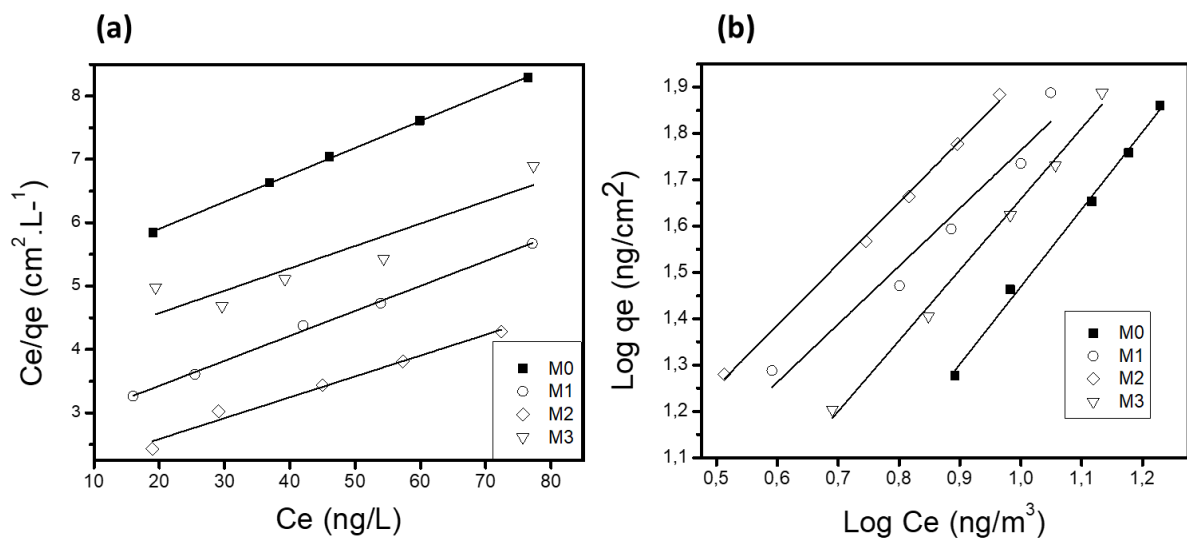


**Figure 4.13** Isotherm data fitting for adsorption of E1 by PES/O-MWCNT membranes (a) linear regression form of Langmuir isotherm and (b) linear regression form of the logarithmic form of the Freundlich isotherm. Experimental conditions: 72 h contact time, 100 ng/L solution of E1, pH  $\sim 6$ , at 20 °C, 260 rpm, and no background electrolyte was used. The data were obtained from Figure 4.8.

**Table 4.5** Langmuir and Freundlich fitted parameters for E1 adsorption by PES/O-MWCNT membranes.

Fitted isotherm	Parameters	Membrane type			
		M0	M1	M2	M3
Langmuir	$q_o$ (mg/g)	23.8	25.6	31.2	25.6
	$b$ (L/mg)	0.008	0.015	0.016	0.009
	$R_L$	0.546	0.404	0.376	0.525
	$R^2$	0.99	0.95	0.91	0.79
Freundlich	$K_F$ (mg/g)(L/mg) <sup>1/n</sup>	0.62	3.25	3.89	1.37
	$1/n$	1.67	1.25	1.33	1.53
	$R^2$	0.99	0.98	0.99	0.99

In summary, PES/O-MWCNT membranes showed improved adsorption of E1 hormone even though their pore sizes are large (~ 90 kDa) compared to those of typically used NF or RO membranes (~ 200 – 400 Da) for hormone removal [11]. Pressure requirements and ultimately, energy consumption follows the order RO > NF > UF > MF, which means that RO/NF membranes offer almost complete removal of small-size solutes, but less convenient because of high energy requirements [65]. Therefore, in addition to the presence of high adsorbing O-MWCNTs in the membrane matrix, the large pore sizes of the PES/O-MWCNT allowed E1 access to internal adsorption sites.

#### 4.3.6.3. pH dependence of E1 adsorption by PES/O-MWCNT membranes

It has been shown from Sections 4.3.6.1 and 4.3.6.2 that under neutral pH conditions; a micropollutant of smaller size than the pore size of the membrane used, can be removed by the membrane as a consequence of hydrophobic interactions, hydrogen bonding interactions and  $\pi$ - $\pi$  interactions. In this section, the influence of solution pH on E1 removal by PES membranes containing various loadings of O-MWCNTs is investigated. Zeta potential measurements discussed in Section 4.3.5., have already demonstrated that a change in pH of the solution has a direct effect on a charge assumed by the membrane due to the dissociation of functional groups on the active sites on the membrane. It can be seen from Fig. 4.14 that an increase in solution pH below the pKa value of E1 led to a slight increase in E1 adsorption by all membranes evaluated, with the highest increase of 66% for M0, 77% for M1, 86% for M2 and 73% for M3 obtained at around pH 9. Above pH 10, a slight decline in percentage of E1 adsorbed was observed. The initial increase in adsorption can be linked to hydrogen bonding interaction between the the  $-OH$  groups of E1 and the  $-COO$  groups or  $-S=O$  groups on the PES membrane surface. This is because at a pH below the pKa value of E1 (= 10.5), E1 hormone is undissociated and in possession of all protons necessary to form hydrogen bonds with the negatively charged membrane surface. However, at a pH above the pKa value of E1, the  $-OH$  groups of E1 undergo deprotonation and the hormone becomes negatively charged [11]. It was established from zeta potential measurements that M2 becomes negatively charged under alkaline conditions. Therefore, the slight decrease in adsorption above pH 10 is attributable to charge repulsion, as E1 carries a similar charge as the membrane surface. Similar results have also been reported by other researchers [16, 63]. Therefore, in addition to hormone removal through hydrophobic interactions, electrostatic interactions between the membrane surface and the charged hormone can also enhance the removal capacity of the membrane. The

results obtained on pH dependence of E1 adsorption by PES/O-MWCNT membranes allow for the establishment of the dominant adsorption mechanism. If hydrogen bonding were the dominant mechanism responsible for E1 adsorption, then the removal of E1 would increase drastically at lower pH values. This is because from zeta potential measurements, it was established that membranes are positively charged or protonated at lower pH values (-COO groups of O-MWCNTs exists as -COOH, -S=O of PES chain transitions to -SO<sub>2</sub>H) and E1 has not undergone dissociation, *i.e.*, the -OH groups of E1 are still intact. As such, the extent of hydrogen bonding between the membrane surface and E1 would increase. However, the results obtained and given in Fig. 4.14 ran contrary to this fact. Hence, it can be assumed that the observed increase in E1 adsorption is dominated by  $\pi$ - $\pi$  interactions between PES/O-MWCNT membranes and E1.

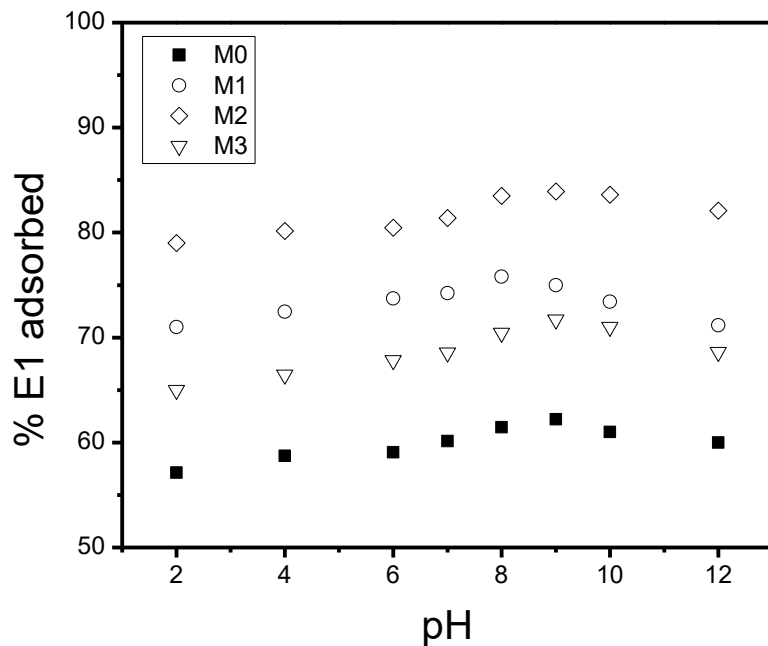


**Figure 4.14** Influence of pH on E1 removal by PES/O-MWCNT membranes. Experimental conditions: 72 h contact time, 25 cm<sup>2</sup> membrane area, initial E1 concentration of 100 ng/L, at 20 °C, 260 rpm.

#### 4.3.6.4. Regeneration of PES/O-MWCNT membranes

Fig. 4.15 shows the regeneration efficiencies of PES membranes containing various loadings of O-MWCNTs after five adsorption–regeneration cycles using ethanol/water solvent mixture. High regeneration efficiencies were observed for PES membranes containing O-MWCNTs, namely 90% for M1, 95% for M2 and 91% for M3 after five cycles, while the bare PES membrane, M0 was found to have a regeneration efficiency of 83%. The observed results are due to strong partitioning of E1 in the ethanol-water solution based on its high octanol-water partition coefficient ( $\log K_{ow} = 3.13$ ), leading to enhanced desorption from the membrane material [35]. Moreover, the –OH groups in ethanol could destabilise the existing hydrogen bond interactions between E1 and –S=O groups or E1 and –COO groups of the PES/O-MWCNT polymer backbone, thereby displacing adsorbed E1 into the ethanol-water solution. The SEM surface images of membrane M2 (Fig S4.3) after five regeneration cycles show that there was no significant change in membrane surface compared to that of M2 in Fig.4.3. Furthermore, the FTIR spectra of M2 after five regeneration cycles still have the same characteristic functional groups identified for M2 prior to E1 adsorption (Fig S4.3). The results obtained suggest that the adsorption of E1 into PES/O-MWCNT membranes is reversible and that the regeneration process used did not cause any damage to the membrane material.

In a separate experiment, Milli-Q water was used instead of the ethanol/water solvent mixture at 20 °C for desorption of E1 from membrane M1. It was found that the regeneration efficiency of M1 was below 5%, even though the washing time was increased beyond 30 min (Fig. S4.4). The results suggest that PES/O-MWCNT membranes are stable in water and that the adsorbed E1 molecules will have low leachability into the treated water.

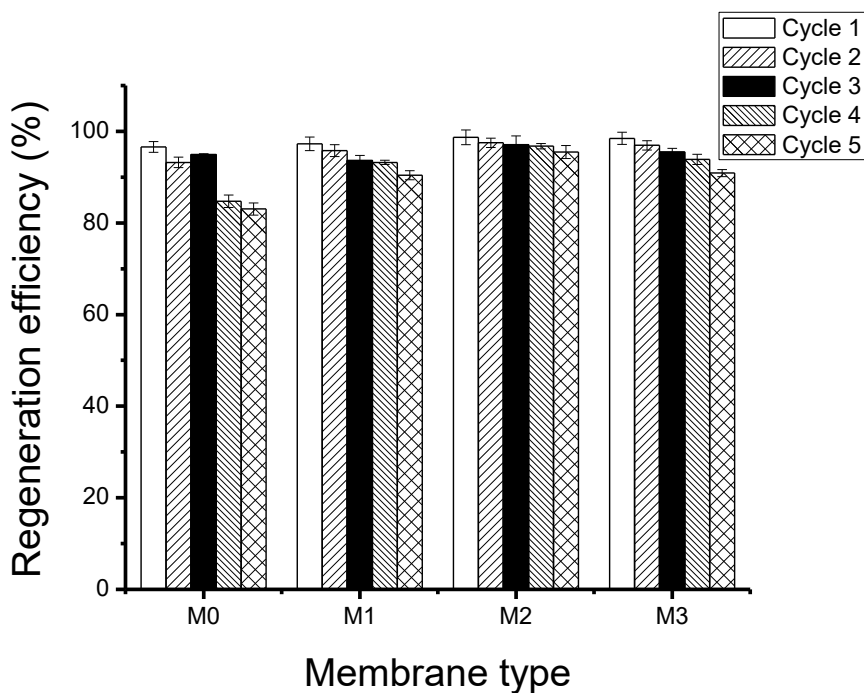


**Figure 4.15** Regeneration efficiency of PES/O-MWCNT membranes. Experimental conditions: 72 h E1 contact time, ethanol/water (1:1) washing solvent, 25 cm<sup>2</sup> membrane area, initial E1 concentration 100 ng/L, 20 °C, 260 rpm.

#### 4.4. Limitations of the study and further work

Chemical adsorption of E1 into PES/O-MWCNT membranes via hydrogen bonding and  $\pi$ - $\pi$  interactions provides an alternative means for the removal of low concentration of E1 from water sources. Moreover, the stability of E1-adsorbed PES/O-MWCNT membranes in water at room temperature and the effective regeneration of the membrane material after successive adsorption-desorption cycles, are particularly desirable for potential application in the treatment of real water samples. However, a few aspects still need to be addressed in the study in greater detail. Firstly, there is a need to further investigate, the membrane preparation methods that can increase the availability of the incorporated O-MWCNTs for maximum contact with estrone molecules. Such preparative methods should ensure maximum exposure of O-MWCNTs while minimising leaching. This will ensure rapid removal of estrone at higher

adsorption capacities than those currently achieved in the study. Moreover, the effect of E1 solution chemistry *i.e.*, varying solution ionic strength and the presence of competing organic compounds such as natural organic matter, for adsorption sites on PES/O-MWCNT membranes, still needs to be evaluated in greater detail. Prolonged regeneration cycles of the membranes should be investigated and the search for greener, recyclable washing solvents for estrone needs to be conducted.

#### **4.5. Conclusion**

The adsorptive removal of natural hormone E1 by PES/O-MWCNT mixed-matrix membranes, was investigated by conducting batch adsorption experiments. PES/O-MWCNT membranes were first synthesised and characterised using various surface and membrane performance techniques and the following results were obtained:

- (i) SEM images indicated that membrane microstructure changes with the O-MWCNTs content in the PES matrix, *i.e.* the membrane morphology transitioned from an open-porous finger-like morphology for bare PES membrane to a dense and less porous substructure for PES membranes with the highest loading of O-MWCNTs.
- (ii) Isoelectric points of PES/O-MWCNT membranes shifted to lower pH values with an increase in O-MWCNT loading due to the presence of negatively charged acidic functional groups of O-MWCNTs on the PES membrane surface.
- (iii) Molecular weight cut-off (MWCO) determination results of PES/O-MWCNT were in agreement with SEM results, in that the membrane pore sizes slightly decreased with an increase in O-MWCNT content.

- (iv) The prepared PES/O-MWCNT membranes became more hydrophilic as the content of O-MWCNTs was increased. However, pure water flux decreased correspondingly. This finding revealed that membrane pore sizes had a dominant effect on resultant membrane pure water flux over membrane surface hydrophilicity.

Adsorptive removal of E1 increased with an increase in O-MWCNT content followed by a decline with further increments. The enhancement in E1 adsorption under neutral pH conditions was attributable to (i) the presence of highly adsorbing O-MWCNTs in PES matrix (large surface area-to-volume ratio of O-MWCNTs), (ii) hydrogen bonding interactions between PES/O-MWCNT and E1 and (iii)  $\pi$ - $\pi$  interactions between graphene sheets of O-MWCNTs and aromatic rings of E1. Studying the influence of pH on E1 adsorption by PES/O-MWCNT membranes provided evidence that  $\pi$ - $\pi$  interactions were the dominant adsorption mechanism instead of hydrogen bonding. The adsorption kinetics of E1 by PES/O-MWCNT membranes followed the pseudo-second-order kinetic model. The E1 adsorption rate by the PES/O-MWCNT membranes was slow as equilibrium was only reached after 24 h. The Freundlich isotherm provided a better fit to the adsorption data than the Langmuir isotherm. The PES/O-MWCNT membranes maintained high adsorption capacities after five adsorption-regeneration cycles as evidenced by regeneration efficiencies of above 90%. The SEM and FTIR analysis provided evidence that the continuous adsorption-regeneration cycles did not induce any damage to the membrane material. The study herein will be beneficial for quantitative predictions of the adsorptive removal of other organic compounds or hormones which have similar physical and chemical properties as E1, by large pore-size PES UF membranes.

## 4.6. References

- [1] E. Stumm-Zollinger, G.M. Fair, Biodegradation of steroid hormones, *Journal of the Water Pollution Control Federation*, 37 (1965) 1506-1510.
- [2] M.J. Benotti, R.A. Trenholm, B.J. Vanderford, J.C. Holady, B.D. Stanford, S.A. Snyder, Pharmaceuticals and endocrine disrupting compounds in US drinking water, *Environmental Science & Technology*, 43 (2008) 597-603.
- [3] P. Westerhoff, Y. Yoon, S. Snyder, E. Wert, Fate of endocrine-disruptor, pharmaceutical, and personal care product chemicals during simulated drinking water treatment processes, *Environmental Science & Technology*, 39 (2005) 6649-6663.
- [4] P. Roefer, S. Snyder, R.E. Zegers, D.J. Rexing, J.L. Fronk, Endocrine-disrupting chemicals in a source water, *Journal American Water Works Association*, 92 (2000) 52-58.
- [5] T. Manickum, W. John, Occurrence, fate and environmental risk assessment of endocrine disrupting compounds at the wastewater treatment works in Pietermaritzburg (South Africa), *Science of the Total Environment*, 468 (2014) 584-597.
- [6] Y. Yoon, P. Westerhoff, S.A. Snyder, E.C. Wert, J. Yoon, Removal of endocrine disrupting compounds and pharmaceuticals by nanofiltration and ultrafiltration membranes, *Desalination*, 202 (2007) 16-23.
- [7] Y. Yoon, P. Westerhoff, S.A. Snyder, E.C. Wert, Nanofiltration and ultrafiltration of endocrine disrupting compounds, pharmaceuticals and personal care products, *Journal of Membrane Science*, 270 (2006) 88-100.
- [8] M. Jayle, O. Crepy, The excretion and measurement of urinary phenolsteroids, in: *Ciba Foundation Symposium-Estimation of Steroid Hormones (Book I of Colloquia on Endocrinology)*, Wiley Online Library, 1952, pp. 84-103.
- [9] J. Legler, A. Jonas, J. Lahr, A.D. Vethaak, A. Brouwer, A.J. Murk, Biological measurement of estrogenic activity in urine and bile conjugates with the in vitro ER-CALUX reporter gene assay, *Environmental Toxicology and Chemistry*, 21 (2002) 473-479.
- [10] L.D. Nghiem, A.I. Schäfer, M. Elimelech, Removal of natural hormones by nanofiltration membranes: measurement, modeling, and mechanisms, *Environmental Science & Technology*, 38 (2004) 1888-1896.
- [11] A.I. Schafer, I. Akanyeti, A.J. Semiao, Micropollutant sorption to membrane polymers: a review of mechanisms for estrogens, *Advances Colloid Interface Science*, 164 (2011) 100-117.
- [12] A. Schäfer, L. Nghiem, T. Waite, Removal of the natural hormone estrone from aqueous solutions using nanofiltration and reverse osmosis, *Environmental Science & Technology*, 37 (2003) 182-188.
- [13] A.R.D. Verliefde, Rejection of organic micropollutants by high pressure membranes (NF/RO), Doctoral Thesis, Delft University of Technology, Delft, Netherlands (2008).
- [14] X. Jin, J. Hu, S.L. Ong, Removal of natural hormone estrone from secondary effluents using nanofiltration and reverse osmosis, *Water Research*, 44 (2010) 638-648.
- [15] E.A. McCallum, H. Hyung, T.A. Do, C.-H. Huang, J.-H. Kim, Adsorption, desorption, and steady-state removal of 17 $\beta$ -estradiol by nanofiltration membranes, *Journal of Membrane Science*, 319 (2008) 38-43.

- [16] L. Nghiem, A. Schäfer, T. Waite, Adsorptive interactions between membranes and trace contaminants, *Desalination*, 147 (2002) 269-274.
- [17] C. Sheng, A.A. Nnanna, Y. Liu, J.D. Vargo, Removal of Trace Pharmaceuticals from Water using coagulation and powdered activated carbon as pretreatment to ultrafiltration membrane system, *Science of the Total Environment*, 550 (2016) 1075-1083.
- [18] C.E. Gökçe, S. Arayici, Adsorption of 17 $\beta$ -estradiol and estrone by activated carbon derived from sewage sludge, *Desalination and Water Treatment*, 57 (2015) 2503-2514.
- [19] P. Oleszczuk, B. Pan, B. Xing, Adsorption and desorption of oxytetracycline and carbamazepine by multiwalled carbon nanotubes, *Environmental Science & Technology*, 43 (2009) 9167-9173.
- [20] B. Pan, D. Lin, H. Mashayekhi, B. Xing, Adsorption and hysteresis of bisphenol A and 17 $\alpha$ -ethinyl estradiol on carbon nanomaterials, *Environmental Science & Technology*, 42 (2008) 5480-5485.
- [21] K. Yang, B. Xing, Adsorption of organic compounds by carbon nanomaterials in aqueous phase: Polanyi theory and its application, *Chemical Reviews*, 110 (2010) 5989-6008.
- [22] X. Qu, P.J. Alvarez, Q. Li, Applications of nanotechnology in water and wastewater treatment, *Water Research*, 47 (2013) 3931-3946.
- [23] A. Kiran Kumar, S. Venkata Mohan, Removal of natural and synthetic endocrine disrupting estrogens by multi-walled carbon nanotubes (MWCNT) as adsorbent: Kinetic and mechanistic evaluation, *Separation and Purification Technology*, 87 (2012) 22-30.
- [24] J. Lee, Carbon nanotube-enhanced membrane for advanced water treatment, Doctoral Thesis, University of Sydney, Australia (2016).
- [25] G. Kaminska, J. Bohdziewicz, J. Calvo, P. Prádanos, L. Palacio, A. Hernández, Fabrication and characterisation of polyethersulfone nanocomposite membranes for the removal of endocrine disrupting micropollutants from wastewater. Mechanisms and performance, *Journal of Membrane Science*, 493 (2015) 66-79.
- [26] A.M. Soto, C. Sonnenschein, K.L. Chung, M.F. Fernandez, N. Olea, F.O. Serrano, The E-SCREEN assay as a tool to identify estrogens: an update on estrogenic environmental pollutants, *Environmental Health Perspectives*, 103 (1995) 113.
- [27] D.M.C. Albert R. Cunningham, Seena A. Iype, and Suzanne L. Cunningham, *Endocrine Disruption Modeling*, CRC Press, 2009.
- [28] A.R. Verliefde, E. Cornelissen, S. Heijman, J. Verberk, G. Amy, B. Van der Bruggen, J. Van Dijk, The role of electrostatic interactions on the rejection of organic solutes in aqueous solutions with nanofiltration, *Journal of Membrane Science*, 322 (2008) 52-66.
- [29] K. Kimura, G. Amy, J. Drewes, Y. Watanabe, Adsorption of hydrophobic compounds into NF/RO membranes: an artifact leading to overestimation of rejection, *Journal of Membrane Science*, 221 (2003) 89-101.
- [30] S.A. Snyder, J. Leising, P. Westerhoff, Y. Yoon, H. Mash, B. Vanderford, Biological and physical attenuation of endocrine disruptors and pharmaceuticals: implications for water reuse, *Groundwater Monitoring & Remediation*, 24 (2004) 108-118.

- [31] L.-F. Liu, X. Huang, X. Zhang, K. Li, Y.-L. Ji, C.-y. Yu, C.-J. Gao, Modification of polyamide TFC nanofiltration membrane for improving separation and antifouling properties, *RSC Advances*, 8 (2018) 15102-15110.
- [32] S. Singh, K. Khulbe, T. Matsuura, P. Ramamurthy, Membrane characterisation by solute transport and atomic force microscopy, *Journal of Membrane Science*, 142 (1998) 111-127.
- [33] Y. Yoon, P. Westerhoff, J. Yoon, S.A. Snyder, Removal of 17 $\beta$  estradiol and fluoranthene by nanofiltration and ultrafiltration, *Journal of Environmental Engineering*, 130 (2004) 1460-1467.
- [34] L. Mdlalose, M. Balogun, K. Setshedi, L. Chimuka, A. Chetty, Adsorption of phosphates using transition metals-modified bentonite clay, *Separation Science and Technology*, (2018) 1-12.
- [35] J. Han, W. Qiu, J. Hu, W. Gao, Chemisorption of estrone in nylon microfiltration membranes: Adsorption mechanism and potential use for estrone removal from water, *Water Research*, 46 (2012) 873-881.
- [36] V. Vatanpour, S.S. Madaeni, R. Moradian, S. Zinadini, B. Astinchap, Fabrication and characterisation of novel antifouling nanofiltration membrane prepared from oxidised multiwalled carbon nanotube/polyethersulfone nanocomposite, *Journal of Membrane Science*, 375 (2011) 284-294.
- [37] M. Son, H. Park, L. Liu, H. Choi, J.H. Kim, H. Choi, Thin-film nanocomposite membrane with CNT positioning in support layer for energy harvesting from saline water, *Chemical Engineering Journal*, 284 (2016) 68-77.
- [38] J.-H. Choi, J. Jegal, W.-N. Kim, Fabrication and characterisation of multi-walled carbon nanotubes/polymer blend membranes, *Journal of Membrane Science*, 284 (2006) 406-415.
- [39] L. Bai, H. Liang, J. Crittenden, F. Qu, A. Ding, J. Ma, X. Du, S. Guo, G. Li, Surface modification of UF membranes with functionalised MWCNTs to control membrane fouling by NOM fractions, *Journal of Membrane Science*, 492 (2015) 400-411.
- [40] R. Saranya, G. Arthanareeswaran, D.D. Dionysiou, Treatment of paper mill effluent using Polyethersulfone/functionalised multiwalled carbon nanotubes based nanocomposite membranes, *Chemical Engineering Journal*, 236 (2014) 369-377.
- [41] R. Sengur-Tasdemir, V.R. Mokkaapati, D.Y. Koseoglu-Imer, I. Koyuncu, Effect of polymer type on characterisation and filtration performances of multi-walled carbon nanotubes (MWCNT)-COOH-based polymeric mixed-matrix membranes, *Environmental technology*, 39 (2018) 1226-1237.
- [42] P.-C. Ma, N.A. Siddiqui, G. Marom, J.-K. Kim, Dispersion and functionalisation of carbon nanotubes for polymer-based nanocomposites: a review, *Composites Part A: Applied Science and Manufacturing*, 41 (2010) 1345-1367.
- [43] J. Mulder, *Basic Principles of Membrane Technology*, Springer Science & Business Media, New York, USA, 2012.
- [44] A.K. Shukla, J. Alam, M. Alhoshan, L.A. Dass, M. Muthumareeswaran, Development of a nanocomposite ultrafiltration membrane based on polyphenylsulfone blended with graphene oxide, *Scientific Reports*, 7 (2017).

- [45] C. Zhao, X. Zhou, Y. Yue, Determination of pore size and pore size distribution on the surface of hollow-fiber filtration membranes: a review of methods, *Desalination*, 129 (2000) 107-123.
- [46] D. Rana, T. Matsuura, Surface modifications for antifouling membranes, *Chemical Reviews*, 110 (2010) 2448-2471.
- [47] E. Celik, L. Liu, H. Choi, Protein fouling behavior of carbon nanotube/polyethersulfone composite membranes during water filtration, *Water Research*, 45 (2011) 5287-5294.
- [48] S. Zinadini, A.A. Zinatizadeh, M. Rahimi, V. Vatanpour, H. Zangeneh, Preparation of a novel antifouling mixed-matrix PES membrane by embedding graphene oxide nanoplates, *Journal of Membrane Science*, 453 (2014) 292-301.
- [49] K. Zhu, G. Wang, Fabrication of high-performance ultrafiltration membranes using zwitterionic carbon nanotubes and polyethersulfone, *High Performance Polymers*, 30 (2018) 602-611.
- [50] A. Tiraferri, C.D. Vecitis, M. Elimelech, Covalent binding of single-walled carbon nanotubes to polyamide membranes for antimicrobial surface properties, *ACS Applied Material & Interfaces*, 3 (2011) 2869-2877.
- [51] A. Tiraferri, Y. Kang, E.P. Giannelis, M. Elimelech, Superhydrophilic thin-film composite forward osmosis membranes for organic fouling control: fouling behavior and antifouling mechanisms, *Environmental Science & Technology*, 46 (2012) 11135-11144.
- [52] D.L. Arockiasamy, J. Alam, M. Alhoshan, Carbon nanotubes-blended poly (phenylene sulfone) membranes for ultrafiltration applications, *Applied Water Science*, 3 (2013) 93-103.
- [53] D. Mattia, H. Leese, K.P. Lee, Carbon nanotube membranes: from flow enhancement to permeability, *Journal of Membrane Science*, 475 (2015) 266-272.
- [54] T. Luxbacher, Electrokinetic properties of natural fibres, in Ryszard Kozlowski (Ed.), *Handbook of natural Natural fibresFibres*, Woodhead Publishing, Birmingham, Ala., USA, 2012, pp. 185-215.
- [55] J.n. Shen, C.c. Yu, H.m. Ruan, C.j. Gao, B. Van der Bruggen, Preparation and characterisation of thin-film nanocomposite membranes embedded with poly(methyl methacrylate) hydrophobic modified multiwalled carbon nanotubes by interfacial polymerisation, *Journal of Membrane Science*, 442 (2013) 18-26.
- [56] M. Elimelech, W.H. Chen, J.J. Waypa, Measuring the zeta (electrokinetic) potential of reverse osmosis membranes by a streaming potential analyzer, *Desalination*, 95 (1994) 269-286.
- [57] A.E. Childress, M. Elimelech, Effect of solution chemistry on the surface charge of polymeric reverse osmosis and nanofiltration membranes, *Journal of Membrane Science*, 119 (1996) 253-268.
- [58] L. Schaeffer, The Role of Functional Groups in Drug–Receptor Interactions, in: *The Practice of Medicinal Chemistry*, Elsevier, 2008, pp. 464-480.
- [59] A. Akbari, E. Aliyarizadeh, S.M.M. Rostami, M. Homayoonfal, Novel sulfonated polyamide thin-film composite nanofiltration membranes with improved water flux and anti-fouling properties, *Desalination*, 377 (2016) 11-22.

- [60] G. Kaminska, M. Adamczak, J. Bohdziewicz, Retention of bisphenol A and caffeine on PES/PES-CNTs membranes-performance and effect of different conditions, *Desalination and Water Treatment*, 134 (2018) 109-114.
- [61] W. Chen, L. Duan, D. Zhu, Adsorption of polar and nonpolar organic chemicals to carbon nanotubes, *Environmental Science & Technology*, 41 (2007) 8295-8300.
- [62] C.A. Hunter, J.K. Sanders, The nature of  $\pi$ - $\pi$  interactions, *Journal of the American Chemical Society*, 112 (1990) 5525-5534.
- [63] M. Tagliavini, F. Engel, P.G. Weidler, T. Scherer, A.I. Schäfer, Adsorption of steroid micropollutants on polymer-based spherical activated carbon (PBSAC), *Journal of Hazardous Materials*, 337 (2017) 126-137.
- [64] A.J.C. Semião, A.I. Schäfer, Removal of adsorbing estrogenic micropollutants by nanofiltration membranes. Part A—Experimental evidence, *Journal of Membrane Science*, 431 (2013) 244-256.
- [65] C.P. Silva, M. Otero, V. Esteves, Processes for the elimination of estrogenic steroid hormones from water: a review, *Environmental Pollution*, 165 (2012) 38-58.

**CHAPTER 5**  
**MACROVOID-FREE PES/SPSF/O-MWCNT ULTRAFILTRATION MEMBRANES**  
**WITH IMPROVED MECHANICAL STRENGTH, ANTIFOULING AND**  
**ANTIBACTERIAL PROPERTIES**

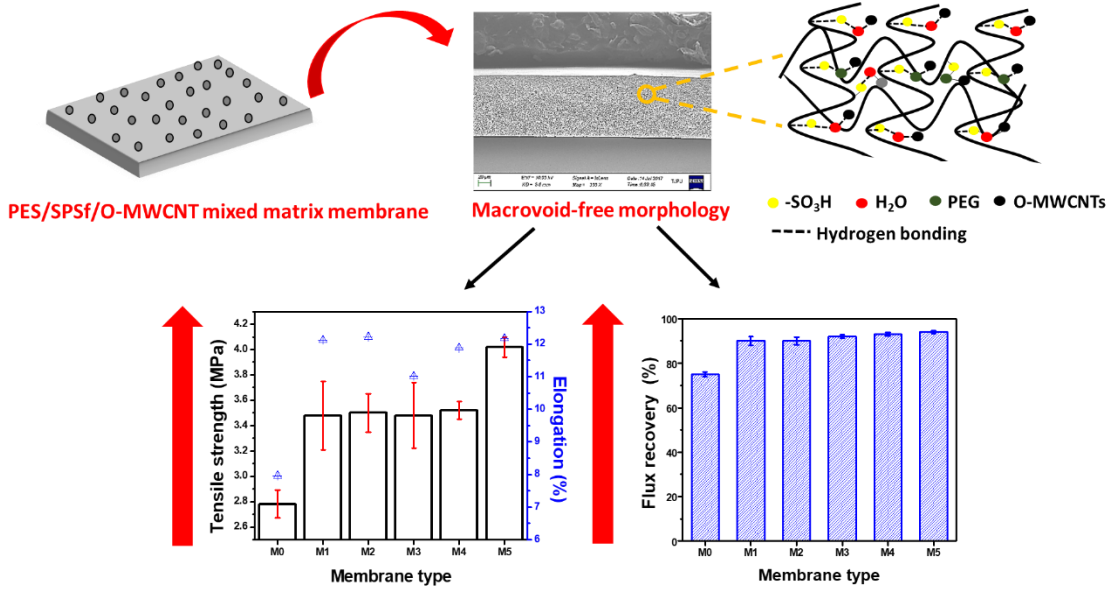
---

**Summary of the chapter**

Macrovoid-free polyethersulfone/sulfonated polysulfone (PES/SPSf) ultrafiltration (UF) membranes containing oxidised multi-walled carbon nanotubes (O-MWCNTs) were fabricated via a non-solvent induced phase-separation method using H<sub>2</sub>O-PEG 20kDa as a non-solvent additive. The results showed that the fully sponge-like morphology of the PES/SPSf membranes could be achieved as the content of O-MWCNTs in the casting solutions was increased, due to the formation of strong hydrogen bonds between SPSf, H<sub>2</sub>O, PEG 20kDa and O-MWCNTs. Such morphology provided excellent mechanical strength properties with the highest of  $4.02 \pm 0.08$  MPa obtained for the membrane containing 0.1 wt.% O-MWCNTs. Microscopic analysis revealed homogenous distribution of O-MWCNTs in the PES/SPSf mixed-matrix membranes. Moreover, pure water flux initially increased from 598 to 713 L/m<sup>2</sup> h followed by a decline to 590, 560, 553 and 578 L/m<sup>2</sup> h as the content of O-MWCNTs was increased from 0 wt.% to 0.005, 0.01, 0.03, 0.05 and 0.1 wt.%, respectively. A rejection of > 99% for bovine serum albumin (BSA) was achieved by membranes containing 0.05 wt.% O-MWCNTs. The water flux recovery ratio of membranes containing O-MWCNTs was found to be higher (> 90%) than that of pristine PES/SPSf (75%) even after the second fouling and cleaning stage. Furthermore, it was found that only 85% of *E. coli* bacteria were killed by pristine PES/SPSf, compared to 99% by PES/SPSf membrane with the highest O-MWCNT loading. The fabricated flat-sheet membranes display attractive features for use as UF membranes in the pre-treatment stage of water treatment.

**Keywords:** oxidised multi-walled carbon nanotubes; polyethersulfone; sulfonated polysulfone; macrovoid-free structure; tensile strength; antifouling

### Graphical abstract



2

<sup>2</sup> N.N. Gumbi, M. Hu, B.B. Mamba, J. Li, E.N. Nxumalo, Macrovoid-free PES/SPSf/O-MWCNT ultrafiltration membranes with improved mechanical strength, antifouling and antibacterial properties, *Journal of Membrane Science*, 566 (2018) 288-300.

## 5.1. Introduction

Pressure-driven membrane processes have been applied extensively to address deteriorating water quality caused by the presence of both traditional as well as newly emerging pollutants in water [1, 2]. However, the membrane performance tends to be limited largely by fouling; as a consequence of the deposition of organic, biological and colloidal substances on the membrane surface and within the membrane pores [3]. The membrane surface (top layer or skin layer) plays a key role during the separation process, as it is the initial contact point with the feed solution. Therefore, by modifying membrane surface properties such as hydrophilicity, surface charge and roughness, membrane fouling can be minimised. Of the known surface modification strategies, improving membrane surface hydrophilicity is theorised to have a central function in controlling the fouling behaviour of membranes. The antifouling behaviour of hydrophilic membranes is believed to occur as a result of the creation of a strong hydration layer that hinders the attachment or adsorption of particulates on the membrane surface [4].

One of the commonly used strategies aimed at improving membrane surface hydrophilicity is polymer blending, also referred to as grafting, a process where a hydrophobic polymer is mixed with a hydrophilic polymer at particular weight ratio(s) provided that the two polymers are of reasonable compatibility [5]. It is essential to ensure that the two polymers are of adequate miscibility in order to bring about significant improvements in structural and surface properties of the membrane [6]. The Schneier theory is often used to assess the compatibility between two polymers, wherein a molar enthalpy of mixing ( $\Delta H_m$ ) greater than 0.01 cal/mol suggests that the polymers are immiscible and therefore incompatible with each other whereas  $\Delta H_m$  that is lower than 0.01 cal/mol suggests that the polymers are miscible at those weight ratios [6]. In a study by Li and co-workers, polyethersulfone (PES), a commonly used polymer in membrane

fabrication, was blended with sulfonated polysulfone (SPSf) and the effect of SPSf on the compatibility, membrane morphology and performance of PES was investigated [5]. It was shown that PES and SPSf are entirely miscible at all weight ratios with  $\Delta H_m < 0.01$  cal/mol and that the sulfonic acid groups of SPSf allowed for improvements in membrane surface hydrophilicity, which subsequently led to significantly high water fluxes and high fouling resistance [5]. Several other research groups have also reported on the improvements in membrane surface hydrophilicity which subsequently led to enhanced membrane performances as a result of the presence of sulfonated polymers such as SPSf [7], sulfonated polyethersulfone (SPES) [8, 9] and sulfonated polyphenylene sulfone (sPPSU) [10], in polymer blend membranes.

Despite the advantages presented above, highly sulfonated polymers when used alone, or at higher contents during fabrication of polymer blends, give rise to membranes with high swelling ratios and therefore, compromised mechanical strength properties [11]. This occurs because the introduction of highly polar sulfonic acid groups in the polymer matrix decreases the aggregative state of the polymer, thereby expanding the polymer matrix and increasing polymer chain mobility, making the material more flexible [12]. For example, Widjojo et al., reported that the sPPSU membrane substrate which had the highest degree of sulfonation (5 mol.%) showed the weakest mechanical strength among all polymer weight ratios evaluated [10]. Similarly, Fang et al., showed that lower fraction (10% compared to 30%) and higher molecular weights (110 000 and 141 000 g/mol) of SPES used in the polymer blend are preferable for achieving higher membrane mechanical strength properties [8]. In addition to this, the membrane morphology, in particular the membrane cross-sectional structure plays a fundamental role in controlling the mechanical strength properties of a membrane. It has been shown that sulfonated polymer blend membranes that are free of macrovoids and finger-like

structures in their membrane sub-layer exhibit higher mechanical strength properties than their macrovoid-containing counterparts [7, 13, 14]. While the existence of macrovoids reduces flow resistance during filtration processes, their absence in membranes is highly favoured as they are weak mechanical points which may lead to membrane collapse, particularly when the membranes are operated under high pressures [15].

Recent years have witnessed an exponential growth on the use of nanostructured materials, such as graphene oxide (GO), carbon nanotubes (CNTs), titanium dioxide (TiO<sub>2</sub>) and several other nanomaterial hybrids, in membrane surface modification, enhancement of the membrane structure and subsequently improvement in the membrane performance behaviour. Several studies have used oxidised multi walled-walled carbon nanotubes (O-MWCNTs) in polymeric mixed-matrix membranes, particularly for UF and NF applications with the aim of improving or enhancing membrane physicochemical and performance properties such as mechanical strength, hydrophilicity, porosity, pure water permeability, antifouling and antibiofouling properties. Indeed, in all of these studies, the presence of O-MWCNTs has been shown to lead to significant enhancement in membrane structural and surface properties [16-25], in particular, due to the hydrophilic nature of the O-MWCNTs. Unfortunately, the addition of O-MWCNTs has been found to lead to the generation of a membrane morphology with finger-like structures and/or macrovoids that span the entire membrane cross-section, due to their hydrophilic nature [19-25]. As already highlighted, such morphology tends to compromise the mechanical strength of the membrane even through the O-MWCNTs incorporated may possess strong reinforcement properties. This means that upon subjection to external stresses, the load is predominantly transferred to the O-MWCNTs in the composite rather than being shared between the polymer matrix and the O-MWCNTs

Possible strategies that can be and have been adopted towards the elimination of macrovoids in the presence of CNTs include the addition of solvents such as isopropanol in the coagulation bath [10] or solvent evaporation prior to immersion into the coagulation bath. While the adoption of these strategies often lead to the elimination of macrovoids, they often result in severe reduction in pure water permeability due to the formation of a dense membrane structure. Therefore, a casting solution composition that allows for the formation of a macrovoid-free UF membrane, with high mechanical strength properties, without a compromise in high water permeabilities, in the presence of O-MWCNTs in the membrane matrix, is desirable. Furthermore, the optimal properties of the polymer-carbon nanotube interface required in order to obtain significant improvements in tensile strength have been established. Sulfonated polymer-blend UF membranes have been prepared numerous times, as PES/SPSf, PES/SPES or as sulfonated polymers alone such sPPSU and have been shown to display attractive features, including sponge-like sublayer structures which eliminate mechanically weak macrovoids in the membrane [7, 8]. Although sponge-like structures have been obtained for these sulfonated polymer blends, tensile strength values were usually low ([6], [7], [8]).

The aim of the current study is to improve the desirable characteristics for PES/SPSf membranes (high water flux, solute rejection, and antifouling properties) while also improving their tensile strength and antibacterial properties using O-MWCNTs as nanoadditives. To achieve this, PES/SPSf blend membranes were prepared with and without O-MWCNTs via a non-solvent induced gelation phase-separation method used previously [7]. The performance of the prepared membranes was investigated by pure water flux and rejection of bovine serum albumin (BSA). The contact angles of the membranes were measured to evaluate the surface hydrophilicity while the surface morphology and cross-sectional structures were studied using

diverse microscopic and spectroscopic techniques. A comprehensive investigation was also carried out to determine the antifouling and antibacterial properties of PES/SPSf modified membranes. Our results shed light on the development of UF membranes with fully sponge-like morphology and good permeability for the creation of a stable hydraulic environment and long-term mechanical stability without the use of a support fabric.

## **5.2. Experimental**

### **5.2.1. Materials**

Polyethersulfone (PES) (Veradel® 3000P, Mw = 62,000 g/mol) was supplied by Solvay Advanced Polymers (Belgium) and SPSf (25% degree of sulfonation) was purchased from Yanjin Technology Co. Ltd, Tianjin (China). Polyethylene glycol (PEG) (Mw = 20 000 g/mol) was purchased from Tianjin Kermel Chemical Reagent Co. Ltd. (China). All the materials were dried in an oven at 70 °C for 24 h before use. Dimethyl acetamide (DMAc) was purchased from BASF (Germany) and used without further purification, while bovine serum albumin (BSA) (Mw = 68 000 g/mol) was purchased from Beijing Probe Bioscience Co. Ltd (China). Reverse osmosis water was used as the non-solvent additive and coagulation bath. *Escherichia coli* (*E. coli*, ATCC8739, gram-negative) was supplied by Tianjin Medical University. Beef extract, peptone and agar powder were provided by Tianjin Sanjiang Chemical Technology Co, Ltd.

### **5.2.2. Preparation of O-MWCNTs**

Multi-walled carbon nanotubes (MWCNTs) were synthesised in-house, via nebulised spray pyrolysis method of toluene and ferrocene mixture, using a procedure described elsewhere

[26]. The synthesised MWCNTs collected were further oxidised by treatment with 35% HNO<sub>3</sub> under reflux, to obtain O-MWCNTs. See Appendix B Supplementary Material section for the detailed procedure on the synthesis and characterisation of O-MWCNTs.

### **5.2.3. Membrane preparation**

All the membranes were prepared by a non-solvent induced phase-separation method, following a previously reported procedure [7]. Briefly, weighed amounts of PES, SPSf, and PEG were dispersed in DMAc solvent. Water (H<sub>2</sub>O) was then added dropwise as a non-solvent additive in the casting solution at 8 wt.%. For casting solutions containing O-MWCNTs, weighed amounts of O-MWCNTs were first dispersed in DMAc solvent by ultrasonication prior to the addition of polymers. The compositions of the casting solutions are shown in Table 5.1. The mixture was then stirred for 8 h at 70±1 °C on a hot plate equipped with a stirrer. The solutions formed were allowed to settle and cool to room temperature followed by degassing under vacuum overnight. The solutions were then cast on a glass plate by using an automated membrane applicator (Elcometer 4340, England), with the casting knife set at a gap height of 200 µm, and immediately immersed in the water coagulation bath maintained at 25 °C. After a few minutes, membranes peeled off from the glass plate and were placed in a freshwater bath at room temperature (~25 °C) in order to wash off any residual solvent and additives. The prepared membranes were all kept in deionised water for 24 h prior to testing and analyses. Every membrane sheet was inspected under light to detect defects, such as thin spots and pinholes. It should be noted that an optimal PES/SPSf polymer weight ratio of 84:16 was maintained throughout the membrane systems, based on previous work [5], and a total polymer concentration of 22 wt.% was used. The concentration (wt.%) of PEG 20kDa used was based on the PEG20kDa content that gave optimal water flux and BSA rejection values in the

presence of O-MWCNTs (see Supplementary material section). Membranes were labelled as M0 to M5, to represent the increase in O-MWCNT loading in the dope solutions and those prepared in the absence of PEG20kDa were labelled as M0-1 and M5-1 (see Table 5.1).

**Table 5.1** Composition of casting solutions for PES/SPSf/O-MWCNTs membrane blends.

Membrane	PES (g)	SPSf (g)	DMAc (g)	H <sub>2</sub> O (g)	PEG (g)	O-MWCNTs (g)	O-MWCNTs* (wt. %)
M0	9.24	1.76	39	4	10	0	0
M1	9.24	1.76	39	4	10	0.0025	0.005
M2	9.24	1.76	39	4	10	0.005	0.01
M3	9.24	1.76	39	4	10	0.015	0.03
M4	9.24	1.76	39	4	10	0.025	0.05
M5	9.24	1.76	39	4	10	0.050	0.1
M0-1	9.24	1.76	39	4	0	0	0
M5-1	9.24	1.76	39	4	0	0.050	0.1

\*The concentration of O-MWCNTs is calculated via plus method

#### 5.2.4. Membrane characterisation

A digital rotational viscometer (NDJ-8S, Hengping Instrument Company, Shanghai China) was used to measure the viscosity of PES/SPSf and PES/SPSf/O-MWCNT casting solutions, at a shear rate of  $10 \text{ s}^{-1}$  at different temperatures.

Membrane surface and cross-sectional morphology was studied using field emission scanning electron microscope (FESEM, Hitachi S4800, Japan). For analyses of membrane cross-

sectional morphology, vacuum-dried membranes were freeze-fractured in liquid nitrogen followed by coating with gold. Atomic force microscopy (AFM: WiTec Alpha300) was used to analyse the surface topography and roughness of the prepared membranes. Small squares of the prepared membranes (approximately 1 cm<sup>2</sup>) were cut and glued into a glass substrate. The surface roughness parameters of the membranes are expressed in terms of the roughness average (Sa) and the root mean square (Sq) values.

Transmission electron microscope (TEM) analysis was performed on a FEI Tecnai™ (T12) Spirit transmission electron microscope operating at 120 kV. The O-MWCNT samples were dispersed in methanol by ultrasonication and loaded into a copper grid. For imaging of mixed-matrix membrane, the membrane samples having an approximate thickness of 100 μm were embedded with epoxy resin, thereafter ultrathin sections of approximately 100 nm were cut in a Leica ultra-microtome and mounted on a copper grid for analysis.

Attenuated total reflectance Fourier transform-infrared (ATR-FTIR) spectrometer (PerkinElmer, Germany) to used to assess functional groups present on the membrane surface. Water contact angle measurements were carried out using a contact angle goniometer (DSA30E Krüss GmbH, Hamburg, Germany) sessile drop method to evaluate membrane hydrophilicity. The contact angle values reported were recorded after the first 3 s of the adherence of the water droplet on the membrane surface. In total, six readings were taken from different spots on the membrane surface and the average value was reported

The mechanical properties of pristine PES/SPSf and O-MWCNT modified PES/SPSf composite membranes were analysed by measuring tensile stress using SAXSpace small and wide-angle X-ray scattering (SAXS/WAXS) system (Anton Paar GmbH, Graz, Austria) with

an integrated TS 600 tensile stage. The dried membrane samples (10 mm wide and 50 mm long) were mounted on the sample holder of the instrument and the measurements taken at a speed of 2 mm/min. The cross-sectional area (mm<sup>2</sup>) of each membrane sample was determined from membrane thickness and width prior to mounting on the sample stage. Three measurements were taken for each membrane type and the average value was reported.

The thickness of the membranes (wet membranes) was determined by using a digital micrometer. Membrane porosity was determined according to a dry-wet weight method. First, the membrane samples stored in deionised water were removed and lightly dabbed with a filter paper to remove excess water followed by weighing. The wet membrane was then dried under vacuum (at a temperature of 60 °C) for 24 h and weighed. Membrane porosity was calculated according to Eq. (5.1) as:

$$\varepsilon(\%) = \frac{W_w - W_d}{\rho_w A \delta} \times 100\% \quad (5.1)$$

where  $\varepsilon$  is the porosity of membrane,  $W_w$  is the weight (g) of THE wet membrane,  $W_d$  is the weight (g) of dry the membrane,  $\rho_w$  is the density of pure water (g/cm<sup>3</sup>),  $A$  is the membrane area (cm<sup>2</sup>) and  $\delta$  is the thickness of membrane (cm).

The mean pore radius was calculated using the Guerout–Elford–Ferry equation [27]:

$$r_m = \sqrt{\frac{(2.9 - 1.75\varepsilon - 0.75\varepsilon^2) Q}{\varepsilon \cdot a \cdot \Delta P}} \quad (5.2)$$

where  $r_m$  is the mean pore radius (nm),  $\varepsilon$  is the membrane porosity,  $\eta$  is the water viscosity (8.9×10<sup>-4</sup> Pa.s),  $L_m$  is the membrane thickness (m),  $Q$  is the volume of permeated water per

unit time ( $\text{m}^3/\text{s}$ ),  $a$  is the effective area of the membrane ( $\text{m}^2$ ), and  $\Delta P$  is the operating pressure (MPa).

### 5.2.5. Membrane performance tests

To evaluate the performance of membranes, pure water flux measurements were carried out using a self-made cross-flow filtration system with an effective membrane area of  $12.57 \text{ cm}^2$ . Firstly, membranes were compacted for 1 h at 0.15 MPa using deionised water to obtain a stable flux. The pressure was reduced to 0.1 MPa in order to collect permeate samples for pure water flux measurements. Pure flux ( $J_{wl}$ ) was calculated according to Eq. (5.3) as:

$$J_{wl} = \frac{V}{A \times t} \quad (5.3)$$

where  $V$  is the volume of permeate (L),  $A$  is the effective membrane area ( $\text{m}^2$ ) and  $t$  is the permeation time (h).

Membrane solute rejection was investigated using BSA as model solutes at 1g/L. The BSA concentration was measured by Ultraviolet-visible (UV-Vis) spectrophotometer (Tianmei UV1102, Shanghai, China) at 280 nm.

Membrane solute rejection  $R$  (%) was calculated using Eq. (5.4):

$$R(\%) = \left( 1 - \frac{C_p}{C_f} \right) \times 100 \quad (5.4)$$

where  $C_p$  and  $C_f$  are solute concentrations in the permeate and feed solution, respectively.

The antifouling propensity of membranes was investigated using BSA as a model protein foulant. The overall fouling process included three pure water filtration stages and two fouling stages. Each stage was operated for 60 min. After each fouling stage, the fouled membranes were thoroughly washed with deionised water, thereafter the water flux of “clean” membranes denoted as  $J_{w2}$  measured under the same operating conditions. The water flux recovery FRR (%) was calculated using Eq. (5.5):

$$\text{FRR}(\%) = \frac{J_{w2}}{J_{w1}} \times 100 \quad (5.5)$$

The antibacterial properties of M0 (without O-MWCNTs) and M5 membranes (with the highest O-MWCNT loading) were evaluated by a shake flask test using *E. coli* bacteria as the model Gram negative bacteria. The bacteria were cultivated in liquid lysogeny broth (LB) consisting of beef extract (5 g), peptone (10 g), and NaCl (10 g) at pH = ~7.4 and then placed in an incubator-shaker overnight at 37 °C. Thereafter, 1 mL of the *E. coli* overnight culture was used to inoculate a flask containing 50 mL of freshly prepared LB. The mixture was then cultured at 37 °C in an incubator shaker for another 5 h to obtain a bacterial suspension in the exponential growth phase. In order to further evaluate the antibacterial performance against *E. coli*, the membrane (5 cm<sup>2</sup>) coupons were immersed into the bacterial suspension (10 mL, 1 × 10<sup>6</sup> CFU/mL) in sealed bottles and the mixtures in the bottles were shaken in an incubator shaker at 120 rpm and 37 °C for 6 h. After that, the number of viable *E. coli* cells was estimated by counting the colony forming units (CFUs) on the agar plates. The bactericidal activity was expressed as the ratio of colonies on the control plate to the number of colonies counted on the sample plate (bacteria killing ratio or sterilisation ratio) and was calculated by Eq. (5.6):

$$\text{Bacterial killing ratio (\%)} = \frac{N_B - N_S}{N_B} \times 100 \quad (5.6)$$

where  $N_B$  and  $N_S$  are the number of colonies on the control plate and the sample plate, respectively. Each membrane sample was measured three times.

### **5.3. Results and discussion**

#### **5.3.1. Dispersion of O-MWCNTs in PES/SPSf matrix**

The solubility parameters of common solvents used for the dispersion of MWCNTs and some membrane materials are listed in Table 5.2. The MWCNTs have good dispersion in solvents with a high dispersive component ( $\delta_d$ ), but precipitate in solvents with high polar component ( $\delta_p$ ) or high hydrogen-bonding component ( $\delta_h$ ) (as shown in Table 5.2) due to their hydrophobic nature [26]. Therefore, based on the above explanation, the polar solvent dimethylacetamide (DMAc) was selected as the solvent for dispersion of O-MWCNTs in this study. Due to the small difference between the solubility parameters between of DMAc and PES, the DMAc is also a good solvent for dissolving PES/SPSf blend mixtures. The smaller the difference between solubility parameters of solvent and polymer, the stronger the polymer-solvent interaction [28].

**Table 5.2** Solubility parameters of different solvents and PES [19, 28].

Solvents	Solubility parameters (MPa <sup>0.5</sup> )			
	$\delta_d$	$\delta_p$	$\delta_h$	$\delta_t$
DMAc	16.8	11.5	10.2	22.7
NMP	18	12.3	7.2	22.9
DMSO	18.4	16.4	10.2	26.6
DMF	17.4	13.7	11.3	24.8
PES	17.6	10.4	7.8	21.9

The dispersion of O-MWCNTs in the casting solution was evaluated by determining the stability of the casting solution immediately after preparation as well as after 4 weeks of preparation. It can be seen in Fig. 5.1(a) and 5.1(b), that the casting solutions containing O-MWCNTs remained stable and homogeneously mixed in solution even after 4 week of preparation and storage at room temperature. This indicates good dispersion and interfacial bonding between O-MWCNTs and the polymer solution. Moreover, visual observation of the mixed-matrix PES/SPSf membranes containing different loadings of O-MWCNTs clearly showed that the added O-MWCNTs are homogeneously distributed on the membrane surface and that the colour intensity increases with content added (Fig.5.1c). This suggests that the incorporated O-MWCNTs incorporated migrate spontaneously to the membrane surface thereby contributing towards the improvement of membrane surface properties [29]. A similar behaviour has also been reported by other researchers when functionalised MWCNTs were incorporated into the PES membrane matrix [19, 22].

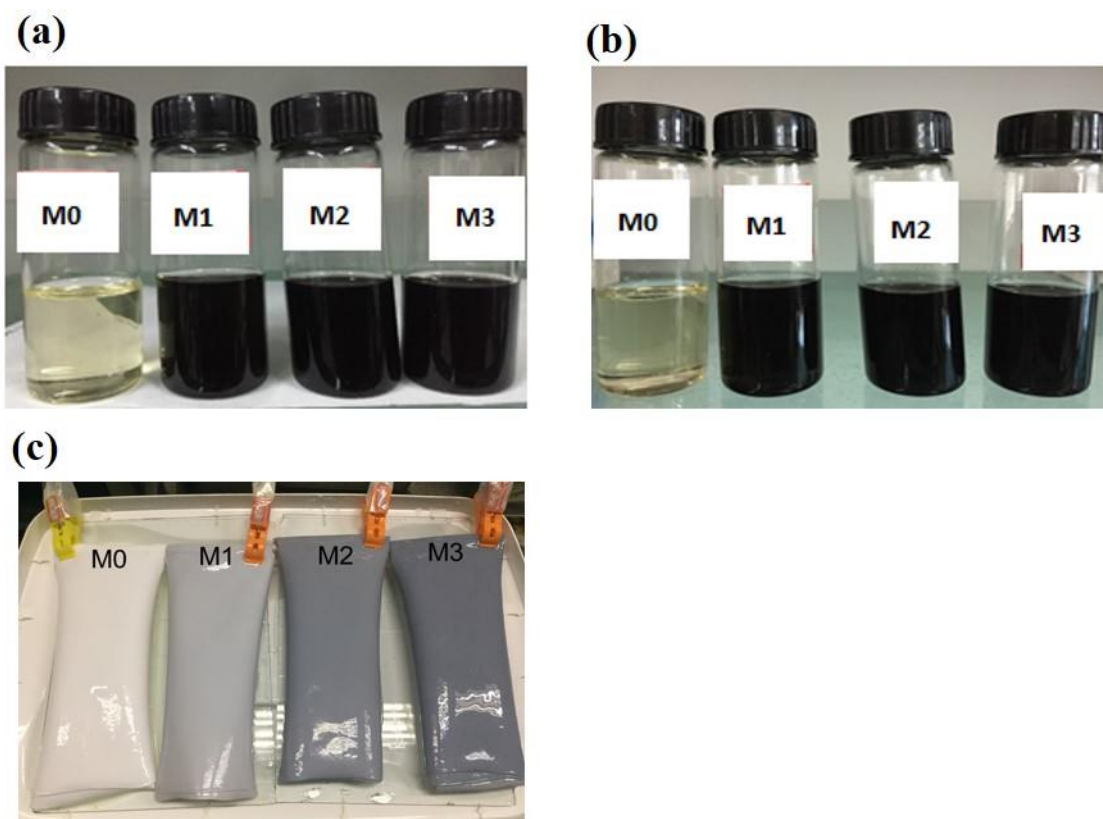


**Figure 5.1** Digital photographs of PES/SPSf/O-MWCNT casting solutions (a) taken immediately after preparation, (b) taken after 4 weeks of preparation and (c) photograph showing the physical appearance of PES/SPSf/O-MWCNT membranes.

To further confirm the presence and distribution of O-MWCNTs in the PES/SPSf membrane matrix, the membrane containing the highest O-MWCNT loading (M5) was observed by TEM imaging. For comparison, a TEM image of O-MWCNTs was acquired (Fig.5.2). In Fig.5.2(b) it can be seen that the incorporated O-MWCNTs are present in the membrane matrix, at low contents vis-à-vis the polymer material. This is expected since 1.0 wt.% of O-MWCNTs were added compared to 22 wt.% of PES/SPSf polymer. Moreover, they are irregularly distributed in the membrane matrix and exist as individual tubes, with fewer segments of entanglement or agglomeration. The good distribution of O-MWCNTs in the PES/SPSf matrix will facilitate

improvements in membrane structural properties, in particular, the enhancement of membranes mechanical strength, as envisaged in this study.

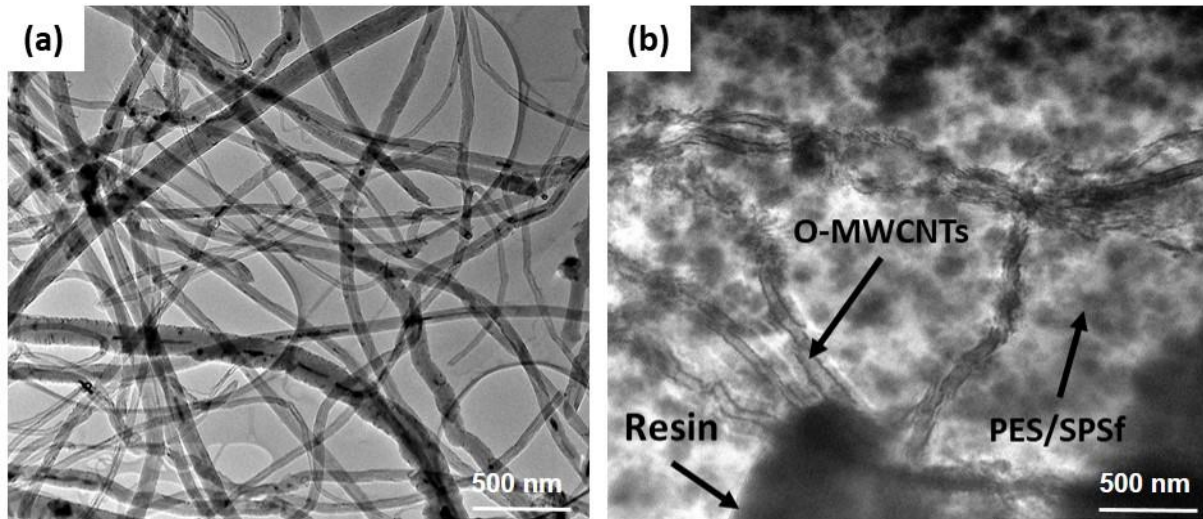


**Figure 5.2** TEM images of (a) O-MWCNTs and (b) microtomed specimen of PES/SPSf/O-MWCNT membrane (M5).

### 5.3.2. Viscosity measurements

The PES/SPSf casting solutions containing different loadings of O-MWCNTs were prepared via a non-solvent induced phase-separation method and their viscosities were determined at different temperatures (45 to 60 °C) at a shear rate of  $0.1 \text{ s}^{-1}$ . Viscosity is an important parameter for casting solutions since it affects the phase separation kinetics and therefore the final membrane morphology. It can be seen in Fig.5.3 that an increase in O-MWCNT content from 0. wt.% for M0 to 0.1 wt. % for M5 led to an increase in the viscosity of the casting solution. For example at 45 °C, the viscosity of M0 was 837 mPa s, 1045 mPa s for M1, 1195 mPa s for M2, 1320 mPa s for M3, 1330 mPa. s for M4 and 1350 mPa s for M5. This increase in viscosity can be linked to the formation of multiple hydrogen bonds i.e. first between the -COOH groups of O-MWCNTs, the H<sub>2</sub>O molecules and the sulfonic acid (-SO<sub>3</sub>H) groups as

substituents of the PES polymer chains and secondary hydrogen bonding interactions are formed between the sulfonic (O=S=O) groups of the PES chains, H<sub>2</sub>O and the -COOH groups of O-MWCNTs (Fig. 5.4). The formation of these hydrogen bonds restricts the mobility of polymer chains hence the increase in the viscosity of casting solution viscosity. Moreover, as higher amounts of O-MWCNTs leads to an increase in the number of hydrogen bonds forming between the components of the casting solution also increases. Generally, an increase in the viscosity of the casting solution leads to a decline in the diffusion rate between solvent and non-solvent during the phase separation process. This further leads to a delayed demixing of solvent and non-solvent and subsequently the suppression of macrovoids in the membrane sublayer, formation of a denser structure and enhanced mechanical strength properties [30, 31]. The influence of viscosity on membrane morphology is discussed in Section 3.4. Additionally, it was found that all casting solutions display a similar trend of a decline in viscosity with increments in temperature (from 45 to 60 °C). For example, for membrane M5, the viscosity values were found to decline from 1357 > 1127 > 1002 > 935 mPa s at 45 °C, 50 °C, 55 °C and 60 °C respectively. The decline in viscosity can be attributed to the increase in kinetic energy of molecules at high temperatures, which leads to an increase in polymer chain mobility.

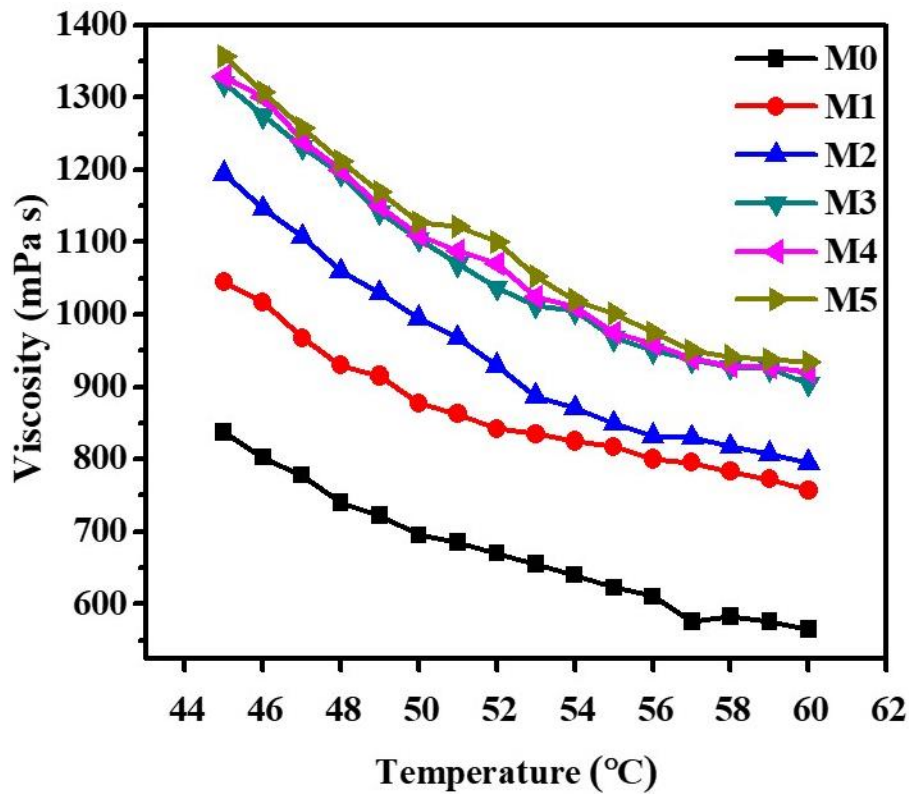


**Figure 5.3** Effect of temperature on viscosity of PES/SPSf and PES/SPSf/O-MWCNT casting solutions.

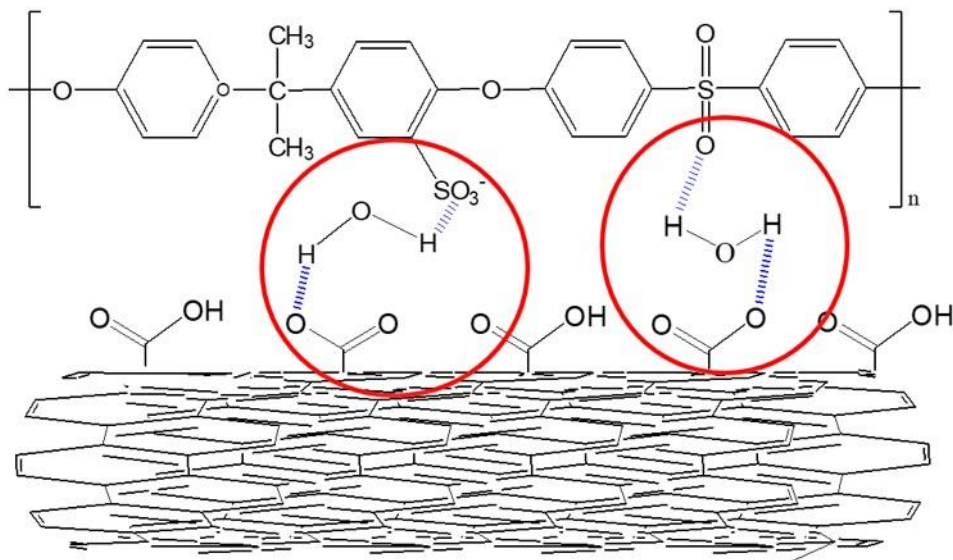


**Figure 5.4** Hydrogen bonding interaction between SPSf, H<sub>2</sub>O and O-MWCNTs.

### 5.3.3. ATR- FTIR analyses of PES/SPSf and PES/SPSf/O-MWCNT membranes

In order to study the functional groups present on the membrane surfaces, ATR-FTIR analysis was carried out. The ATR-FTIR spectra of all flat-sheet membranes are shown in Fig. 5.5. All spectra show distinctive peaks at  $\sim 3435\text{ cm}^{-1}$  corresponding to  $-\text{OH}$  stretching vibrations,  $2879\text{ cm}^{-1}$  for  $-\text{C}-\text{H}$  stretch,  $\sim 1643\text{ cm}^{-1}$  for the  $-\text{C}=\text{O}$  of the O-MWCNTs and in the same range  $\sim 1235 - 1250\text{ cm}^{-1}$ ,  $1000 - 1072\text{ cm}^{-1}$  and  $1119 - 1150\text{ cm}^{-1}$  corresponding to the asymmetric and symmetric stretching of  $-\text{SO}_3\text{H}$  and  $\text{O}=\text{S}=\text{O}$  groups of SPSf polymer [8, 32, 33]. Fig. 5.5 shows that O-MWCNTs consist of a broad peak around  $3500\text{ cm}^{-1}$  due to  $-\text{OH}$  stretching vibrations, and a peak at  $1600\text{ cm}^{-1}$  which can be attributed to the  $-\text{C}=\text{O}$  stretching vibration of the carboxylic acid group. These identified chemical functional groups, enable further interaction of O-MWCNTs with the polymer matrix. Moreover, all the FTIR spectra of the PES/SPSf membranes containing O-MWCNTs (M1 to M5), exhibit broad  $-\text{OH}$  functional group peak in the same region ( $\sim 3500\text{ cm}^{-1}$ ) which is absent in the spectrum of pristine PES/SPSf membrane (Fig. 5.5). This confirms successful incorporation of O-MWCNTs and their interaction with the  $-\text{SO}_3$  groups of the PES/SPSf membrane matrix. Moreover, the intensity of the  $-\text{OH}$  absorption band for the PES/SPSf/O-MWCNT membranes increases with O-MWCNT content, suggesting that hydrogen bonding has taken place between the  $-\text{SO}_3\text{H}$  of the polymer,  $\text{H}_2\text{O}$  and the O-MWCNTs. The ATR-FTIR spectra provided evidence that the increase in the viscosity of the casting solution with increments in O-MWCNT content is due to the formation of hydrogen bonds within the polymer matrix

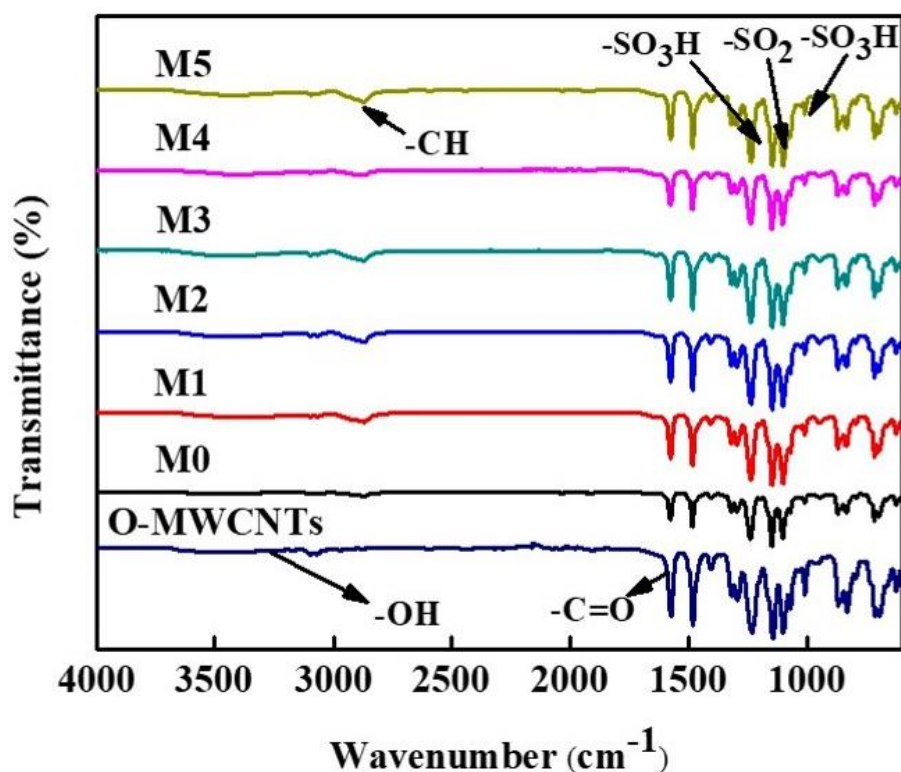


**Figure 5.5** ATR-FTIR spectra of PES/SPSf and PES/SPSf/O-MWCNT membranes.

#### 5.3.4. Morphological studies

The SEM surface and cross-sectional images of membranes M0 – M5 prepared by varying the O-MWCNT loading are shown in Fig.5.6. All the membranes exhibited similar top surface SEM images with no visible pores even at high magnifications of 50,000. Moreover, an increase in O-MWCNT loading did not change the cross-sectional morphology of the membrane, *i.e.* the sponge-like morphology was maintained even at higher O-MWCNT loadings. The hydrogen bonding interaction between O-MWCNTs, high molecular-weight PEG 20kDa, H<sub>2</sub>O molecules and the polymer matrix was found to be much stronger and dominant over any other individual influence imparted by O-MWCNTs alone in the membrane structure. Typically, because of their hydrophilic nature, O-MWCNTs enhance the phase-separation process by increasing the affinity of the polymer solution for the non-solvent (water)

during the coagulation process leading to the creation of a membrane structure with finger-like structures in the sub-layer [23, 27, 34, 35]. This claim was further substantiated by preparing two casting solutions; labelled M0-1 and M5-1 in Table 5.1. We found that in the absence of O-MWCNTs, the membrane cross-section structure of M0-1 is fully sponge-like, whereas the inclusion of O-MWCNTs transforms the membrane morphology of M5-1 to fully finger-like (Fig. 5.7). If the rate of non-solvent (water) influx in the polymer solution during the solvent-non-solvent exchange process exceeds that of solvent outflow, the resultant membrane structure is likely to consist of finger-like structures, the opposite is true for sponge-like morphology [36, 37].

Careful examination of the cross-sectional SEM images at higher magnifications (Fig. 5.6), shows that while all the membranes consist of an interconnected network pore structure, the interstitial spaces between the porous internal structures become less open as the content of O-MWCNTs is increased and the structure becomes more compact. Similar behaviour based on the ability of PEG to increase pore interconnectivity has also been reported by other studies [13, 38]. Firstly, the interstitial spaces between the interconnected pores are more open for M1 in comparison to those of M0, following which they become less open and more compact for M2, M3 and M4 and then open again for M5. This is because the added O-MWCNTs are hydrophilic in nature, and initially enhance the phase-separation process. However, their influence on the overall phase separation process is eventually surpassed by the presence of high molecular-weight PEG and water as non-solvent additives. This results in the final membrane morphology being completely sponge-like with an open cell internal structure. The cellular structures were found to become less open with further increments in O-MWCNTs due to partial aggregation of O-MWCNTs at higher loadings. The observed patterns in membrane

internal morphology play a significant role in membrane permeability and selectivity and mechanical strength properties.

In our case, the addition of both high molecular-weight PEG 20kDa and H<sub>2</sub>O in the presence of O-MWCNTs assisted in the formation of a membrane structure with no finger-like structures and macrovoids. The PEG 20kDa improves pore interconnectivity thus preventing the formation of macrovoids; whereas H<sub>2</sub>O increases casting solution viscosity and brings dope solution viscosity closer to the binodal composition where the suppression of macrovoids is favoured [38]. Fig. 5.6 shows that the addition of high molecular-weight PEG 20kDa assisted in the formation of porous, open cellular internal structures with interconnected pores. Boom et al. [39], earlier used a model for mass transfer to investigate the role of high molecular-weight additives in membrane formation, particularly on the mechanistic pathway that is responsible for characteristic structures for PVP-containing membranes. The findings of that study showed that for quaternary systems (consisting of a polymer, solvent, additives and non-solvent), the spinodal decomposition mechanism is followed which can be an explanation for the high interconnectivity of the pores in membranes containing high molecular weight PVP. In their study, the interconnected pores were in fact a continuous polymer (PES) lean phase intertwined by a continuous polymer (PES) rich phase which forms the membrane matrix [39, 40]. In addition to increasing casting solution viscosity and improving pore interconnectivity thereby eliminating macrovoid formation, PEG of high molecular weight such as PEG20kDa, becomes trapped in the membrane matrix after the solvent and non-solvent exchange processes because of its lower mobility in the coagulation bath. Consequently, the entrapped residual PEG molecules in the membrane matrix contribute towards the improvements of membrane hydrophilicity. It is our thought, therefore, that the state of the polymer solution prior to immersion into the coagulation bath is critical in determining the ultimate membrane

morphology. Therefore, it is vital to determine the viscosity of the casting solutions prior to casting the membrane and immersion into the coagulation bath.

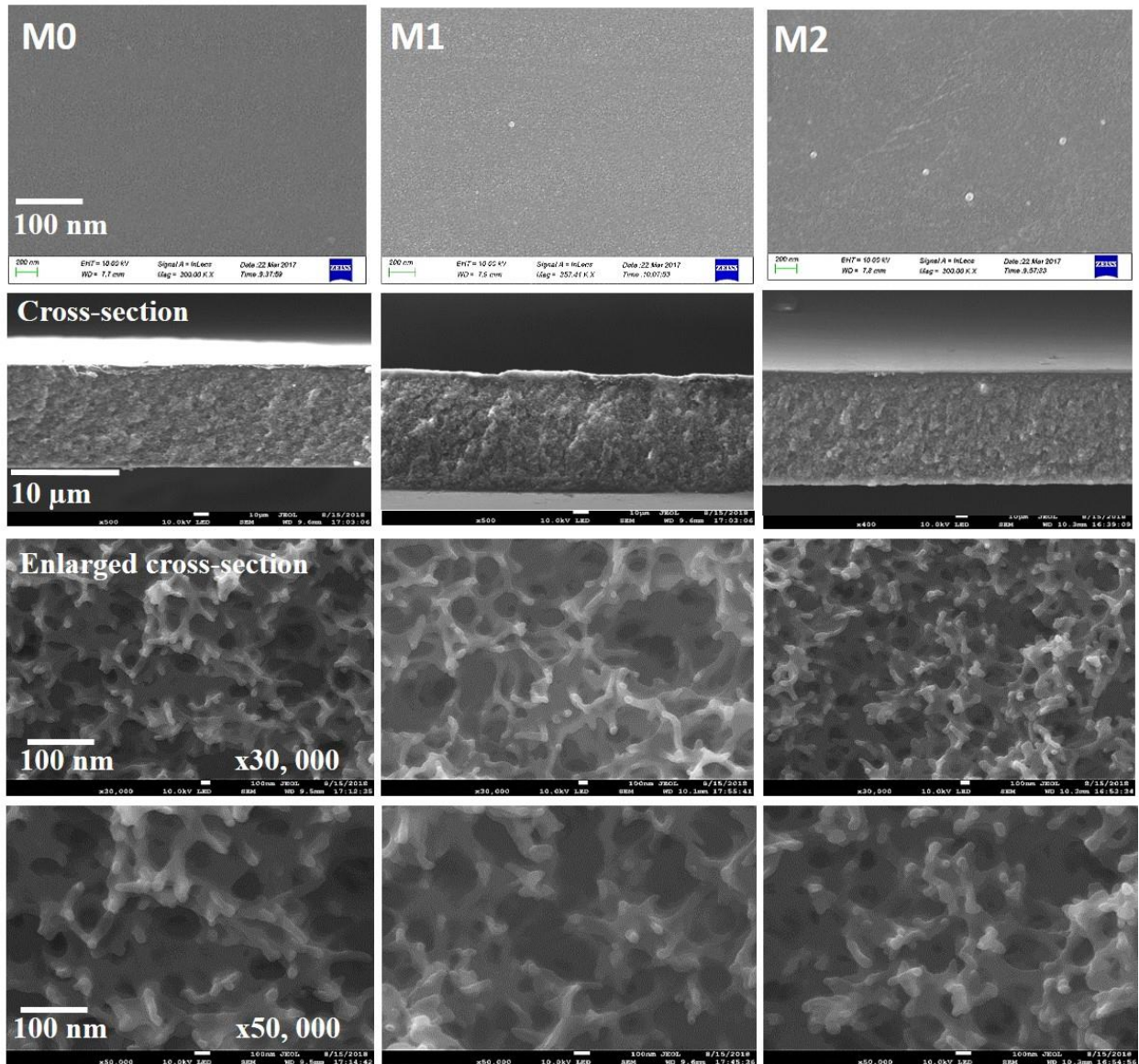


**Figure 5.6** SEM surface and cross-sectional images of PES/SPSf/O-MWCNT membranes: M0, M1, M2, M3, M4 and M5.

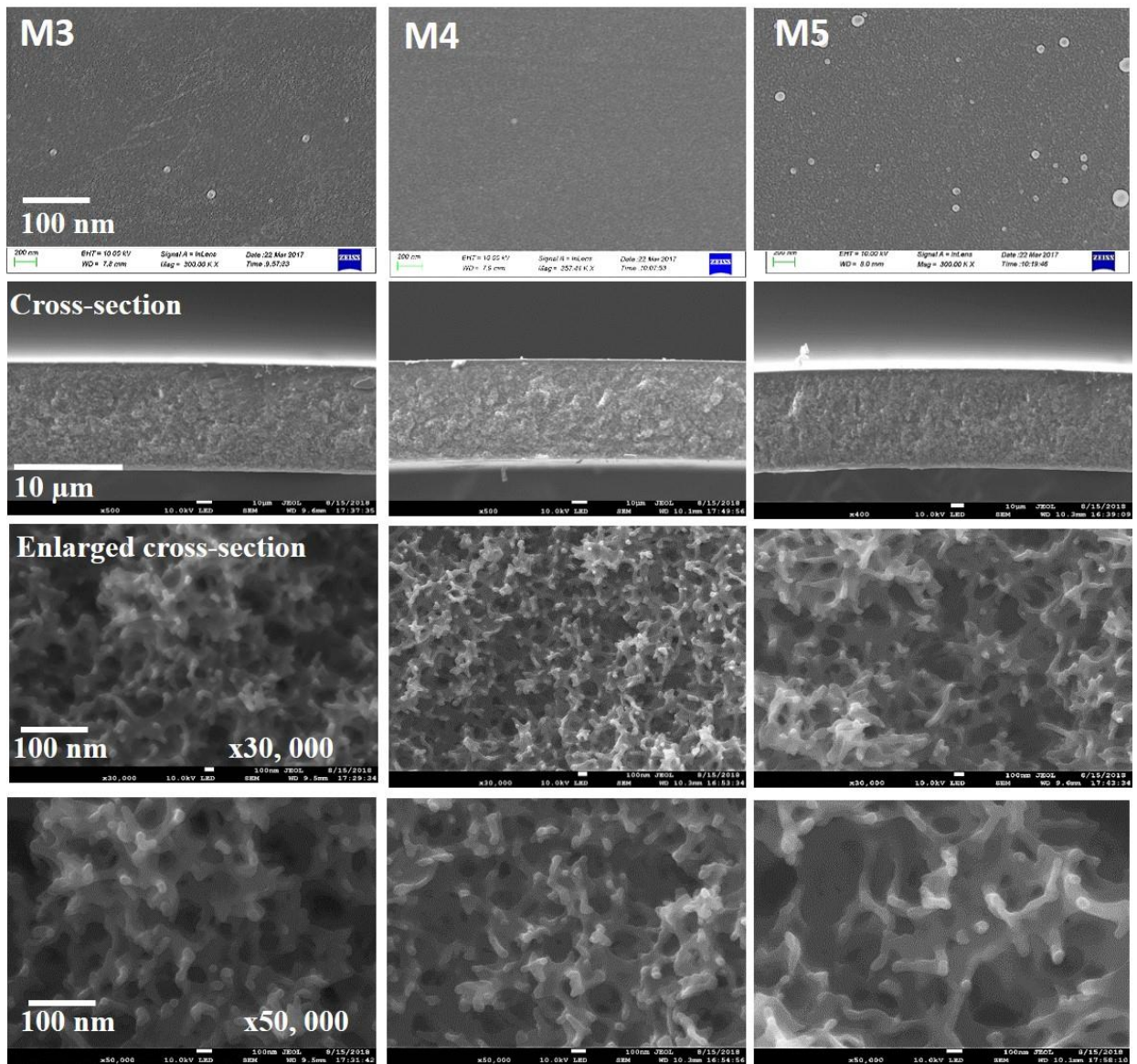
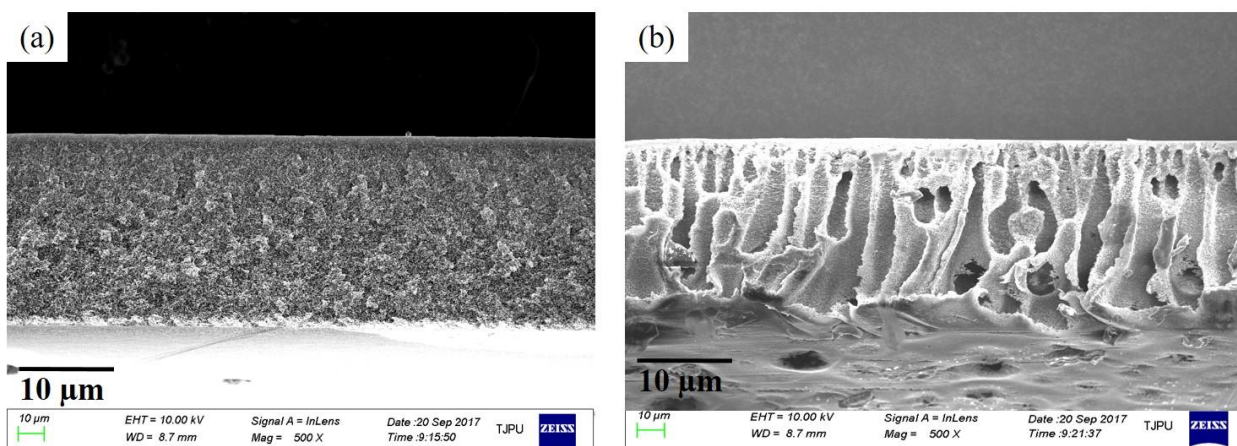
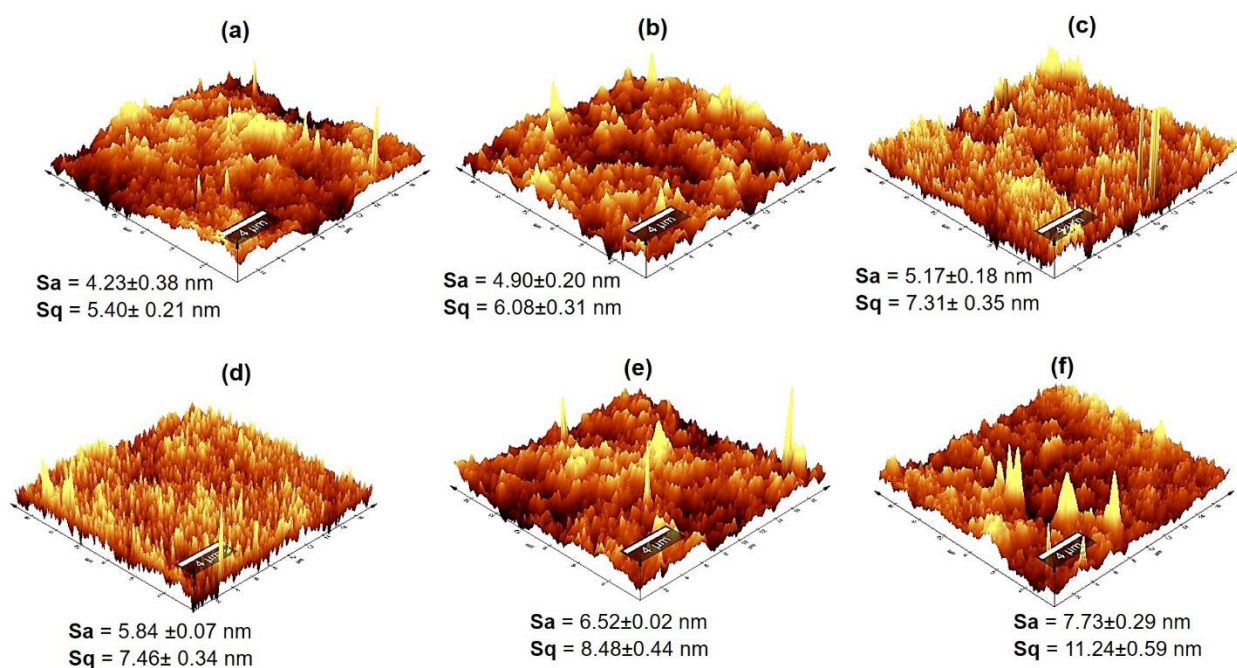


Figure 5.6 continued



**Figure 5.7** SEM cross-sectional images of PES/SPSf/O-MWCNT membranes (a) M0-1 and (b) M5-1.

Membrane surface topography and roughness were analysed using AFM and the results are displayed in Fig.5.8. It can be seen that the surface roughness values, in particular the root mean square roughness value ( $S_q = 5.40 \text{ nm}$ ) of the pristine PES/SPSf membranes (M0) are slightly lower compared to those of membranes containing O-MWCNTs (M1 - M5). This can be attributed to the presence of hydrophilic O-MWCNTs which migrate spontaneously to the membrane interface thereby generating rougher membrane surfaces. It can also be observed that amongst the PES/SPSf membranes containing O-MWCNTs, surface roughness values increase with an increase in O-MWCNT content. At higher loadings, O-MWCNTs begin to agglomerate, thereby increasing the membrane hydrophilicity. An increase in membrane roughness signals an increase in the effective membrane area caused by the nodular shapes having ridges and valleys, which is beneficial in the improvement of fluxes [41].



**Figure 5.8** AFM topographical images and surface roughness values of PES/SPSf/O-MWCNT membranes (a) M0, (b) M1, (c) M2, (d) M3, (e) M4, and (f) M5.

### 5.3.5. Contact angle and tensile strength measurements

Contact angle measurements were carried out in order to determine the changes in PES/SPSf membranes surface hydrophilicity upon inclusion of O-MWCNTs. Fig.5.9 shows that upon the inclusion of O-MWCNTs, the contact angle values decreased from  $67.2^\circ$  for pristine PES/SPSf membrane (M0) to  $47.6^\circ$  for M5 containing the highest loading of O-MWCNTs, suggesting an improvement in membrane hydrophilicity. Our findings are similar to those reported by other researchers [34, 42]. However, subtle differences of between  $2^\circ \geq 8^\circ$  in contact angles were observed for membranes with different O-MWCNT content, implying that a small amount of O-MWCNTs is sufficient to increase the membrane's hydrophilicity. The improved hydrophilicity with the addition of O-MWCNTs endows the membranes with enhanced fouling resistance. Typically, the contact angle value of a membrane of higher surface roughness will be larger compared to that of a membrane with lower surface roughness, even though both

membranes are of similar hydrophilic nature [3]. In our case, the results displayed an opposite behaviour to this observation, in that although the roughness values obtained for O-MWCNT-incorporated membranes were slightly higher than those of pristine membrane (as discussed in Section 5.3.4.), the influence of surface roughness on contact angle values obtained was significantly low. This finding can be ascribed to the fact that the magnitude by which the surface roughness increased after the inclusion of O-MWCNTs, was at the lower end of the nanometre range (from 5.8 nm for M0 to 11.2 nm for M5) and could not have brought about any significant changes in contact angle values measured

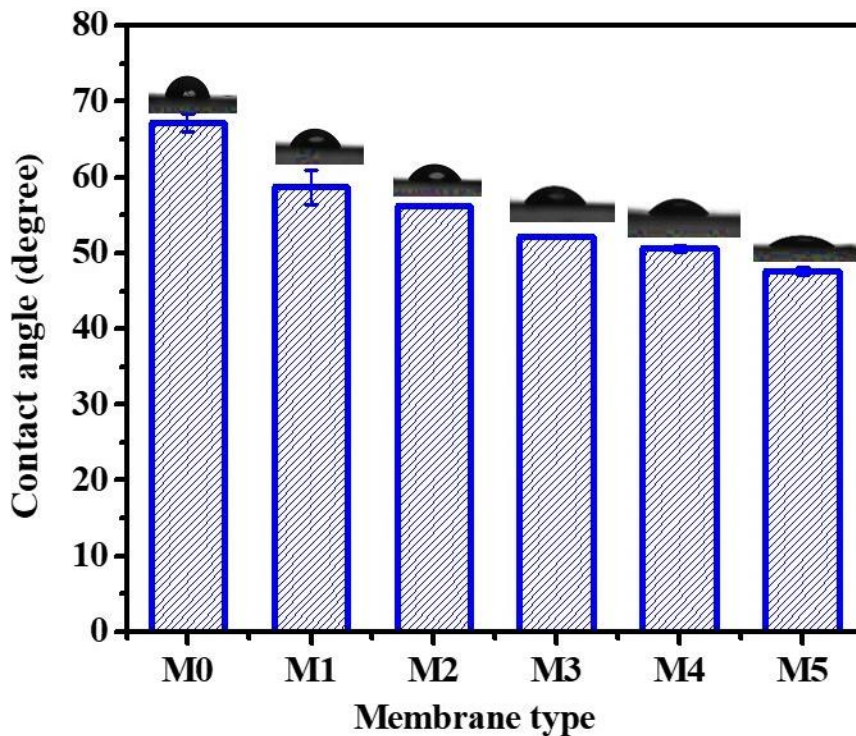


**Figure 5.9** Water contact angle values of the pristine PES/SPSf membrane and PES/SPSf/O-MWCNT blend membranes.

The most important requirement from MWCNTs as reinforcing fillers in composites is that when external forces are applied to the composite as a whole, those stresses are efficiently

transferred to the nanotubes, allowing them to take a disproportionate share of the load [43]. Mechanical strength properties of our PES/SPSf composite membranes have been expressed in terms of tensile strength and elongation at break. It can be observed from Fig. 5.10 that the tensile strength of the membranes increased after the addition of O-MWCNTs and with an increase in O-MWCNT content. Membrane M0 was found to have a tensile strength of 2.78 MPa at elongation at break of 7.9% which then showed a gradual increase with increasing O-MWCNT content for membranes M1- M4, until 4.02 MPa (at elongation at break of 12.2%) was attained for membrane M5 containing the highest O-MWCNT loading (Fig. 5.10). This indicates that the interfacial interactions via hydrogen bonding and electrostatic interactions between the O-MWCNTs and the polymer matrices are well established. Moreover, homogenous distribution of O-MWCNTs in the PES/SPSf mixed-matrix membrane as displayed from TEM analysis in Fig. 5.2, assisted in the improvements in tensile strength. The fabricated PES/SPSf/O-MWCNT membranes in this study displayed better mechanical strength (2.78 MPa for M0 – 4.02 MPa for M5) compared to those in previous studies on sulfonated polymer blends (SPSf, SPES, SPPSU) ultrafiltration membrane supports reported in the literature [7, 8, 11, 44]. It should also be noted that the tensile strength of membrane M5-1 is lower than that of membranes M0-1, M1-M5 and even much lower compared to that of pristine M0. This is attributed to the difference in membrane structure, i.e., macrovoids and finger-like structures in the membrane cross-sectional structure of M5-1 act as mechanically weak points when external force are applied to the membrane. This then reduces the overall mechanical strength of the membrane. It is quite clear that the membrane morphology plays a crucial role in governing the mechanical reinforcement process.

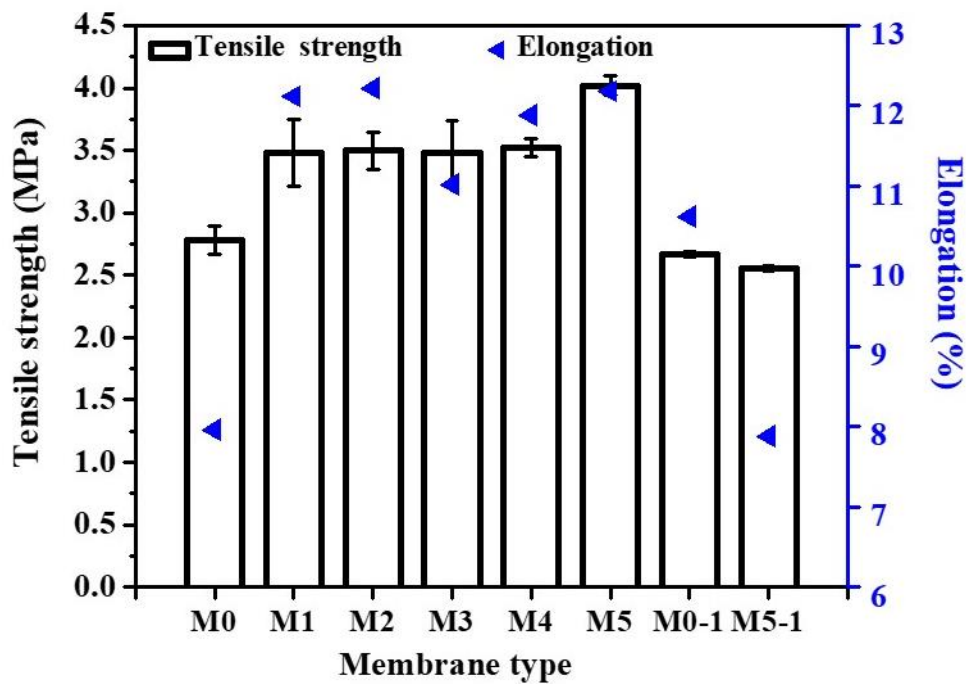


**Figure 5.10** Tensile strength and elongation at break of the pristine PES/SPSf membrane and PES/SPSf/O-MWCNT blend membranes.

### 5.3.6. Performance tests: Pure water flux and BSA rejection

The fabricated PES/SPSf ultrafiltration membranes containing different O-MWCNT loadings were evaluated for their performance in terms of pure water flux and BSA rejection and the results are summarised in Table 5.3. The data given in Table 5.3 indicate that pure water flux initially increased with the inclusion of O-MWCNTs followed by a decrease with further increments in O-MWCNT content. For instance, pure water flux of M0 without O-MWCNTs was found to be 598 L/m<sup>2</sup> h, and then increased to 713 L/m<sup>2</sup> h for M1 (19% increase in flux) followed by a decline to 590 L/m<sup>2</sup> h, 560 L/m<sup>2</sup> h, 553 L/m<sup>2</sup> h and 578 L/m<sup>2</sup> h for M2, M3, M4 and M5 respectively. The initial increase in pure water flux is attributed to the improvements in membrane hydrophilicity (as shown in Fig.5.9), decrease in membrane thickness and increase in bulk porosity of M1 (Table 5.3). Increments in membrane hydrophilicity enhance water permeation through the membrane. For the PES/SPSf blend membranes containing

different O-MWCNT contents, the pure water flux was found to decrease with an increase of O-MWCNT content ( $M4 > M3 > M2$ ), due to the decreased mean pore radius of the membranes (Table 5.3) caused by agglomeration of O-MWCNTs at higher loadings. Furthermore, considering the multiple hydrogen bonds forming between SPSf, H<sub>2</sub>O and O-MWCNTs, it can be expected that the presence of O-MWCNTs within the polymer matrix will lead to a slight reduction in membrane pore sizes. Although membrane hydrophilicity of all membranes containing O-MWCNTs was found to be higher than that of M0, ultimately the membranes with larger pore sizes will have higher fluxes, i.e., the influence of pore size supersedes that of hydrophilicity. It is important to mention that although pure water fluxes in this study were found to decrease with increments in O-MWCNT content, the water fluxes obtained for M2 to M4 membranes are still reasonably high for ultrafiltration membranes with sponge-like morphology [45, 46]. Previous studies have demonstrated that the sponge-like morphology can be produced in the presence of O-MWCNTs through the use of (i) high polymer concentrations (ii) addition of solvents with low miscibility with water (such as isopropanol) in the coagulation bath [47] or (iii) via solvent evaporation prior to immersion in the water coagulation bath. However, these strategies lead to the formation of membranes with very low water fluxes or permeabilities compared to those achieved in this study, as a result of the formation of a very dense membrane top layer with tiny surface pores.

When the O-MWCNT content of the blend membranes was 0.005 wt.% (M1), the hydrophilic O-MWCNTs enhanced the phase-separation, resulting in the formation of bigger pore sizes and higher pure water flux. However, when the content of O-MWCNTs was above 0.01 wt.%, the viscosity of the casting solution increased, thereby delaying the phase separation and resulting in a smaller pore sizes and lower pure water fluxes. The increase in pore sizes for M5 with 0.1 wt.% O-MWCNTs was presumably due to the steric hindrance and electrostatic

interactions between the O-MWCNTs or between the O-MWCNTs and the polymer matrix causing the O-MWCNTs to irregularly collocate in the membrane. This irregular positioning favoured an increase the pore sizes of the membrane. Celik et al., also reported similar phenomenon when the O-MWCNT content in the PES matrix was increased from 0.5 to 4 wt.% [21].

Conversely, the rejection of BSA initially decreased from 96.4% for M0 to 95.2% for M1 and then increased to 97.3%, 99.9% and 100% for M2, M3 and M4 with an increase in O-MWCNT content, as a result of the reduction in mean pore radius of membranes. Based on the results presented in Table 5.3, membrane M3 depicts favourable membrane performance characteristics for an ultrafiltration membrane, *i.e.*, (i) small pore sizes, (ii) high porosity, (iii) moderately high water flux and (iv) high solute rejection. An ultrafiltration membrane with smaller pore sizes but higher porosity (one with a large number of pores that are smaller in size) is more desirable since such a membrane is capable of avoiding to a large extent, the permeability-selectivity trade-off of membranes. The small pore sizes favours the rejection of solutes while the large number of pores is beneficial for the improvement of flux [48].

Current membranes without O-MWCNTs have been shown to reject BSA molecules to large extent, ranging between 70% and 99% (Table 5.4) [5,7,49-52]. In comparison, the PES/SPSf/O-MWCNT membranes fabricated in this study were able to reject > 99.9% of BSA molecules using membrane M4 containing 0.05 wt.% O-MWCNTs while maintaining reasonably high water fluxes. In addition to this, after two stages of fouling with BSA and cleaning with deionised water, an initial water flux of up to 93% was recovered.

**Table 5.3** Effect of SPSf, H<sub>2</sub>O and O-MWCNT interaction on membrane porosity, mean pore radius and thickness.

<b>Membrane</b>	<b>Bulk porosity (%)</b>	<b>Mean pore radius (nm)</b>	<b>Thickness (μm)</b>	<b>Pure water flux (L/m<sup>2</sup> h)</b>	<b>BSA rejection (%)</b>
M0	85±1.57	50.7±0.16	129±3.06	598±1.16	96.4±0.22
M1	86±1.16	51.1±3.92	116±2.16	713±2.90	95.2±0.65
M2	87±2.02	45.4±1.95	102±2.98	590±1.90	97.3±0.50
M3	88±1.30	41.3±2.05	104±2.35	560±1.300	99.9±1.99
M4	88±0.48	40.9±1.33	108±2.52	553±4.30	100±0.45
M5	84±0.12	46.9±0.63	116±2.16	578±1.68	98.5±0.24

**Table 5.4** BSA rejection and water permeability values for various UF membranes.

<b>Membrane composition</b>	<b>Membrane type</b>	<b>Water permeability</b>	<b>BSA rejection (%)</b>	<b>Ref</b>
PES/SPSf	Flat-sheet	1467 L/m <sup>2</sup> .h.bar @ 1 bar	92.0, 91.4	[5]
PES/SPSf/H <sub>2</sub> O	Flat-sheet	858 L/m <sup>2</sup> .h.bar @ 1 bar	90.5, 98.7	[7]
PES modified with PVP, Pluronic 31R1, and star-like Tetronic 904	Flat-sheet	PES= 2.2 L/m <sup>2</sup> .h.bar @ 1 bar	90	[49]
			66	
		PES/PVP= 40 L/m <sup>2</sup> .h.bar @ 1 bar	63	
		PES-P31R1= 116 L/m <sup>2</sup> .h.bar @ 1 bar	70	
	PES-T904= 64 L/m <sup>2</sup> .h.bar @ 1 bar			
PES/PVDF	Hollow fibre	30 L/m <sup>2</sup> .h.bar @ 3 bar	89.2	[50]
PVDF-g-PNIPAAm	Hollow fibre	13100 L/m <sup>2</sup> .h.bar	84	[51]
PES/PEI	Hollow fibre	130.1 L/m <sup>2</sup> .h.bar	99.3	[52]
PES/SPSf/O-MWCNT	Flat-sheet	560 L/m <sup>2</sup> .h.bar	100	This work

### 5.3.7. Antifouling and antibacterial tests

Fig.5.11 shows time-dependent flux during fouling measurements of fabricated PES/SPSf-O-MWCNT ultrafiltration membranes using BSA as a model protein foulant (1 g/L solution of BSA) at a pressure of 0.1 MPa. The antifouling performance tests included three pure water filtration stages (stages I, III and V) and two fouling stages (stages II and IV) with BSA solutions. After each fouling stage, the membranes were cleaned with deionised water followed by measurement of pure water flux. It can be seen in Fig.5.11 that the initial pure water flux of M0 declined from 597 L/m<sup>2</sup> h to 456 L/m<sup>2</sup> h to 449 L/m<sup>2</sup> h after stage III and IV, whereas that of M5 with the highest O-MWCNT loading only declined from 578 L/m<sup>2</sup> h to 564 L/m<sup>2</sup> h and finally to 544 L/m<sup>2</sup> h after stage III and I. The decline in flux is indicative of membrane fouling. We employed a more quantifiable approach to membrane antifouling properties by calculating the flux recovery ratios (FRR) using Eq. (5). The FRR is a critical parameter for the evaluation of membrane antifouling properties; higher FRR values indicates superior antifouling properties. It is clear from the results given in Fig.5.12 that the FRR values of membranes M1 to M5 containing O-MWCNTs were higher (> 90%) than that of M0 (75%) even after the second fouling and cleaning stage. Moreover, the FRR values were found to increase with the increase in O-MWCNT content, with M5 having the highest FRR (94%). The improvement in antifouling properties of membranes M1 to M5 can be attributed to the improvements in membrane hydrophilicity of these membranes as established from Fig.5.9, with M5 showing the highest hydrophilicity. The creation of a hydration layer on the surface of hydrophilic membranes prevents the attachment of foulants. These results are in agreement with other findings that have been reported in the literature [4, 19, 23, 53]. Therefore, the results obtained indicates that the inclusion of O-MWCNTs in the PES/SPSf matrix leads to improved antifouling properties of the membranes towards protein molecules.

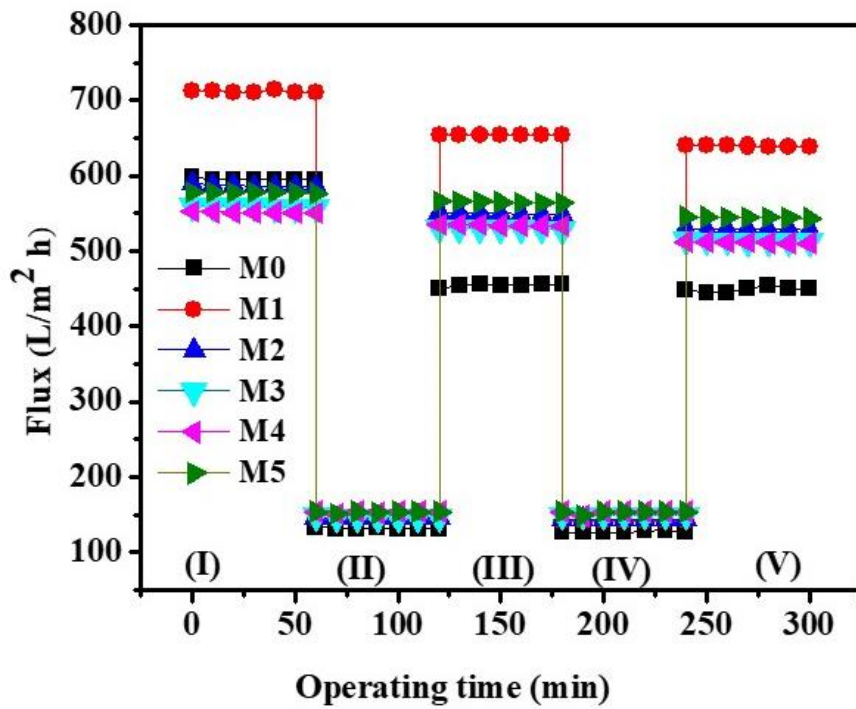


**Figure 5.11** Flux variation of membranes during the pure water filtration and fouling operation with 1g/L BSA solution (stages I, III and V: pure water filtration and II, IV: fouling stage).

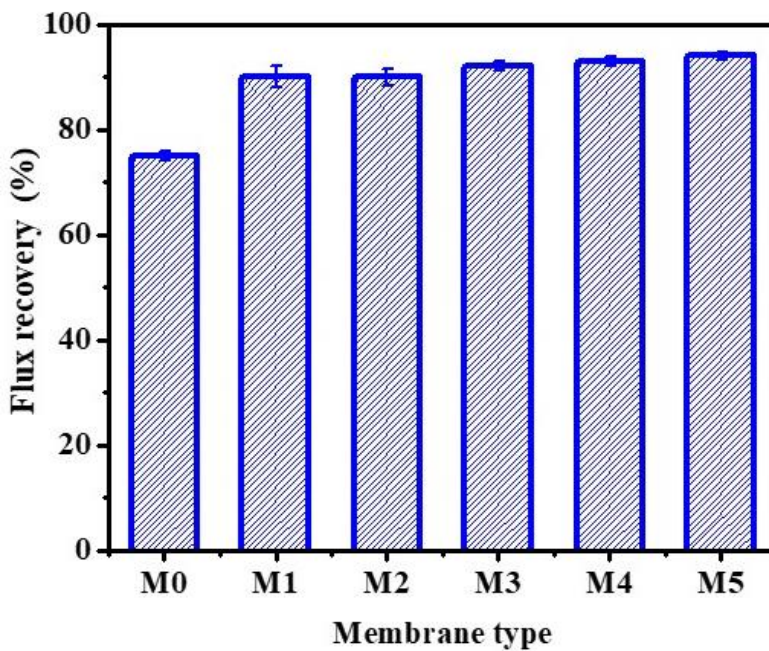


**Figure 5.12** Flux recovery ratios of PES/SPSf/O-MWCNT membranes after the second fouling stage (after stage IV).

Previous studies have demonstrated the antimicrobial activity of CNTs, in particular single-walled carbon nanotubes (SWCNTs) towards Gram-positive and Gram-negative bacteria, and that the bactericidal effects were attributed to either physical interaction by direct contact with the CNT agglomerates or through oxidative stress that compromise the cell membrane integrity of the bacteria [18, 54]. However, due to potential risks to the environment and human health, CNTs cannot be directly added to contaminated water sources like commodity chemicals but should rather be embedded in a host matrix such as a polymer, at a very low CNT content. In this study, membrane M5, which was found to have the best antifouling performance and has the highest loading of O-MWCNTs, was employed for antibacterial tests against *E. coli* bacteria. Its antibacterial activity was compared to that of M0, without O-MWCNTs. The *E. coli* suspension was treated with M0 and M5 membranes by shaking in separate flasks over a predetermined period of time followed by spreading the inoculum on agar plates and incubation. A control sample was also prepared in the absence of a membrane, to assess free growth of the bacterium. The purpose of this test was to observe the bactericidal effect of O-MWCNT-incorporated ultrafiltration membranes in a mixed-matrix format. It can be seen from the photographs in Fig.5.13, that some bacterial colonies could still be counted on the agar plate of M0, whereas only a few remained for M5. The bacterial killing ratio calculated for both membranes was found to be 85% for M0 and 99% of bacteria were killed by M5. Much uncertainty remains as to the exact mechanism that carbon nanotubes or carbon nanotube-containing membranes use to kill the bacteria. It is proposed that in this study that the main mechanism responsible for the death of *E. coli* cells is by direct contact killing whereby the antibacterial functional groups of the O-MWCNTs and O-MWCNT agglomerates penetrate the cell membrane of the bacteria leading to membrane damage and bacterial cell death [18, 55].

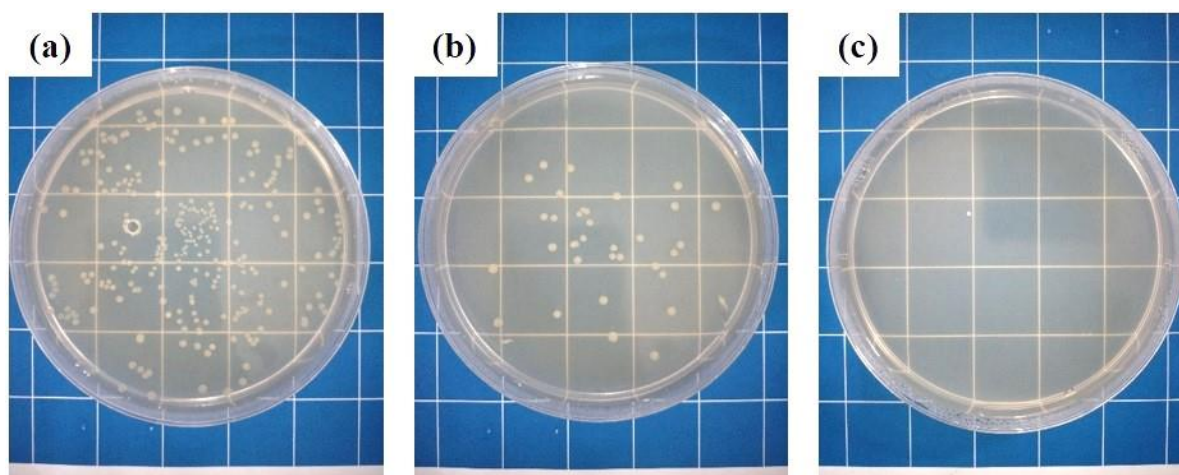


**Figure 5.13** Photographs of agar plates of *E. coli* suspension treated with PES/SPSf membranes: (a) control (without membrane), (b) M0 and (c) M5.

#### 5.4. Conclusion

This study investigated the effects of oxidised multi-walled carbon nanotubes on the morphological structure, surface and performance properties of PES/SPSf ultrafiltration membranes. Membrane hydrophilicity was enhanced in the presence of O-MWCNTs. Membranes containing O-MWCNTs displayed superior antifouling and antibacterial properties compared to pristine PES/SPSf membranes. Microscopic analyses and membrane performance tests revealed that it is possible to maintain a fully sponge-like structure in the presence of O-MWCNTs, without severely compromising the pure water flux. The interaction between O-MWCNTs, the polymer and high molecular-weight PEG/H<sub>2</sub>O mixture led to an increase in casting solution viscosity, which subsequently delayed the demixing rate between solvent and non-solvent, hence the formation of sponge-like structure. In particular, the presence of O-MWCNTs and the fully sponge-like morphology led to improvements in membrane mechanical strength properties. Moreover, hydrogen bonding between SPSf and additives H<sub>2</sub>O, PEG and O-MWCNT led to their strong interfacial interactions and uniform distribution of O-MWCNT in the mixed-matrix membrane, finally resulting in the improvement of membrane

mechanical strength. Therefore, while the reinforcing ability of O-MWCNTs helps achieve maximum improvement in the tensile strength of membranes; the homogenous distribution of CNTs and controlled formation of a sponge-like morphology in the presence of CNTs in the membrane matrix plays an important role. As such, in the absence of support fabrics, membrane morphology plays a fundamental role in governing the final mechanical strength properties of the membrane. The PES/SPSf/O-MWCNT membranes produced in this study, display promising features for the fabrication of fabric-free support substrates with enhanced performance as well as hollow fibre membrane, and for use as ultrafiltration membranes in wastewater treatment.

## 5.5. References

- [1] A. Schäfer, L. Nghiem, T. Waite, Removal of the natural hormone estrone from aqueous solutions using nanofiltration and reverse osmosis, *Environmental Science & Technology*, 37 (2003) 182-188.
- [2] L.D. Nghiem, A.I. Schäfer, M. Elimelech, Removal of natural hormones by nanofiltration membranes: measurement, modeling, and mechanisms, *Environmental Science & Technology*, 38 (2004) 1888-1896.
- [3] D. Rana, T. Matsuura, Surface modifications for antifouling membranes, *Chemical Reviews*, 110 (2010) 2448-2471.
- [4] A. Tiraferri, Y. Kang, E.P. Giannelis, M. Elimelech, Superhydrophilic thin-film composite forward osmosis membranes for organic fouling control: fouling behavior and antifouling mechanisms, *Environmental Science & Technology*, 46 (2012) 11135-11144.
- [5] S. Li, Z. Cui, L. Zhang, B. He, J. Li, The effect of sulfonated polysulfone on the compatibility and structure of polyethersulfone-based blend membranes, *Journal of Membrane Science*, 513 (2016) 1-11.
- [6] B. Schneier, Polymer compatibility, *Journal of Applied Polymer Science*, 17 (1973) 3175-3185.
- [7] L. Zhang, Z. Cui, M. Hu, Y. Mo, S. Li, B. He, J. Li, Preparation of PES/SPSf blend ultrafiltration membranes with high performance via H<sub>2</sub>O-induced gelation phase separation, *Journal of Membrane Science*, 540 (2017) 136-145.
- [8] L.-F. Fang, H.-Y. Yang, L. Cheng, N. Kato, S. Jeon, R. Takagi, H. Matsuyama, Effect of Molecular Weight of Sulfonated Poly (ether sulfone)(SPES) on the Mechanical Strength and Antifouling Properties of Poly (ether sulfone)/SPES Blend Membranes, *Industrial & Engineering Chemistry Research*, 56 (2017) 11302-11311.
- [9] A. Rahimpour, S.S. Madaeni, S. Ghorbani, A. Shockravi, Y. Mansourpanah, The influence of sulfonated polyethersulfone (SPES) on surface nano-morphology and performance of polyethersulfone (PES) membrane, *Applied Surface Science*, 256 (2010) 1825-1831.
- [10] N. Widjojo, T.-S. Chung, M. Weber, C. Maletzko, V. Warzelhan, A sulfonated polyphenylenesulfone (sPPSU) as the supporting substrate in thin film composite (TFC) membranes with enhanced performance for forward osmosis (FO), *Chemical Engineering Journal*, 220 (2013) 15-23.
- [11] L. Luo, T.-S. Chung, M. Weber, C. Staudt, C. Maletzko, Molecular interaction between acidic sPPSU and basic HPEI polymers and its effects on membrane formation for ultrafiltration, *Journal of Membrane Science*, 524 (2017) 33-42.
- [12] R. Guan, H. Zou, D. Lu, C. Gong, Y. Liu, Polyethersulfone sulfonated by chlorosulfonic acid and its membrane characteristics, *European Polymer Journal*, 41 (2005) 1554-1560.
- [13] Y. Feng, G. Han, T.-S. Chung, M. Weber, N. Widjojo, C. Maletzko, Effects of polyethylene glycol on membrane formation and properties of hydrophilic sulfonated polyphenylenesulfone (sPPSU) membranes, *Journal of Membrane Science*, 539 (2017) 27-35.

- [14] K. Zhu, S. Zhang, J. Luan, Y. Mu, Y. Du, G. Wang, Fabrication of ultrafiltration membranes with enhanced antifouling capability and stable mechanical properties via the strategies of blending and crosslinking, *Journal of Membrane Science*, 539 (2017) 116-127.
- [15] N. Peng, T.-S. Chung, K.Y. Wang, Macrovoid evolution and critical factors to form macrovoid-free hollow fiber membranes, *Journal of Membrane Science*, 318 (2008) 363-372.
- [16] M. Fang, K. Wang, H. Lu, Y. Yang, S. Nutt, Covalent polymer functionalisation of graphene nanosheets and mechanical properties of composites, *Journal of Materials Chemistry*, 19 (2009) 7098-7105.
- [17] B. Arash, Q. Wang, V. Varadan, Mechanical properties of carbon nanotube/polymer composites, *Scientific Reports*, 4 (2014) 6479.
- [18] S. Kang, M. Pinault, L.D. Pfefferle, M. Elimelech, Single-walled carbon nanotubes exhibit strong antimicrobial activity, *Langmuir*, 23 (2007) 8670-8673.
- [19] V. Vatanpour, S.S. Madaeni, R. Moradian, S. Zinadini, B. Astinchap, Fabrication and characterisation of novel antifouling nanofiltration membrane prepared from oxidised multiwalled carbon nanotube/polyethersulfone nanocomposite, *Journal of Membrane Science*, 375 (2011) 284-294.
- [20] J. Zhang, Z. Xu, W. Mai, C. Min, B. Zhou, M. Shan, Y. Li, C. Yang, Z. Wang, X. Qian, Improved hydrophilicity, permeability, antifouling and mechanical performance of PVDF composite ultrafiltration membranes tailored by oxidised low-dimensional carbon nanomaterials, *Journal of Materials Chemistry A*, 1 (2013) 3101-3111.
- [21] E. Celik, H. Park, H. Choi, H. Choi, Carbon nanotube blended polyethersulfone membranes for fouling control in water treatment, *Water Research*, 45 (2011) 274-282.
- [22] E. Celik, L. Liu, H. Choi, Protein fouling behavior of carbon nanotube/polyethersulfone composite membranes during water filtration, *Water Research*, 45 (2011) 5287-5294.
- [23] V. Vatanpour, M. Esmaeili, M.H.D.A. Farahani, Fouling reduction and retention increment of polyethersulfone nanofiltration membranes embedded by amine-functionalised multi-walled carbon nanotubes, *Journal of Membrane Science*, 466 (2014) 70-81.
- [24] E.-S. Kim, G. Hwang, M.G. El-Din, Y. Liu, Development of nanosilver and multi-walled carbon nanotubes thin-film nanocomposite membrane for enhanced water treatment, *Journal of Membrane Science*, 394 (2012) 37-48.
- [25] S. Qiu, L. Wu, X. Pan, L. Zhang, H. Chen, C. Gao, Preparation and properties of functionalised carbon nanotube/PSF blend ultrafiltration membranes, *Journal of Membrane Science*, 342 (2009) 165-172.
- [26] L.M. Cele, N.J. Coville, The negative effects of alcohols on carbon nanotube synthesis in a nebulised spray pyrolysis process, *Carbon*, 47 (2009) 1824-1832.
- [27] A.K. Shukla, J. Alam, M. Alhoshan, L.A. Dass, M. Muthumareeswaran, Development of a nanocomposite ultrafiltration membrane based on polyphenylsulfone blended with graphene oxide, *Scientific Reports*, 7 (2017).
- [28] Z.-L. Xu, F.A. Qusay, Polyethersulfone (PES) hollow fiber ultrafiltration membranes prepared by PES/non-solvent/NMP solution, *Journal of Membrane Science*, 233 (2004) 101-111.

- [29] J.-H. Choi, J. Jegal, W.-N. Kim, Fabrication and characterisation of multi-walled carbon nanotubes/polymer blend membranes, *Journal of Membrane Science*, 284 (2006) 406-415.
- [30] E. Saljoughi, M. Amirilargani, T. Mohammadi, Effect of PEG additive and coagulation bath temperature on the morphology, permeability and thermal/chemical stability of asymmetric CA membranes, *Desalination*, 262 (2010) 72-78.
- [31] G.R. Guillen, Y. Pan, M. Li, E.M. Hoek, Preparation and characterisation of membranes formed by non-solvent induced phase separation: a review, *Industrial & Engineering Chemistry Research*, 50 (2011) 3798-3817.
- [32] N. Zhao, T. Liu, Z. Liu, Y. Su, H. Yu, J. Ma, Y. Yang, Z. Jiang, Synthesis and properties of sulfonated biphenyl poly (ether sulfone) and its mixed-matrix membranes containing carbon nanotubes for gas separation, *Journal of Applied Polymer Science*, (2017).
- [33] R.P. Pandey, A.K. Thakur, V.K. Shahi, Sulfonated polyimide/acid-functionalised graphene oxide composite polymer electrolyte membranes with improved proton conductivity and water-retention properties, *ACS Applied Materials & Interfaces*, 6 (2014) 16993-17002.
- [34] M. Kumar, M. Ulbricht, Low fouling negatively charged hybrid ultrafiltration membranes for protein separation from sulfonated poly (arylene ether sulfone) block copolymer and functionalised multiwalled carbon nanotubes, *Separation and Purification Technology*, 127 (2014) 181-191.
- [35] S. Zinadini, A.A. Zinatizadeh, M. Rahimi, V. Vatanpour, H. Zangeneh, Preparation of a novel antifouling mixed-matrix PES membrane by embedding graphene oxide nanoplates, *Journal of Membrane Science*, 453 (2014) 292-301.
- [36] A.J. Reuvers, Membrane formation: diffusion induced demixing processes in ternary polymeric systems, Doctoral Thesis, University of Twente, Enschede, the Netherlands, 1987.
- [37] H. Strathmann, K. Kock, P. Amar, R. Baker, The formation mechanism of asymmetric membranes, *Desalination*, 16 (1975) 179-203.
- [38] P. Sukitpaneevit, T.-S. Chung, High performance thin-film composite forward osmosis hollow fiber membranes with macrovoid-free and highly porous structure for sustainable water production, *Environmental Science & Technology*, 46 (2012) 7358-7365.
- [39] R. Boom, I. Wienk, T. Van den Boomgaard, C. Smolders, Microstructures in phase-inversion membranes. Part 2. The role of a polymeric additive, *Journal of Membrane Science*, 73 (1992) 277-292.
- [40] I. Wienk, R. Boom, M. Beerlage, A. Bulte, C. Smolders, H. Strathmann, Recent advances in the formation of phase-inversion membranes made from amorphous or semi-crystalline polymers, *Journal of Membrane Science*, 113 (1996) 361-371.
- [41] O. Mahlangu, R. Nackaerts, J. Thwala, B. Mamba, A. Verliefde, Hydrophilic fouling-resistant GO-ZnO/PES membranes for wastewater reclamation, *Journal of Membrane Science*, 524 (2017) 43-55.
- [42] M. Kumar, M. Ulbricht, Novel antifouling positively charged hybrid ultrafiltration membranes for protein separation based on blends of carboxylated carbon nanotubes and aminated poly (arylene ether sulfone), *Journal of Membrane Science*, 448 (2013) 62-73.
- [43] J.N. Coleman, U. Khan, W.J. Blau, Y.K. Gun'ko, Small but strong: a review of the mechanical properties of carbon nanotube-polymer composites, *Carbon*, 44 (2006) 1624-1652.

- [44] N. Widjojo, T.-S. Chung, M. Weber, C. Maletzko, V. Warzelhan, The role of sulphonated polymer and macrovoid-free structure in the support layer for thin-film composite (TFC) forward osmosis (FO) membranes, *Journal of Membrane Science*, 383 (2011) 214-223.
- [45] L. Yu, Y. Zhang, B. Zhang, J. Liu, H. Zhang, C. Song, Preparation and characterisation of HPEI-GO/PES ultrafiltration membrane with antifouling and antibacterial properties, *Journal of Membrane Science*, 447 (2013) 452-462.
- [46] H. Zhao, L. Wu, Z. Zhou, L. Zhang, H. Chen, Improving the antifouling property of polysulfone ultrafiltration membrane by incorporation of isocyanate-treated graphene oxide, *Physical Chemistry Chemical Physics*, 15 (2013) 9084-9092.
- [47] G. Kaminska, J. Bohdziewicz, J.I. Calvo, P. Prádanos, L. Palacio, A. Hernández, Fabrication and characterisation of polyethersulfone nanocomposite membranes for the removal of endocrine disrupting micropollutants from wastewater. Mechanisms and performance, *Journal of Membrane Science*, 493 (2015) 66-79.
- [48] G. Arthanareeswaran, D. Mohan, M. Raajenthiren, Preparation, characterisation and performance studies of ultrafiltration membranes with polymeric additive, *Journal of Membrane Science*, 350 (2010) 130-138.
- [49] A. Abdel-Karim, T.A. Gad-Allah, A.S. El-Kalliny, S.I. Ahmed, E.R. Souaya, M.I. Badawy, M. Ulbricht, Fabrication of modified polyethersulfone membranes for wastewater treatment by submerged membrane bioreactor, *Separation and Purification Technology*, 175 (2017) 36-46.
- [50] T.-Y. Liu, R.-X. Zhang, Q. Li, B. Van der Bruggen, X.-L. Wang, Fabrication of a novel dual-layer (PES/PVDF) hollow fiber ultrafiltration membrane for wastewater treatment, *Journal of Membrane Science*, 472 (2014) 119-132.
- [51] X. Shen, Y. Zhao, Q. Zhang, L. Chen, Dry-wet spinning of temperature-sensitive PVDF hollow-fiber membranes at different bore fluid flow rates, *Journal of Polymer Research*, 20 (2013) 136.
- [52] B. Govardhan, S. Chandrasekhar, S. Sridhar, Purification of surface water using novel hollow fiber membranes prepared from polyetherimide/polyethersulfone blends, *Journal of Environmental Chemical Engineering*, 5 (2017) 1068-1078.
- [53] A. Rahimpour, M. Jahanshahi, B. Rajaeian, M. Rahimnejad, TiO<sub>2</sub> entrapped nanocomposite PVDF/SPES membranes: Preparation, characterization, antifouling and antibacterial properties, *Desalination*, 278 (2011) 343-353.
- [54] C. Yang, J. Mamouni, Y. Tang, L. Yang, Antimicrobial activity of single-walled carbon nanotubes: length effect, *Langmuir*, 26 (2010) 16013-16019.
- [55] J. Meng, X. Zhang, L. Ni, Z. Tang, Y. Zhang, Y. Zhang, W. Zhang, Antibacterial cellulose membrane via one-step covalent immobilization of ammonium/amine groups, *Desalination*, 359 (2015) 156-166.
- [56] R.A. DiLeo, B.J. Landi, R.P. Raffaele, Purity assessment of multiwalled carbon nanotubes by Raman spectroscopy, *Journal of Applied Physics*, 101 (2007) 064307.
- [57] Y. Liu, C. Pan, J. Wang, Raman spectra of carbon nanotubes and nanofibers prepared by ethanol flames, *Journal of Materials Science*, 39 (2004) 1091-1094.

**CHAPTER 6**  
**RELATING THE PERFORMANCE OF SULFONATED THIN-FILM COMPOSITE**  
**NANOFILTRATION MEMBRANES TO STRUCTURAL PROPERTIES OF**  
**MACROVOID-FREE PES/SPSF/O-MWCNT SUPPORT MEMBRANES**

---

**Summary of the chapter**

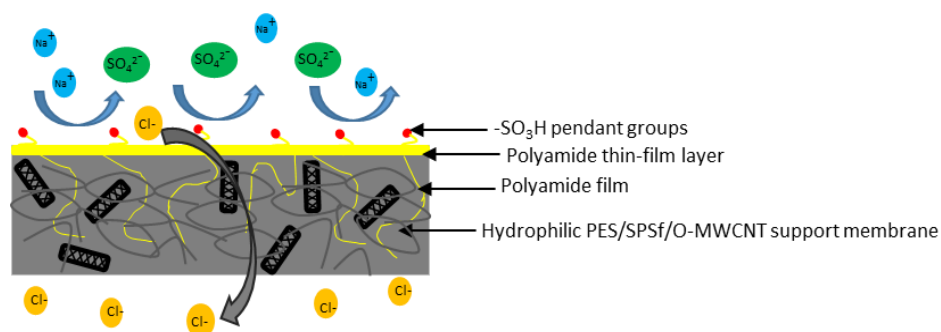
This chapter describes the synthesis of sulfonated thin-film composite nanofiltration (TFC NF) membranes on macrovoid-free polyethersulfone/sulfonated polysulfone/oxidised multi-walled carbon nanotube (PES/SPSf/O-MWCNT) ultrafiltration membrane supports via an interfacial polymerisation method. During the deposition of the selective polyamide film layer, the aqueous phase solution consisted of a mixture of piperazine (PIP) and 2,4-diaminobenzene sulfonic acid (2,4-DABSA) and the organic phase solution consisted of trimesoyl chloride (TMC). The deposition of the sulfonated polyamide thin-film layer was confirmed by ATR-FTIR, SEM, AFM, contact angle and zeta potential measurements. The TFC NF membranes fabricated on PES/SPSf/O-MWCNT support membrane showed a 35% improvement in pure water flux with comparable salt rejections from those prepared on PES/SPSf support membranes. The presence of hydrophilic O-MWCNTs in the PES/SPSf support membrane allowed for the formation of a thin polyamide layer on the top surface for enhanced water permeability and a possibility of thin polyamide rejection layer within the support membrane pore channels. The addition of low monomer weight ratio of 2,4-DABSA in the amine mixture, led to the generation of a sulfonated TFC NF membrane with superior membrane performance in terms of pure water permeability (30.2 L/m<sup>2</sup>.h.bar), monovalent/bivalent salt selectivity ( $\alpha_{\text{NaCl/Na}_2\text{SO}_4} = 25.0$ ) at low operating pressures (3 bar) and salt concentrations in the range

of brackish water. Moreover, sulfonated TFC NF membrane exhibited good antifouling properties against BSA, with FRR of 96.4% after 3 cycles of fouling and cleaning.<sup>3</sup>

The performance of the sulfonated TFC NF membrane remained fairly stable over a 10-day period of pure water flux and Na<sub>2</sub>SO<sub>4</sub> rejection testing. The use of a macrovoid-free PES/SPSf/O-MWCNT support membrane provided the mechanical support for the TFC NF membrane, and also their open, cellular network microstructure, combined with high hydrophilicity and large surface pore sizes were beneficial in the reduction of polyamide layer thickness, and subsequently in the enhancement of TFC NF membrane performance in comparison to their pristine counterparts (PES/SPSf supports). Overall, the fabricated sulfonated TFC NF membrane displayed promising features for application as pretreatment membranes for lower-pressure softening and desalination of brackish water.

**Keywords:** sulfonated thin-film composite membranes, macrovoid-free structure, oxidised multi-walled carbon nanotubes, permeability, selectivity, antifouling.

### Graphical abstract



<sup>3</sup> N.N. Gumbi, J. Li, B.B. Mamba, E.N. Nxumalo, Relating the performance of sulfonated thin-film composite nanofiltration membranes to structural properties of macrovoid-free polyethersulfone/sulfonated polysulfone/O-MWCNT supports, *Desalination*, 474 (2020) 114176.

## 6.1. Introduction

Thin-film composite (TFC) membranes are significantly gaining popularity in the nanofiltration (NF), reverse osmosis (RO) and forward osmosis (FO) separation processes of wastewater remediation [1]. Polyamide TFC membranes are generally prepared via the interfacial polymerisation (IP) reaction between polyfunctional amine and acyl chloride monomers at the interface between two immiscible solvents, over a porous polymeric support [2, 3]. The IP process is based on the diffusion of the amine monomer from the aqueous phase to the organic phase due to the relatively low solubility of the acyl chloride monomer in the aqueous phase [4]. The key advantage of TFC membranes over other membrane types is the ability to independently tailor the structural properties of each layer, i.e., polyamide skin layer and porous support layer. Therefore, they present a unique technique to achieve a composite membrane of desired selectivity and permeability, while maintaining good mechanical integrity and compression resistance. As such, several research studies have focused on either the optimisation of the polyamide layer properties [5-7] or on the optimal support membrane properties [3, 8-10] to develop a TFC membrane with enhanced separation performance, chemical tolerance and fouling resistance. The initial contact point with the feed solution, polyamide layer properties, including film thickness, hydrophilicity and cross-linking degree have a significant effect on the performance of the TFC membrane.

Although the polyamide layer of the TFC membrane is responsible for the majority of the permeation and selectivity of the composite membrane, the morphology and surface properties of the porous support membrane, have a direct influence on the nature of the ultrathin polyamide layer formed [11]. There are still conflicting views on ideal support membrane characteristics for deposition of the polyamide layer, particularly on whether hydrophilic

properties of the support membrane contribute towards diminishing the performance of the TFC membrane or improving it.

Widjojo et al. [12], reported that for FO applications; a higher degree of hydrophilicity of support membrane was more favourable for the enhancement in pure water flux of the TFC membrane than the membrane cross-sectional morphology. Ghosh and Hoek [3], conducted a comprehensive study on the impacts of the polysulfone (PSf) support membrane structural properties, in particular the pore size and hydrophilicity, on the performance of the resultant polyamide TFC membranes. It was found that the support membrane labelled PSf-6 which had pores that were twice as large as those PSf-1 and PSf-2 supports but was of equal hydrophobicity as PSf-1 and PSf-2; produced the most permeable composite polyamide membrane. On the other hand, the most hydrophilic support, namely PSf-3 which had intermediate pore sizes between those of PSf-1 and PSf-2, produced the least permeable composite membrane. It was concluded that larger and hydrophobic support layer pores produce more permeable and rough composite membranes because less polyamide forms within the pores [3]. The authors explained that the m-phenylene diamine (MPD) aqueous monomer diffused more slowly out of the pores of the hydrophilic support membranes due to hydrogen bonding interactions between the MPD and the polar functional groups of polymeric additives which were used to make the support membranes hydrophilic. Nonetheless, it is entirely possible that, more than the hydrophobicity/hydrophilicity of the support membrane, the size of the pores had a greater impact on the observed enhancement in pure water flux of the composite polyamide membrane produced from the PSf-6 support membrane.

Singh et al. [8], investigated the effect of pore sizes of PSf support membranes (70 nm versus 150 nm) on the salt rejection and water permeation efficiency of TFC membranes. It was reported that the TFC membrane formed over the support with small pore-sized had superior salt rejection but lower water flux compared to the TFC membrane formed over supports with large pore sizes. This observation was attributable to reduced penetration of polyamide film into the support with small pore-sizes whereas a thinner, more porous polyamide skin layer is formed over the supports with large pore sizes since the membrane pores are largely plugged with polyamide film [8].

Fathizadeh et al. [13], investigated the effect of surface properties such as membrane hydrophilicity and pore size of PES support substrates as well as the effect of lag time (i.e., time spent on removing the excess MPD solution from the surface of the support layer prior to immersion into TMC organic phase solution) on the surface and performance properties of polyamide TFC membranes. The following findings were obtained from that study: (i) support membranes with large pore sizes and low hydrophilicity produced TFC membranes with high water and salt permeability at low lag times (e.g. 0 min) and (ii) support membranes with large pore sizes and high hydrophilicity produced TFC membranes with high water and salt permeability at maximum lag time (e.g. 8 min) investigated. An increase in lag time allows for the diffusion of MPD deeper into the support membrane pores and the formation of a thinner polyamide film on top of the support membrane, with less surface roughness. It was concluded that the lag time had a more significant influence on the separation performance of the polyamide TFC membranes than the pore size and hydrophilicity of support membranes [13]. A subsequent study by Fathizadeh et al. [14], showed that the wet/dry state of a hydrophilic polyethersulfone (PES) support membrane prior to the IP process has a significant effect on the performance of the TFC membrane. The study showed that TFC membranes synthesised

over wet PES supports have a lower cross-linking degree and higher water fluxes compared to TFC membranes formed over dry PES supports.

From the studies discussed above, it can be clearly seen that apart from process operating conditions or post-treatment conditions, the state of the support membrane prior to immersion in the aqueous phase solution, the pore sizes of the support layer and the lag time during the IP process all play a crucial role in affecting the polyamide layer properties and subsequently, the performance of the TFC membrane.

To date, the pore sizes of the support membrane have been identified as having a significant effect on the polyamide layer formed as well as on the performance of the resultant TFC membranes. However, only scant reports are available on the influence of other support membrane morphological features such as the presence or the absence of finger-like structures and macrovoids, on the performance of the TFC membranes. Yip et al. [15] and Wang et al. [16], reported that the support membrane structure for TFC FO membranes should consist of a thin layer of sponge-like morphology on top and finger-like morphology at the bottom, in order to realise enhanced membrane performance. Tiraferri et al. [10], reported that the finger-like morphology in the support membrane for TFC FO applications, is more favourable than the sponge-like morphology for the reduction of internal concentration polarisation (ICP). It is important to highlight a clear distinction in support membrane properties of TFC membranes for osmotically-driven processes such as FO and pressure-retarded reverse osmosis (PRO) and those for pressure-driven processes such as NF and RO. For FO applications, the presence of sponge-like structures in the membrane sublayer is deemed a hindrance to mass transfer across the TFC membranes and a major contributor to ICP, whereas in pressure-driven processes such as NF and RO, the sponge-like morphology of the support layer is desired for mechanical

stability of the TFC membranes [17]. Nonetheless, some research studies have reported that even for NF/RO applications, support membrane structures with sponge-like morphology are highly undesirable as they lead to the generation of TFC NF/RO membrane with reduced water fluxes but increased salt rejections [18, 19]. Ding et al. [19], evaluated the effects of support layer polymer concentration on the performance of the TFC RO membranes. They reported that increasing the polymer concentration changed the substructure morphology from finger-like to sponge-like morphology, which was accompanied by a decline in surface porosity and water permeability of the TFC membrane. Similar findings were previously reported by Misdan and coworkers [20].

In a recent study, macrovoid-free polyethersulfone /sulfonated polysulfone/oxidised multi-walled carbon nanotube (PES/SPSf/O-MWCNT) ultrafiltration membranes were prepared with enhanced hydrophilicity, water flux, mechanical strength and antifouling properties [21]. Besides their macrovoid-free nature, the characteristic physicochemical properties highlighted make these mixed-matrix UF membranes desirable candidates for use as support membranes for polyamide layer deposition. To investigate the effect of support membrane structural properties (such as. hydrophilicity and pore size) on the TFC NF membrane performance, PES/SPSf/O-MWCNT supports membranes (with and without O-MWCNTs) were used for the fabrication of TFC NF membranes via the IP process. The morphology and surface characteristics of the substrates were related to the resultant TFC NF membrane performance. Additionally, to further improve the surface properties of TFC NF membrane in terms of water permeability, monovalent/bivalent salt selectivity and fouling resistance, the use of mixed diamine monomers (piperazine (PIP) and 2,4- diaminobenzene sulfonic acid (2, 4-DABSA) for the IP reaction with TMC (as shown in Fig. 6.1), was systematically investigated.

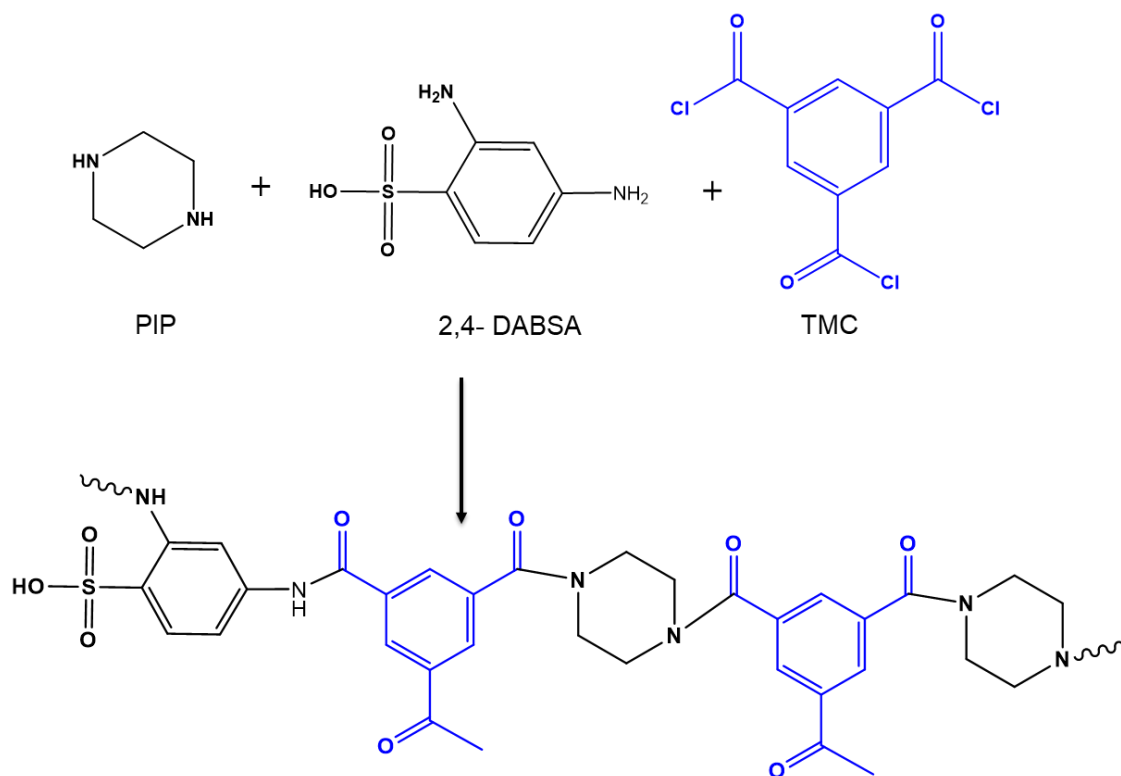


**Figure 6.1.** Interfacial polymerisation reaction scheme between PIP, 2,4-DABSA and TMC.

## 6.2. Experimental

### 6.2.1. Materials

Piperazine (PIP, reagent plus 99%), 2,4- diaminobenzene sulfonic acid (2,4-DABSA,  $\geq 98\%$ ), 1,3,5-benzenetricarbonyl trichloride (TMC, 98%), sodium dodecyl sulphate (SDS, 98.5%), sodium hydroxide (NaOH), and anhydrous hexane (95%) were all purchased from Sigma-Aldrich (Germany). Sodium chloride (NaCl), calcium chloride ( $\text{CaCl}_2$ ), magnesium sulphate ( $\text{MgSO}_4$ ) and sodium sulphate ( $\text{Na}_2\text{SO}_4$ ) salts for membrane selectivity tests, were purchased from Merck (South Africa). All chemicals were used without further purification unless otherwise stated.

### **6.2.2. Preparation of thin-film composite nanofiltration (TFC NF) membrane**

The detailed procedure on non-solvent-induced phase-separation (NIPS) preparation of PES/SPSf/O-MWCNT support membranes has been discussed in our previous work [21] and in Chapter 5. The characteristic physicochemical properties of the support membranes used in the study, have been summarised in Table 6.1. The support membranes that had been previously stored in deionised water were dabbed dry to remove excess water droplets and placed into a frame where the top surface of the membrane was contacted with the aqueous phase solution containing 2 wt.% PIP/2,4-DABSA and 0.1 wt.% SDS, for 2 min. The pH of the aqueous phase solution was adjusted to 10 using 1 mM NaOH, in order to ensure complete dissolution of 2,4-DABSA. Thereafter, the excess aqueous phase solution was removed from the membrane surface using a rubber roller and a lag time of 6 min was allowed in dry air before contact with the organic phase solution. The saturated support membrane was then contacted with TMC in hexane solution for 60 s to allow the interfacial polymerisation reaction to occur and for the deposition of the active polyamide layer. The TMC concentration was varied between 0.05 - 0.3 wt.%. The nascent membrane was then removed from the frame and cured in the oven at 60 °C for 5 min, followed by rinsing with deionised water at ambient temperature and storage in deionised water at 4 °C until use. The PIP/2,4-DABSA monomer weight ratios were varied as follows: 100:0; 75:25; 50:50 and 0:100. The TFC membranes prepared on PES/SPSf support membranes were labelled as NF\_M0 and those prepared on PES/SPSf/O-MWCNT supports were coded as NF\_M1 as shown in Table 6.2.

### 6.2.3. Membrane characterization

Attenuated total reflectance Fourier transform-infrared (ATR–FTIR) spectrometer (Perkin Elmer, Germany) was used to record spectra in the range of 500 – 4000  $\text{cm}^{-1}$  to confirm successful deposition of the polyamide film layer by assessing the functional groups present on the membrane surfaces. Field emission scanning electron microscope (FESEM, Hitachi S4800, Japan) was used to characterise changes in membrane morphologies with the diamine monomer ratio. For cross-sectional viewing, vacuum-dried membranes were freeze-fractured in liquid nitrogen followed by coating with 5 nm gold. Atomic force microscopy (AFM: WITec Alpha300) in non-contact mode was used to analyse membrane surface topography and roughness. Membrane samples were dried in desiccators prior to AFM analysis. Contact angle measurements were carried out using a contact angle goniometer (DSA30E Krüss GmbH, Hamburg, Germany) using sessile drop method to evaluate membrane hydrophilicity. The contact angle values reported were recorded after the first 3 s of the adherence of the water droplet on the membrane surface. An average of six readings were taken from different spots on the membrane surface and the average value was reported. The surface charge of TFC membranes was analysed using zeta potential measurements on the electrokinetic analyser (SurPASS Anton Paar, Austria). Membrane samples were mounted into the adjustable gap cell sample holder. The background electrolyte solution used for the measurements was 10 mM potassium chloride (KCl) and the solution pH was adjusted using 0.1 M hydrochloric acid (HCl) and sodium hydroxide (NaOH) solutions.

**Table 6.1** PES/SPSf support membranes physicochemical characteristics\*.

<b>Membrane used</b>	<b>Membrane type</b>	<b>PWP (L/m<sup>2</sup>.h.bar)</b>	<b>MWCO (kDa)</b>	<b>Contact angle (°)</b>	<b>Tensile strength (MPa)</b>	<b>FRR (%)</b>
M0	PES/SPSf	598 ± 1.16	79.8	67.2	2.78	75%
M1	PES/SPSf/O-MWCNT	713 ± 0.26	88.2	58.7	3.48	90%

\*support membrane synthesis and characteristics has been discussed in detail in Chapter 5.

**Table 6.2** Compositions of aqueous and organic phase solutions for TFC NF membrane preparation.

<b>Membrane</b>	<b>TMC (wt.%)</b>	<b>PIP (wt.%)</b>	<b>2,4-DABSA (wt.%)</b>
NF_M0	0.10	2.00	0.00
NF_M1	0.10	2.00	0.00
NF_M1_0	0.10	2.00	0.00
NF_M1_25	0.10	1.50	0.50
NF_M1_50	0.10	1.00	1.00
NF_M1_100	0.10	0.00	2.00

#### 6.2.4. Membrane performance tests

To evaluate the performance of membranes, pure water flux measurements were carried out using dead-end stirred cells (Sterlitech™ HP4750) with an effective membrane area of 12.60 cm<sup>2</sup> (Fig. 6.2). The membrane samples were compacted at 0.4 MPa for 1 h using deionised water to obtain a stable flux. The pressure was reduced to 0.3 MPa for pure water flux

measurements and salt rejection experiments. Pure flux ( $J_{w1}$ ) was calculated according to Eq. 6.1 as:

$$J_{w1} = \frac{V}{A \times t} \quad (6.1)$$

where  $V$  is the volume of permeate (L),  $A$  is the effective membrane area ( $m^2$ ) and  $t$  is the permeation time (h).

To evaluate the separation performance of TFC NF membranes, salt rejection experiments were carried out using 2000 ppm solutions of NaCl, CaCl<sub>2</sub>, MgSO<sub>4</sub> and Na<sub>2</sub>SO<sub>4</sub> to simulate brackish water concentrations [22]. Each salt solution was tested separately. The concentration of salts in the feed and permeate samples were measured using a Eutech instruments, 700 CON bench-top conductivity meter ((Eutech Instruments Pty Ltd, Singapore). Membrane solute rejection  $R$  (%) was calculated using Eq. 6.2 as:

$$R(\%) = \left( 1 - \frac{C_p}{C_f} \right) \times 100 \quad (6.2)$$

where  $C_p$  and  $C_f$  are solute concentrations in the permeate and feed solution, respectively.

The monovalent/bivalent salt selectivity ( $S_{NaCl/Na_2SO_4}$ ) was calculated from the rejection ( $R$ ) values of NaCl and Na<sub>2</sub>SO<sub>4</sub> using Eq.6.3 as:

$$S_{NaCl/Na_2SO_4} = \frac{(100 - R_{NaCl})}{(100 - R_{Na_2SO_4})} \quad (6.3)$$

Fouling experiments were conducted using BSA as a model protein foulant (0.1 g/L). The fouling process included four pure water filtration stages and three fouling stages. Each stage

was operated for 60 min. After each fouling stage, the fouled membranes were thoroughly washed with deionised water, thereafter the water flux of “clean” membranes denoted as  $J_{w2}$  was measured. The water flux recovery ( $FRR$ ) (%) and total flux decline rate ( $FDR_t$ ) were calculated after three cycles of fouling and cleaning using Eq. 6.4 and 6.5 as follows:

$$FRR(\%) = \frac{J_{w2}}{J_{w1}} \times 100 \quad (6.4)$$

$$FDR_t(\%) = \left(1 - \frac{J_{BSA}}{J_{w1}}\right) \times 100 \quad (6.5)$$

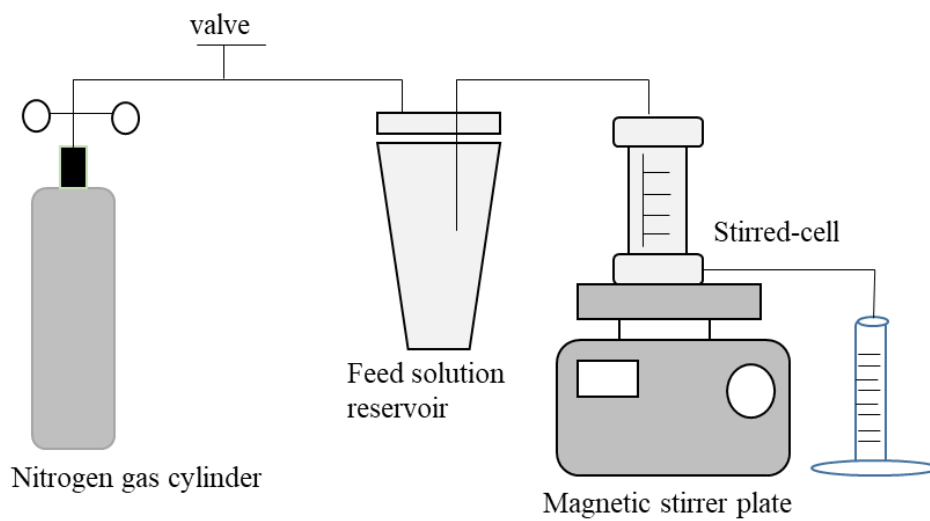


**Figure 6.2.** Schematic diagram of stirred-cell membrane permeation test unit.

### 6.3. Results and discussion

#### 6.3.1. Effect of TMC concentration on TFC NF membrane performance: PES/SPSf versus PES/SPSf/O-MWCNT support membranes

The effect of TMC concentration on TFC NF membrane performance in terms of pure water flux and salt rejection was investigated in order to find optimum reaction conditions. Fig. 6.3 shows the effect of TMC concentration on pure water flux of TFC NF membranes prepared on M0 and M1 support membranes. For both support membranes used, the pure water flux declined significantly with an increase in TMC concentration, from 124.9 L/m<sup>2</sup>.h to 18.8 L/m<sup>2</sup>.h for the NF\_M0 membrane and from 169.3 L/m<sup>2</sup>.h to 26.0 L/m<sup>2</sup>.h for the NF\_M1 membrane. On the other hand, the rejection of salts by both TFC NF membranes increased with an increase in TMC concentration and follows the order Na<sub>2</sub>SO<sub>4</sub> > MgSO<sub>4</sub> > NaCl (Fig. 6.4). To explain the observed performance results, SEM surface image analysis of the TFC NF membranes was conducted (shown in Fig. 6.5). It can be seen from the surface images that at low TMC concentration (e.g. at 0.05 wt.%), the polyamide layer does not become fully formed on the surface of the support membranes, i.e., there are spaces in between in polyamide granules deposited on the support membrane. This suggests that there is an insufficient amount of TMC monomers reaching the reaction zone at the interface between two immiscible phases for the formation of the polyamide film [23]. With further increments in TMC concentration, the polyamide layer formed became dense and largely covered the active surface of the support membrane. As such, at low TMC contents, the TFC membrane exhibits the behavior of a UF membrane, by displaying high water fluxes (> 100 L.m<sup>2</sup>.h). Therefore, the TMC concentration of 0.1 wt.% gave optimum TFC NF membrane performance for both support membranes evaluated.

It is important to note that although the increase in TMC concentration similarly affects the performance of both NF\_M0 and NF\_M1, the NF\_M1 membrane prepared on a PES/SPSf/O-MWCNT support membrane exhibited better performance compared to NF\_M0. In fact, NF\_M1 showed a 35% improvement in pure water fluxes with comparable salt rejections as NF\_M0. The enhancement in performance behaviour of NF\_M1 membrane can be attributed to the larger pore sizes and improved hydrophilicity of the PES/SPSf/O-MWCNT support membrane used which provided better adhesion on the polyamide layer compared to PES/SPSf support membrane [3, 8]. The presence of hydrophilic O-MWCNTs in the PES/SPSf support membrane allows for the hydrogen bond interactions with PIP aqueous solution, leading to the formation of a thin polyamide layer on the top surface which is responsible for enhanced water permeability of the membrane and thin polyamide rejection layer within the support membrane pore channels [8].

Recently, Lau et al., in their comprehensive review on microporous substrates for polyamide TFC membranes summarised the requirements for an ideal support membrane prepared via NIPS method as: (i) pore size: 20–150 nm, (ii) bulk porosity: 50–70%, (3) contact angle: 40–60° and (4) pure water flux: >100 L/m<sup>2</sup>.h, regardless of materials used to fabricate the support [24]. The PES/SPSf/O-MWCNT support membrane used for fabrication of NF\_M1 meets these requirements. Moreover, the possession of a macrovoid-free morphology by the support membrane did not diminish the TFC NF membrane performance as previously speculated by other researchers [19, 25]. The TFC NF membrane performance was comparable and in some instances higher than that achieved on a support membrane with finger-like morphology [20, 23, 26]. The sponge-like or macrovoid-free morphology of the support membranes reported from previous studies had been obtained via an increase in polymer concentration, particularly PSf concentration [20, 25]. The sponge-like morphology achieved

in this manner becomes very dense and less porous, hence the decline in TFC membrane permeability. In this study, the macrovoid-free morphology of the support membrane consisted of open intercellular structures and was achieved through interfacial interactions between O-MWCNTs, the polymer and high molecular-weight PEG/H<sub>2</sub>O mixture [21]. High molecular-weight PEG improved pore interconnectivity thus preventing the formation of macrovoids; whereas H<sub>2</sub>O increased casting solution viscosity and brought the polymer solution viscosity closer to the binodal composition where the suppression of macrovoids is favoured. As such further investigations in this study on TFC NF performance variables are based on the TFC NF membranes prepared on the PES/SPSf/O-MWCNT support.

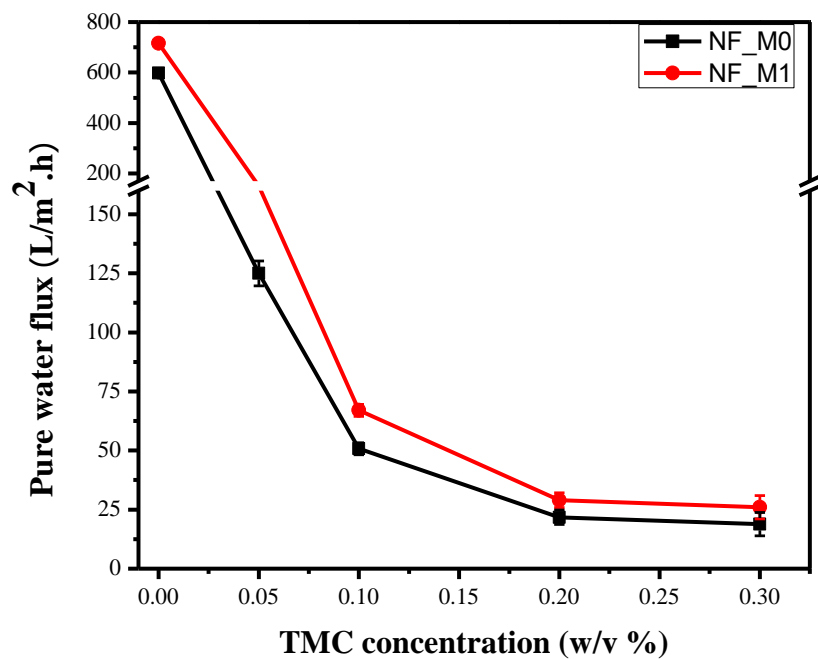


**Figure 6.3.** Effect of TMC concentration on pure water flux of TFC membranes. Experimental conditions: PIP concentration = 2 wt.%, IP reaction time = 30 s.

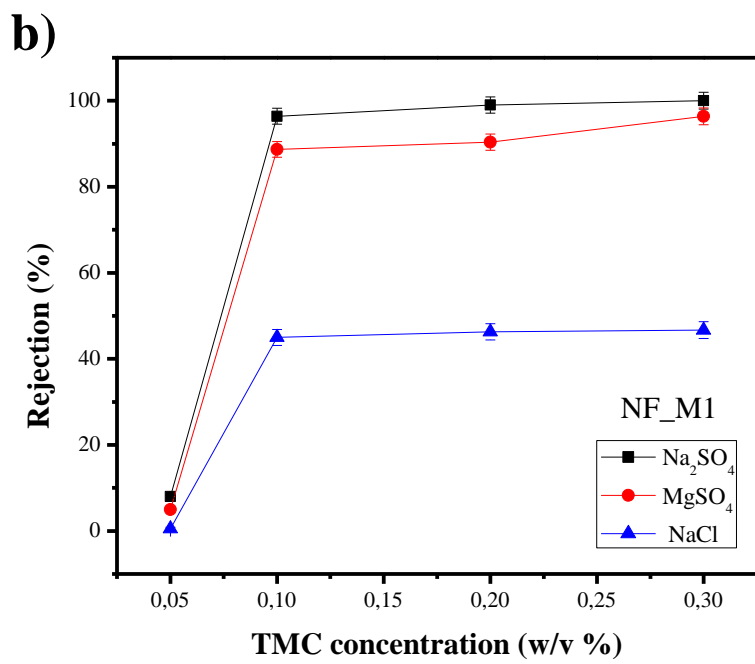
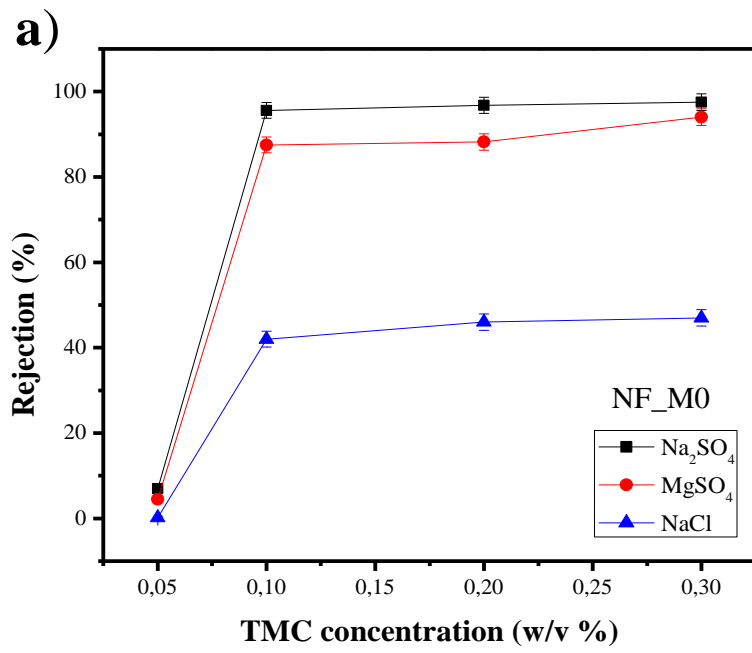


**Figure 6.4.** Salt rejection performance of (a) NF\_M0 and (b) NF\_M1 membranes. Experimental conditions: PIP concentration = 2 wt.%, IP reaction time = 30 s.

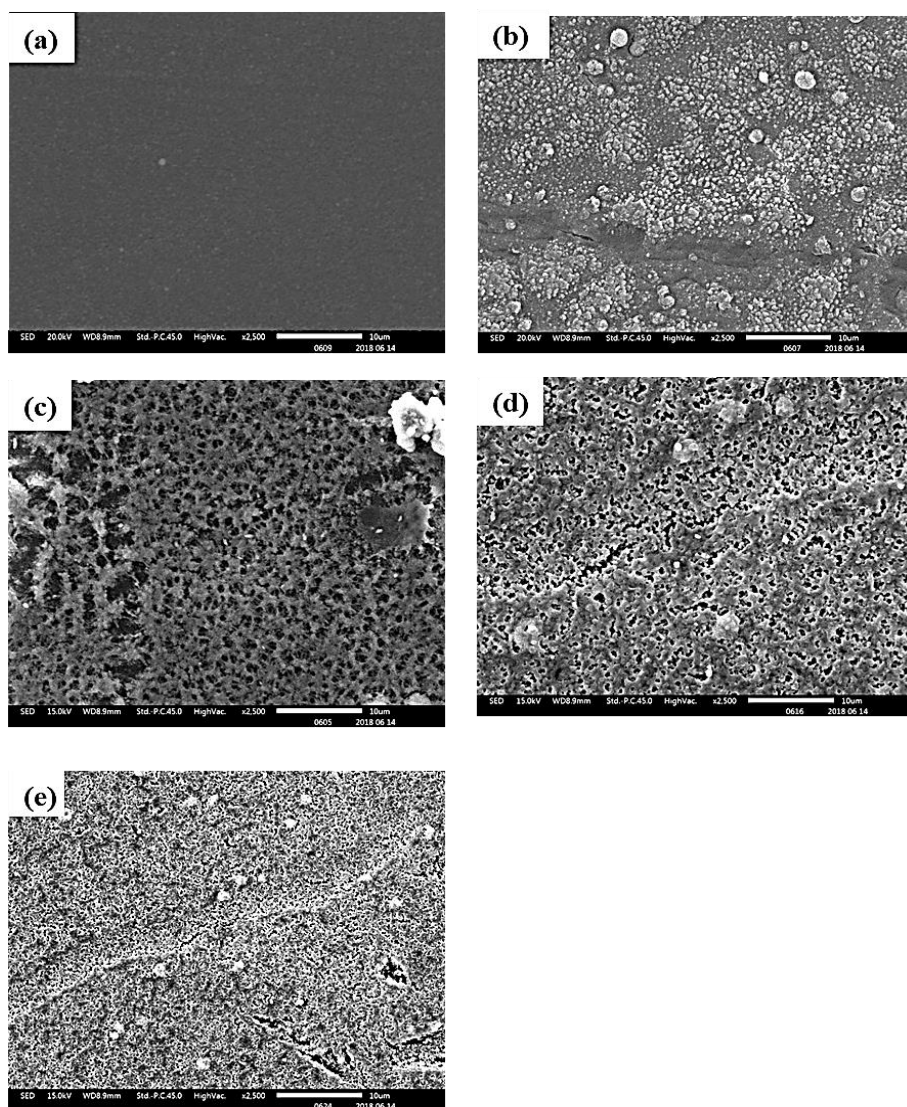


**Figure 6.5** SEM surface images of NF\_M1 membranes prepared from different concentrations of TMC: (a) 0.0 wt.%, (b) 0.05 wt.%, (c) 0.1wt.%, (d) 0.2 wt.% and (e) 0.3 wt.%. Experimental conditions: PIP concentration = 2 wt.%, IP reaction time = 30 s.

### 6.3.2. Effect of interfacial polymerisation reaction time on pure water flux and $\text{Na}_2\text{SO}_4$ rejection

The effect of interfacial polymerisation (IP) reaction time, *i.e.* contact time between the aqueous and organic phase for polyamide film deposition, was evaluated in order to obtain optimum TFC NF membrane performance. The investigation was conducted in NF\_M1

membrane prepared using 0.1 wt.% TMC and 2 wt.% PIP monomers. In general, the IP process is rapid and takes place within a few seconds of contact between the two immiscible phases [2]. As shown in Fig. 6.6, the increase in reaction time from 10 s to 30 s initially led to an increase in pure water flux from  $57.31 \pm 1.53$  L/m<sup>2</sup>.h to  $67.03$  L/m<sup>2</sup>.h  $\pm 0.58$ , and a slight decline in Na<sub>2</sub>SO<sub>4</sub> rejection from 98.4% to 98.1%. The increase in pure water flux can be attributed to the increase in availability of monomers reaching the reaction interface for the formation of polyamide layer. However, with further increments in reaction time to 60 s, pure water flux decreased to  $51.4 \pm 0.32$  L/m<sup>2</sup>.h, and Na<sub>2</sub>SO<sub>4</sub> rejection increased to 98.7%. The decline in pure water flux can be attributed to the increase in crosslinking degree with the growth of dense polyamide layer with low-free volume at longer reaction times, hence the accompanying increase in Na<sub>2</sub>SO<sub>4</sub> rejection from 98.4% [27]. Similar results were reported by Huang et al.[26]. Therefore, an IP reaction time of 30 s gave optimal TFC NF membrane performance for the monomers used and their concentration.

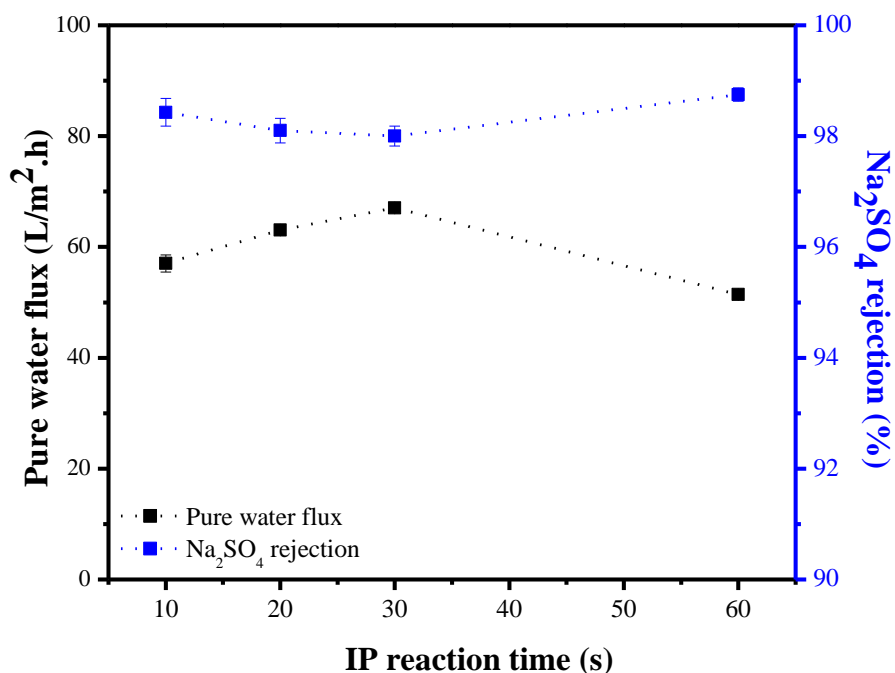


**Figure 6.6.** Effect of IP reaction time on pure water flux and salt rejection of NF\_M1 membrane. Experimental conditions: PIP concentration = 2 wt.%, TMC concentration = 0.1 wt.%.

### 6.3.3. Effect of monomer weight ratio on membrane separation performance of TFC NF membranes

Although TFC NF membranes prepared to date including commercial ones from Dow FilmTec (NF270, NF400, *etc.*) using PIP monomer have shown promising performance features in terms of pure water permeability, salt rejection and chlorine tolerance [18, 28], there is still room for further improvements in membrane performance properties and to develop fouling resistant TFC NF membrane. Sulfonic-acid group containing amine monomers have the potential to improve membrane surface hydrophilicity, thereby improving pure water permeability of the membrane and improving membrane fouling resistance. In this work, different weight ratios of 2,4-DABSA monomer were combined with PIP monomer in the aqueous phase to improve the properties of the semi-aromatic polyamide layer formed. As shown in Fig. 6.7, pure water flux

initially increased from  $67.03 \pm 1.53 \text{ L/m}^2\cdot\text{h}$  to  $90.70 \pm 2.31 \text{ L/m}^2\cdot\text{h}$  when the PIP:2,4-DABSA monomer weight ratio was increased from 100:0 to 75:25. However, with further increments to 50:50 and 0:100, pure water flux declined to  $45.3 \pm 1.45 \text{ L/m}^2\cdot\text{h}$ . The initial increase in pure water flux at low 2,4-DABSA contents can be explained by the fact that in addition to the introduction of hydrophilic pendant sulfonic acid groups in the polyamide chain (Fig. 6.1), the phenyl backbone of 2,4-DABSA has a strong affinity for the organic phase, hence the formation of the polyamide film proceeds immediately at the reaction interface [29]. Therefore, the combination of the rigid but hydrophilic 2,4-DABSA with the PIP monomer, results in an increase in microporosity of the polyamide layer and backbone stiffness, which in turn led to the enhancement of membrane permeability. At higher 2,4-DABSA/PIP monomer weight ratios (50:50 and 0:100), pure water flux declined due to the increase in number of amidic hydrogens present in the amide linkages on polyamide thin-film layer [18]. Hydrogen bonds can form via the amide link of the semi-aromatic polyamide layer and excess carboxylate groups from unreacted acyl chloride monomers, during water filtration. The hydrogen bonds formed can then offer resistance to water transport, thus reducing membrane permeability while increasing the salt rejection rate [30].

Salt rejection by all membranes followed the order  $\text{Na}_2\text{SO}_4 > \text{MgSO}_4 > \text{NaCl}$ . The salt rejection pattern displayed is typical for negatively charged NF membranes surfaces [29]. The high rejection of  $\text{Na}_2\text{SO}_4$  and  $\text{MgSO}_4$  salts compared to  $\text{NaCl}$  can be explained by Donnan exclusion separation mechanism; membranes with negatively charged surfaces show more favourable rejections for divalent anions and monovalent cations [31]. It was easier for the negatively charged membrane surface to reject the divalent anion with the high valence ( $-\text{SO}_4^{2-}$ ) than the monovalent anion ( $-\text{Cl}^-$ ). With regards to lower rejection rates of  $\text{MgSO}_4$  compared to  $\text{Na}_2\text{SO}_4$ , this is attributable to the recombination between the rejected  $-\text{SO}_4^{2-}$  anions on the membrane

surface with  $Mg^{2+}$  cations, thereby shielding the effective membrane surface charge and reducing the Donnan exclusion effects and rejection performance [32]. The rejection of salts by the TFC NF membranes prepared with 2,4-DABSA monomer (NF\_M1\_25, NF\_M1\_50 and NF\_M1\_100), was found to be higher than that of the TFC NF membrane prepared with PIP only (NF\_M1\_0). This was due to the increased cross-linking of the polyamide layer. The cross-linking degree of the polyamide layer also increases as the content of 2,4-DABSA in the mixed amine monomer is increased. It can be concluded that at higher 2,4-DABSA monomer weight content and lower PIP concentration, the TFC membrane formed behaves less like an NF membrane and displays the behaviour of an RO membrane. Therefore, the optimum separation performance was found for the TFC NF membrane NF\_M1\_25, which showed a high water flux ( $90.70 \text{ L/m}^2\cdot\text{h}$ ) and optimum salts rejection of  $Na_2SO_4$  (98.1%),  $MgSO_4$  (91.4%), and  $NaCl$  (54.4%) respectively.

The pure water flux of TFC NF membranes was further investigated as a function of operating pressure, as shown in Fig. 6.8. Pure water flux of all the membranes was found to increase with an increase in pressure applied. Moreover, by calculating the inverse of the slope of the fitting line in Fig. 6.8, the membrane hydraulic resistance ( $R_m$ ) can be obtained [33]. The  $R_m$  value initially decreased from  $6.5 \times 10^{-2} \text{ m}^{-1}$  for NF\_M1\_0 to  $5.4 \times 10^{-2} \text{ m}^{-1}$  for NF\_M1\_25 followed by an increase to  $8.1 \times 10^{-2} \text{ m}^{-1}$  for NF\_M1\_50 and  $8.5 \times 10^{-2} \text{ m}^{-1}$  for NF\_M1\_100. The decline in hydraulic resistance is indicative of the weak resistance of the NF\_M1\_25 membrane to hydraulic pressure; and a subsequent enhancement in membrane permeability owing to the introduction of hydrophilic sulfonic acid groups and possible reduction in polyamide layer thickness. On the other hand, an increase in  $R_m$  value can be attributed to reduced membrane permeability as result of the presence of a dense and strongly cross-linked polyamide layer on the support membrane surface.

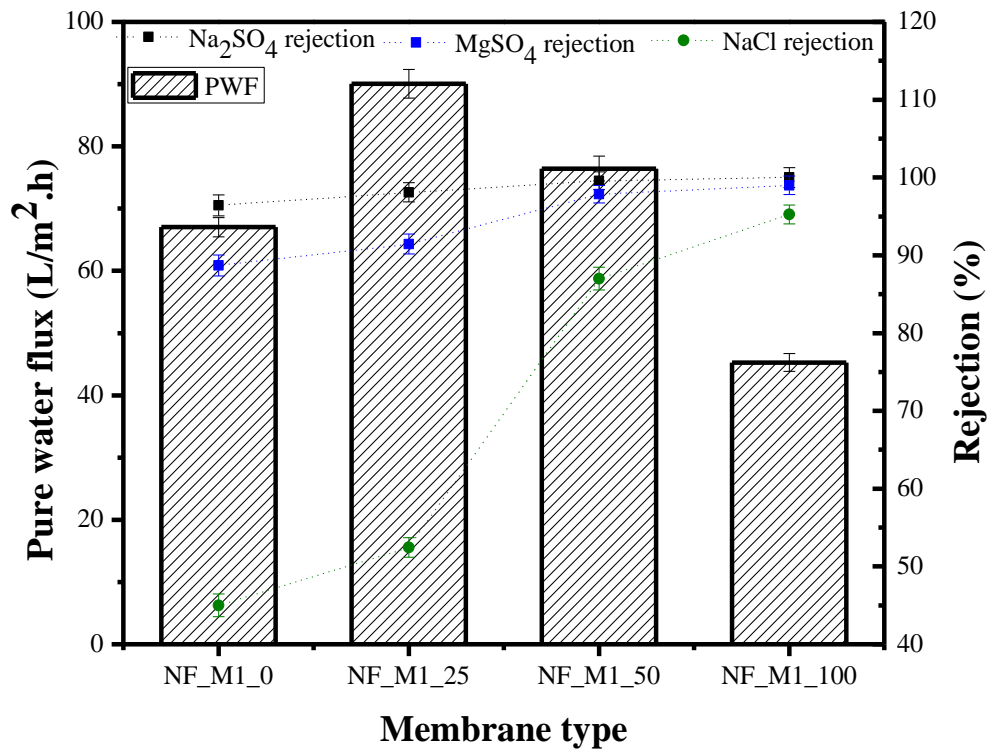


**Figure 6.7.** Effect of 2,4-DABSA monomer weight on pure water flux and salt rejection of TFC NF membranes.

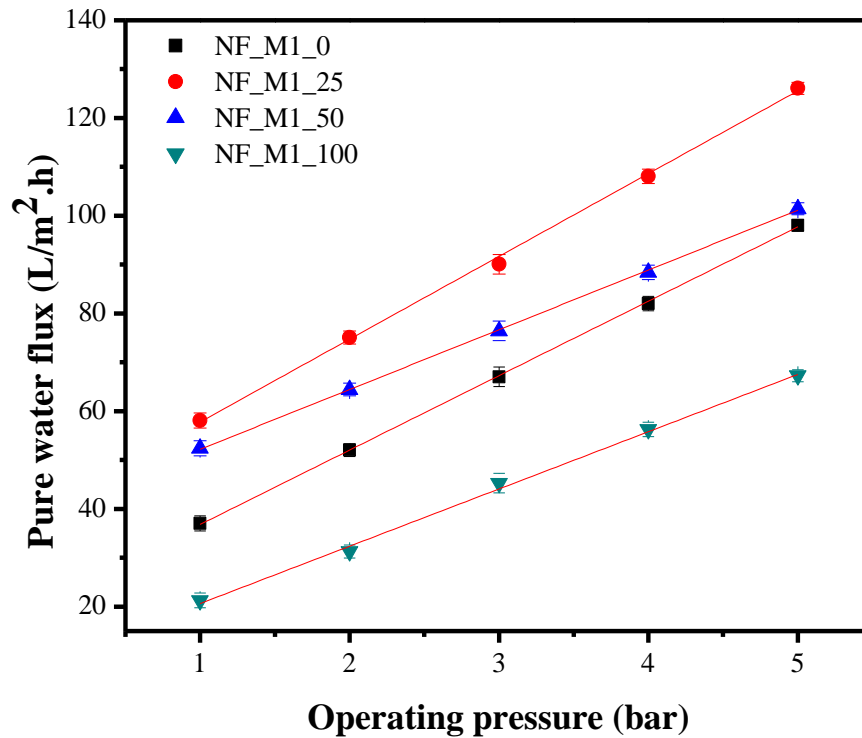


**Figure 6.8.** Pure water flux of TFC NF membranes as a function of operating pressure.

As shown in Fig. 6.9, the permeate flux of salt solutions were found to be lower (36.03 - 42.31 Lm<sup>2</sup>.h for NF\_M1\_0; 47.01 – 52.07 L/m<sup>2</sup>.h for NF\_M1\_25; 44.42 – 47.42 L/m<sup>2</sup>.h for NF\_M1\_50; and 37.27 – 39.28 L/m<sup>2</sup>.h for NF\_M1\_100) compared to pure water fluxes owing to concentration polarisation on the membrane surface [34]. Nonetheless, permeation fluxes of 47.1 – 52.07 L/m<sup>2</sup>.h for NF\_M1\_25 for example, are still reasonably high for nanofiltration performance under low pressure application.

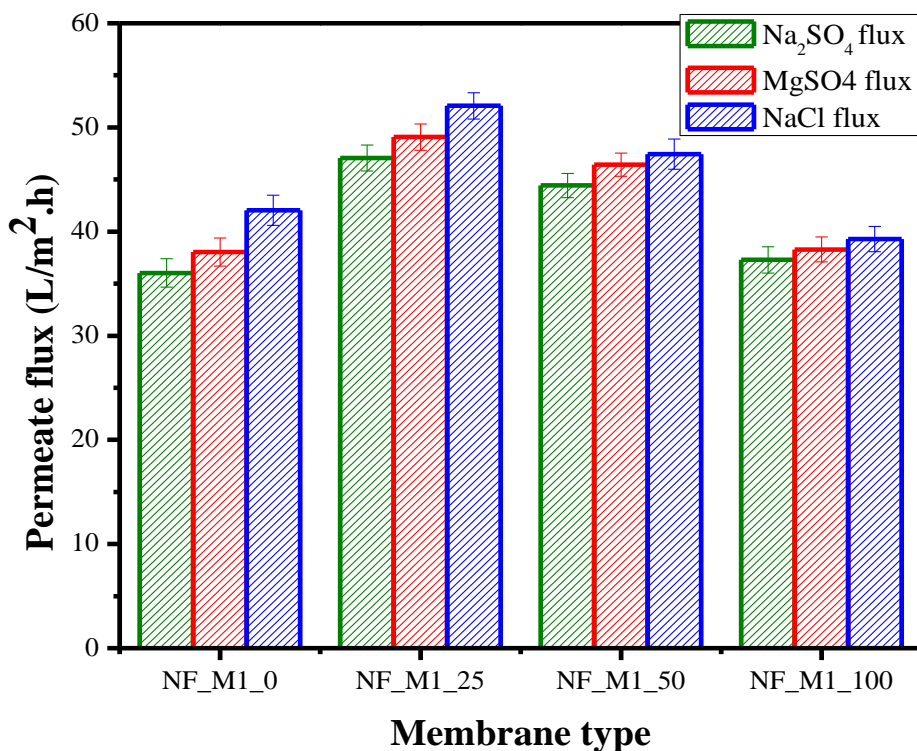


**Figure 6.9.** Salt flux of TFC NF membranes prepared from different 2,4-DABSA monomer weight ratios.

To evaluate the performance of our sulfonated TFC NF membranes with those previously reported in the literature, a comparison was made based on pure water permeability (PWP), salt selectivity and operating pressure (Table 6.3). Based on the data reported in Table 6.3, the NF\_M1\_25 membranes exhibited high water permeability and high monovalent/bivalent salt selectivity at low operating pressures and at salt concentrations in the range of brackish water salinity. The enhanced performance compared to previous works of sulfonated TFC NF is attributable to the properties of the combined effect of negative charged polyamide surface with structural properties of the PES/SPSf/O-MWCNT support membrane used; the high hydrophilicity and large surface pore size ensures the formation of a thin polyamide layer on top of the support, in turn enhancing the permeability of the formed TFC NF membranes. On the other hand, the presence of pendant sulfonic acid groups, increases the negative surface

charge of the membrane thereby increasing the rejection of salts. Correspondingly, the sulfonated TFC NF membrane fabricated in this study, display promising features to use as pretreatment membranes for the desalination of brackish water.

**Table 6.3** Comparison of sulfonated TFC NF membrane performance in terms of pure water permeability and salt selectivity.

<b>Monomers/support</b>	<b>PWP (L/m<sup>2</sup>.h.bar<sup>-1</sup>)</b>	<b>Salt concentration (ppm)</b>	<b>Salt selectivity (NaCl/Na<sub>2</sub>SO<sub>4</sub>)</b>	<b>Operating pressure (bar)</b>	<b>Ref</b>
BDSA+PIP/PES	12.3	2000	12.1	4	[26]
2,5-DABSA+PIP/PAN	20.4	1000	13.6	3	[23]
BDSA/PSf	16.6	1000	9.7	6	[29]
SPEEK/PPEsk	14.4	1000	4.2	2.5	[35]
BAPBS/PSf	12.1	1000	7.5	6	[36]
2,5-DABSA+PIP/PES	11.5	1420	30.0	4	[37]
2,4-DABSA +PIP /PES/SPSf/O- MWCNT	30.2	2000	25.0	3	This work

BDSA - 2,2'-benzidinedisulfonic acid, PAN – polyacrylonitrile, PSf- polysulfone, SPEEK - sulfonated poly (phthalazinone ether sulfone ketone), PPEsk – poly (phthalazinone ether sulfone ketone), BAPBS - potassium 2,5-bis(4-aminophenoxy) benzenesulfonate

#### 6.3.4. ATR- FTIR analyses of TFC NF membranes

To evaluate the changes in surface functional groups upon introduction of the polyamide layer on the support membrane and the components thereof, ATR-FTIR analysis of TFC NF membranes was conducted. It can be seen from Fig. 6.10 that all membranes contain the peaks

at  $\sim 1087\text{ cm}^{-1}$  and  $1235\text{ cm}^{-1}$  corresponding to the  $-\text{SO}_2$  symmetric and asymmetric stretching of the sulfonic acid groups in the support layer polymer backbone. Traces of the support layer can be detected from spectra of the TFC NF membranes, suggesting that the polyamide layer deposited does not completely cover the effective surface area of the support membrane. A shoulder peak at  $1632\text{ cm}^{-1}$  is characteristic of the  $-\text{C}=\text{O}$  groups of the amide bond [38]. The emergence of the doublet peaks at  $\sim 3101 - 3052\text{ cm}^{-1}$  is due to the  $-\text{NH}$  stretching vibrations. The  $-\text{C}=\text{O}$  overtone of the  $-\text{CONH}$  bond is represented by the broad peak at  $3409\text{ cm}^{-1}$ . Moreover, the NF\_M1\_100 membranes which is made up entirely of the 2,4-DABSA amine monomer with TMC, shows an additional high intensity peak at  $1702\text{ cm}^{-1}$  due to  $-\text{C}=\text{O}$  groups from unreacted acyl chloride monomers. This occurs as a result of the rapid diffusion of the 2,4-DABSA monomer into the organic phase to form a dense and highly cross-linked polyamide layer, thus preventing more monomers to reach the reaction zone [26]. The peaks identified with their corresponding functional groups confirm successful deposition of the polyamide film layer on the support membrane surface.

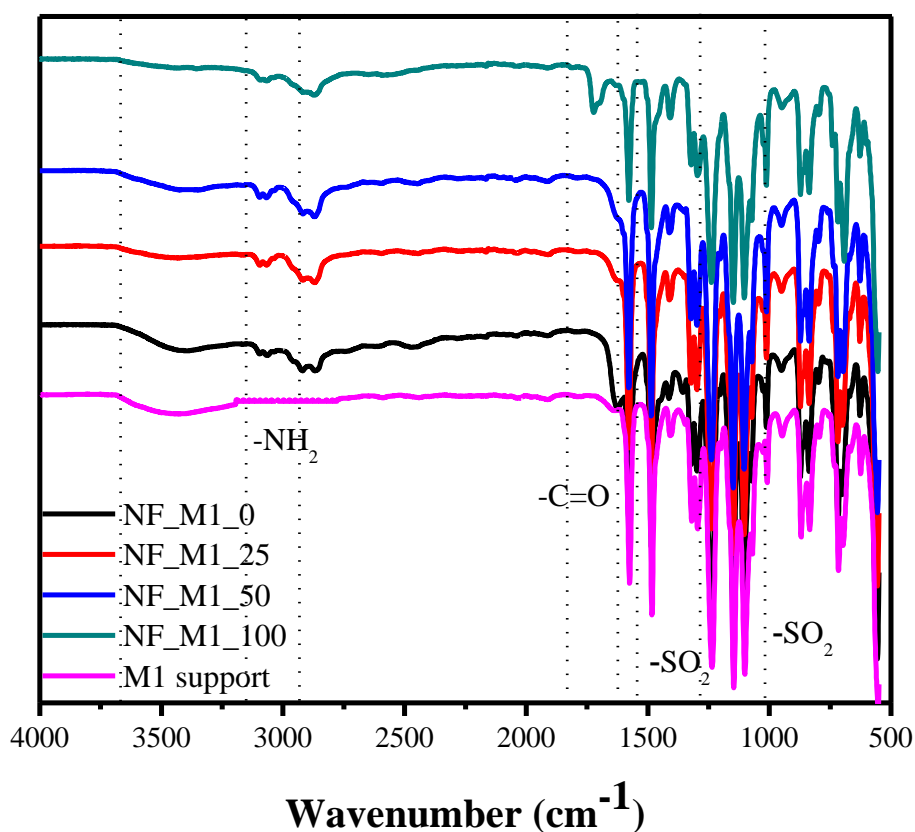


**Figure 6.10.** FTIR spectra of TFC NF membranes prepared from different 2,4-DABSA monomer weight ratios.

### 6.3.5. Microstructure analysis

The surface and cross-sectional morphologies of the support and TFC NF membranes were analysed by FE-SEM in order to evaluate (i) changes in membrane morphology of the support membrane upon the introduction of the polyamide film and (ii) the nature of the polyamide film formed from different amine monomer weight ratios. As shown in Fig. 6.11, the surface morphology changed from a relatively smooth surface for the M1 support membrane to a granular surface for the NF\_M1\_0 membrane. The granular morphology is typical for polyamide TFC NF membranes made from PIP monomers [27]. Upon introduction of the lower content of 2,4-DABSA monomer (NF\_M1\_25), the membrane surface changed from

polyamide granules to consist of cross-linked structures with ridge-and-valley morphology. This is due to the increase in cross-linking degree of the polyamide layer upon the inclusion of the aromatic diamine monomer. With further increments in 2,4-DABSA monomer weight ratio, the polyamide layer deposited on the membrane surface was found to become denser and more tightly cross-linked with low-free volume on the support membrane surface. Close examination of the SEM cross-sectional images at higher magnifications and rough estimation of the polyamide film thickness showed an increase in polyamide film thickness (from 50 – 150 nm) with an increase in the 2,4-DABSA monomer weight ratio. The increase in polyamide film thickness is in line with observed TFC NF membrane performance in terms of pure water flux and salt rejection as discussed in section 6.3.3. The inset in cross-sectional image of the support membrane M1, shows the internal structure of the macrovoid-free support layer morphology at higher magnifications. It can be seen that the macrovoid-free structure consists of open, cellular network structures that allow for the enhancement in water permeabilities of the support and the fabricated TFC NF membranes. As such, a macrovoid-free support is able to generate TFC NF membranes with enhanced water permeabilities.

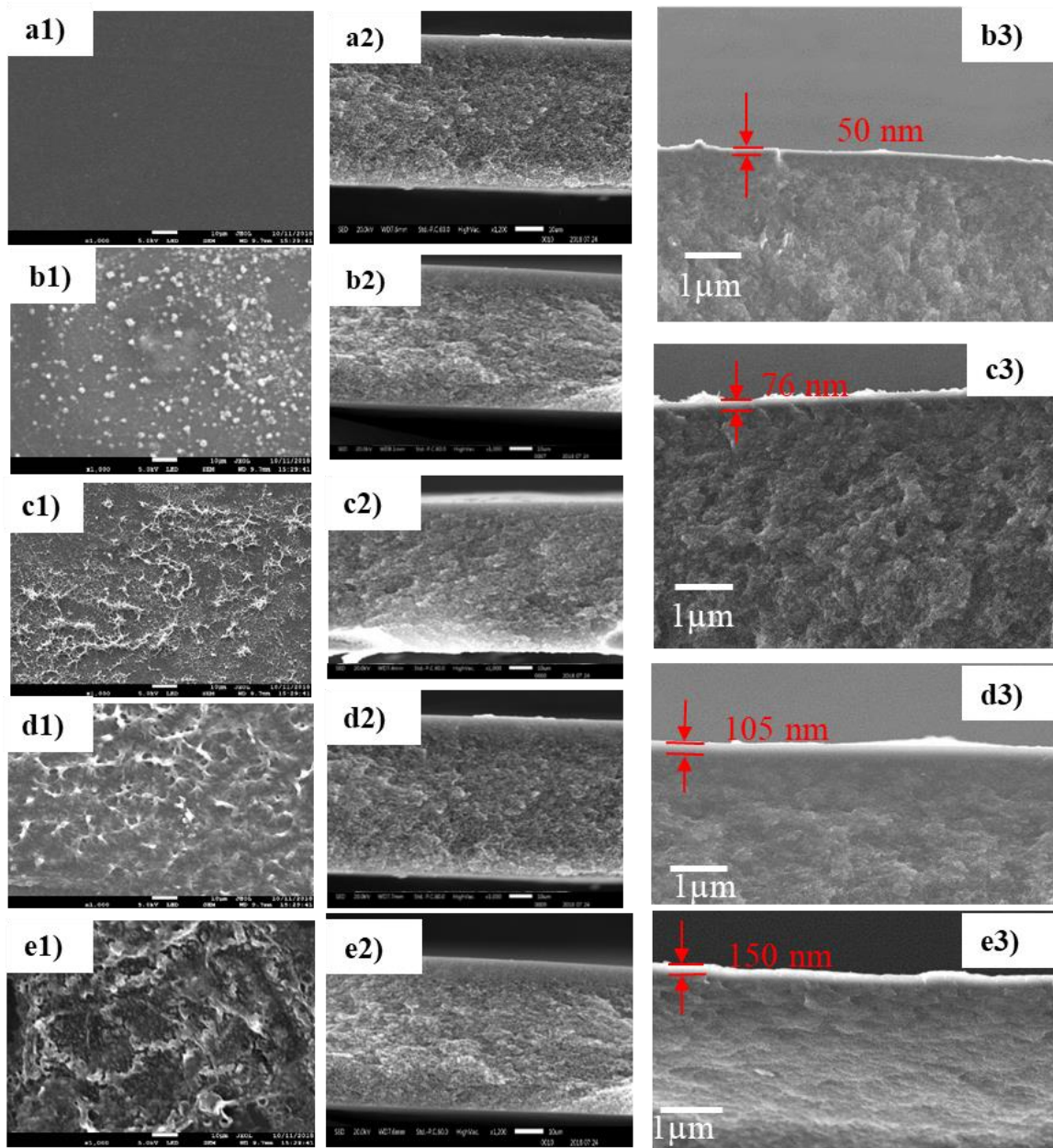


**Figure 6.11** SEM surface (1) and cross-sectional images (2 and 3) of UF support and TFC NF membranes; (a) M1 support UF membrane, (b) NF\_M1\_0, (c) NF\_M1\_25, (d) NF\_M1\_50 and (e) NF\_M1\_100.

The surface characterisation of the support UF membrane and TFC NF membranes by AFM was conducted to evaluate changes in membrane surface roughness upon deposition on the polyamide layer. It can be seen in Fig. 6.12 that the roughness parameters ( $S_a$  and  $S_q$ ) of TFC NF membranes were much larger than those of the support membrane, owing to the presence

of the rigid polyamide layer on the support membrane surface. The roughness results are in agreement with findings from SEM analysis (Fig. 6.11). Moreover, upon the introduction of the lower contents of the 2,4-DABSA monomer, surface roughness initially declined from  $S_q = 48.3$  nm for NF\_M1\_0 to  $S_q = 32.7$  nm for NF\_M1\_25 membranes. The PIP monomer with a smaller molecular-weight and higher partition coefficient ( $M_w = 86.4$  g/mol,  $\log K_{ow} = -1.50$ ) than that of the 2,4-DABSA monomer ( $M_w = 188.20$  g/mol,  $\log K_{ow} = -4.65$ ), easily diffuses into the reaction interface to react with acyl chloride monomer, thereby generating smoother membrane surface [26, 39]. However, with further increments in 2,4-DABSA monomer weight ratio, the surface roughness of membranes NF\_M1\_50 and NF\_M1\_100 increased to  $S_q = 51.4$  nm and 60.9 nm due to the increased in cross-linking degree of the polyamide layer formed from the majority of the aromatic diamine monomer. Moreover, the increase density of sulfonic acid groups inside the polyamide chains results in swelling of the polyamide film thereby increasing membrane surface roughness [23].

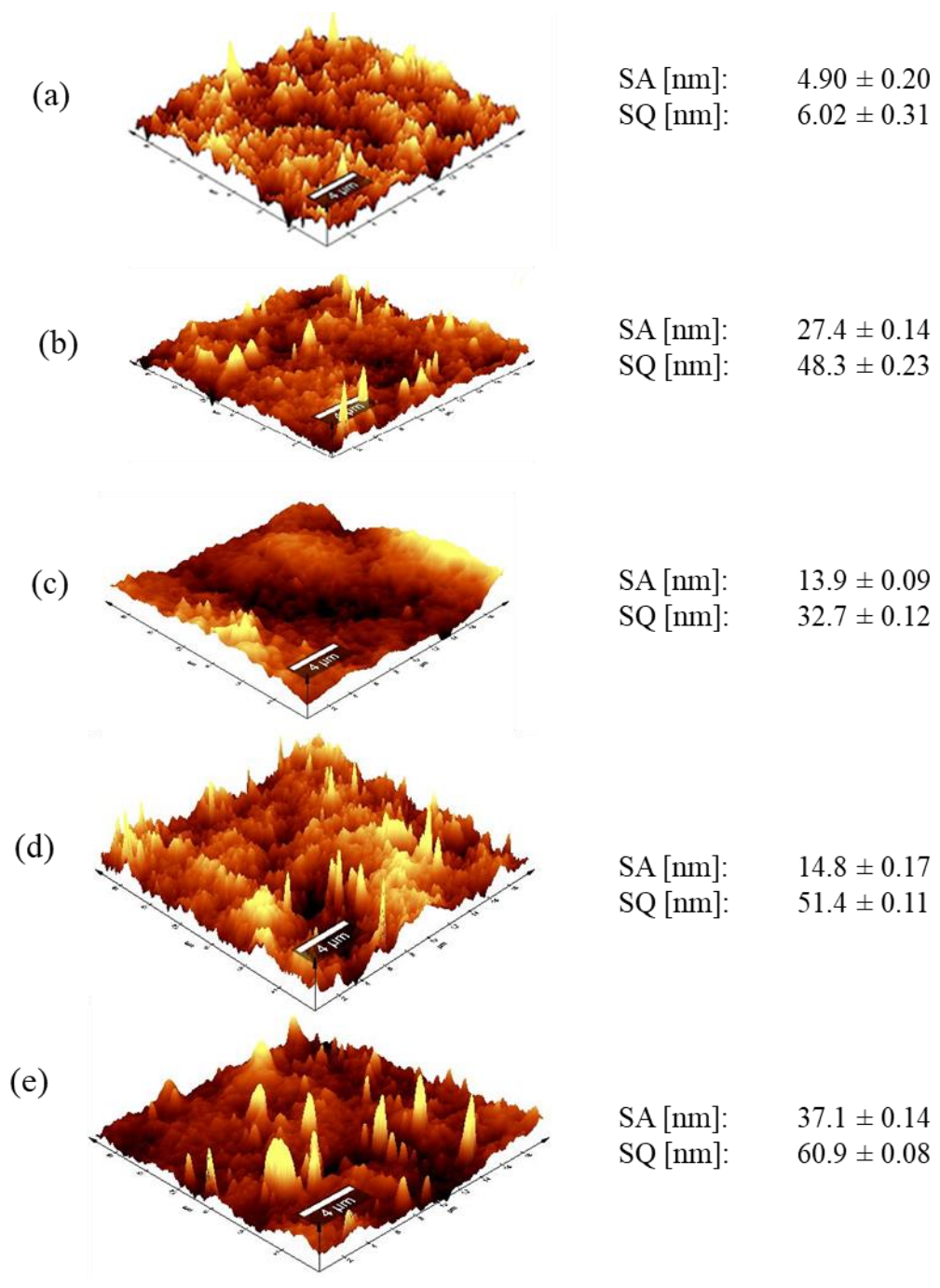


**Figure 6.12** AFM topographic images of support UF and TFC NF membranes; (a) M1 support UF membrane, (b) NF\_M1\_0, (c) NF\_M1\_25, (d) NF\_M1\_50 and (e) NF\_M1\_100.

### 6.3.6. Contact angle and surface charge measurements

Contact angle measurements were conducted to study the changes in surface hydrophilicity of the polyamide TFC NF membranes induced by different 2,4-DABSA monomer weight ratios. It can be seen from Fig. 6.13 that the contact angle value of NF\_M1\_0 membrane made from PIP amine monomer only is much lower ( $35.9^\circ$ ) than that of the support UF membrane (M1 =  $58.7^\circ$ ) (Table 6.1), suggesting that the presence of the polyamide bonds improves the hydrophilicity of the membranes. With the incorporation of low contents of 2,4-DABSA monomer, the contact angle of the NF\_M1\_25 membrane decreased further to  $29.8^\circ$ , owing to the presence of both polyamide groups on the membrane surface and the pendant sulfonic acid groups of the 2,4-DABSA monomer in the polyamide chain. However, with further increments in the 2,4-DABSA monomer weight ratio, a slight decline in surface hydrophilicity was observed for NF\_M1\_50 and NF\_M1\_100 membranes as evidenced by an increase in contact angle values to  $43.2^\circ$  and  $65.6^\circ$ . It would be expected that at higher 2,4-DABSA monomer weight ratios, the membrane surface hydrophilicity of the polyamide TFC membrane would increase due to the increase in density of the sulfonic acid groups in the polyamide chain, and a large number of unreacted acyl chloride groups on the membrane surface or properly washed out during TFC NF membrane preparation. However, the increase in cross-linking degree of the polyamide film at higher 2,4-DABSA monomer weight ratio, reduces the water absorption ability of the membrane surface, thus reducing membrane hydrophilicity [18].

The surface charge of TFC NF membranes was determined by measuring their zeta potential values at neutral pH of 6.6. Membrane surface charge played a vital role in the separation of salts since the Donnan exclusion effects are governed by the surface charge (see discussion in Section 6.3.3). As shown in Fig. 6.14, all the TFC NF membranes are negatively charged at the

neutral pH; the membranes become more negatively charged as the 2,4-DABSA monomer weight ratio is increased. This phenomenon is attributable to the increase in density of pendant sulfonic acid groups on the polyamide chain, and unreacted acyl chloride monomers on the membrane surface that become hydrolysed into carboxylate groups as observed from ATR-FTIR analysis. Similar findings were previously reported by Ghaee et al. [40], for thin-film nanocomposite membranes manufactured using a mixture m-phenylenediamine (m-PDA) and 2,4-DABSA monomers on a PSf support layers.

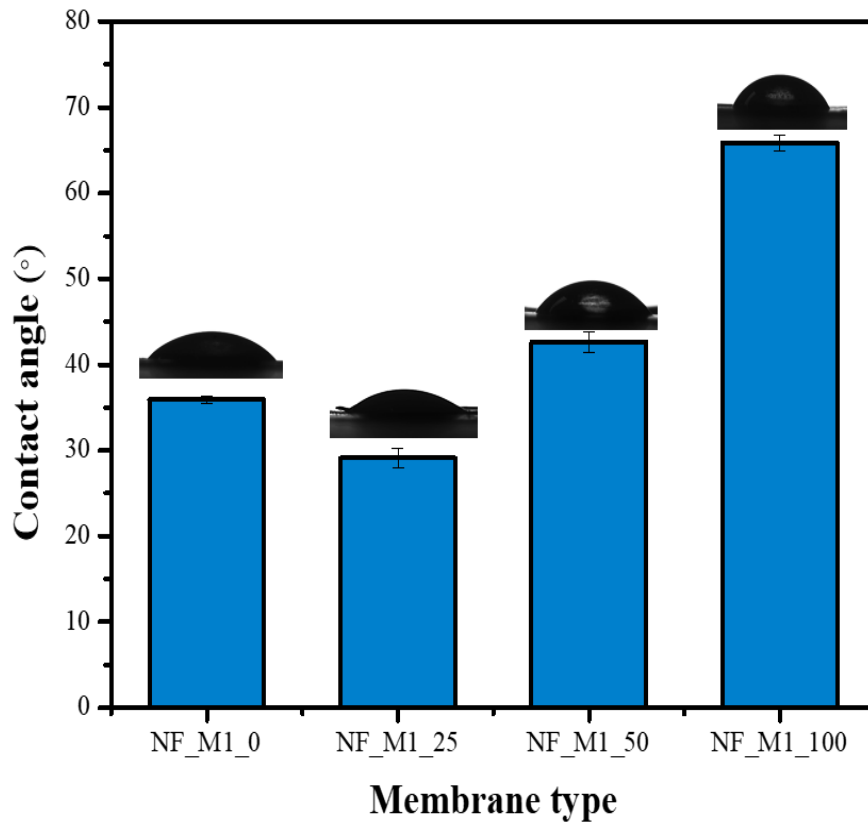


**Figure 6.13** Contact angle values of TFC NF membranes prepared from different 2,4-DABSA monomer weight ratios.

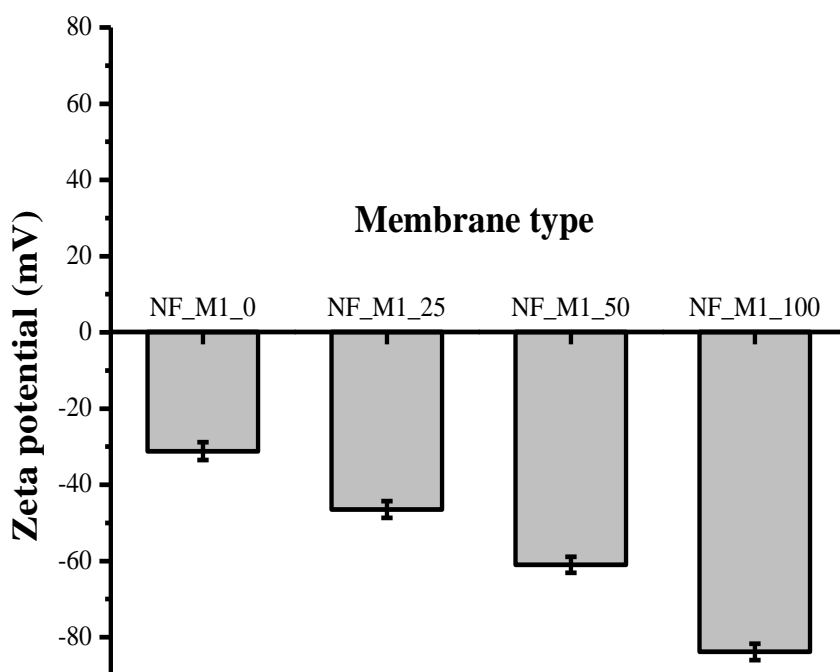


**Figure 6.14** Zeta potential of TFC NF membranes prepared with different 2,4-DABSA monomer weight ratios.

### 6.3.7. Antifouling tests and performance stability

Antifouling tests were conducted on three representative TFC NF membranes, namely NF\_M1\_0, NF\_M1\_25 and NF\_M1\_100, over three fouling and cleaning cycles using BSA solution as a model foulant (0.1 g/L BSA solution) and deionised water as a cleaning solution. The permeability was measured every 10 min and the normalised flux of the membrane ( $J_1/J_0$ ) was plotted against filtration time as given in Fig. 6.15. To better quantify the fouling resistance of the membranes, the flux decline rate (FDR) and flux recovery ratio (FRR) were calculated from the results plotted in Fig. 6.15. Although the FDR of all the membranes was above 38%, the FRR after three fouling and cleaning stages was found to be the highest for NF\_M1\_25 at 96.9% compared to 88.9% for NF\_M1\_0 and 76.4% for NF\_M1\_100. The increase in FRR for NF\_M1\_25 membranes is attributable to the increase in membrane hydrophilicity and decrease in surface roughness, which minimises the adsorption of BSA molecules on the membrane

surface. On the other hand, the increase in surface roughness of NF\_M1\_100 led to an increase in membrane fouling propensity owing to the large number of attachment sites for BSA molecules on the membrane surface [41].

Long-term membrane performance stability tests were carried out on the best performing TFC NF membrane in the series, namely NF\_M1\_25, under a pressure of 3 bar, using pure water flux and Na<sub>2</sub>SO<sub>4</sub> rejection experiments over a period of 10 days. It can be seen from Fig. 6.16 that both pure water flux and salt rejection remained fairly constant, with minor variations over the testing period. This finding suggests that the sulfonated polyamide layer was efficiently attached into the support membrane surface and did not detach during prolonged filtration. This is indicative of the good compatibility between the deposited sulfonated polyamide layer and the PES/SPSf/O-MWCNT support membrane used [24].

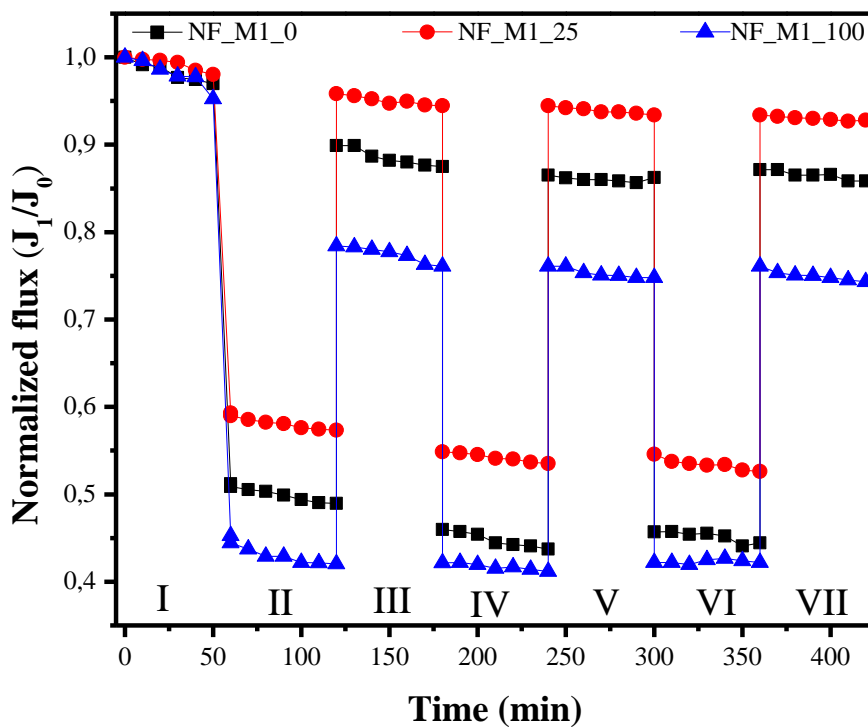


**Figure 6.15** Normalised flux of TFC NF membranes using BSA as model foulant.

**Table 6.4** Antifouling performance parameters of TFC NF membranes.

Membrane used	FDR (%)	FRR (%)
NF_M1_0	48.8	88.9
NF_M1_25	39.5	96.9
NF_M1_100	58.8	76.4

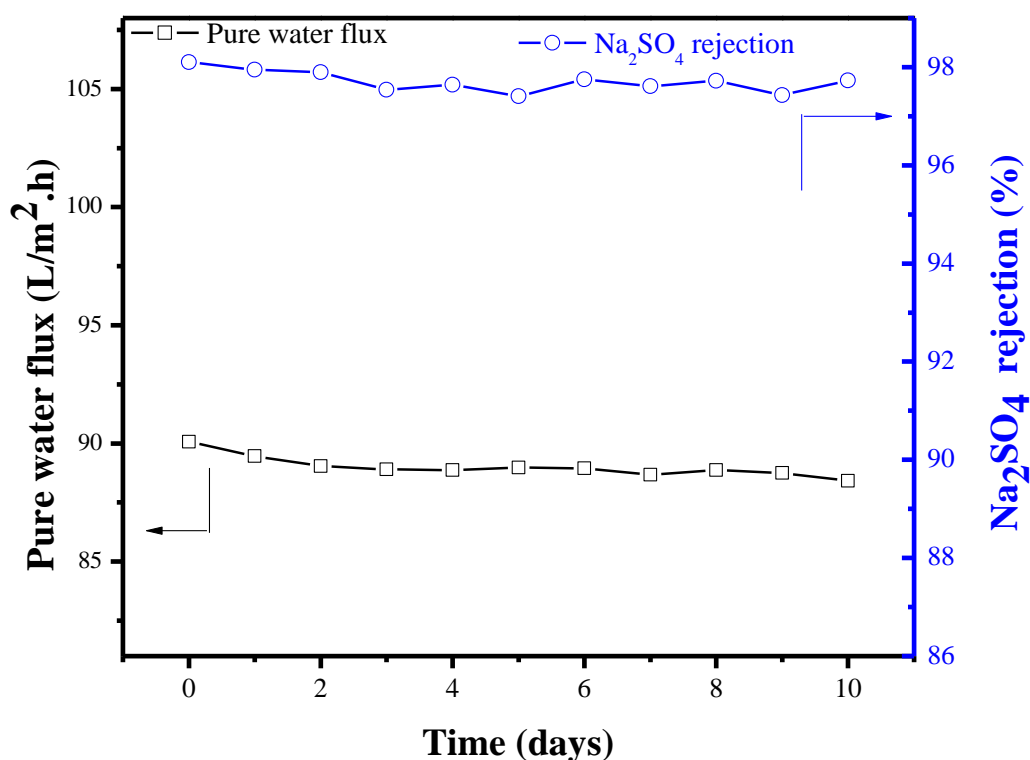


**Figure 6.16** Performance stability of NF\_M1\_25 membrane based on pure water flux and Na<sub>2</sub>SO<sub>4</sub> rejection.

#### 6.4. Conclusion

The study demonstrated the ability of macrovoid-free PES/SPSf/O-MWCNT ultrafiltration membranes to be used as support membranes for the deposition of a sulfonated polyamide thin-film layer. The open, cellular network structure of the support membrane morphology combined with high hydrophilicity and large surface pore sizes were beneficial in the reduction

of polyamide layer thickness, and subsequently in the performance enhancement of TFC NF membrane performance. The presence of hydrophilic O-MWCNTs in the PES/SPSf support membrane allows for the hydrogen bonding interactions with the PIP monomer, leading to the formation of a thin polyamide layer on the top surface which is responsible for enhanced water permeability and the formation of a polyamide rejection layer within the support membrane pore channels. The combination of traditional PIP monomer used for TFC NF membrane fabrication with low amounts of 2,4-DABSA monomer (75:25 PIP/2,4-DABSA) led to significant improvements in membrane pure water permeability (30.2 L/m<sup>2</sup>.h. bar), monovalent/bivalent salt selectivity (25.0) at low operating pressure of 3 bar, at salt concentrations in the range of brackish water salinity compared to those previously reported in literature. The rejection of salts under neutral conditions followed the order Na<sub>2</sub>SO<sub>4</sub> > MgSO<sub>4</sub> > NaCl, which is consistent with negatively charged membrane surfaces based on the Donnan exclusion effect. The antifouling tests showed that the NF\_M1\_25 membrane with low content of the 2,4-DABSA monomer had the highest fouling resistance against BSA molecules, with an FDR of 39% and a high FRR of 96.4%. The TFC NF membrane performance in terms of pure water flux and Na<sub>2</sub>SO<sub>4</sub> rejection remained fairly stable over a 10-day period of testing, suggesting good compatibility between the polyamide layer and the support membrane. The fabricated sulfonated TFC NF membrane on PES/SPSf/O-MWCNT membrane supports display promising features for use in the desalination of environmental brackish waters. Sulfonated TFC NF membranes with a hollow fibre configuration can also be prepared following the method presented in this study, as they present more opportunities for practical applications.

## 6.5. References

- [1] W. Lau, A. Ismail, N. Misdan, M. Kassim, A recent progress in thin film composite membrane: a review, *Desalination*, 287 (2012) 190-199.
- [2] M.T.M. Pendergast, E.M. Hoek, A review of water treatment membrane nanotechnologies, *Energy & Environmental Science*, 4 (2011) 1946-1971.
- [3] A.K. Ghosh, E.M. Hoek, Impacts of support membrane structure and chemistry on polyamide-polysulfone interfacial composite membranes, *Journal of Membrane Science*, 336 (2009) 140-148.
- [4] L. Li, S. Zhang, X. Zhang, G. Zheng, Polyamide thin film composite membranes prepared from isomeric biphenyl tetraacyl chloride and m-phenylenediamine, *Journal of Membrane Science*, 315 (2008) 20-27.
- [5] E.-S. Kim, G. Hwang, M.G. El-Din, Y. Liu, Development of nanosilver and multi-walled carbon nanotubes thin-film nanocomposite membrane for enhanced water treatment, *Journal of Membrane Science*, 394 (2012) 37-48.
- [6] B.-H. Jeong, E.M. Hoek, Y. Yan, A. Subramani, X. Huang, G. Hurwitz, A.K. Ghosh, A. Jawor, Interfacial polymerisation of thin film nanocomposites: a new concept for reverse osmosis membranes, *Journal of Membrane Science*, 294 (2007) 1-7.
- [7] F.-Y. Zhao, Y.-L. Ji, X.-D. Weng, Y.-F. Mi, C.-C. Ye, Q.-F. An, C.-J. Gao, High-flux positively charged nanocomposite nanofiltration membranes filled with poly (dopamine) modified multiwall carbon nanotubes, *ACS Applied Materials & Interfaces*, 8 (2016) 6693-6700.
- [8] P.S. Singh, S. Joshi, J. Trivedi, C. Devmurari, A.P. Rao, P. Ghosh, Probing the structural variations of thin film composite RO membranes obtained by coating polyamide over polysulfone membranes of different pore dimensions, *Journal of Membrane Science*, 278 (2006) 19-25.
- [9] H.I. Kim, S.S. Kim, Plasma treatment of polypropylene and polysulfone supports for thin film composite reverse osmosis membrane, *Journal of Membrane Science*, 286 (2006) 193-201.
- [10] A. Tiraferri, N.Y. Yip, W.A. Phillip, J.D. Schiffman, M. Elimelech, Relating performance of thin-film composite forward osmosis membranes to support layer formation and structure, *Journal of Membrane Science*, 367 (2011) 340-352.
- [11] A.K. Ghosh, B.-H. Jeong, X. Huang, E.M. Hoek, Impacts of reaction and curing conditions on polyamide composite reverse osmosis membrane properties, *Journal of Membrane Science*, 311 (2008) 34-45.
- [12] N. Widjojo, T.-S. Chung, M. Weber, C. Maletzko, V. Warzelhan, The role of sulphonated polymer and macrovoid-free structure in the support layer for thin-film composite (TFC) forward osmosis (FO) membranes, *Journal of Membrane Science*, 383 (2011) 214-223.
- [13] M. Fathizadeh, A. Aroujalian, A. Raisi, Effect of lag time in interfacial polymerisation on polyamide composite membrane with different hydrophilic sub layers, *Desalination*, 284 (2012) 32-41.

- [14] M. Fathizadeh, A. Aroujalian, A. Raisi, Preparation and characterisation of thin film composite reverse osmosis membranes with wet and dry support layer, *Desalination and Water Treatment*, 56 (2015) 2284-2295.
- [15] N.Y. Yip, A. Tiraferri, W.A. Phillip, J.D. Schiffman, M. Elimelech, High performance thin-film composite forward osmosis membrane, *Environmental Science & Technology*, 44 (2010) 3812-3818.
- [16] R. Wang, L. Shi, C.Y. Tang, S. Chou, C. Qiu, A.G. Fane, Characterisation of novel forward osmosis hollow fiber membranes, *Journal of Membrane Science*, 355 (2010) 158-167.
- [17] N. Peng, T.-S. Chung, K.Y. Wang, Macrovoid evolution and critical factors to form macrovoid-free hollow fiber membranes, *Journal of Membrane Science*, 318 (2008) 363-372.
- [18] J.M. Gohil, P. Ray, A review on semi-aromatic polyamide TFC membranes prepared by interfacial polymerisation: Potential for water treatment and desalination, *Separation and Purification Technology*, 181 (2017) 159-182.
- [19] C. Ding, J. Yin, B. Deng, Effects of polysulfone (PSf) support layer on the performance of thin-film composite (TFC) membranes, *Journal of Chemical and Process engineering*, 1 (2014) 1-8.
- [20] N. Misdan, W. Lau, A. Ismail, T. Matsuura, Formation of thin film composite nanofiltration membrane: effect of polysulfone substrate characteristics, *Desalination*, 329 (2013) 9-18.
- [21] N.N. Gumbi, M. Hu, B.B. Mamba, J. Li, E.N. Nxumalo, Macrovoid-free PES/SPSf/O-MWCNT ultrafiltration membranes with improved mechanical strength, antifouling and antibacterial properties, *Journal of Membrane Science*, 566 (2018) 288-300.
- [22] H. Dong, L. Zhao, L. Zhang, H. Chen, C. Gao, W.W. Ho, High-flux reverse osmosis membranes incorporated with NaY zeolite nanoparticles for brackish water desalination, *Journal of Membrane Science*, 476 (2015) 373-383.
- [23] A. Akbari, E. Aliyarizadeh, S.M.M. Rostami, M. Homayoonfal, Novel sulfonated polyamide thin-film composite nanofiltration membranes with improved water flux and anti-fouling properties, *Desalination*, 377 (2016) 11-22.
- [24] W.-J. Lau, G.-S. Lai, J. Li, S. Gray, Y. Hu, N. Misdan, P.-S. Goh, T. Matsuura, I.W. Azelee, A.F. Ismail, Development of microporous substrates of polyamide thin film composite membranes for pressure-driven and osmotically-driven membrane processes: A review, *Journal of Industrial and Engineering Chemistry*, (2019).
- [25] J. Lee, H. Yoon, J.H. Yoo, D.-C. Choi, C.H. Nahm, S.H. Lee, H.-R. Chae, Y.H. Kim, C.-H. Lee, P.-K. Park, Influence of a sublayer structure of thin-film composite reverse osmosis membranes on the overall water flux, *Environmental Science: Water Research & Technology*, 4 (2018) 1912-1922.
- [26] B.-Q. Huang, Z.-L. Xu, H. Ding, M.-C. Miao, Y.-J. Tang, Antifouling sulfonated polyamide nanofiltration hollow fiber membrane prepared with mixed diamine monomers of BDSA and PIP, *RSC Advances*, 7 (2017) 56629-56637.
- [27] Y. Liu, S. Zhang, Z. Zhou, J. Ren, Z. Geng, J. Luan, G. Wang, Novel sulfonated thin-film composite nanofiltration membranes with improved water flux for treatment of dye solutions, *Journal of Membrane Science*, 394 (2012) 218-229.

- [28] A. Ismail, M. Padaki, N. Hilal, T. Matsuura, W. Lau, Thin film composite membrane—Recent development and future potential, *Desalination*, 356 (2015) 140-148.
- [29] J. Hu, Z. Lv, Y. Xu, X. Zhang, L. Wang, Fabrication of a high-flux sulfonated polyamide nanofiltration membrane: Experimental and dissipative particle dynamics studies, *Journal of Membrane Science*, 505 (2016) 119-129.
- [30] J. Jegal, S.G. Min, K.H. Lee, Factors affecting the interfacial polymerisation of polyamide active layers for the formation of polyamide composite membranes, *Journal of Applied Polymer Science*, 86 (2002) 2781-2787.
- [31] H. Tang, J. He, L. Hao, F. Wang, H. Zhang, Y. Guo, Developing nanofiltration membrane based on microporous poly (tetrafluoroethylene) substrates by bi-stretching process, *Journal of Membrane Science*, 524 (2017) 612-622.
- [32] M. Aiba, T. Tokuyama, S. Baba, H. Matsumoto, H. Tomioka, T. Higashihara, M. Ueda, Improvement in semipermeable membrane performance of wholly aromatic polyamide through an additive processing strategy, *Journal of Polymer Science Part A: Polymer Chemistry*, 52 (2014) 1275-1281.
- [33] D.L. Arockiasamy, J. Alam, M. Alhoshan, Carbon nanotubes-blended poly (phenylene sulfone) membranes for ultrafiltration applications, *Applied Water Science*, 3 (2013) 93-103.
- [34] J. Zhu, S. Yuan, A. Uliana, J. Hou, J. Li, X. Li, M. Tian, Y. Chen, A. Volodin, B. Van der Bruggen, High-flux thin film composite membranes for nanofiltration mediated by a rapid co-deposition of polydopamine/piperazine, *Journal of Membrane Science*, 554 (2018) 97-108.
- [35] S. Zhang, X. Jian, Y. Dai, Preparation of sulfonated poly (phthalazinone ether sulfone ketone) composite nanofiltration membrane, *Journal of Membrane Science*, 246 (2005) 121-126.
- [36] Z. Lv, J. Hu, J. Zheng, X. Zhang, L. Wang, Antifouling and high flux sulfonated polyamide thin-film composite membrane for nanofiltration, *Industrial & Engineering Chemistry Research*, 55 (2016) 4726-4733.
- [37] X.-Z. Wei, Z.-Q. Gan, Y.-J. Shen, Z.-L. Qiu, L.-F. Fang, B.-K. Zhu, Negatively-charged nanofiltration membrane and its hexavalent chromium removal performance, *Journal of Colloid and Interface science*, (2019).
- [38] G.N.B. Baroña, J. Lim, B. Jung, High performance thin film composite polyamide reverse osmosis membrane prepared via m-phenylenediamine and 2, 2'-benzidinedisulfonic acid, *Desalination*, 291 (2012) 69-77.
- [39] C. Hansch, A. Leo, D. Hoekman, Exploring QSAR: fundamentals and applications in chemistry and biology, American Chemical Society Washington, DC, 1995.
- [40] A. Ghaee, M. Zerafat, P. Askari, S. Sabbaghi, B. Sadatnia, Fabrication of polyamide thin-film nanocomposite membranes with enhanced surface charge for nitrate ion removal from water resources, *Environmental technology*, 38 (2017) 772-781.
- [41] D. Rana, T. Matsuura, Surface modifications for antifouling membranes, *Chemical Reviews*, 110 (2010) 2448-2471.

## CHAPTER 7

### GENERAL CONCLUSIONS AND RECOMMENDATIONS

---

#### 7.1. General conclusions

The study has provided proof of concept by demonstrating the ability of O-MWCNT-incorporated polymeric membranes to be effectively used as adsorptive membranes (for the removal of steroid hormones), as molecular-sieving UF membranes and as support membranes for the preparation of TFC NF membranes. Whilst a significant amount of work has been covered in the area of CNT/polymer composite mixed-matrix membranes in the previous years, the study has shed new insights on the following aspects of O-MWCNT-enhanced polymer composite membranes:

- The addition of hydrophilic O-MWCNTs in polymer matrices does not always lead to the enhancement of membrane permeability. In as much as phase-separation kinetics are accelerated during coagulation, leading to the formation of a porous membrane structure, the presence of O-MWCNTs in an otherwise “vacant” polymer matrix can induce pore plugging and a subsequent decrease in membrane permeability.
- Membrane pore size has the upper hand over hydrophilic effects in PES/O-MWCNT membranes and dictates the resultant mixed-matrix membrane permeability and selectivity performance.
- O-MWCNT content in the polymeric mixed-matrix composite membranes is the determining factor of the changes (enhancement or deterioration thereof) in modified membrane properties.

- Large pore-sized PES/O-MWCNT UF membranes can effectively adsorb low-molecular-weight steroid hormones via hydrogen bonding and  $\pi$ - $\pi$  interactions between graphene sheets of O-MWCNTs and aromatic rings of the hormones.
- Macrovoid-free morphology does not automatically translate into reduced membrane performance, in terms of increasing membrane resistance to water flow. The preparation method by which a sponge-like and macrovoid-free structure was created is vital. A sponge-like membrane morphology created through excessive increase in polymer concentrations, or by solvent evaporation prior to immersion in the coagulation bath or addition of solvent in the coagulation bath with low miscibility with the solvent used to dissolve the polymer, becomes dense and tightly packed, leading to reduced membrane permeability.
- The enhancement in mechanical strength properties of O-MWCNT-incorporated mixed-matrix membranes is only fully realised through the combination of O-MWCNTs and the proper control of membrane morphology by preventing the formation of macrovoid and finger-like structures. Although MWCNTs are well-known for their remarkable mechanical strength properties, previous studies have failed to realise significant enhancements in mechanical properties of composite membranes in the presence of MWCNTs. This is due to the fact that the membrane morphology, in most instances, possessed finger-like structures and macrovoids in the membrane sub-layer.
- The presence of hydrophilic O-MWCNT in the support membrane layer of TFC NF membrane, allows for hydrogen bonding interactions with the PIP monomer, leading to the formation of a thin polyamide layer on the top surface of the support membrane and polyamide rejection later within the pores of the support membrane substrate.

- The combination of low amounts of sulfonic acid monomer (2,4-DABSA) with the traditional PIP monomer used in the fabrication TFC NF membrane, led to significant improvements in membrane pure water permeability, monovalent/bivalent salt selectivity, at low operating pressures, and at salt concentrations in the range of brackish waters compared to those previously reported in literature.

## 7.2. Recommendations

Although the study has provided significant insights on the membrane structure and performance of O-MWCNT incorporated mixed-matrix membranes; the study can be extended further to incorporate the suggestions below:

- Identify membrane preparation method with the prospect of increasing the availability of O-MWCNTs in PES UF membrane, while minimising leachability; for maximum contact with the target steroid hormones or other class of EDCs, rapid adsorption kinetics and further improvements in adoptive capacity of the membrane.
- Evaluate, in more detail the effect of changes in solution chemistry on the adsorptive removal of steroid hormones, by varying ionic strength of the solution and testing for competitive adsorption in the presence of other organic pollutants such as natural organic matter. This will give conclusive evidence on the favourable separation mechanism by which the membranes are able to remove steroid hormones.
- Isolation and systematic evaluation of where exactly on the membrane does adsorption occur (membrane surface adsorption vs adsorption inside the membrane pores).
- Employ methods that could adequately measure the polyamide layer thickness formed on top of the support membrane and confirm the penetration and formation of the polyamide rejection layer within the support membrane pores.

- Prepare O-MWCNT nanocomposite UF and TFC NF membranes, with hollow fibre configuration, as they could offer higher packing densities and presents more opportunities for practical applications.
- Test the performance of the prepared UF and NF membranes on environmental brackish waters and real water samples contaminated with EDCs.

Indeed, research in the field of O-MWCNT mixed-matrix membranes will continue to grow due to prospects that the fabricated membranes present, particularly for water remediation applications. Interfacial interactions between the incorporated O-MWCNTs and the polymer matrices present ample opportunities for improvement in nascent polymer membrane properties, provided that homogenous dispersion of the incorporated O-MWCNTs can be effectively controlled as well as the resultant membrane sub-layer morphology. The O-MWCNT mixed-matrix membranes can benefit further from development of methods that can control dispersion of O-MWCNTs in the polymer matrix. Recently, Hu et al., demonstrated that the use of ultra-low contents of graphene oxide aqueous dispersion for PES/SPSf membrane modification, can result in significant enhancements in membrane permeability, antifouling and antibacterial properties [1]. Perhaps the preparation of O-MWCNT aqueous dispersions could be a starting point in the inhibiting of O-MWCNT agglomeration within the polymer matrices. As such, the content of O-MWCNT incorporated plays major role in control the membrane performance. Fabricated O-MWCNT-mixed-matrix membranes are envisaged to take centre-stage once the health concerns and cost of implications of O-MWCNTs have been adequately addressed. It is strongly believed that due to continued demand for MWCNTs, research on cost-effective methods for mass production of MWCNTs will also continue to grow leading to a significant drop in prices for MWCNTs.

### 7.3. Reference

1. Hu M., Cui Z., Li J., Zhang L., Mo Y., Dlamini D.S., Wang H., He B., Li J., Matsuyama H., Ultra-low graphene oxide loading for water permeability, antifouling and antibacterial improvement of polyethersulfone/sulfonated polysulfone ultrafiltration membranes. *Journal of Colloids and Interface Science*, 552 (2019), 319 -331.

## APPENDICES

### Appendix A-Supplementary material

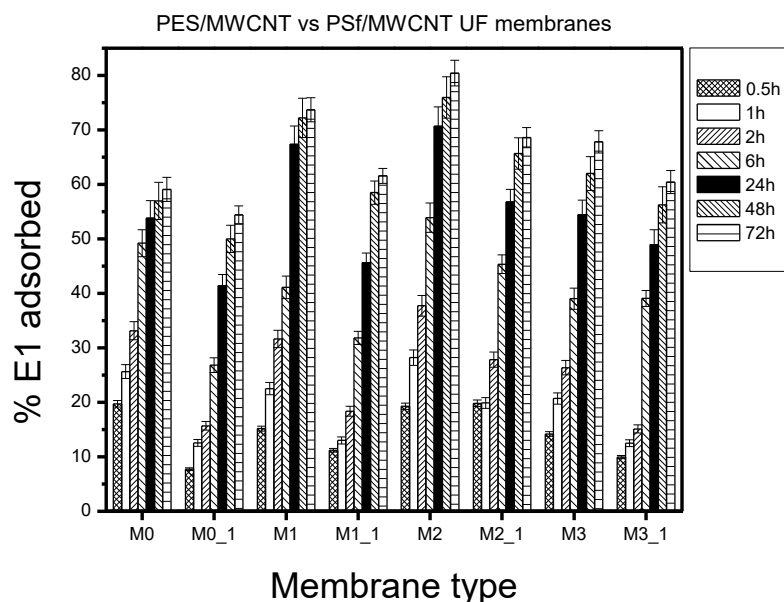


**Figure S4. 1** Comparison of E1 adsorption on PES/O-MWCNT membranes vs PSf/MWCNT membranes. Experimental conditions: 72 h contact time, 25 cm<sup>2</sup> membrane area, 100 ng/L of E1 solution, pH ~6, at 20 °C, 260 rpm. Membranes denoted as M0\_1, M1\_1, M2\_1 and M3\_1 were prepared from PSf-based casting solutions with various loadings of O-MWCNTs.

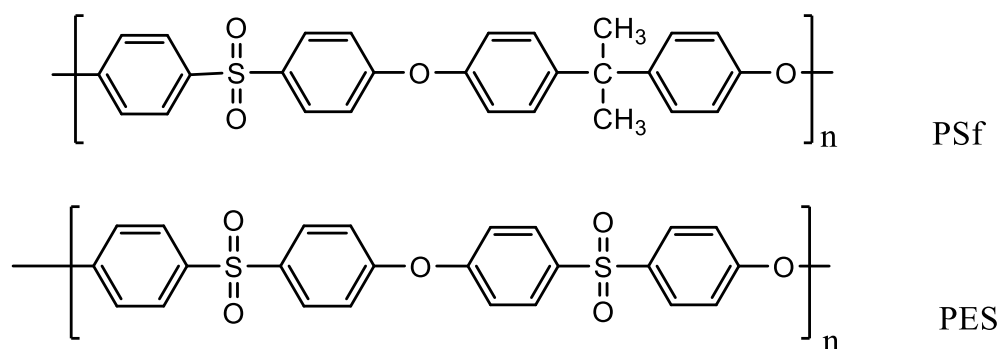


**Figure S4. 2** Chemical structures of PSf and PES.

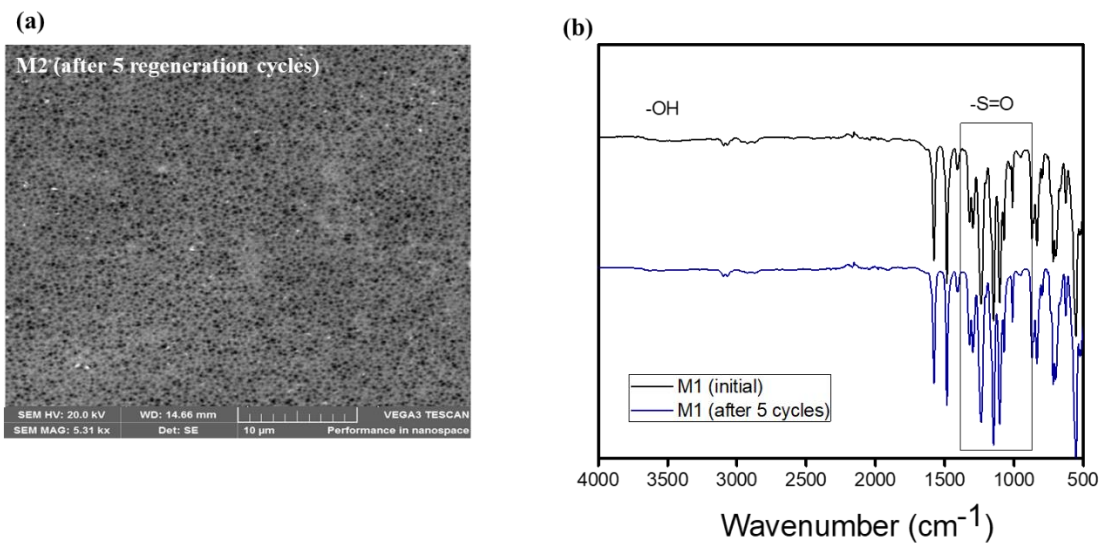


**Figure S4. 3.** SEM surface image of M2 after five adsorption-regeneration cycles.

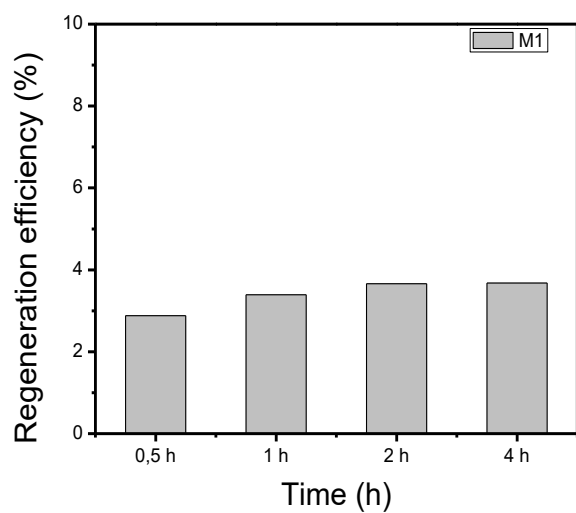


**Figure S4. 4** Regeneration efficiency of M1 using Milli-Q water at 20 °C as a washing solvent.

## **Appendix B. Supplementary material**

### **S5.6.1. Synthesis and characterisation of O-MWCNTs using nebulized spray pyrolysis method**

The synthesis, functionalisation and characterisation of O-MWCNTs were carried out using known and widely documented procedure. MWCNTs were prepared using a chemical vapour deposition method via nebulized spray pyrolysis (see Fig. S1) [1]. Briefly, a mixture containing 2.00 g of ferrocene (catalyst) in 20 ml of toluene (carbon source) was nebulized into quartz tube that was placed horizontally inside a furnace. Dr Hielscher UM20-1.6 MHz nebuliser and frequency controller were used to produce the “mist” which was carried into a furnace (Elite TSH 12/500-2216). Argon and hydrogen gases were also passed through the quartz tube at a flow rate of 500 sccm and 60 sccm and were used as carrier gases to create an inert reaction atmosphere. The synthesis time was maintained at 30 min at a reaction temperature of 850 °C. Upon cooling of the quartz tube reactor, the MWCNTs grown around the quartz tube walls were collected. For the removal of residual metal catalyst and oxidation, MWCNTs were refluxed in 35% HNO<sub>3</sub> for 4 h at 120 °C followed by washing with deionised water until a neutral pH of the washing solution was obtained. The purified CNT sample was dried in an oven at 60 °C for 24 h.

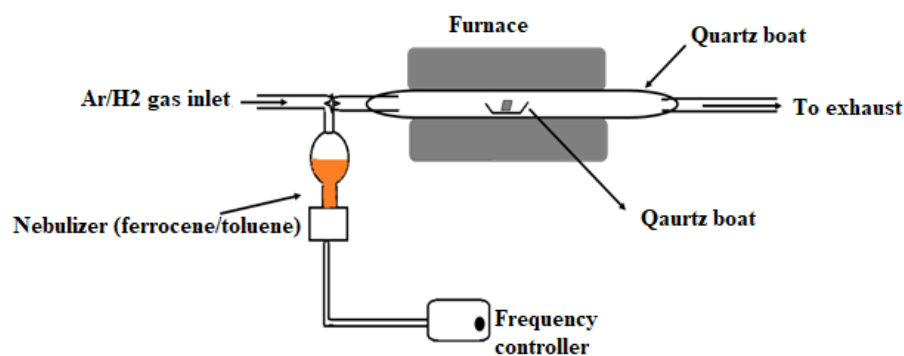


**Figure S5. 1.** Experimental set-up for the nebulized spray pyrolysis method.

## S5.6.2. Characteristic properties of O-MWCNTs

### S5.6.2.1. TEM analysis of MWCNT and O-MWCNTs

The small particles observed within the MWCNT tangles Fig. S5.2 (a) are due to the presence of residual ferrocene catalyst used during the MWCNT growth process. These metal particle residues were removed by treatment with 35% HNO<sub>3</sub> and H<sub>2</sub>SO<sub>4</sub> (Fig. S2b). The characteristic properties of as-synthesized MWCNTs and O-MWCNTs, in terms of their outer diameters and ET surface area values are summarized in Table S5.1.

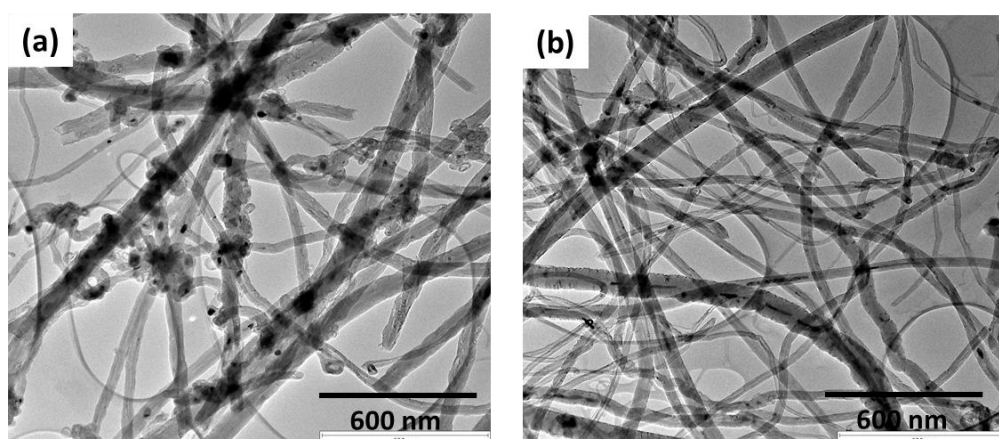


**Figure S5.2.** TEM analysis of (a) as-synthesized MWCNTs and (b) O-MWCNTs.

**Table S5. 1** Characteristics of MWCNTs.

	Outer diameter (nm)	Length ( $\mu\text{m}$ )	BET mean surface area ( $\text{m}^2/\text{g}$ )	BET mean pore volume ( $\text{cm}^3/\text{g}$ )
MWCNTs	10–25	2.0–18.0	208.7	0.17
O-MWCNTs	10–14	1.5–13.0	292.2	0.31

### S5.6.2.2. FTIR spectroscopy analysis of MWCNTs

In Fig. S5.3, the FTIR spectra analyses shows that acid treatment induces the presence of oxygen-containing, hydrophilic functional groups such as  $-\text{OH}$  and  $-\text{COO}$  groups in the carbon nanotube backbone. The intensity of the  $-\text{OH}$  band for the O-MWCNTs, is sharper and intense than for as the as-synthesized MWCNT sample, suggesting successful oxidation of the MWCNTs.

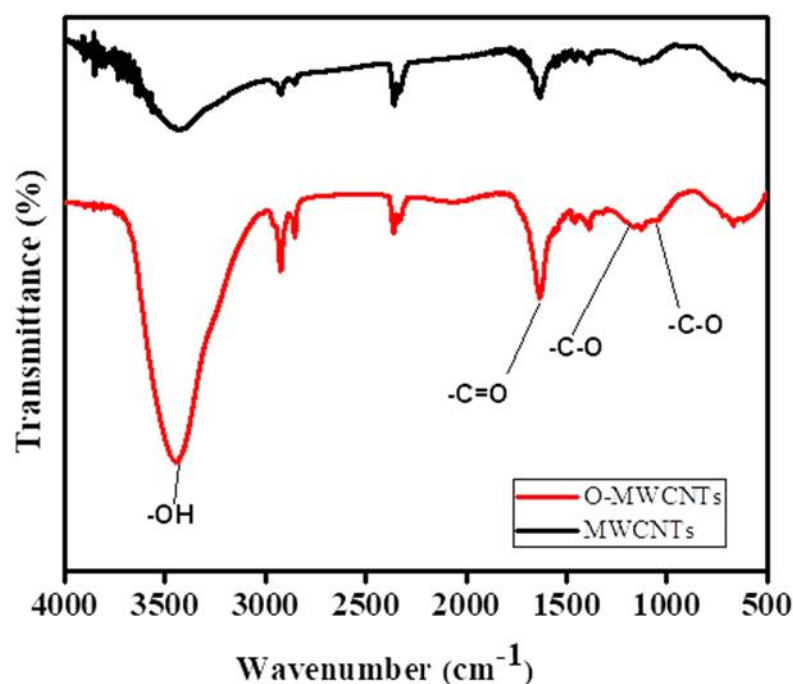


**Figure S5. 3** FTIR spectra of as-synthesized MWCNTs and O-MWCNTs.

### S5.6.2.3. Raman spectroscopy analysis

Raman spectra were collected on a Jobin-Yvon T6400 micro-Raman spectrometer at ambient temperature using a tunable spectra Physics dye laser with a 636.4 nm excitation source. Raman spectroscopy analysis was carried out in order to investigate the purity of MWCNTs after acid oxidation and the removal of metal catalyst impurities as well as to examine the degree of structural disorder induced during treatment. Raman spectra for both pristine and functionalised MWCNTs in Fig. S4 displays three characteristic peaks of multi-walled CNTs at  $\sim 1353\text{ cm}^{-1}$  (D- band),  $\sim 1580\text{ cm}^{-1}$  (G- band) and at  $\sim 2690\text{ cm}^{-1}$  (G'- band). D- band relates to the disorder induced feature within the O-MWCNT lattice by the presence of amorphous carbon and other impurities. On the other hand, the G-band is indicative of the graphitic nature of the O-MWCNTs and G'- band relates to the long-range order within the O-MWCNT sample and occurs as a result of two-phonon second order scattering process [2]. Further, the  $I_D/I_G$  ratio can be used as a measure of the degree of order in CNTs; the higher the  $I_D/I_G$  ratio or the closer this value is to 1, the less ordered the CNTs are [3]. In Fig. S5.4, not only has the D band intensity of the functionalised CNTs decreases but the  $I_D/I_G$  ratio decreased from 0.72 for the as-synthesized CNTs to 0.34 for functionalised CNTs. This suggests that acid treatment of CNTs was effective in removing amorphous carbon and the catalyst residues that causes structural disorder in CNTs. The graphitic nature of CNTs has therefore improved after acid treatment.

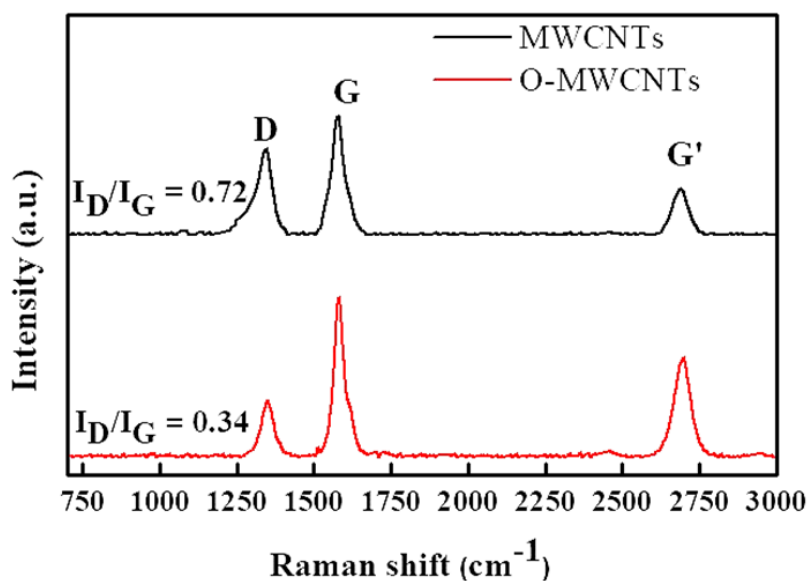


**Figure S5. 4.** Raman spectra of as-synthesized MWCNTs and O-MWCNTs.

#### S5.6.2.4. TGA analysis

TGA can be used as an effective tool to assess the thermogravimetric stability of MWCNTs and to measure the efficiency of the purification methods used in the removal of metal catalyst residues, *i.e.* metal content of the MWCNTs can be accurately determined. The TGA scan of pristine MWCNTs in Fig. S5.5a, shows that the MWCNTs does not undergo complete decomposition *i.e.* about ~6% of sample remain. This mass fraction corresponds to the weight of residual ferrocene catalyst or iron oxides. However, after acid treatment the O-MWCNTs undergo complete decomposition. This suggests that acid oxidation was effective in removing the metal particle residues and is agreement with findings from Raman spectroscopy analysis of these O-MWCNTs. Similar observations were reported by Dileo and coworkers [2]. DTA maxima in Fig. S5.5a and S5.5b were used to estimate the decomposition temperature of the MWCNTs. This increase in decomposition temperature from *ca.* 622 °C for pristine MWCNTs to *ca.* 632 °C for functionalised MWCNTs indicates an improvement in the thermal stability of MWCNTs upon removal of amorphous carbon and other metal catalyst impurities.

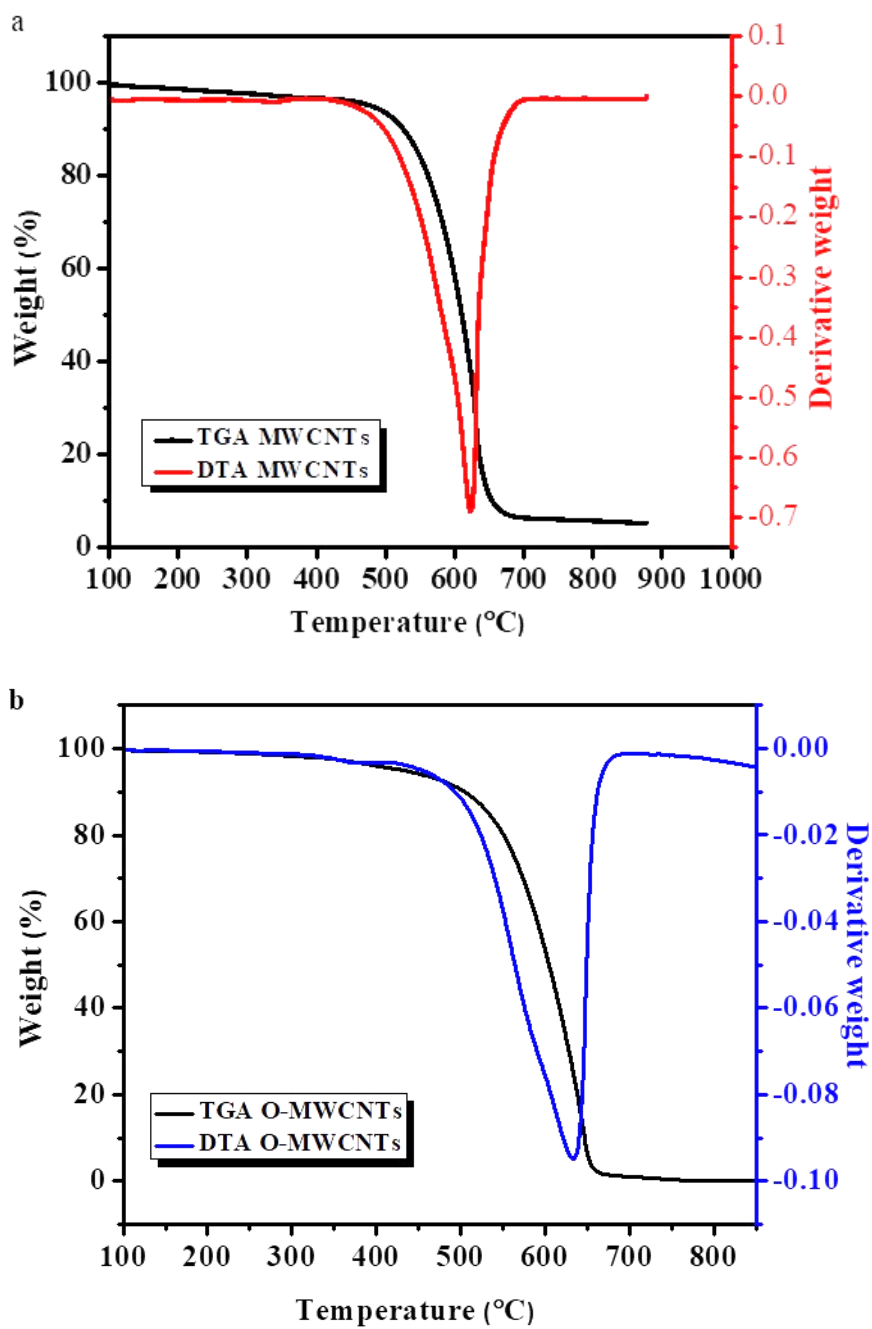


**Figure S5.5** TGA and DTA curves for (a) pristine MWCNTs and (b) functionalised O-MWCNTs

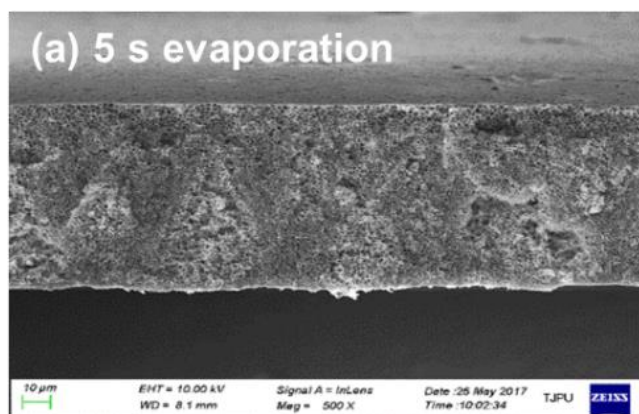


**Figure S5. 6** SEM cross-sectional image of PES/SPSf membrane with 0.03wt.% O-MWCNT (5s of solvent evaporation) prepared in the absence of PEG20kDa and H<sub>2</sub>O; Pure water flux (17.55 L/m<sup>2</sup>.h at 0.2MPa).

### S5.6.3. Controlling the formation of sponge-like morphology for PES/SPSf/O-MWCNT membranes.

#### Effect of H<sub>2</sub>O contents on the morphology and performance properties of PES/SPSf blend membranes - A step towards establishing the influence of the interaction between O-MWCNTs, H<sub>2</sub>O and SPSf on the membrane morphology

Casting knife gap height was set at 300 μm

Coagulation bath temperature set at 25°C

Solvent evaporation time for 0 s.

**Table S5.2** Casting solution composition: Effect of H<sub>2</sub>O concentration on membrane structural and performance properties.

Membrane	Polymer (wt. %)	PES (g)	SPSf (g)	DMAc (g)	H <sub>2</sub> O (g)	H <sub>2</sub> O (wt. %)
M0	22	9.24	1.76	39	0	0
M1	22	9.24	1.76	39	1.5	3
M2	22	9.24	1.76	39	2.5	5
M3	22	9.24	1.76	39	3.5	7
M4	22	9.24	1.76	39	4	8

M5	22	9.24	1.76	39	4.5	9
M6	22	9.24	1.76	39	5	10

### S5.6.3.1. Viscosity measurements

The physical appearance of PES/SPSf casting solutions containing different contents of C was monitored at 70 °C (immediately after casting solution preparation) and at 25 °C (room temperature), Fig. S5.6. All solutions were transparent and homogenous at 70 °C, except for M6 which contained 10wt% of H<sub>2</sub>O (addition of too H<sub>2</sub>O resulted in instant separation into two layers). However, at 25 °C (room temperature), casting solutions M4 and M5 became turbid, and M5 eventually solidified indicating complete gelation [14]. Casting solutions containing little (3 – 7 wt%) to no H<sub>2</sub>O, remained transparent at room temperature.

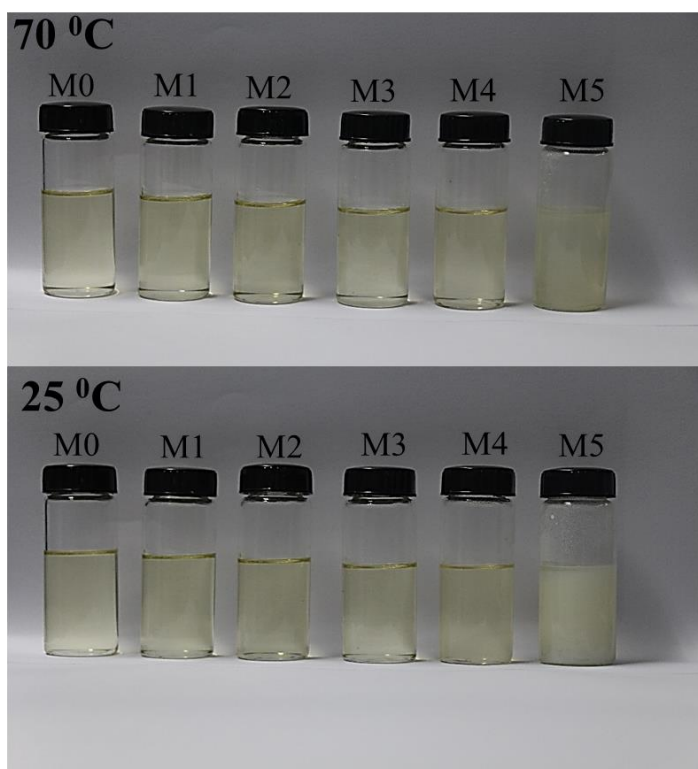


**Fig. S5.7:** Physical appearance of PES/SPSf casting solutions with different H<sub>2</sub>O contents at 70 °C and 25 °C.

Generally, an increase in viscosity of the casting solution tends to slow down the diffusion rate between solvent and non-solvent during the coagulation process. This can lead to a delayed demixing and subsequently the suppression of macrovoids in the membrane sublayer and formation of a denser structure [1]. The viscosity of casting solutions increases with an increase in additive mass of H<sub>2</sub>O (Fig. S5.7). This is due to the formation of hydrogen bonds between H<sub>2</sub>O molecules and the –SO<sub>3</sub><sup>-</sup> groups of the polymer chains, thus restricting the mobility of polymer chains, hence the increase in casting solution viscosity. The number of hydrogen bonds formed increases with additive H<sub>2</sub>O content.

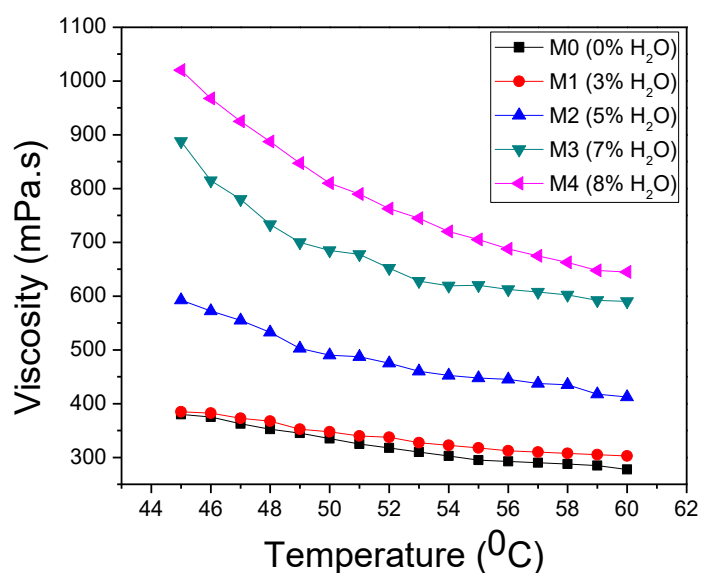


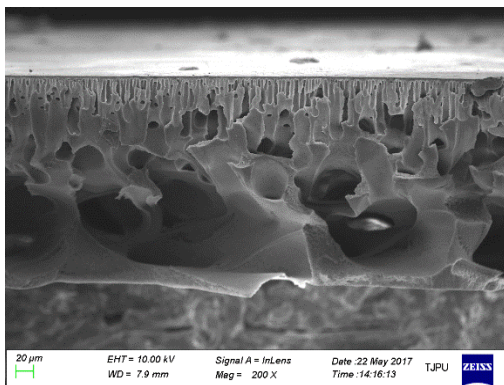
**Fig. S5.8:** Viscosity measurements of PES/SPSf casting solutions containing different additive mass of H<sub>2</sub>O as a function of temperature.

### S5.6.3.2. SEM analyses

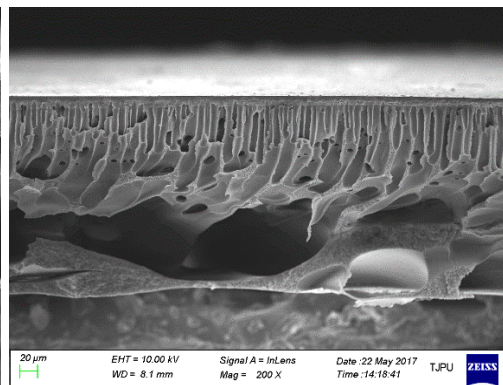
In Fig. S5.8 all membranes exhibit the typical asymmetric structure of a thin dense top layer and porous sublayer. However, clear changes in membrane morphology can be observed when comparing cross-sectional image of M0 derived from PES/SPSf casting solution without H<sub>2</sub>O to those of PES/SPSf composite membranes containing H<sub>2</sub>O. For membranes M0 to M3, at low

H<sub>2</sub>O contents, the membrane sublayer consists of finger-like structures and macrovoids towards the bottom layer of the membrane cross-section. However, with further increments in H<sub>2</sub>O content M4 to M5, the membrane morphology changes from finger-like to sponge-like. The change in membrane morphology to sponge-like is brought about by the delay in demixing rate between solvent and non-solvent during membrane formation, which is induced by the increase in casting solution viscosity at higher H<sub>2</sub>O contents. The addition of H<sub>2</sub>O in the PES/SPSf solution, leads to strong hydrogen bond interactions between H<sub>2</sub>O molecules and SO<sub>3</sub><sup>-</sup> groups of the polymer, which then restricts the movement of the polymer chains hence the increase solution viscosity.

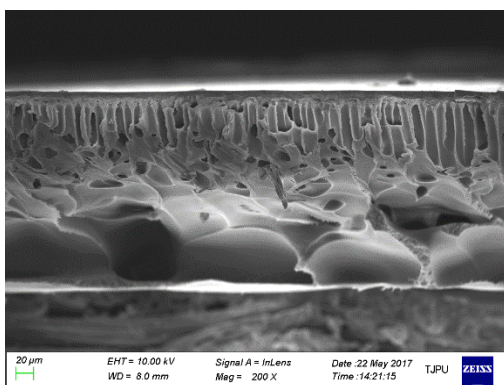
a)



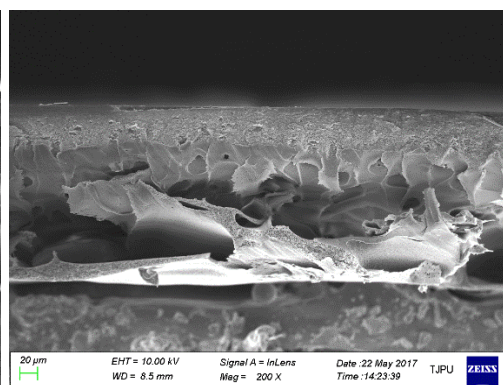
b)



c)



d)



e)

f)

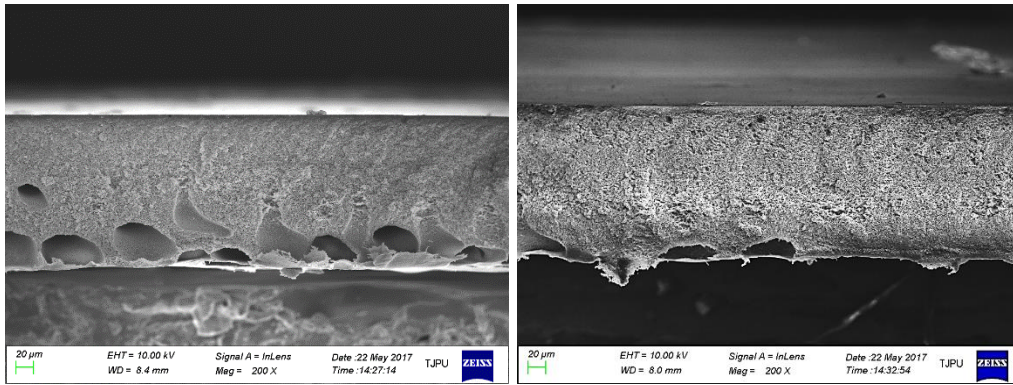


**Fig. S5.9** SEM cross-sectional images of PES/SPSf membranes with different contents of H<sub>2</sub>O: a) M0 (0 wt.%), b) M1 (3 wt.%), c) M2 (5 wt.%), d) M3 (7wt.%), e) M4 (8 wt.%) and f) M5 (9 wt.%).

### *S5.6.3.3. Performance tests: Effect of H<sub>2</sub>O content on pure water flux and solute rejection*

In **Error! Reference source not found.**S5.9, pure water flux of PES/SPSf composite membranes first increases with an increase in H<sub>2</sub>O content but decreases with further increments. Initially, pure water flux increases from 371.57 L/m<sup>2</sup>.h for M0 membrane without H<sub>2</sub>O to 486.89 L/m<sup>2</sup>.h and 511.31 L/m<sup>2</sup>.h for M1 and M2. This occurs as a result of the increase in size and number of macrovoids in the membrane sublayer of M1 and M2 (see Fig. S5.8), which reduces the resistance in water permeation through the membrane. However, with further increments in water content, pure water flux decreases to 481.13 L/m<sup>2</sup>.h, 438.26 L/m<sup>2</sup>.h and 428.73 for M3, M4 and M5 but is still significantly higher than that of pristine membrane (M0). It was established in Figs. S5.6 and S5.7, that the addition of higher H<sub>2</sub>O contents enhances the viscosity of casting solutions thereby generating sponge-like morphology in the membrane sublayer. Although porous, the sponge like morphology may lead to slight increase in resistance to water permeation, hence the reduction in pure water flux at high H<sub>2</sub>O contents. The pure water flux of M3 to M5 is still higher than that of M0. This is behavior can be correlated to the fact that at high nonsolvent concentrations, the thermodynamic stability of the casting solution is reduced, which then causes phase separation to proceed faster due to low

compatibility between nonsolvent additive and polymer solution [14, 15]. Therefore, a more porous membrane is generated. All membranes displayed high rejection for BSA (>99% rejection).

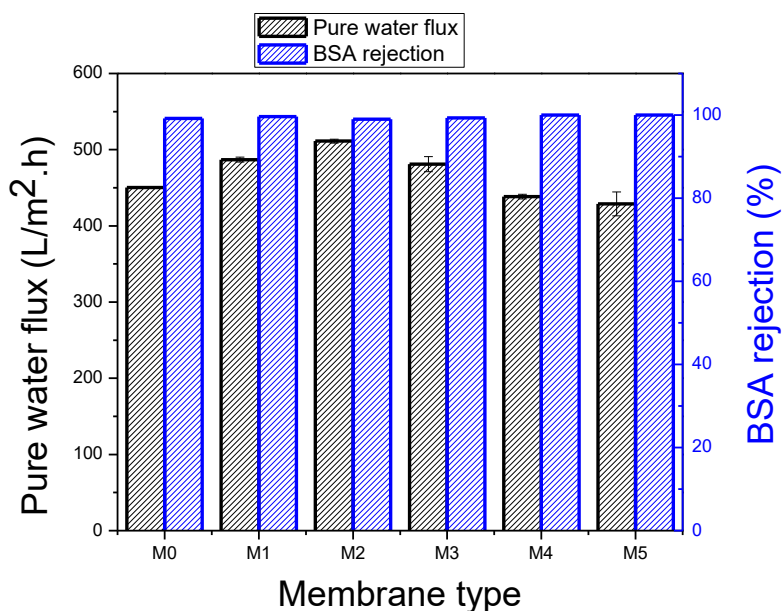


**Fig. S5.10** Pure water flux and BSA rejection for PES/SPSf composite membranes containing different contents of H<sub>2</sub>O, at applied pressure of 0.1MPa.

#### S5.6.4 Interaction between H<sub>2</sub>O, SPSf and O-MWCNTs: Effect of O-MWCNT content

Casting knife gap height was set at 200 μm

Coagulation bath temperature set at 25°C

Solvent evaporation time for 0 s.

**Table S5.3.** Composition of casting solutions.

Membrane	PES (g)	SPSf (g)	DMAc (g)	H <sub>2</sub> O (g)	O-MWCNTs (wt%)	Viscosity (mPa.s) @ 25°C
M0	9.24	1.76	39	4	0	1612.5
M1	9.24	1.76	39	4	0.005	1920.0
M2	9.24	1.76	39	4	0.01	1982.5

M3	9.24	1.76	39	4	0.03	2225.0
M4	9.24	1.76	39	4	0.05	2452.5

Polymer concentration: 22wt%, H<sub>2</sub>O content: 8wt%

#### S5.6.4.1. Viscosity measurements

The results in Fig. S5.10 confirm a known fact that the viscosity of the dope solutions decreases with an increase in temperature. Secondly, the dope solution viscosity increases with an O-MWCNT content. This behaviour can be attributed to the strong hydrogen bond interactions that occur between SPSf, H<sub>2</sub>O and O-MWCNTs, which lead to reduction in polymer chain mobility, thus an increase in solution viscosity [2].

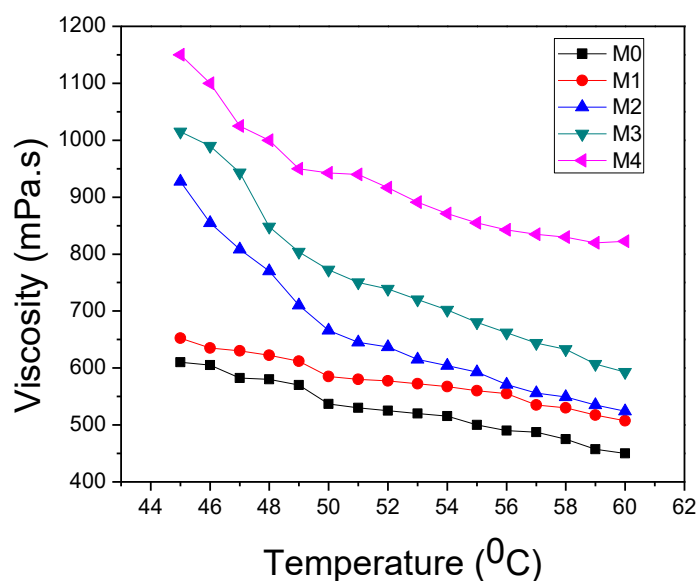
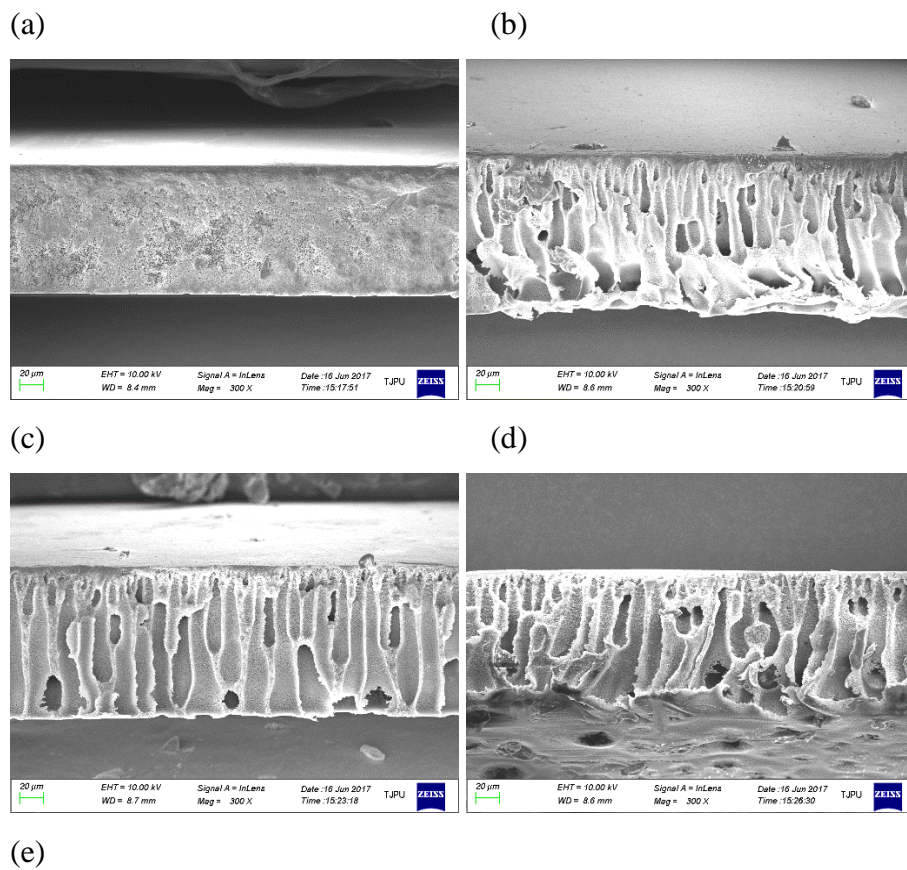


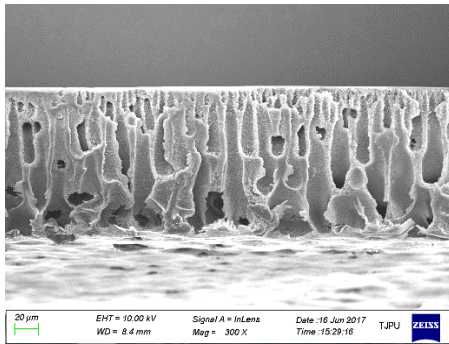
**Fig. S5.11** Effect of temperature on viscosity of casting solutions.

#### S5.6.4.2. SEM analyses

The addition of O-MWCNTs (Fig. S5.11b, c, d, and e) in the PES/SPSf/H<sub>2</sub>O casting solution changes the membrane morphology from sponge-like (Fig. S5.11a) to fully finger-like

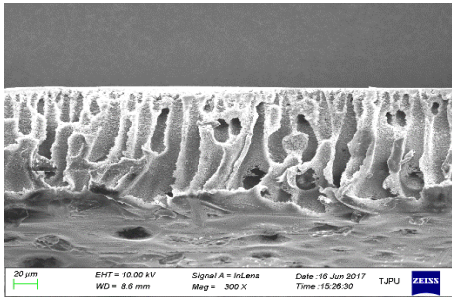
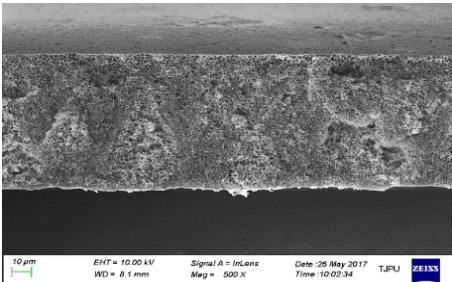
structure. This can be attributed to the hydrophilic nature of O-MWCNTs, which reduces the thermodynamic stability of the casting solution thereby causing phase separation in water coagulation bath to proceed faster. Previously, we reported that the addition of 0.016wt% O-MWCNTs in the 22 wt% PES/SPSf/H<sub>2</sub>O casting solution, combined with solvent evaporation (20s) prior to immersion in the water coagulation bath, leads to the formation of a membrane with sponge-like structure. It is now clear from the present results that in the absence of solvent evaporation, O-MWCNTs induces the formation of finger-like structure in the membrane sublayer due to their highly hydrophilic nature.





**Fig. S5.12** Cross-sectional SEM images of PES/SPSf/H<sub>2</sub>O membranes containing different contents of O-MWCNTs: (a) 0 wt%, (b) 0.005 wt%, (c) 0.01wt%, (d) 0.03 wt% and (e) 0.05wt%.

**Table S5.4** Effect of evaporation time on PES/SPSf/H<sub>2</sub>O/O-MWCNT membrane morphology.

PES/SPSf/OMWCNT (evaporation time = 0s)	PES/SPSf/OMWCNT (evaporation time = 20s)
 <p>O-MWCNT= 0.03 wt%            PWF = 333.46 L/m<sup>2</sup>.h            Mechanical strength = 2.39±0.01 MPa</p>	 <p>O-MWCNT= 0.02 wt%            PWF= 17.55 L/m<sup>2</sup>.h            Mechanical strength = 3.16±0.1 MPa</p>

#### S5.6.4.3. Performance tests: Interaction between H<sub>2</sub>O, SPSf and O-MWCNTs

Pure water flux was found to decrease to a certain extent, with an increase in O-MWCNT content (Table S5.4). Pure water flux for M0 without O-MWCNTs was found to be 666.92 L/m<sup>2</sup>.h, and this reduced to 524.01 L/m<sup>2</sup>.h, 514.48 L/m<sup>2</sup>.h, 333.46 L/m<sup>2</sup>.h, and 498.60 L/m<sup>2</sup>.h for M1, M2, M3 and M4 respectively. O-MWCNTs are hydrophilic in nature and therefore,

their addition in the membrane matrix was expected to enhance pure water flux as reported by numerous researchers in the field. The reduction in pure water flux can be related to agglomeration of O-MWCNTs in the membrane matrix which led to a reduction in mean pore radius as shown in Table S5.4. Considering the multiple hydrogen bonds forming between SPSf, H<sub>2</sub>O and O-MWCNTs, it can be expected that the presence of O-MWCNTs within the polymer matrix may lead to slight reduction in membrane pore size. Although pure water flux reduced with increments in O-MWCNT content, the fluxes obtained for M1 to M4 are still reasonably high. Similar results have also been obtained reported by others [16, 17]. Fig. S5.12 shows the effect of O-MWCNT content on membrane PEG 10kDa rejection. It can be seen that the maximum rejection obtained for PEG 10kDa was 26% by M3. Also, the PEG 10kDa rejection was found to increase with O-MWCNT content (2%, 13%, 15%, 22% for M0, M1, M2 and M4), as a result of the reduction in mean pore radius of membranes.

Membrane porosity increased while mean pore radius decreased with increments in O-MWCNT content (Table S5.4). This property can prove to be advantageous for the fabrication of our membranes. This is because a membrane that is best suited for any application is the one with many pores that are smaller in size [18]. Such a membrane is capable of avoiding to large extent, the permeability-selectivity trade-off that membranes are known to suffer from. The small pore sizes will favour the rejection of solutes while the large number of pores is beneficial for the improvement of flux.

The mechanical strength of membranes reduced with increments in O-MWCNTs content (Table S5.4). The decrease in mechanical strength for membranes containing O-MWCNTs can be attributed to the presence of finger-like structures in the membrane sublayer as shown in Fig. S5.11.

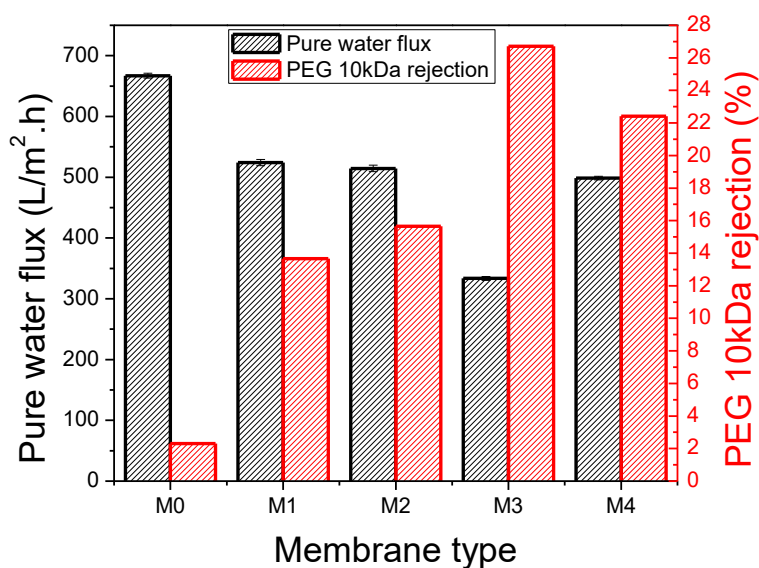


**Fig. S5.13** Effect of O-MWCNT content on pure water flux and PEG 10kDa rejection.

**Table S5.5.** Effect of SPSf, H<sub>2</sub>O and O-MWCNT interaction on membrane porosity, mean pore radius and thickness.

Membrane	Porosity (%)	Mean pore radius (nm)	Thickness (μm)	Pure water flux (L/m <sup>2</sup> .h)	BSA rejection (%)	Mechanical strength (MPa)
M0	71.8	66.2±2.0	146±2.8	666.9±4.0	92.8	2.29±0.23
M1	86.2	48.9±2.6	142±2.5	524.0±5.1	92.9	2.19±0.20
M2	87.8	47.8±4.9	139±3.9	514.5±5.4	97.7	1.94±0.06
M3	88.3	35.3±0.2	128±2.1	333.5±3.0	92.8	2.39±0.01
M4	90.8	42.0±1.3	130±3.6	498.6±2.9	94.6	1.97±0.09

### S5.6.5. Controlling the formation of sponge-like morphology in the presence of O-MWCNTs by adding PEG20kDa at different weight percentages

Casting knife gap height was set at 200 μm

Coagulation bath temperature set at 25°C

Solvent evaporation time for 0 s.

**Table S5.6** Composition of casting solutions

Membrane	PES (g)	SPSf (g)	DMAc (g)	H <sub>2</sub> O (g)	O-MWCNTs (wt%)	PEG 20kDa (g)	PEG 20kDa (wt%)	Viscosity (mPa.s) @ 25 °C
M0	9.24	1.76	39	4	0.005	8	16	1607.5
M1	9.24	1.76	39	4	0.005	9	18	1612.5
M2	9.24	1.76	39	4	0.005	10	20	1717.5
M3	9.24	1.76	39	4	0.005	11	22	1837.5
M4	9.24	1.76	39	4	0.005	12	24	1952.5

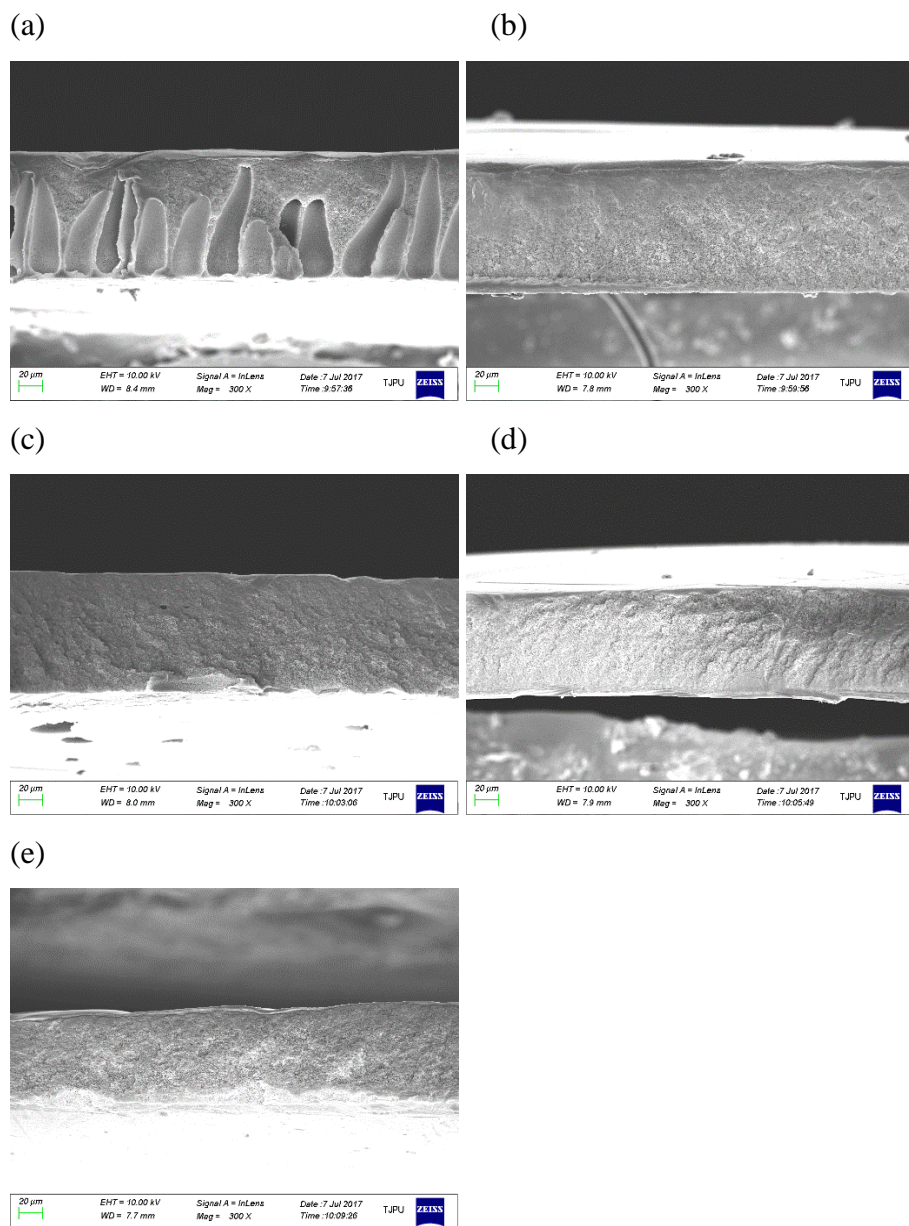
Polymer concentration: 22wt%, H<sub>2</sub>O content: 8wt%

#### ***S5.6.5.1. Viscosity measurements: Effect of PEG20kDa content***

In Table S5.6, casting solution viscosity increases with an increase PEG20kDa content. This behaviour can be attributed to the strong hydrogen bond interactions that occur between PEG, SPSf, H<sub>2</sub>O and O-, which lead to reduction in polymer chain mobility, thus an increase in solution viscosity [2].

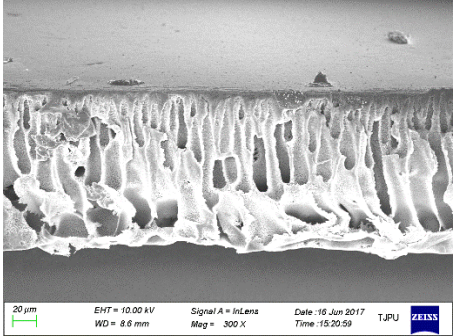
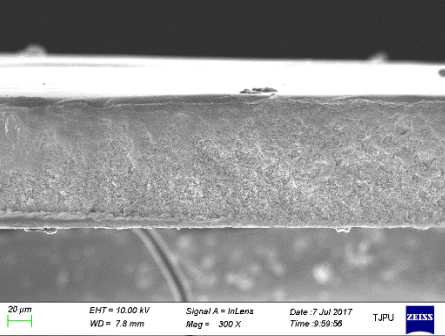
#### ***S5.6.5.2. SEM analyses***

SEM cross-sectional images of PES/SPSf/O-MWCNTs membranes prepared by varying PEG20kDa loading in the casting solution are shown in Fig. S5.13a. The addition of PEG20kDa at low concentrations (16wt%) in the PES/SPSf/O-MWCNTs casting solution led to the formation of finger-like structures in the membranes sublayer. However, with further increments in PEG20kDa loadings (18 - 24 wt%), the membrane morphology was transformed to fully sponge-like structure in Fig. S5.13b, c, d, e. This can be attributed to the increase in casting solution viscosity, which led to delayed demixing between solvent and nonsolvent during membrane formation, hence the formation of sponge-like morphology.



**Figure S5.14** Cross-sectional SEM images of PES/SPSf/O-MWCNTs membranes containing different contents of PEG 20kDa: (a) 16 wt%, (b) 18 wt%, (c) 20 wt%, (d) 22 wt% and (e) 24 wt%.

**Table S5.7** Effect of PEG20kDa on PES/SPSf/O-MWCNT membrane morphology.

PES/SPSf/H <sub>2</sub> O/OMWCNT (without PEG20kDa)	PES/SPSf/H <sub>2</sub> O/OMWCNT (with 18wt% PEG20kDa)
 <p data-bbox="212 884 534 1025">                     O-MWCNT= 0.005 wt%                      PWF = 524.0 L/m<sup>2</sup>.h                      BSA rejection = 93%                 </p>	 <p data-bbox="794 884 1114 1025">                     O-MWCNT= 0.005 wt%                      PWF= 676.99 L/m<sup>2</sup>.h                      BSA rejection = 94%                 </p>

### S5.6.5.3. Performance tests

Pure water flux was found to increase with an increase in PEG20kDa content (Fig. S5.14). Pure water flux increased from 390.93 L/m<sup>2</sup>.h for M1, to 676.98 L/m<sup>2</sup>.h, 727.86 L/m<sup>2</sup>.h, 753.27 L/m<sup>2</sup>.h and 824.73 L/m<sup>2</sup>.h, for M2, M3, M4 and M5. PEG additive is hydrophilic in nature and not all of it is removed during membrane formation, thus improving the hydrophilicity of the membranes [2]. Therefore, the enhancement in membrane hydrophilicity led to improved water fluxes. BSA rejection was found to increase (from 90.9% for M1 to 99.3% for M5) with an increase in PEG20kDa loading. Generally, membranes are known to suffer from selectivity-permeability trade-off, where an increase in flux is accompany by a decrease in rejection. An opposite behavior was displayed by these membranes due to the presence of O-MWCNTs.

Although present at significantly low concentration (0.005 wt%), O-MWCNTs were able to influence the rejection properties of PES/SPSf blend membranes.

Although a higher polymer concentration (22wt%) was used in this work, water fluxes for M5 of 824.73 L/m<sup>2</sup>.h is only slightly reduced compared to that previously reported by Zhang et al [19], of 858.5 L/m<sup>2</sup>.h for 18 wt% polymer concentration. The reason for this is the fact that a lower casting thickness was used (200µm instead of 300 µm) and also due to the presence of hydrophilic O-MWCNTs in the casting solution.

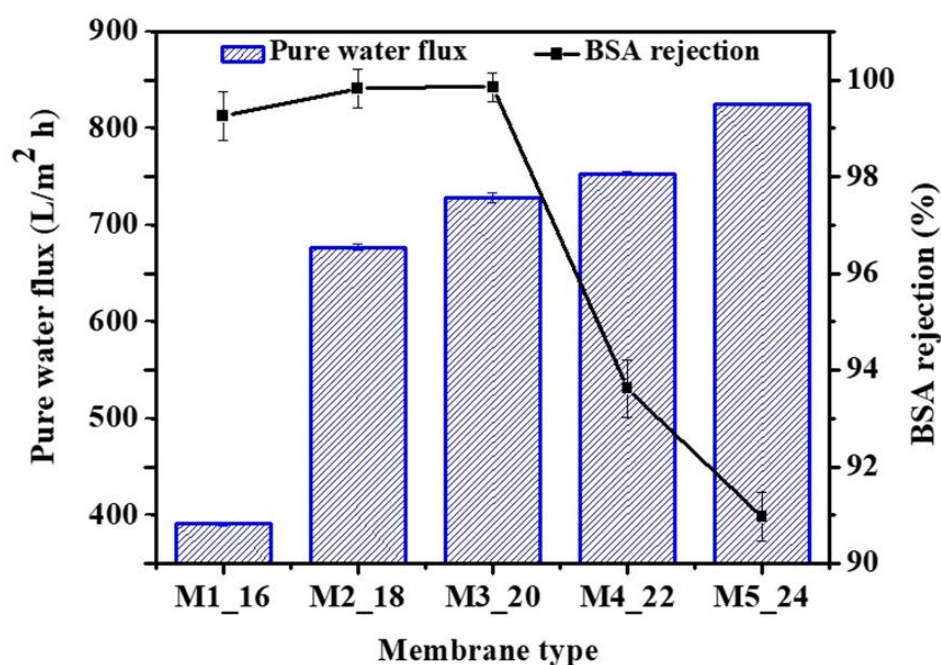


**Figure S5.15** Pure water flux and BSA rejection of PES/SPSf/O-MWCNT membranes containing various contents of PEG 20kDa (O-MWCNT content = 0.005wt.%, PEG 20kDa content = 16, 18, 20, 22 and 24 wt.%).

## References

- [1] L.M. Cele, N.J. Coville, The negative effects of alcohols on carbon nanotube synthesis in a nebulised spray pyrolysis process, *Carbon*, 47 (2009) 1824-1832.
- [2] R.A. DiLeo, B.J. Landi, R.P. Raffaele, Purity assessment of multi-walled carbon nanotubes by Raman spectroscopy, *Journal of Applied Physics*, 101 (2007) 064307.
- [3] Y. Liu, C. Pan, J. Wang, Raman spectra of carbon nanotubes and nanofibers prepared by ethanol flames, *Journal of Materials Science*, 39 (2004) 1091-1094.

## Appendix C- Supplementary materials

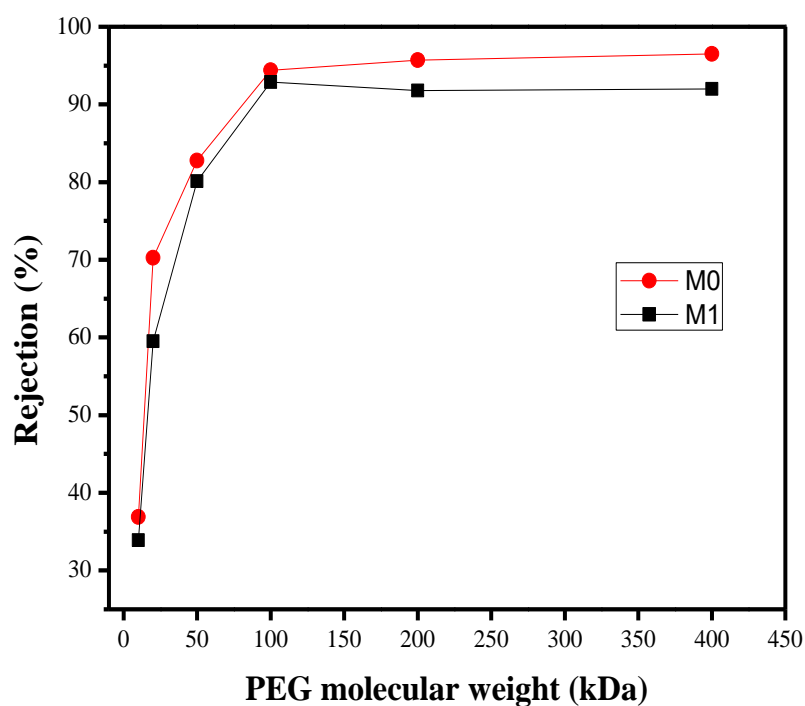


**Figure S6.1.** MWCO determination of M0 and M1 support membranes used for fabrication of TFC NF membranes.

**Table S6.1.** Composition of TFC NF membranes prepared on M0 and M1 supports.

<b>Membrane</b>	<b>TMC (wt.%)</b>	<b>PIP (wt.%)</b>
<b>M0 support</b>		
NF_M0_0.05	0.05	2.00
NF_M0_0.1	0.10	2.00
NF_M0_0.2	0.20	2.00
NF_M0_0.3	0.20	2.00
<b>M1 support</b>		
NF_M1_0.05	0.05	2.00
NF_M1_0.1	0.10	2.00
NF_M1_0.2	0.20	2.00
NF_M1_0.3	0.20	2.00

**Table S6.2.** Thickness values of TFC NF membranes.

<b>Membrane</b>	<b>Thickness (um)</b>
NF_M0	117 ± 1.14
NF_M1_0	119 ± 1.11
NF_M1_25	122 ± 1.13
NF_M1_50	123 ± 1.83
NF_M1_100	126 ± 1.72